Cell-free yet Cell-based Tissue Engineered Vascular Graft

by

Katherine Lorentz

Bachelor of Science in Biomedical Engineering, University of Minnesota Twin Cities, 2013

Master of Science in Biomedical Engineering, Carnegie Mellon University, 2015

Submitted to the Graduate Faculty of the

Swanson School of Engineering in partial fulfillment

of the requirements for the degree of

Doctor of Philosophy

University of Pittsburgh

2020

UNIVERSITY OF PITTSBURGH

SWANSON SCHOOL OF ENGINEERING

This dissertation was presented

by

Katherine Lorentz

It was defended on

June 2, 2020

and approved by

Steven R. Little PhD, Chairman of the Department of Chemical and Petroleum Engineering and the William Kepler Whiteford Endowed Professor in the Departments of Chemical and Petroleum Engineering, Bioengineering, Immunology, and Ophthalmology

Kacey G. Marra PhD, Professor in the Departments of Plastic Surgery and School of Medicine

Morgan V. Fedorchak PhD, Assistant Professor in the Departments of Ophthalmology, Bioengineering, Chemical Engineering, and Clinical & Translational Sciences

Edith Tzeng PhD, Chief of Vascular Surgery at the VA Pittsburgh Healthcare System and UPMC Professor of Surgery

Justin S. Weinbaum PhD, Research Assistant Professor in the Departments of Bioengineering and Pathology

Dissertation Director: David A. Vorp PhD, Associate Dean for Research and the John A. Swanson Professor of Bioengineering, Professor of Cardiothoracic Surgery, Surgery, and Chemical and Petroleum Engineering

Cell-free yet Cell-based Tissue Engineered Vascular Graft

Katherine Lorentz, PhD

University of Pittsburgh, 2020

Cardiovascular disease (CVD) is currently the leading cause of death worldwide resulting in 647,000 annual deaths in the United States alone. A common treatment is revascularization to bypass arterial blockages from CVD; however, currently clinical options are associated with a high failure rate[1]. The field of tissue engineering holds promise, and several groups have been working towards the development of an appropriate tissue engineered vascular graft. This dissertation focused on the development and in vivo testing of three different graft options: (1) custom silk (Antheraea assama (AA) and Bombyx mori (BM)) functionalized with macrophage attractant (C-C motif chemokine ligand 2, CCL2) loaded microparticles or (2) cellular secretions (conditioned media, CM), and (3) BM silk functionalized with extracellular vesicles (EVs). Each graft was assessed after 1 week and 8 weeks for patency and remodeling in a rat model. All graft types showed increased acute patency after 1 week in comparison to blank controls (scaffold only, no payload); however, graft failure due to stenosis was observed in the CCL2 and CM groups after 8 weeks. An increased macrophage presence and higher occurrence of stenosis was observed in response to both the CCL2 and CM functionalized scaffolds when compared to the EV group. Additionally, an increased occurrence of stenosis was observed in response to the inclusion of AA silk compared to BM silk possibly due to the increased RGD binding sites present within the AA silk fibroin. Overall, results have shown a more complete and positive remodeling response to BM silk treated with EVs characterized by increased patency, neotissue formation, extracellular matrix deposition, and a reduction in stenosis. The three TEVGs tested in this dissertation, particularly

the EV functionalized BM silk scaffold, show promising potential for future studies and translation. The development of a TEVG which leverages the positive remodeling effects of cellular secretions, yet is cell-free, offers a lower risk of immune rejection and more easily translatable arterial graft option in comparison to previous cell-based options. A successful TEVG technology has the potential to improve the outcomes of small diameter revascularization including the 371,000 coronary bypass surgeries performed in the US annually.

Table of Contents

List of Tables

List of Figures

List of Abbreviations

αSMA - α smooth muscle actin

AA- Antherea assama

ASC – adipose stem cell or adipose-derived stem cell

AV fistula – arteriovenous fistula

BM – Bombyx mori

BM MNC – bone marrow mononuclear cell

CABG – coronary artery bypass grafting

CAD – coronary artery disease

CCL2 – C-C motif chemokine ligand 2

CM – conditioned media

CVD – cardiovascular disease

EC – endothelial cell

ECM – extracellular matrix

EPC – endothelial progenitor cell

ePTFE - polytetrafluoroethylene

EV – extracellular vesicle

FBS – fetal bovine serum

FGF – fibroblast growth factor

FITC – fluorescein isothiocyanate

H&E – hematoxylin and eosin

IACUC – Institutional Animal Care and Use Committee

ID – inner diameter

IFC – immunofluorescent chemistry

IHC - immunohistochemistry

IL – interleukin

IPSC – induced pluripotent stem cell

ITA – internal thoracic artery

LDL – low-density lipoprotein cholesterol

M1 – inflammatory type macrophage

M2 – regulatory type macrophage

MCP 1 – monocyte chemoattractant protein 1 also known as CCL2

MIRM – McGowan Institute for Regenerative Medicine

MSC – mesenchymal stem cell

NO – nitric oxide

OD – outer diameter

PBS – phosphate buffered solution

PCL – polycaprolactone

PCI – percutaneous coronary intervention

PDGF – platelet-derived growth factor

PETE – polyethylene terephthalate

PGA – polyglycolic acid

PGS – poly(glycerol-sebacate)

PLA - poly-lactic acid

PLGA – poly (lactic co-glycolic acid)

PLLA – poly-l-lactic acid

PSR – picro Sirius red

PU - polyurethane

RA – radial artery

RGD -arginine-glycine-aspartate tripeptide

SF - silk fibroin

SVF – stromal vascular fraction

SVG – saphenous vein graft

TEVG - tissue-engineered vascular graft

TF – tissue factor

TNF - α - transforming necrosis factor α

tPA – tissue plasminogen activator

uPA – urokinase plasminogen activator

VBL – Vascular Biomechanics Laboratory

VEGF – vascular endothelial growth factor

VSMC – vascular smooth muscle cell

VVG – Verhoff's Van Geison

vWF – von Willebrand Factor

List of Company Locations

Abcam: Cambridge, UK

Aligent Technologies: Santa Clara, CA

ATCC: Manassas, VA

Atlanta Biologics: Atlanta, GA

BioTek Instruments: Vermont, MA

Baracco: Monroe Township, NJ

BD Bioscience: Franklin Lakes, NJ

Beckman Coulter: Pasadena, CA

Brandtech Scientific: Essex, CT

Butler Schein: Columbus, OH

Cell Applications Inc.: San Diego, CA

Charles River: Wilmington, MA

Covidien: Minneapolis, MN

Eppendorf: Hauppauge, New York

Ethicon: New Alexandria, PA

Exel Int.: Redondo Beach, CA

GE: Chicago, IL

Gibco: Gaithersburg, MD

GraphPad: San Diego, CA

Invitrogen: Carlsbad, CA

Jackson ImmunoReserach Laboratories: West Grove, PA

JOEL: Peabody, MA

Kospira: Lake Forest, IL

Malvern Panalytical: Malvern, UK

McGowan Institute for Regenerative Medicine: Pittsburgh PA

McKesson Medical-Surgical: Irving, TX

Millex: Duluth, GA

Nikon: Tokyo, Japan

Novus Biologicals: Centennial, CO

ProteinTech: Rosemount, IL

R&D Systems: Minneapolis, MN

RoosterBio: Fedrick, MD

Sigma Aldrich: St. Louis, MO

SonoSite, Inc.: Bothell, WA

Thermo Scientific – Pittsburgh, PA

Tokai Hit Co.: Shizuoka, Japan

Vacu-Statt II: Scanlan, MN

1.0 Introduction

This dissertation aimed to develop a cell-free tissue-engineered vascular graft (TEVG) for the treatment of blockages requiring revascularization, e.g. arterial blockages. To lead toward a clinically translatable technology, this project has tested various combinations of extracellular proteins, materials, and bioactive factors to stimulate in vivo vascular tissue formation. However, to develop a successful TEVG, it is important to understand the underlying anatomy of the vascular tissue we aim to replicate and the limitations of current clinical treatments and in the field of vascular tissue engineering. This initial introductory chapter will focus on the anatomy of the arterial tissue and review the current state of CVD treatments and the field of TEVGs to give a clearer understanding of the work done and the potential impact of the resulting findings.

1.1 Cardiovascular System Overview

The cardiovascular system is comprised of the heart and a closed system of arteries, veins, and capillaries that deliver fluids, nutrients, cells, and bioactive signals throughout the body[2]. The heart acts as the muscular pump, which circulates the blood to the organs and tissues, delivering necessary nutrients and signaling factors. This complex delivery system is broken into two main circuits: [1] The pulmonary circuit, which provides blood flow to the lungs for re-oxygenation, and [2] the systemic circuit which is responsible for circulating the oxygen-rich blood throughout the rest of the body[2]. This dissertation focuses on finding a vascular replacement suitable for the arteries of the high-pressure systemic system.

1.1.1 Blood Vessel Anatomy and Function

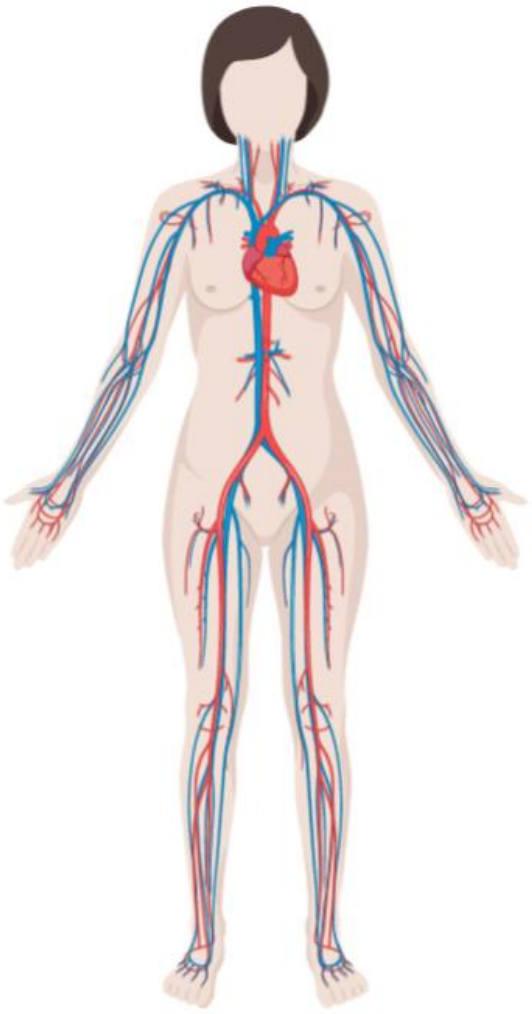

Figure 1. Diagram of the circulatory system

The systemic circulation can be divided into two halves, arterial (blue) and venous (red) (**Figure 1**)[3], which combine to form the circulatory system. Blood travels throughout the pulmonary system to exchange carbon dioxide for oxygen. The reoxygenated blood returns to the left atrium of the heart to begin its journey through the arterial system. As the heart contracts, blood is expelled from the left ventricle and into the aorta[4]. The aorta branches multiple times to form a network of vessels (in descending size: aorta, arteries, and arterioles) that vary in size from 30 mm (aorta) to 10 μm (smallest arterioles) inner diameter (ID)[4]. The arterioles then connect to the capillaries (smallest vessels connecting the arteries to veins), which allow for cargo exchange (e.g., oxygen delivery and carbon dioxide uptake) between the blood and tissues due to their thin walls[3]. Deoxygenated blood is carried back through the capillaries, which converge at multiple points to form the venous network of venules (smallest), veins, and finally, the vena cava (largest), which returns into the heart[4].

The veins and arteries of the systemic system are further divided by their functionality and environment. Two main factors that contribute to the different environmental stressors of vessels are flow rate and pressure[2-4]. The blood flow rate, or the velocity of flow through a specific level of vessel hierarchy, is inversely proportional to the total cross-sectional area of the vessels in that level. Although the diameter of each individual artery becomes smaller with more branching, the overall cross-sectional area of all the branching arteries increases, becoming far larger than the aorta itself and hence having a slower flow rate[2].

The pressure observed within the vessel refers to the force of the blood against the vessel wall as it circulates throughout the body. Blood ejecting from the left ventricle of the heart into the aorta and branching arteries causes an increase in force upon the vessel walls and a corresponding increase in observed pressure[2,4]. The highest pressure is observed within the left ventricle itself

and is propagated to the aorta and branching arteries; luminal pressure lessens as the blood travels further from the heart. This decreasing pressure gradient translates to much higher pressures within arteries than veins[4].

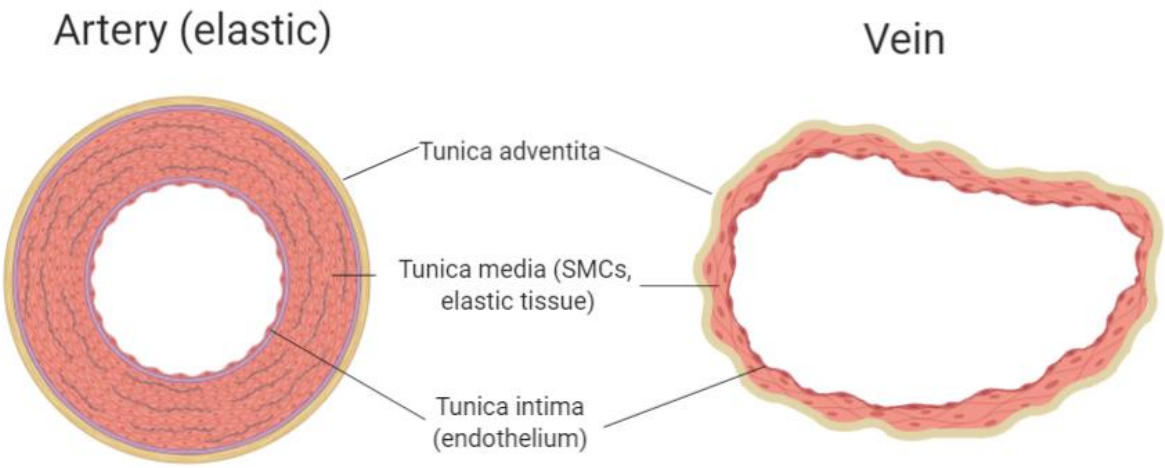

Figure 2. Gross anatomy of arteries vs. veins

As shown in **Figure 2**, the gross anatomy of arteries and veins differ. Even further, arteries themselves can be broken into elastic and muscular subtypes based on their size and distance from the heart[5]. Elastic arteries are the largest arteries, such as the aorta and pulmonary arteries, which are closest to the heart[2,4]. To receive ejected blood at high pressures, elastic arteries contain higher amounts of collagen and elastin when compared to muscular arteries. Muscular arteries branch from elastic arteries drawing blood flow towards the extremities. The tunica media of muscular arteries is thicker and contains more vascular smooth muscle cells (VSMCs) to maintain blood flow. Additionally, they also contain well defined elastic layers at the intima/media and media/adventitia interfaces[4]. This dissertation focuses on the development of an elastic arterial

conduit for application in cardiac arterial bypass and peripheral arterial revascularization (**Figure 3**).

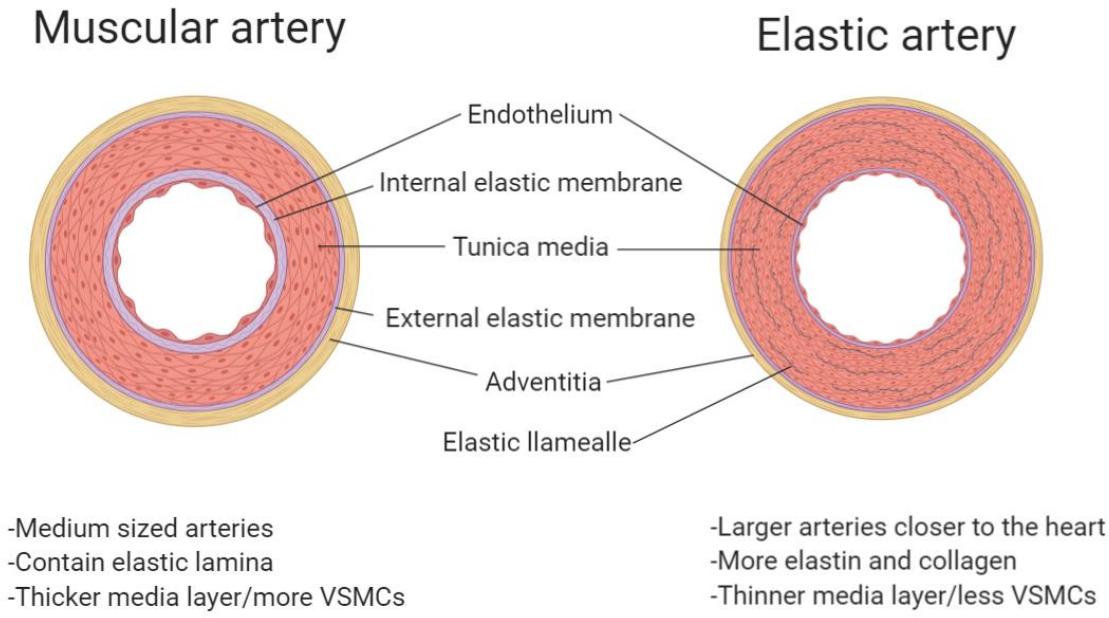

Figure 3. Muscular vs. elastic arterial wall cross-section

1.2 Coronary Artery Disease

Cardiovascular disease (CVD) is currently the leading cause of death within the United States, resulting in a staggering 647,000 annual deaths[6]. The term "CVD" encompasses a broad range of disorders of the heart and vasculature, ranging from heart attacks to strokes. In many types of CVD, revascularization is a potential treatment where the damaged vasculature is bypassed with a vessel like conduit. Due to the broad nature of CVD, many types of TEVGs have been developed for specific applications including arteriovenous fistulas (connecting a vein and artery for use in

hemodialysis)[7,8], large diameter vascular grafts (suited for larger arteries such as the carotid)[9,10], and small diameter vascular grafts (designed for coronary artery bypass and peripheral artery revascularization applications)[11-20]. The sheer volume of illnesses associated with CVD makes a complete summary of each beyond the scope of this dissertation. Instead, I have chosen to focus specifically on coronary artery disease (CAD) and current treatments.

CAD is the most common type of CVD, accounting for about 365,000 annual deaths associated with heart disease[6,21]. Nearly 18 million adults have CAD or about 6.7% of the US population[22]. Of these diagnosed patients, approximately 371,000 revascularization surgeries requiring a bypass graft occur each year[21]. CAD refers to the narrowing or complete blockage of the arteries supplying blood to the heart[23]. The blockage of the coronary arteries restricts oxygen and nutrient supply to the myocardium, eventually leading to cardiac failure[23,24]. Blockages usually form over time, beginning with the narrowing of the luminal space due to intimal hyperplasia and progressing into plaque blockage known as atherosclerosis.

Intimal hyperplasia describes the narrowing of the vessel's luminal space due to the accumulation of cells within the tunica intima[25]. VSMC proliferation and migration within this layer cause an increased number of cells and intimal thickening (**Section 1.2.2**). While intimal hyperplasia is described here as a diseased state, it is actually a wound healing response to vascular injury. Most occurrences of intimal hyperplasia are associated with vascular cell activation, which can be affected by injury, age, and increased inflammation.[5]. Vascular cells undergo phenotypic changes in response to vascular injury (**Sections 1.2.1.1** and **1.2.2.1**), which, if left activated, progresses into intimal hyperplasia[5]. Even in a healthy individual, the natural expansion of vascular cells over time leads to hyperplasia[26], which is reflected in the high occurrence within aging populations[26]. Over time, hyperplasia progresses into atherosclerosis.

Atherosclerosis refers to the narrowing of the arteries supplying blood to the heart due to plaque accumulation within the lumen[23]. Atherosclerosis usually begins with increased accumulation of low-density lipoprotein cholesterol (LDL) particles from circulating blood into the intimal layer, where they are oxidized into pro-inflammatory particles[27] activating the surrounding vascular cells (**Sections 1.2.1.1** and **1.2.2.1**). The inflammatory state is further exacerbated as inflammatory cells are attracted and lead to large plaque formations within the luminal space[27]. Both genetic and environmental factors play a role in the development of atherosclerosis[23,24]. Studies have linked 15 genetic variants to an increased propensity for CAD associated with LDL, arterial hypertension, triglycerides, high-density lipoprotein cholesterol, and thrombosis[23,28]. In addition to these genetic risk factors, many lifestyle choices increase CAD occurrence and atherosclerosis progression such as diabetes[29], smoking[30], sedentary lifestyle[31], and consumption of a high-fat diet[32].

Both intimal hyperplasia and its progression into atherosclerosis can occur in many different ways; however, the main causes of CAD can be traced to endothelial cells (EC) (**Section 1.2.1**), VSMC (**Section 1.2.2**), and the vascular extracellular matrix (**Section 1.2.3**)[24].

1.2.1 Endothelial Cell Function

The lumen of arteries consists of a monolayer of endothelial cells (EC) acting as a buffer between the vessel wall and blood[33]. This continuous endothelium lines the entirety of the circulatory system regulating nutrient delivery and blood flow throughout every part of the body. The importance of this single layer of cells cannot be overstated and is evident through the sheer number of ECs, up to 6×10^{13}, working to regulate vessel function[34]. The endothelium plays many roles ranging from cellular to whole organ functions. At an organ level, the continuous lining of

ECs acts as a buffer between tissue and blood. At a cellular level, with slight variation throughout the vascular tree, the endothelium is responsible for regulating the exchange of nutrients between blood and tissue, thrombosis, blood flow through vascular tone, host inflammatory response, and angiogenesis[3,35,36]. Cellular EC functions such as secretion, proliferation, and migration are regulated through environmental cues allowing for the maintenance of surrounding tissues[35,37]. Two of the main roles of ECs are providing an antithrombotic lining at the blood interface and controlling vascular tone.

The endothelium encounters all circulating molecules, toxins, and potential threats and acts as a protective barrier. There are a host of surface proteins and cellular secretions associated with ECs aimed at preventing platelet aggravation and thrombosis[35,36,38]. In particular, ECs produce tissue plasminogen activator (tPA) that aids in breaking down blood clots after repair of the vessel wall[38]. Another anti-thrombotic function of ECs is the production and surface binding of tissue factor pathway inhibitor to inhibit tissue factor (TF), the receptor for factor VII, a pro-coagulant[36,38]. Healthy ECs also regulate coagulation through the expression of many different anticoagulants (thrombomodulin, endothelial protein C receptor, heparin-like proteoglycans, etc.)[39]. Through these modes of anti-platelet adhesion, clot disruption, and anti-coagulation, vascular ECs work to prevent clot formation. This cellular function of the endothelium to prevent thrombosis is an important factor in TEVG development.

The second role of ECs that will be discussed in this section is a broader organ systems function: regulation of vascular tone. The control of vessel tone is less relevant in the development of TEVGs since the main goal is to simply restore flow around a small portion of the vasculature; however, it is an important homeostasis function and must therefore be discussed. Vascular tone is regulated by the ECs through the secretion of vasodilatory (nitric oxide (NO), endothelium-

derived hyperpolarizing factor, and prostacyclin) and vasoconstrictive (thromboxane and endothelin-1) factors[40]. For example, the endothelium can respond to excessive shearing forces by producing endothelin – 1 causing vasoconstriction. Similarly, ECs can stimulate vasodilation in response to various mechanical and environmental stimuli through the production of NO[36,41]. This regulation of vascular tone is essential in maintaining blood pressure and proper flow within organs and tissues.

Overall, healthy ECs maintain a non-thrombogenic lining and maintain vascular tone. EC activation leads to disruption of the functions described above and eventual vascular dysfunction such as hyperplasia[5].

1.2.1.1 Endothelial Cell Dysfunction and CAD

EC activation can be induced in multiple ways, including uneven flow (such as at branching points), infection, and physical injury. Activation of vascular ECs is usually the first stage of intimal hyperplasia and is characterized by the loss of normal EC functioning (vascular tone and anti-coagulation) combined with an increased expression of VSMC-activating and inflammatory cell-attracting factors[5]. Increased EC secretion of platelet-derived growth factor (PDGF), fibroblast growth factor (FGF), and stromal cell-derived factor 1 activate surrounding VSMCs (**Section 1.2.2.1**). Dysfunctional ECs secrete pro-inflammatory factors (various interleukins (IL), tumor necrosis factor α (TNF-α), monocyte chemoattractant protein 1, monocyte colony-stimulating factor and granulocyte-monocyte colony-stimulating factor) to attract and regulate circulating leukocytes[5]. Activated ECs express adhesion molecules (vascular cell adhesion molecule 1, intracellular adhesion molecule 1, P-selectin, and E-selectin) which enable leukocyte binding and migration into the intima[5]. Additionally, dysfunctional ECs have shown an increased permeability to circulating LDL leading to an accumulation of both macrophages and LDL within

the intimal space[42]. This combined increase in VSMCs and inflammatory environment leads to the thickening of the intima and subsequent narrowing of the luminal space (i.e., intimal hyperplasia).

Another component of EC dysfunction relevant to this dissertation is the increased risk of clot formation. As previously described (**Section 1.2.1**), a healthy endothelium provides an anti-thrombotic lining between the blood and tissue, whereas dysfunctional endothelium loses many of its anti-thrombotic properties[39]. Firstly, activated ECs, recruited leukocytes, and activated VSMCs can secrete TF, increasing the production of thrombin[39]. Secondly, activated ECs express a host of surface receptors and cellular secretions (VWF, P-selectin, angiopoietin-2, and endothelin-1) to promote platelet aggregation in response to injury[39]. These two effects increase the risk of thrombus formation due to EC activation.

1.2.1.2 Endothelial Cells and TEVGs

In the case of vascular grafts, EC function is a crucial component of TEVG success as ECs are the "first responders" to vascular injury. While the idea of a TEVG is to bypass an occluded artery to restore proper blood flow, the act of implanting a scaffold creates a new "site of injury" at each anastomosis. As with any wound, the body responds with a cascade of immune and inflammatory responses controlled through cellular communication using soluble molecules or cytokines. The location of the endothelium between the affected tissue and circulating blood means it plays a crucial role in producing a variety of cytokines to attract circulating leukocytes[35,36,43,44]. An applicable example is the secretion of monocyte chemoattractant protein 1 (MCP-1) or C-C motif chemokine ligand 2 (CCL2) by vascular endothelial cells to attract circulating macrophages to the site of injury[36,45,46]. In addition to leukocyte migration into the scaffold, we also must consider EC migration and proliferation into the vacant lumen.

In the case of a cell-free scaffold as a vascular conduit, a break in the endothelium is created, causing an increased potential for clotting. One of the previously mentioned roles of ECs is angiogenesis or the development of new vasculature from preexisting endothelium[33,36,43]. While healthy, undisturbed, ECs remain quiescent, events such as injury or hypoxia can stimulate ECs migration and proliferation into new vessels[35,47]. The ability of vascular ECs to quickly migrate and proliferate in response to local stimulation allows for endothelium formation within an implanted scaffold. As the endothelium represents the regulatory lining between the blood and body, rapid endothelialization is preferential to restore this barrier quickly. After long term graft remodeling, the presence of an intact endothelium becomes important in normal vascular function as described above (nutrient transport, vessel tone, etc.). In response to the significant role of ECs within vascular grafts, many different studies have attempted to culture and pre-seed scaffolds before implantation[48-50].

1.2.2 Vascular Smooth Muscle Cell Function

VSMCs are the most abundant cell type within the vascular wall. They play a diverse role ranging from direct regulation of vascular tone to cellular deposition of new ECM[4,51,52]. In healthy individuals, VSMCs respond to paracrine cues from the endothelium to relax and contract to alter the vascular tone. Healthy VSMCs maintain a quiescent phenotype characterized by the presence of various contractile proteins necessary in cellular contraction (vessel contraction)[4,51,53]. On a cellular level, VSMCs also play a role in ECM deposition, arterial repair, and transport of substances from the blood to the surrounding tissue. To maintain these various functions in response to physiologic cues, VSMCs display a high level of plasticity[53].

VSMCs can range in phenotype from quiescent and non-proliferative in a healthy state to synthetic and proliferative in response to vascular injury[51,54]. Healthy, contractile cells can be identified through the presence of contractile proteins within the cell, including α-actin, smoothelin, and caldesmon[55]. In contrast, synthetic cells can be identified through the absence of contractile proteins (and a corresponding loss of contractile abilities). The transition or rather activation of VSMCs from a contractile to a synthetic phenotype can be triggered through many pathways (**Section 1.2.2.1**) and is generally associated with vascular dysfunction or injury[55]. In reverse, synthetic VSMCs can shift back towards a contractile phenotype, often referred to as "re-differentiation."[55,56] Both directions of phenotypic switching are important considerations in TEVG design (**Section 1.2.2.2**).

1.2.2.1 Vascular Smooth Muscle Cell Dysfunction and CAD

In the case of injury or vascular disease, VSMCs undergo a phenotypic change towards a synthetic state. This change is associated with increased organelle formation to allow for cellular migration and proliferation. While this unique plasticity allows for vessel repair, it can also be detrimental and contribute to various vascular dysfunctions, including intimal hyperplasia[53,57,58], atherosclerosis[53,59,60], and hypertension[57,58,61]. The switch towards a synthetic state, particularly in the case of CAD), may be triggered by several factors including circulating signaling molecules (such as PDGF and VEGF)[53,58], mechanical cues (low shear stress)[62,63], inflammation[53,58,60], and signaling from the endothelium (PDGF, FGF, TGF-β)[33,34,53] (**Section 1.2.1.1**).

VSMCs play a critical role in the severity and progression of vascular disease. VSMCs express many different endothelial-derived growth factor surface receptors, including receptors for PDGF, FGF, and stromal cell derived fator-1, which are all upregulated during vascular injury by activated ECs (**Section 1.2.1.1**) causing increased migration into the intima. The increased

quantity of VSMCs within the intima causes vessel wall thickening and lumen narrowing, further propagating the inflammatory environment. Over time, the combined VSMC increase, macrophage infiltration, and LDL accumulation (**Section 1.2.1.1**) within the intimal space leads to formations of dead cells and lipid pockets that harden into plaque. Further VSMC and macrophage apoptosis triggered by the inflammatory environment can cause the release of matrix vesicles into the lipid pockets, causing plaque calcification and hardening[64].

While the plastic nature of VSMCs allows for vessel repair and formation, the prolonged activation of cells can be detrimental over time. In the context of vascular grafts, VSMC migration into the scaffold is required for vascular remodeling.

1.2.2.2 Smooth Muscle Cells and TEVGs

After TEVG implantation, host VSMCs must migrate into or otherwise become present in the scaffold pores and proliferate, which requires a synthetic phenotype[55]. In most cases, this VSMC activation occurs due to injury at each end of the implant, and no additional stimuli are required. Once within the scaffold, the cells are also responsible for new ECM deposition (with the aid of recruited fibroblasts) as the scaffold degrades[52,55]. This early vascular remodeling heavily relies upon the infiltration and propagation of VSMCs to form the bulk of newly formed tissue (neotissue). Once the graft has been repopulated, and new ECM deposited, the engrafted cells must then re-differentiate towards a contractile state[56].

Completely remodeled TEVGs should consist of mostly contractile type VSMCs similar to elastic arteries. The re-differentiation of VSMCs back into a contractile state is currently a limiting factor in many TEVG designs[65,66]. Failure of VSMC differentiation back into a contractile phenotype oftentimes results in graft stenosis and occlusion[55,67]. Ideally, VSMC re-differentiation occurs naturally as the graft remodels due to reduced inflammation, alignment of cells in response

to shear, and ECM maturation (vs. scaffold degradation)[55,56,68]. Although simply stated, this environmental change requires TEVG design considerations, including scaffold degradation rate (**Section 1.3.1.4**), porosity (**Section 1.3.1.2**), and material type (**Section 1.3.1.1**) that each alter the VSMC behavior.

Overall, VSMCs are a major contributor to TEVG remodeling and overall success. Their unique plasticity can lend to successful remodeling as well as graft failure depending on the design. In our attempts to develop an effective TEVG, we have established the presence of VSMCs as a key indicator of graft success.

1.2.3 Extracellular Matrix Components

The two main ECM components in arteries are elastin and collagen. Elastin is the most prominent ECM component within the artery wall and is produced by VSMCs in the tunica media. It provides the vessel with the ability to recoil after distention from the high systolic pressures of pulsatile flow[4,51,69]. As elastin plays a key role in arterial response to pressure, the amount found in the vascular wall depends on the distance from the heart (as previously mentioned, as arteries branch pressure decreases, **Section 1.1.1**)[4]. In addition to the tunica media, elastin is also found in a layer called the internal elastic lamina lying between the intima and the media. Similarly, an external elastic lamina is present between the media and adventitia in larger, elastic arteries but not within muscular arteries[51,69,70]. Within the vessel wall, elastic fibers are organized into distinct fenestrated sheets called lamellae circumferentially aligned around the artery[4,51,69]. Smaller elastic fibers interconnect the lamellae and collagen to form an interwoven elastic structure[4,51,69], which anchors VSMCs forming a network of structural support.

While elastin is responsible for the recoil of the vessel wall in response to pressure, collagen is the load-bearing element[4,70,71]. The role of collagen is to provide mechanical strength within an acceptable range. An excess of collagen will cause a stiff matrix inducing VSMC differentiation towards a synthetic phenotype and reduce the vessels' ability to flex with high pressures and increase the risk of cardiovascular disease[67,69,72]. In reverse, an artery with too little collagen is likely to dilate without the mechanical strength to withstand blood pressure. There are 28 known types of collagen occurring throughout the body; however, types I, III, and IV are the most prominent within the arterial wall[71,73]. Each type of collagen is a triple helix woven fiber with varying signaling functions and patterns[71]. Within the tunica media (and adventitia), collagen types I and III fibers are incorporated into the elastin and VSMC structure, which combined provide recoil (elastin), contractility (VSMCs), and strength (collagen).

1.2.3.1 Extracellular Matrix Dysfunction

Healthy vascular ECM supplies a dynamic network of mechanical and environmental cues dictating vascular cell function. Deviations in ECM properties such as stiffness and abundance can detrimentally affect CAD. For example, a component of atherosclerosis is vascular fibrosis characterized by an excess of ECM within the vascular wall[74]. As discussed, arterial wall thickening occurs primarily due to VSMC migration and proliferation within the intimal space where they begin to secrete ECM components, mainly collagen, in their activated state (**Section 1.2.2.1**). Since little to no elastin is produced beyond adolescence, the gradual increase in collagen from constant remodeling over a lifetime results in a slow stiffening of the arterial wall[74]. This stiffening is amplified in many cases of vascular diseases, such as atherosclerosis, due to the highly inflammatory environment. Many studies have also shown that collagen can induce vascular cell activation, intensifying the progression of hyperplasia[74].

1.2.3.2 Extracellular Matrix and TEVGs

Elastin formation in vivo occurs almost exclusively within embryonic development and early infancy lasting for the duration of an individual's life[75,76]. While many studies have attempted to stimulate in vitro elastin formation, the complex, highly organized elastic networks are exceedingly difficult to reproduce[75]. Elastin itself has a half-life of about 74 years[77] and is highly stable, yet many genetic disorders exist associated with abnormal elastin production, including Williams-Beuren Syndrome. Additionally, elastin degradation is related to factors including age[78], lifestyle (smoking)[79], and disease (Marfan Syndrome)[80]. Since elastin production in adults is negligible, stimulating elastin production with vascular grafts presents a unique challenge. In response, various labs have attempted to incorporate elastin artificially within TEVG models with some success[14,81-83]. Elastin production within a construct in vivo has been attempted through the delivery of regulatory factors, including TGF-β[84,85], altering mechanical properties[11], and other in vivo modulatory factors[86,87]. Additionally, the elastic recoil properties of elastin within the arterial wall have been mimicked through the scaffold material itself however scaffold degradation over time makes this an infeasible long term option[88,89].

In comparison to elastin, VSMCs, and ECs, collagen is readily available and easily produced by cells in vivo[90,91]. While collagen remains an important component of the arterial wall, it is not a limiting factor when designing a vascular graft. Overall, the presence of both elastin and collagen within a remodeled TEVG is a good indicator of success. To mimic an artery, a remodeled graft must possess the ability to both recoil and withstand pressure as would a native vessel.

Overall, ECM plays a role in healthy vascular function as well as the progression of vascular disease. The design of a TEVG will ideally mimic the elasticity and strength of a native vessel to not only maintain flow but also prevent chronic vascular cell activation.

1.2.4 Current CAD Treatments

There are two main treatment options for CAD, percutaneous coronary intervention (PCI), also known as "stenting"[92], and bypass. Approximately 480,000 PCI procedures (formally called angioplasty) are performed annually in the US[93]. During PCI, a mesh tube known as a stent is inserted at the blockage site to expand and hold open the lumen of the vessel. There are many types of clinically available coronary stents including bare metal, drug-eluting, and resorbable, often deployed through a catheter and expanded using a balloon[94]. PCI offers a less invasive option in comparison to graft revascularization but is associated with a high occurrence of restenosis (lumen re-narrowing after treatment). In most cases, restenosis is triggered by VSMC dysfunction in response to the stiff metal implant. Newer drug-eluting stent options include antiproliferative and antimitotic drugs to mitigate excessive neointimal proliferation, but the restenosis rate remains about 10%[66]. Overall, PCI is a quicker, less invasive option but is associated with risks including an increased chance of blood clot formation within the stent, excessive bleeding at the catheter insertion site, heart attack during the procedure, kidney damage from the dye used during implantation, stroke due to plaque loosening during catheterization, and coronary artery damage during balloon deployment[66].

The second most common treatment is a bypass procedure (371,000 annual procedures in the US[93]) implanting a graft to reroute blood flow around the blockage to resume circulation[53]. Coronary artery bypass grafting (CABG) is usually recommended over PCI in cases of blockage in any of the major coronary arteries (right coronary, left main coronary, and left anterior descending) and previous PCI failure[95]. While PCI is less invasive and quicker, bypass grafts have been shown to have better long term results with lower occurrences of re occlusion[96]. Current

arterial revascularization surgeries utilize two types of grafts: synthetic scaffolds or autografts isolated from the patient, both of which are accompanied by complications.

Synthetic grafts currently used in clinical applications include polyethylene terephthalate (PETE manufactured by Dacron©) and polytetrafluoroethylene (ePTFE manufactured by Gore©)[97]. Completely synthetic grafts have many advantages including high reproducibility, ease of manufacturing, and "off the shelf" availability. These options are only suitable in larger diameter arteries (>6mm in diameter) due to the larger luminal space reducing the risk of thrombotic failure. In comparison, synthetic grafts in small diameter applications result in high failure rates due to actue thrombosis[98]. An ideal graft should be similar to an artery in strength (collagen), elasticity (elastin), non-thrombogenicity (endothelium), and viscoelasticity (SMCs). Synthetic options offer suitable strength and elasticity but lack the biocompatibility of cell-based options. After implant of a synthetic graft, coagulation factors and adhesive proteins, such as fibrin, are bound to the graft surface due to hydrophobic interaction between the material and blood as well the phenomenon of protein adsorption known as the Vroman effect[99,100]. These surface-bound molecules initiate platelet aggregation and fibrin aggregation resulting in thrombus formation[99]. At larger diameters, the high flow rates and larger lumen prevent synthetic graft occlusion due to this protein adsorption; however, small diameter grafts (<6mm) quickly clot and are therefore an unsuitable graft option. Another limiting factor of synthetic grafts is their inability to grow with the patient, particularly in pediatric applications. While tissue-based grafts can remodel and grow, synthetic conduits must be replaced once the patient outgrows the graft requiring another surgery.

The second graft option, an autograft, is the current clinical gold standard. Autografts are isolated from the patient and commonly include the internal mammary artery/internal thoracic artery (ITA)[101,102], radial artery[103], and saphenous vein[103-105]. The ITA and saphenous vein are the

most commonly used graft types[95,106]. The ITA results in promising long term patency[107], although there are limited long term studies as the use of ITAs only became more popular in recent years. There are two ITAs delivering blood to the chest and breast tissue running along each side of the sternum. In bypass surgeries using the ITA, one end is isolated and sutured below the arterial blockage[101] to reroute the flow of blood. Despite promising results utilizing ITA autografts, ITA failure is more common in patients with multiple revascularizations, intermediate left anterior descending artery stenosis, and multiple blockages[108]. Additional limitations include blockage location, number (if more than two blockages occur), and ITA unsuitability due to poor quality in already disease patients (i.e., diabetes, obesity)[108].

The other gold standard autograft is the saphenous vein graft (SVG) isolated from the upper leg. SVGs are a popular choice for bypass conduits due to their length and accessibility; however, long term results using SVGs show failure rates exceeding 50% after ten years[109] due to intimal hyperplasia and atherosclerosis. Due to the compliance and strength difference between veins and arteries, the much weaker vein graft (**Section 1.1.1**) dilates due to high pressures triggering VSMCs activation and hyperplasia. Over time, this progresses into atherosclerosis and the high long term failure rates associated with SVG[105,109]. Overall, SVGs remain a popular graft option due to the available length as a single SVG is sufficient for multiple bypasses[103]. Various methods are currently employed to strengthen SVGs eliminating graft dilation, including coating the graft in a polymer sheath[110].

Another less commonly used autograft option is the radial artery (RA) which is the major artery within the forearm. Previously, the RA has been associated with high occlusion rates but has become more popular with the advancement in surgical methods and drug treatment[103]. The main complication associated with RA grafts is an arterial spasm or spontaneous contraction of

the VSMCs, preventing flow[103], which is treated using calcium channel blockers. Although there is a resurgence of RA use in bypass procedures, limitations include plaque already existing within the artery and RA hypersensitivity to trauma (due to its muscular nature), resulting in a higher rate of atherosclerosis formation[103,111]. Additionally, harvesting the RA may cause nerve damage and altered sensation of the arm and hand in approximately one-third of patients[112].

As outlined, the low long term patency rates and high risk of thrombosis associated with current clinical options indicate a need for a more suitable graft option. The low biocompatibility and inability of polymer grafts to grow in pediatric cases make them less than ideal options in many cases. The increased risk of thrombosis previously described eliminates them as a small diameter conduit option completely. The high failure rates, complications, and need for secondary surgical sites for graft isolation also render autografts an unappealing option. One additional concern regarding patient-derived grafts is the potential for coexisting morbidities. The patient cohort requiring a bypass graft due to an arterial blockage may likely have atherosclerosis and stenosis within their ITA, RA, and SVG as well. The rising number of patients affected by CVD and the potential of a more suitable graft option has fueled the field of tissue engineering towards the development of a tissue-engineered vascular graft.

1.3 Tissue Engineered Vascular Grafts

Researchers in the field of biomedical engineering have been investigating the production of an ideal tissue-engineered vascular conduit for over thirty years[113]. As was discussed in **Section 1.1.1**, arteries are complex and extremely difficult to replicate. There are also design requirements for TEVGs that depend on their intended application. One potential application mentioned in

Section 1.2 is to provide a connection between the artery and vein known as an AV fistula. This surgical connection facilitates hemodialysis and faces many different barriers to translation than a coronary artery bypass graft (ability to withstand continuous puncture, different pressures, etc.)[98,114]. Another type of TEVG focuses on large diameter applications in pediatric patients to allow for vessel growth over the patient's lifetime[9,10]. Since the different types of vascular grafts have unique sets of requirements, this dissertation will focus on the development of a small diameter (<6mm) TEVG for application in cardiac bypass surgeries. Small diameter TEVGs (simply called TEVGs throughout the remainder of the dissertation) must provide a biomimetic channel to reroute blood flow around an arterial blockage. This section will focus on the progression of development of small-diameter arterial TEVGs and the current state of the field.

1.3.1 Scaffold Material Requirements

Various material types have been tested for use in TEVGs over the years, generally chosen for their mechanical strength, tunability, and durability. Polymer-based grafts alone offer many advantages, including that they are easy to manufacture, shelf-stable, and reproducible; however, the lack of biocompatibility mentioned in **Section 1.2.4** and an increased risk of clotting are the limiting factor of these grafts. Many labs, including ours[17,18,20,115], have attempted to combine synthetic but biodegradable scaffolds with biologic components, such as stem cells, to increase graft patency and acceptance with a high level of success[12,116,117]. Synthetic scaffolds augmented with various anti-thrombogenic coatings have also seen success in research studies[114,118-122]. Other studies have focused on scaffolds fabricated from naturally derived materials, including elastin[11,123], collagen[123,124], silk fibroin[15,125-127], and decellularized ECM[13,14]. These natural material options offer higher biocompatibility in comparison to synthetic materials but lack the

durability and ease of fabrication associated with polymer-based grafts. Overall, material type is an important factor in the resulting graft and affects four major TEVG qualities: biocompatibility, porosity, mechanical strength (compliance), and degradation.

1.3.1.1 Material Options and Biocompatibility

Biocompatibility refers to the level of compatibility between the graft material and host tissues. A successful graft must allow for positive interactions between the surrounding host cells and material surface, i.e., cells must migrate in and bind to the artificial scaffolding. All implanted devices, ranging from prosthetics to bone grafts, must consider biocompatibility when choosing a material type; however, TEVGs present a unique challenge in this regard due to their direct contact with blood. The biocompatibility of TEVGs must also account for platelet aggregation and VSMC activation, as discussed in **Sections 1.2.4** and **1.2.2.1**. Immediately after implantation, the prevention of acute thrombosis in response to material type is critical in overall graft success. In the field of vascular tissue engineering, biocompatibility falls on a scale of compatibility ranging from low, eliciting a higher immune response, to high, showing very little rejection. Generally speaking, synthetic materials fall on the low end of the scale and natural materials towards the higher end.

While most entirely synthetic TEVGs are not suitable, many labs have attempted to increase graft acceptance and biocompatibility by adding biologic elements (e.g. cells[18,20,116], coatings[128-131], etc.). Such approaches leverage the strength, tunability, and reproducibility of synthetic based grafts that are often difficult to achieve using entirely natural options. One main group of synthetic materials used is biodegradable polymers including poly(lactic-co-glycolic acid) (PLGA)[132,133], polyglycolic acid (PGA)[134,135], poly-lactic acid (PLA)[136,137], poly-l-lactic acid (PLLA, an isomer of PLA)[136,138,139], polycaprolactone (PCL)[137,140], polyurethanes (PU)[17,18,20,141],

poly(glycerol-sebacate) (PGS)[142-144] and numerous combinations therein. These polymers display varying degrees of biocompatibility and are often supplemented with a biologic component in response (**Section 1.3.2**). Similarly, these grafts have shown promising results when combined with biologic elements such as cells[18,20,86]. Overall, synthetic materials augmented with biologic components to increase biocompatibility and cellular infiltration offer a promising TEVG option (**Section 1.3.2**).

Naturally sourced materials (elastin, collagen, and silk) have the added advantage of natural binding sites to promote cellular infiltration[145] as well as less toxic degradation byproducts making them an appealing option compared to synthetic materials. Additionally, many natural scaffold designs utilize ECM components which are already present within the body. For example, elastin is naturally occurring within arteries (**Section 1.1.3.2**) and plays a role in VSMC regulation, prevention of thrombosis, and modulation of inflammation[75], which makes it an excellent scaffold material. However, entirely elastin-based scaffolds are expensive to fabricate and lack the mechanical strength necessary for an arterial conduit. Collagen is also present within the arterial wall and can provide the mechanical strength necessary to withstand blood pressure but can also bind von Willebrand Factor (vWF), a blood glycoprotein, and other blood coagulation proteins increasing the risk of thrombosis[146]. Silk based vascular grafts have been explored by many labs[15,16,127,147,148] and remains a promising material option. Silk fibroin isolated from silkworm cocoons or glands offers a natural material option that is both biocompatible and tunable. Previous studies of silk at the blood interface showed no signs of platelet activation[126,149] (i.e., anti-thrombogenic), the mechanical strength to withstand blood pressure[16], and the promotion of cellular infiltration[16,148]. Overall, silk for use in TEVGs is a relatively new area of study but shows great potential.

Another popular natural scaffold type is decellularized ECM. Decellularized ECM scaffolds are fabricated from allogenic or xenogeneic tissues, with the cells removed via decellularization. These scaffold types have the added advantage of a preexisting ECM structure that is very difficult to replicate artificially. Decellularized veins[150] and arteries as TEVGs have a readily made ECM network for cellular infiltration and appropriate mechanical properties[151], yet allogenic sourcing remains an issue. Other human decellularized ECM options include any tubular structure of compatible size, including umbilical arteries[152,153] and small intestine submucosa[154], but these options are still limited in availability. Most studies using decellularized ECM are xenogeneic grafts[151], which addresses the limited availability of human tissues[155]. Another popular approach to ECM based scaffolds is cell-derived ECM[13,156,157]. Notably, this method has been explored by Dr. Robert Tranquillo's lab by culturing VSMC or fibroblasts in a tubular fibrin gel to allow for ECM deposition followed by decellularization[13,158]. Dr. Laura Niklason and colleagues at Humacyte have also explored cell-derived ECM in both benchtop and clinical trials of AV fistula with promising results [157,159]. Cell-derived ECM remains a promising option but may face barriers to clinical translation due to the time, cost, and cell culture required (**Section 1.3.2**).

Both synthetic and natural materials types have varying advantages and disadvantages. Research using all of the mentioned materials types has also explored scaffold augmentation with biologic components such as cells (**Section 1.3.2**), coatings (**Section 1.3.4**), and signaling effects (**Section 1.3.3**) to address many of the disadvantages.

1.3.1.2 Porosity

Another scaffold property affecting graft success is having sufficient porosity to encourage cellular migration. In healthy tissue, a network of ECM provides the scaffolding for cellular attachment and migration. Previous research has shown cells interact and function (including

migration, proliferation, signaling, phenotypic changes, etc.) in response to environmental cues, including porosity[160-162]. Pore size and interconnectivity must be tuned to allow for VSMC into the pores and EC migration along the lumen of the scaffold. A study implanting scaffolds with small (10-30μm ID), medium (30-90μm ID), and large (90+ μm ID) pore sizes showed maximal cellular infiltration in medium-sized pores. In contrast, a lower cell count and incomplete endothelium were observed in the smaller and larger pores[163].

Various methods of fabrication can alter the graft porosity, including salt leaching[164], phase separation[88], and electrospinning[88,165]. Increased porosity is most often accompanied by decreased graft strength resulting in graft dilation under physiologic pressure. Many TEVGs utilize a bilayered approach combining a porous inner layer encouraging cellular migration with a denser outer layer adding the necessary mechanical stability. Our lab has worked with two different bilayered graft types, PEUU[17,88], and silk-based[127], both combining an inner porous layer with an outer electrospun layer producing a biomimetic scaffolding.

1.3.1.3 Compliance, Elasticity, and Burst Pressure

Given that an artery is a mechanically functional organ, the mechanical properties of a replacement must be considered carefully. In the field of vascular biomechanics, compliance describes the ability of a vessel to distend and increase luminal volume in response to increased pressure. For example, veins have high compliance (high volume increase) at low pressures, but low compliance (comparatively lower volume increase) at high pressures), which is one of the critical factors for SVG failures in arterial bypass applications[105]. In the case of vein grafts, a highly compliant vein replacing a lower compliance artery results in dilation of the vein[166]. This dilation activates VSMCs to migrate and proliferate inducing intimal hyperplasia and eventually graft occlusion[105,166]. Compliance mismatch also causes disturbance in flow through the graft,

increasing the risk of thrombosis, particularly in a low flow application[105]. Ideally, compliance should match that of the native artery (4.5-6.2% $mmHg^{-1}$ x 10^{-2} in human arteries[167]).

The elasticity of the graft must also reflect the host artery. In a healthy vessel, elastin allows the vessel to recoil under pulsatile flow (**Section 1.2.3**). In TEVGs, the elastic property can be provided by the material itself. A scaffold without elasticity will be unable to recoil after deformation resulting, in time, in graft dilation and potential rupture. Arterial stiffening occurs naturally with age as elastin fibers degrade, and stiffer collagen fibers remain. This stiffening activates VSMC migration and proliferation, eventually leading to atherosclerosis[168]. A similar phenomenon occurs in stiff scaffolds resulting in high rates of graft failure. Arterial wall stiffness is measured using the β stiffness index and can similarly be applied to scaffolds. Various studies have used both the saphenous vein (β-stiffness = 16.9±7.1) or, more ideally, the arterial wall (femoral β-stiffness = 23.7±0.8)[169] as the gold standard to match.

The third measure of TEVG mechanical properties is burst strength. An implanted scaffold must be strong enough to withstand pulsatile flow and blood pressure in vivo. Burst strength is most commonly compared to the saphenous vein (~1680 mmHg)[98,170] as the clinical gold standard. Unlike compliance and stiffness, many grafts both over[167,171,172]- and under[173-175]-match this value with successful results with different modes of remodeling indicating it may not be as important to match; however, burst pressure is a required ISO measurement towards clinical translation.

1.3.1.4 Degradation

Lastly, the graft material for small diameter arterial bypass or replacement should be biodegradable. The end goal of any TEVG is to provide a temporary scaffolding to promote vascular tissue formation in its place, requiring a degradable material. The rate of degradation should match the rate of new tissue formation, which varies in response to different material types.

Numerous studies have designed quickly degrading grafts designed to promote rapid cellular infiltration and quick scaffold degradation in hopes of reducing a prolonged inflammatory response[138,164,176]. Notably, fast degrading scaffolds have been intensively studied by groups, including Shinoka[11,138], Breuer[11,138], and Wang[177,178] as potential TEVG options. Promising results have been observed in rat[178] and mouse[138] models, but scaling this technology into a human-sized graft remains the current challenge. In comparison, slow degrading materials such as PCL (exceeding 24 months)[179] are more suitable for slow tissue healing. In scaffolds types with slower observed cellular infiltration rates, a longer degradation time may be beneficial to provide mechanical support during neotissue formation. Another concern is the toxicity of scaffold degradation byproducts. Natural materials are more favorable in this sense as their degradation byproducts can be quickly metabolized and excreted. Synthetic materials, while biocompatible, are associated with prolonged inflammatory responses to lingering material[180]. Overall, the tunability of scaffold degradation rates is an important consideration in TEVG design. There is a delicate balance in timing between cellularization/new tissue formation and scaffold degradation, which must be reached and differs with each TEVG type.

1.3.2 Cells in TEVG Applications

The incorporation of cells within scaffolds has evolved over the history of vascular graft research. The addition of cells to both synthetic and natural scaffolds helps overcome many of the biocompatibility limitations outlined. In terms of cell type, a large variety of cells have been studied in TEVGs (**Section 1.3.2.1**), but all meet a few base requirements: (1) non-immunogenic, (2) easily obtained, and (3) able to perform their intended function (e.g., EC must be able to adhere and proliferate within the scaffold)[98,181]. Some studies[116], including those in our lab[18,182], focused

on autologous cell sourcing to minimize the risk of rejection and disease transfer, as observed with xenogeneic cells[98]. More recent studies have studied allogeneic cells as a potential cell source[183,184], but much is still unknown regarding immune response to these cells.

There are currently many different techniques to incorporate cells into scaffolds[181]. One common method is static cell seeding, where a cell suspension is applied directly to the scaffold surface and relies on gravity and cellular adhesion to penetrate the entire scaffold[114,185]. This method is appealing due to its simplicity but often results in uneven cellular distribution, long incubation times necessary for cellular attachment (up to 9 days), increased risk of contamination due to long culture times, and low overall cellular attachment (especially in synthetic scaffolds)[114,185,186]. Dynamic cell seeding addresses many of these issues by utilizing vacuum pressure[17] or centrifugal force[186] to increase cellularity and seeding homogeneity as well as decrease the time required. To date, vacuum cell seeding into porous scaffolds remains a popular option offering even cellular distribution within minutes[17,116] compared to weeks for cell culture methods; however, this method relies heavily on the scaffold material qualities (porosity, elasticity, and strength) to achieve ideal seeding[181]. Dynamic seeding methods also exist to pre-form an endothelium before implantation. Bioreactors mimicking physiologic flow and shear on luminal seeded ECs can induce EC proliferation and migration into a full endothelium in vitro[49] but are limited similar to static seeding in cell culture cost, time and potential for infection.

1.3.2.1 Cell Types and Considerations

Cells for use in TEVGs fall into two categories: vascular cells (particularly ECs) and stem cells. Many early and current studies utilizing cells focused on integrating vascular cells into the scaffold prior to implantation in attempts to implant a graft more closely mimicking the native artery[48,187]. Endothelial cells and endothelial progenitor cells (EPCs) can be isolated from bone

marrow and incorporated into an autologous graft. A pre-formed monolayer of mature ECs is a popular approach[48,140,188,189] to prevent thrombosis. Many of these studies observed positive results in graft patency with the inclusion of an endothelium[190,191] but required extensive bioreactor culture. Alternatively, other studies have used EPCs, which can differentiate into ECs, to lessen culture time and eliminate the need for bioreactor culture[114,192]. Mixed results have been observed using ECs and EPCs depending on the cell sourcing, seeding strategy, and scaffold material[188,193]. While the incorporation of endothelial cells has been a large area of study, smooth muscle cells are generally not pre-seeded due to the potential downfalls of inducing VSMC proliferation and intimal hyperplasia. Additionally, the inherent plasticity of VSMCs introduces the risk of phenotypic change in response to the mechanical stress of seeding.

An alternative cell type is mesenchymal stem cells (MSCs)[187]. MSCs are readily available in a number of tissues such as adipose[194,195], bone marrow[196], and umbilical vein blood[197], making them more convenient to harvest than primary vascular cells. MSCs are highly proliferative in vitro[198] and can easily reach volumes necessary for a human-sized graft. They are also immunomodulatory[198], can recruit ECs and VSMCs[115,198], and can differentiate into vascular cell types (ECs and VSMCs) making them an ideal TEVG cell source.

Another less commonly used cell type is induced pluripotent stem cells (iPSCs) genetically modified to resemble embryonic stem cells and then differentiated into vascular cells[199]. iPSCs offer an appealing alternative to EPCs and ECs in terms of availability but may face regulatory hurdles due to the extensive differentiation and cell culture required[199].

Each of these cell types has seen success in various TEVG designs but are all limited by regulations around cell culture. FDA regulations around the use of stem cells and stem cell culture is a clear barrier to stem cell-based TEVG translation[200,201]. As stem cells and cell-based

technology continues to progress, guidelines governing these technologies also continue to change. In general, the FDA strictly regulates ex vivo handling (i.e., culture expansion, exposure to culture media, etc.), making any technology using culture-expanded cells difficult to translate[200-202]. In order to limit cell manipulation and reduce the time between cell isolation and graft implantation, the Vorp lab has been working with the stromal vascular fraction (SVF) of cells directly isolated from patient adipose tissue[20]. Cell types within the SVF include fibroblasts, macrophages, preadipocytes, and MSCs[203]. SVF isolation takes ~4 hours and potentially eliminates the need for culture expansion if enough adipose tissue is available. This elimination of culture provides a more translatable technology; however, it is a relatively new cell source as applied to TEVGs and requires additional investigation before its potential is fully known. Similarly, bone marrow mononuclear cells (BM MNCs) refer to the cellular isolate from bone marrow before purification into MSCs. This particular cell population includes EPCs, ECs, MSCs, immune cells, and MSCs[114] and has been used in place of MSC with success[116].

1.3.2.2 Role of Stem Cells within TEVGs

As the field of tissue-engineered vascular grafts continues to grow and change, so has the rationale behind the use of stem cells within grafts. Many early studies incorporated MSCs into different TEVG types hypothesizing MSC differentiation into vascular cells[12,17]. Implanting a pre-seeded scaffold was intended to increase graft acceptance by providing already engrafted cells able to differentiate into appropriate vascular phenotypes rather than rely on recellularization from surrounding tissue and circulating cells. As more studies focused on the mechanisms behind scaffold remodeling, it was discovered that initially implanted cells are not present within the remodeled graft disproving this hypothesis[65,116,127,204]. Rather, the cells play a signaling role within the scaffold. Stem cells are able to communicate with surrounding cells through the secretion of

signaling molecules, vesicles (**Section 1.3.3.2**) and cell surface interactions[114,205]. To summarize the scope of cells within grafts, this section will use the term stem cells to refer to MSCs, BM MNCs, and SVF as they all play similar signaling roles within TEVGs. Stem cells influence graft acceptance and remodeling in three main ways: (1) anti-thrombogenicity, (2) immunoregulation, and (3) promotion of remodeling.

The first role of the stem cells is to prevent thrombus formation. Studies from our lab[18,86], as well as others[116,206,207], have shown improved acute patency immediately after implant in scaffolds with stem cells vs. unseeded scaffolds. This improved patency is observed within the first days post-implantation, indicating an immediate thrombogenic regulatory role of the stem cells. While the exact mechanisms behind this anti-thrombogenic effect are unknown, some ideas can be drawn based on the current understanding of stem cells. Thrombosis occurs in two main ways: protein adsorption due to blood and material interactions (intrinsic) or the release of tissue factor (TF) from injured cells (extrinsic)[100]. Vascular injury due to graft implantation extrinsically activates clotting, but this may be counteracted through stem cell secretions. Stem cells secrete urokinase-type plasminogen activator (uPA), which plays a role in plasmin formation and thereby fibrin (clot) degradation[19]. Alternatively, stem cells may function to lessen protein adsorption to the graft surface. As discussed in **Section 1.2.4**, synthetic materials naturally bind blood serum proteins (the Vroman effect[100]), including albumin and fibrinogen, which then bind platelets[205]. Pre-seeding scaffolds, particularly along the lumen, may decrease this effect. While the mechanism behind stem cell regulation of thrombosis (or perhaps, a combination of multiple mechanisms) is unknown, various studies have observed a reduction in platelet adhesion through the delivery of stem cells[19,86,116].

Stem cells also play an immunoregulatory role in inflammatory cell recruitment and polarization. The entire secretome is still an area of study, but more recent studies have focused on inflammatory mediated graft remodeling, particularly through macrophage interaction[138,178,204,208]. A focus of Dr. Breuer and Dr. Shinoka's[65] TEVG work is the increased secretion of CCL2 from seeded cells to promote graft remodeling (**Figure 4**[204]). They hypothesized that stem cells attract macrophages through the secretion of chemokine (C-C motif) ligand 2 (CCL2, also known as monocyte chemotactic protein-1 or MCP-1). These engrafted macrophages then take over the remodeling process. Additionally, secretions have been shown to mediate macrophage polarization from a pro-inflammatory (M1) state towards an anti-inflammatory/immune-regulatory (M2) state[209].

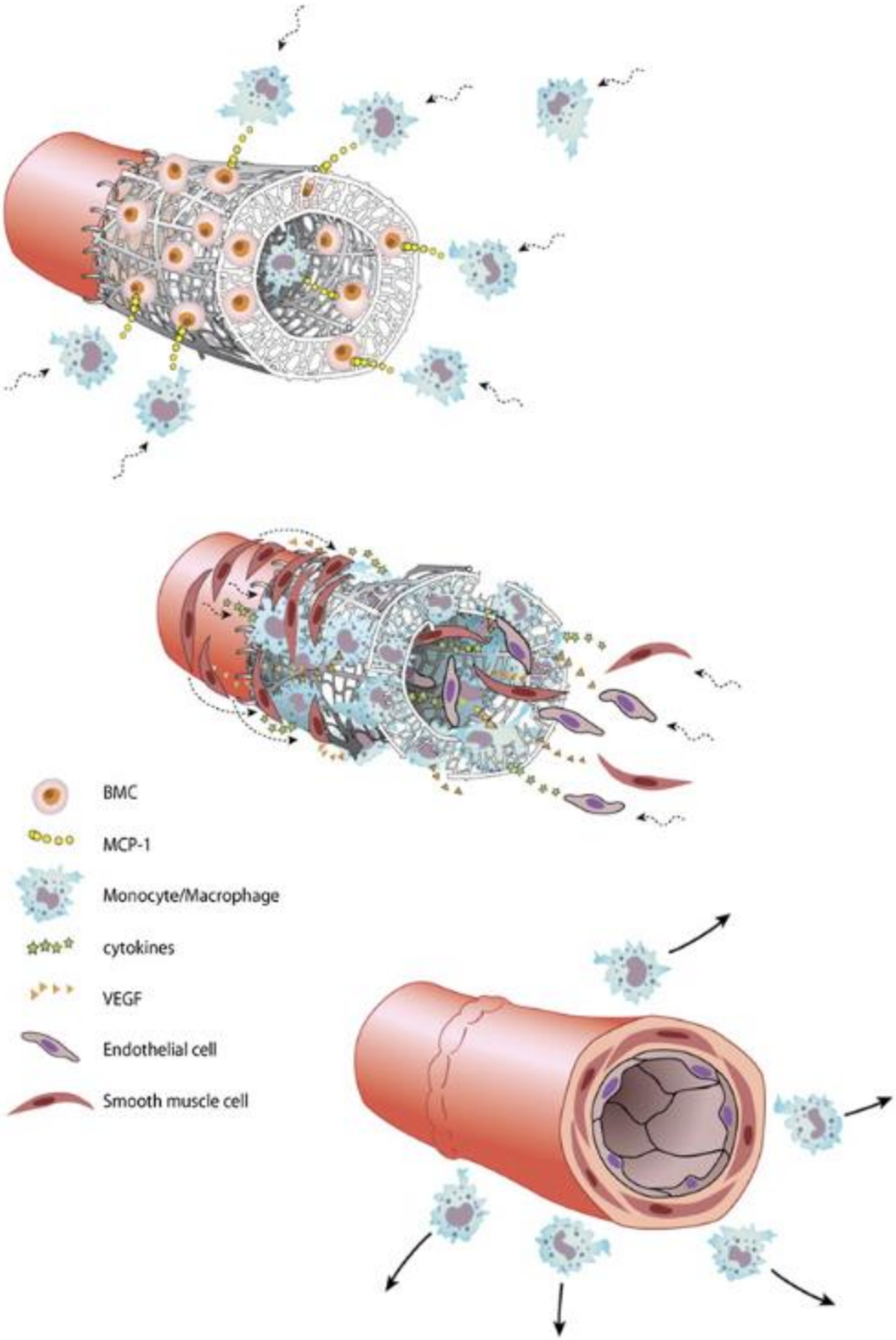

Figure 4. Proposed methods of graft remodeling via host inflammatory response

This proposed mechanism of TEVG remodeling was proposed by Dr. Breuer and Dr. Shinoka[204].

Lastly, the stem cell secretome (**Section 1.3.3**) contains potent pro-remodeling (by way of inducing cell migration) signals[115]. One mode of potential graft remodeling is the recruitment of surrounding vascular cells, which then take over remodeling (i.e., endothelium formation by ECs and ECM deposition/contractile SMCs layer formation by VSMCs). Engrafted cells may provide localized signaling to surrounding host cells to migrate towards and into the scaffold, specifically for EC migration and proliferation[210]. As mentioned, VSMC dysfunction caused by injury or chronic inflammation is a potential mode of graft failure through intimal hyperplasia. A major role of stem cells is to regulate VSMC phenotype and inhibit VSMC proliferation[211]. Much is left to be discovered regarding the role of stem cells in TEVGs and their signaling effects.

1.3.3 Cytokine Signaling in TEVGs

The term cytokine signaling encompasses all cell-secreted proteins and vesicles, which is beyond the scope of this dissertation. This section will focus specifically on three aspects of signaling relevant to this project: (1) macrophage recruitment through MCP-1, (2) MSC secretome applied to vascular cells, and (3) extracellular vesicles.

1.3.3.1 Macrophages and CCL2

The idea of inflammatory mediated graft remodeling is currently being investigated in many labs but was introduced by Dr. Breuer and Dr. Shinoka[204]. In an early study focusing on stem cell immunoregulation in TEVGs, they discovered high levels of CCL2 secreted from seeded cells[204]. Further, increased local delivery of CCL2 encouraged early monocyte recruitment into the scaffolds to begin the wound healing process. The idea of graft remodeling can be thought of by analogy to wound healing and its stages (inflammation, tissue formation, and tissue remodeling).

In vascular injury, endothelial cells secrete CCL2, which attracts tissue-resident and circulating neutrophils and monocytes[46]. From there, tissue-specific signals cause monocyte differentiation into macrophages to begin tissue regeneration[212]. This macrophage population then undergoes polarization (phenotypic change in response to environmental cues) into either classically activated (M1) and alternatively activated (M2) macrophages. The full description of macrophage phenotypes is beyond the scope of this dissertation, but a basic understanding of the M1 and M2 exemplary phenotypes is important in understanding TEVG remodeling.

A pro-inflammatory environment polarizes macrophages towards an M1 type. The M1 macrophage population in healthy tissue remodeling is responsible for microbe phagocytosis and the production of additional pro-inflammatory cytokines to initiate the immune response. This stage of increased inflammation usually occurs within the first days after injury and is a necessary step in the tissue remodeling process; however, prolonged M1 expression can cause chronic inflammation and improper healing[213,214]. One particular macrophage population expresses chemokine receptor CCR2, which binds CCL2. These CCR2 macrophages are recruited immediately after injury and play an inflammatory role (M1)[212]. After the initial inflammatory response, the recruitment of macrophages changes from M1 towards an M2 phenotype associated with cellular migration, proliferation, and new ECM deposition. M2 type macrophage secretions promote host cell migration (VSMCs and ECs) into the injury site (i.e., the scaffold), and promote collagen production from surrounding cells[213,214].

1.3.3.2 Conditioned Media

As described in **Section 1.3.2.2**, cellular secretions from stem cells have many different effects on TEVG remodeling. Cells in culture secrete a unique combination of growth factors and vesicles containing proteins, surface markers, and mRNA into the media. MSCs, in particular, can

secrete a wide variety of signals affecting neighboring cell migration, proliferation, differentiation, chemoattraction, etc[215]. In vivo, these secretions vary in response to environmental cues to regulate cell function. As discussed in **Section 1.3.2.2**, stem cell secretions within TEVGs also have multiple roles whose exact mechanisms are unknown; however, several MSC cellular secretions (in addition to CCL2) are known to play a role specifically in vascular remodeling: VEGF[140,216], TGFβ[217,218], and uPA[19,219].

VEGF mostly affects endothelial cells, which play a regulatory role in vascular healing and TEVG remodeling (**Section 1.1.2.1**)[220]. VEGF is secreted by smooth muscle cells and macrophages (both M1 and M2)[221], during wound healing. As indicated by its name, VEGF's main role is to promote EC growth and proliferation and inhibit EC apoptosis[222]. Many different studies have functionalized scaffolds with VEGF to promote rapid endothelialization and observed improved patency and endothelium formation[140,216].

TGF-β is a growth factor that promotes VSMC and EC proliferation and migration[223], macrophage polarization towards an M2 phenotype[224], and ECM production by VSMCs[225]. In vivo, increased TGF-β secreted by VSMC and EC can have detrimental effects leading to intimal hyperplasia[217]. TEVG studies focusing on TGF-β have shown inhibition of TGF-β receptors improve graft patency and stenosis[217,218].

Lastly, uPA plays an anti-thrombogenic role within TEVGs (**Section 1.3.2.2**). The secretion of uPA from cells within the scaffold works to break down clots as they form. Our lab has shown decreased uPA production of seeded cells increases graft failure via acute thrombosis[19].

Conditioned media has the advantage of containing the entirety of the cell secretome - a feat impossible to achieve artificially. Delivery of conditioned media in place of engrafted cells has the potential to mimic the robust cell secretome without requiring the cells themselves, which

bypasses the many regulations around stem cell technologies (**Section 1.3.2**). However, this potential application faces limitations around cell culture and the inclusion of xenogeneic components within the media, including fetal bovine serum (FBS) and bovine serum albumin (BSA).

1.3.3.3 Extracellular Vesicles

Extracellular vesicles (EVs) are also contained with the conditioned media and are an important means of intercellular communication. EVs are lipid bilayer encased packages naturally secreted from cells. There are various types of EVs identified by size and contents that are secreted (**Figure 5**[226]). Microvesicles usually range from 100-1000nm in diameter and are loaded with growth factors and genetic information, though they cannot replicate like a cell. As shown in **Figure 5**, microvesicles bud from the lipid bilayer of cells and therefore contain surface proteins that can provide surface protein communication between cells[226]. Exosomes are smaller, 30-150 nm in size, and are produced when multivesicular bodies filled with intraluminal vesicles fuse with the cell membrane releasing into the intracellular space[226]. Lastly, apoptotic bodies are vesicles released from a dying cell and can attract immune cells for removal via phagocytosis[226]. All three types fall under the umbrella term "extracellular vesicle" and provide a more complex signaling effect than growth factors alone. Vesicles have an advantage over conditioned media since unnecessary culture media components (fetal bovine serum, fungizone, penicillin, streptomycin, and bovine serum albumin) are removed during EV isolation.

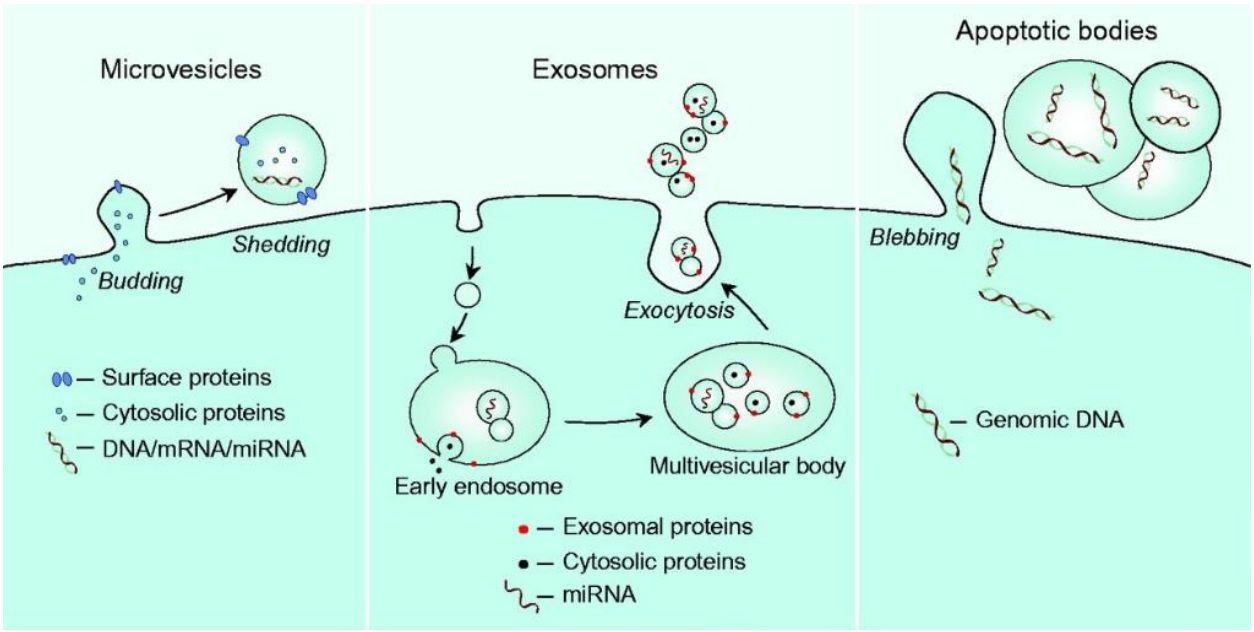

Figure 5. Formation and contents of cell-secreted bodies

1.3.4 Acellular Grafts

Despite all the positive effects of stem cells within TEVGs, they also provide the main limiting factor towards clinical translation. Some labs have attempted to design a more easily translatable[129,138,178], cell-free graft in response to the strict FDA regulations surround stem cells[200-202]. The main limitation of acellular grafts is the low biocompatibility of any material, synthetic or natural, at the blood interface. One popular approach to increasing graft patency and compatibility is to encourage host cell recruitment through the delivery of various peptides, growth factors, and antibodies. As mentioned in **Section 1.3.1.1**, many synthetic materials lack cellular binding sites slowing the rate of host cell infiltration. Various labs have coated synthetic materials with arginine-glycine-aspartate (RGD) peptides[128,129,227,228] to provide EC binding sites in attempts to stimulate early endothelium formation and thrombosis prevention. Various studies have combined other EC

binding peptides with RGD to enhance rapid endothelization, including YIGSR[229,230], mussel adhesive proteins[188], REDV[230], and cRRE[231]. This popular approach shows promising results in vivo to enhance EC cell recruitment[228,232,233], but effective RGD binding to the graft material remains a limiting factor.

Another approach to acellular grafts is the inclusion of anticoagulants such as heparin. A regiment of anticoagulants is generally prescribed following any revascularization surgery, but inclusion into the scaffold itself offers localized, sustained delivery at the site at risk of clotting[130,131,234]. Grafts have been coated in heparin through cross-linked collagen[234] and luminal surface modifications[130,235], yet a long term, controlled delivery at the blood interface has yet to be developed. Some studies combined multiple anticoagulants such as heparin, nitric oxide, or thrombomodulin to provide a more robust anti-clotting treatment[131,236,237]. This multi-factor delivery is similarly limited by failing to achieve a sustained, controlled release, which is further complicated with the delivery of multiple treatments.

1.3.5 Current In Vivo Studies

As is clear from the considerations and previous research explained above, there are many different approaches to TEVGs currently under investigation. Below, Table 1 summarizes a list of some relevant in vivo studies and their current status within the field.

Table 1. Summary of current in vivo TEVG research.

Scaffold material	Intended application	Current in vivo model	Cell source	Main findings	Group
Cell seeded grafts					
Polyester (urethane urea) (TIPS + ES)	Small diameter aortic graft	Rat abdominal aortic grafts	Xenogeneic SVF/MSCs	Seeded cells improved graft patency for up to 8 weeks.	Vorp and colleagues[17,19]
Silk fibroin	Small diameter aortic graft	Rat abdominal aortic grafts	Allogenic SVFs	Unseeded grafts displayed higher patency	Vorp and colleagues[127]
50:50 PLCL copolymer woven with PLA or PGA	Large diameter pediatric graft	Human clinical trials	Autologous BM MNCs	11 years after implant: no graft specific complications, 28% showed stenosis, complete scaffold degradation	Shinoka, Breuer, and colleagues[9]
PGA mesh with outer layer PLCL copolymer	Small diameter vein grafts	Mouse inferior vena cava interposition grafts	Autologous BM MNCs	BM MNCs reduced platelet adhesion to graft, increased MCP1 production, and graft patency	Shinoka, Breuer, and colleagues[116,204]
PGA/P4HB	Large diameter aortic graft	In vivo ovine model (pulmonary)	Human peripheral blood induced pluripotent stem cells	Grafts were patent at 2 years, complete scaffold degradation but an excessive amount of collagen was observed	Hoerstrup and colleagues[238]
In situ biotube formation around a nylon mold	AV fistula	Canine carotid to jugular graft	Allogenic implants	Tubes were up to 50cm long and remained patent after 3 months. The strength and burst pressure were about 60% compared to human carotid	Iwai and colleagues[239]

Table 1 (continued)

Scaffold material	Intended application	Current in vivo model	Cell source	Main findings	Group
PCL and type I collagen	Small diameter arterial graft	Ovine carotid arterial graft	Allogenic primary vascular cells	Grafts were preconditioned to form EC and SMC layers. Patency was achieved at 6 months in seeded vs. clotting in unseeded	Atala and colleagues[240]
ePTFE with a seeded endothelium	Femoral popliteal bypass	Human trials	Autologous EC monolayer	Improved patency was observed in grafts with an preseeded endothelium	Zilla and colleagues[241]
Acellular synthetic grafts					
Resobrbale PLCL reinforced with PLA nanofibers	Small diameter vein grafts	Mouse inferior vena cava grafts		Quick graft resorption to remodel tissue via inflammation	Shinoka, Breuer, and colleagues[11]
PGA+cadaver vascular cells in a bioreactor for 8 weeks then de-celled (ECM from vascular cells + PGA degradation)	AV fistula	Human clinical trials		Full recellularization of grafts. 1 year post: 28% patent, 38% primary patent, 89% secondary patent	Niklason and colleagues[7]
Allogenic fibroblast-derived ECM, decellularized	AV fistula	Human clinical trials		No degradation or dilation after 11 months and no chronic inflammation	L'Heureux and colleagues[242]
PGS and PCL	Small diameter aortic grafts	Rat abdominal aortic grafts		Positive remodeling observed at 90 days – neotissue formed.	Wang and colleagues[178]

Table 1 (continued)

Scaffold material	Intended application	Current in vivo model	Cell source	Main findings	Group
Knitted PGA lumen, PCL middle, and PLLA woven outer shell	Large diameter aortic graft	In vivo thoracic descending aortic graft		All grafts patent up to 1 year. Full endothelium and SMC layer present. Collagen and elastin present in graft.	Sawa and colleagues[243]
Polyester knitted mesh center with collagen lumen and outer shell	Small diameter aortic graft (specific for low flow settings)	Sheep carotid graft		92% patency after 14 weeks but mixed results: adherent thrombi, necrosis, and disintegration in some cases.	Linder and colleagues[244]
Neonatal human dermal fibroblasts in bovine fibrin and cultured for 5 weeks before de-cellularization	AV fistula	Axillary artery and brachial vein graft in baboons		60% primary patency after 6 months. Explanted grafts were re-cellularized, with no calcification or stenosis.	Tranquillo and colleagues[14]
Ovine dermal fibroblasts in fibrin gels with 2-week static culture and 5 weeks bioreactor culture then de-cellularization	Large diameter arterial graft	Ovine pulmonary arterial grafts		100% patency at 50 weeks. Complete remodeling with substantial elastin and collagen deposition. The graft grew with the sheep.	Tranquillo and colleagues[245]
SIS rolled and coated with heparin and VEGF	Small diameter arterial grafts	Ovine carotid arterial graft		Heparin only completely occluded but heparin + VEGF showed 92% patency over 3 months	Andreadis and colleagues[246]
Silk fibroin gel ES into tubes	Small diameter arterial grafts	Rat abdominal aortic grafts		Patent at 4 weeks with the presence of SCMs and ECs detected.	Kaplan and colleagues[149]

Table 1 (continued)

Scaffold material	Intended application	Current in vivo model	Cell source	Main findings	Group
Silk fibroin in a woven tube	Small diameter vascular graft	Rat abdominal aortic grafts		85% patency up to 1 year with neotissue formation and collagen deposition.	Sata and colleagues[126]
Silk fibroin at varying concentrations	Small diameter arterial graft	Rat abdominal aortic grafts		Grafts remained patent up to 3 months. A 2.5% silk coating showed the best results (lower stenosis, better cell infiltration)	Asakura and colleagues[247,248]
PCL and tropoelastin	Small diameter arterial graft	Mouse infrarenal abdominal aortic graft		Tropoelastin delivery significantly reduced intimal hyperplasia after 8 weeks. 100% graft patency was observed	Weiss and colleagues[82,249]

2.0 Chapter 2: C-C Motif Chemokine Ligand 2 Functionalized Silk Scaffolds

Many different approaches to tissue-engineered vascular grafts combine a base scaffold with a biologic component. This chapter focuses on a novel combination of silk-based scaffolds and CCL2 loaded microparticles (MPs) for use as a TEVG. This study was the result of a collaboration between Dr. David Vorp's Vascular Biomechanics Laboratory (VBL) at the University of Pittsburgh, Dr. Biman Mandal from the Indian Institute of Guwahati, Dr. Steven Little at the University of Pittsburgh, Dr. Morgan Fedorchak at the University of Pittsburgh, and Dr. Charles Sfeir from the University of Pittsburgh.

Previous work from the VBL combined polyester(urethane urea) (PEUU) scaffold with a variety of stem cell types producing promising results in rat models[17-20,250]. Collectively, these studies showed increased patency in cell-seeded constructs compared to unseeded scaffolds indicating a signaling role played by the engrafted cells (**Section 1.3.2.2**). Despite these promising results, the regulations governing stem cell use in implanted devices limit the translatability of cell-based constructs (**Section 1.3.2.1**). To circumvent this barrier, we have developed a cell-free immunoregulatory-based TEVG comprised of a silk scaffold functionalized with CCL2-loaded MPs fabricated in collaboration with Dr. Sfeir. By incorporating CCL2, we had hoped to encourage early host macrophage recruitment to the scaffold to begin the wound healing process (**Figure 4**).

Additionally, this study utilized silk-based scaffolds in collaboration with Dr. Mandal. As discussed in the introduction (**Section 1.3.1**), silk offers many potential advantages in tissue engineering due to its natural biocompatibility. There are many types of silk isolated from different kinds of silkworms and spiders that have been applied to tissue engineering[147,251,252]. Very broadly, the types of silkworm silk can be isolated into two classes based on the main diet of the silkworm:

mulberry and non-mulberry. The majority of studies applying silk-based scaffolds to the cardiovascular application have utilized mulberry silk, specifically *Bombyx mori* (BM) silk, due to its tunability (elasticity, mechanic strength, porosity) and ease of access; however, the study of non-mulberry silk is a relatively new area of study[253]. Dr. Mandal's laboratory is one of the leading labs exploring non-mulberry silk-based scaffolds for tissue engineering[147,251,254] with a specific focus on *Antheraea assama* (AA) silk. The novel research using AA silk has shown scaffold tunability and the ability to support vascular cell growth in vitro[251,255]. AA silk also contains a naturally occurring RGD peptide, which has been shown to prevent acute thrombosis in vivo[228], making it a promising material choice for a TEVG.

2.1 Methods

2.1.1 Silk Scaffold and MP Fabrication

Silk scaffolds were designed and fabricated in collaboration with Dr. Biman Mandal and a Ph.D. student visiting from Dr. Mandal's lab, Prerak Gupta. Silk fibroin (SF) was isolated and purified following a related, previously published protocol[147] and stored at 4°C in dehydrated pellets until use. Two aqueous SF solutions were made from (1) cocoons of BM silk in a 6% w/v solution and (2) glands of matured fifth instar larvae of AA in a 2% w/v solution. The two solutions were combined in a 1:1 ratio resulting in a 4% w/v custom silk blend and injected into custom tubular molds of rat aortic size (**Figure 6**). This custom blend was designed to leverage the biocompatibility and tunability of BM silk with the increased potential for cellular infiltration associated with AA silk[147].

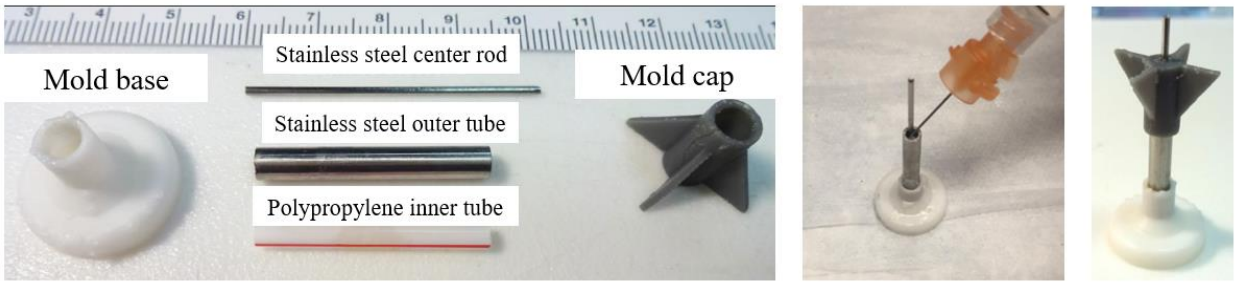

Figure 6. Silk scaffold fabrication mold.

The solution was then incubated at 37°C for 20 minutes to allow for hydrogel formation. After gelation, the mold cap and stainless steel center rod were removed to reveal the lumen of the scaffold. The scaffold was then frozen at -20°C overnight (12-18 hours) before lyophilization for 24 hours. After lyophilization, the scaffolds were removed from the mold and soaked in 80% ethanol to form a porous, tubular scaffold. This porous tube was then electrospun (ES) with a 1:1 mixture of 10% w/v polycaprolactone (PCL) (Sigma Aldrich) and 10% w/v BM silk in 1,1,1,3,3,3-Hexafluoro-2-propanol (HFIP, Sigma Aldrich). To ES, the mixture was ejected from a 5 mL syringe at 100 μL/min through a 23 gauge blunt tip needle placed 10 cm from the scaffold. The scaffold was mounted to a linear (50 mm/sec) and rotation motor (200 rpm) in a chemical hood at ~25°C. The resulting custom, bi-layered scaffold is called a “lyogel” scaffold.

CCL2 was loaded into PLGA microparticles following a previously published protcol[256,257] in collaboration with Dr. Sfeir. Water loaded PLGA MPs served as a negative control throughout this study fabricated in collaboration with Dr. Little and Dr. Fedorchak. Cargo was loaded using a water-oil-water double emulsion procedure resulting in loaded PLGA MPs containing CCL2 or water.

Scaffolds were functionalized with CCL2 loaded (or unloaded "blank") poly(lactic-co-glycolic acid) (PLGA) microparticles (5-15 μm in diameter) by incorporation into the silk solution. After the 4% w/v custom silk solution was fabricated, 3mg of MPs were incorporated into 1 mL of the SF mixture and blended to form a homogenous solution. The scaffolds were then assembled in the same way as described above. Three types of scaffolds were tested: (1) "lyogel" fabricated using just lyogel silk, (2) "Blank" fabricated using water loaded PLGA microparticles loaded into lyogel silk (negative control), and (3) "CCL2" fabricated using CCL2 loaded microparticles in lyogel silk. Even MP distribution throughout the length of mold was tested by incorporating fluorescein isothiocyanate (FITC) loaded MPs into scaffolds. Scaffolds were then divided longitudinally into five equally sized pieces and imaged using an upright fluorescent microscope (Eclipse 90i, Nikon) and imaging software (NIS Elements, Nikon). The resulting images were qualtitatively assesed for MP distribution.

2.1.2 Measuring CCL2 Release

The release of CCL2 from the MPs was assessed to ensure proper release after incorporation into silk scaffolds. Approximatly 0.5 cm long scaffolds of each type (lyogel, CCL2, and Blank, n=4 of each) were weighed prior to release. Each scaffold was then placed in 2.0 mL Eppendorf tubes filled with 1 mL of phosphate buffered solution (pH 7.4, PBS, Gibco), mounted in an end-over-end turner, and incubated at 37°C for 24 hours. Each day, the scaffolds were removed and placed in a new 1 mL PBS. The remaining releasate was centrifuged at 16,000 rpm to remove any silk or PLGA degradation. The resulting supernatant was isolated and stored at -20°C until use. Samples were then analyzed using a CCL2 ELISA kit (DY479, R&D Systems) and ancillary reagent kit 2 (DY008, R&D Systems) following the manufacturer's protocol. Absorbance

was measured using a plate reader (Synergy HT, BioTek Instruments) and normalized to the initial weight of each scaffold portion.

2.1.3 Scaffold Implantation

All animal protocols were approved by the Institutional Animal Care and Use Committee (IACUC, University of Pittsburgh, Pittsburgh, PA) to ensure the ethical treatment of each animal. Each MP-impregnated construct was implanted as an abdominal, infrarenal, interposition graft in a Lewis rat (**Figure 7**). Rats were anesthetized using 4% isoflurane (Butler Schein) and maintained using a mixture of 1% isoflurane and ketamine (50 mg/kg hydrated in lactated ringers electrolyte solution). Deep anesthesia was assessed through respiratory rate monitoring and a lack of deep pain response (pedal reflex). After anesthesia, the abdomen was shaved and prepared using a 7.5% povidone-iodine solution followed by a 70% ethanol wash. A midline incision was made along the prepared abdomen, and the aorta was then exposed. Using micro forceps, a 3 cm portion of the aorta between the renal branches and lower trifurcation was isolated, and micro clamps (Vascu-Statt II) were applied to stop blood flow through the isolated portion. The aorta was then severed in the middle of the clamped length resulting in a ~1cm gap due to elastic recoil. A 1cm scaffold was dipped in a 5% heparin solution (McKesson Medical-Surgical) and sutured as end-to-end anastomoses with 6-10 interrupted sutures per end (10-0 prolene, J496G, Ethicon). Once the graft was secured, the distal then proximal clamps were removed to restore blood flow. If leaking was detected, clamps were replaced for a maximum of 10 minutes, and additional sutures were applied, followed by a bolus of 5% heparin solution over the suture site to avoid stagnant blood clotting within the graft. The muscle and skin layers were closed separately using running 3-0 polyglactin resorbable sutures (J215H, Ethicon). Rats recovered on heating pads and were monitored for signs

of distress for 24 hours post-implantation. Post-operation, each rat received a subcutaneous injection of 0.05mg/kg buprenorphine every 12 house for 48 hours. Anticoagulants were administered orally for 4 weeks post-operation (dipyridamole – 250 mg/kg for the first 7 days, 100 mg/kg for the following 3 weeks; aspirin – 200 mg/kg for the first 7 days, 100 mg/kg for the following 3 weeks).

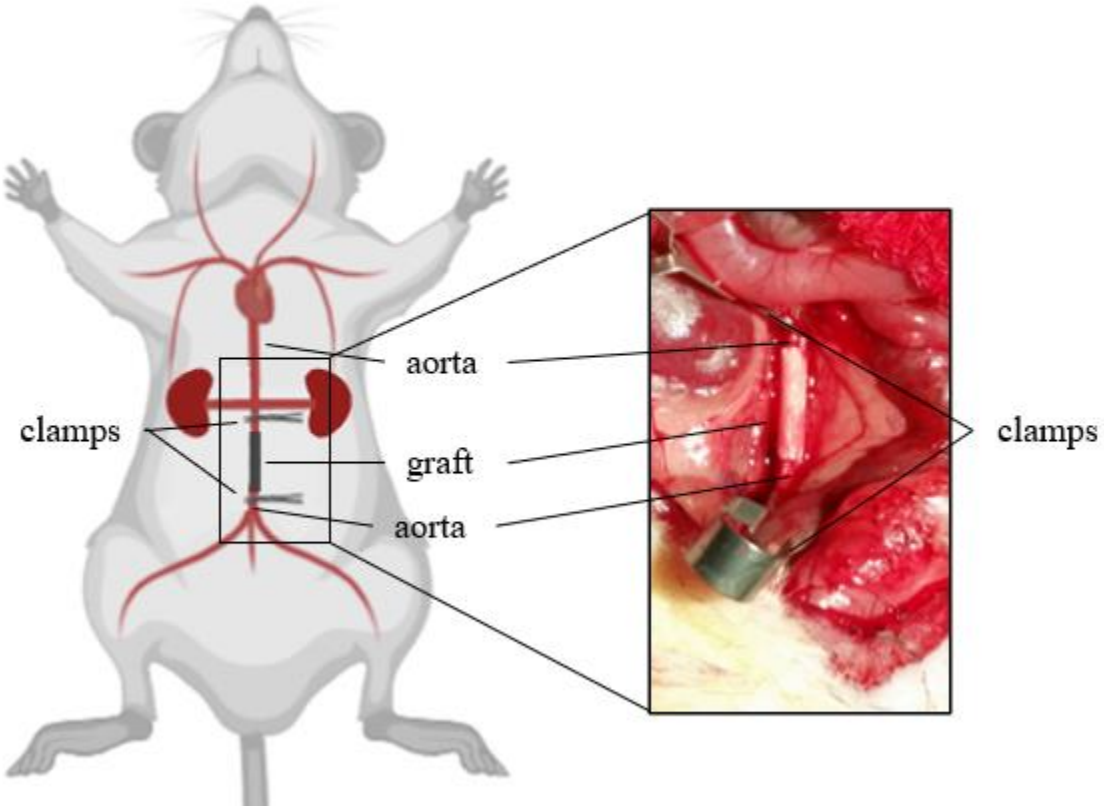

Figure 7. Diagram of TEVG implant in a rat model.

TEVGs were implanted as infrarenal aortic interposition grafts as depicted.

2.1.4 TEVG Explant and Patency Determination

Grafts were explanted at 1 and 8 weeks to observe the early macrophage and late remodeling response to the implanted materials (**Figure 8**). The rats were anesthetized with 5% isoflurane and euthanized by a lethal intracardiac injection of a 1:1 mixture of heparin (40IU, McKesson Medical-Surgical) and potassium chloride (100mg/kg, Kospira). Immediately after euthanasia, a 22G catheter (22G x 1 in, Safelet IV catheter, Exel Int.) was inserted into the left ventricle of the heart, and a contrast agent (Isovue (iopamidol injection), Bracco) was injected under angiography (GE OEC 9800 Plus, GE) to determine patency. The graft was then removed and processed for mechanical testing and imaging. Each explant was sectioned and fixed.

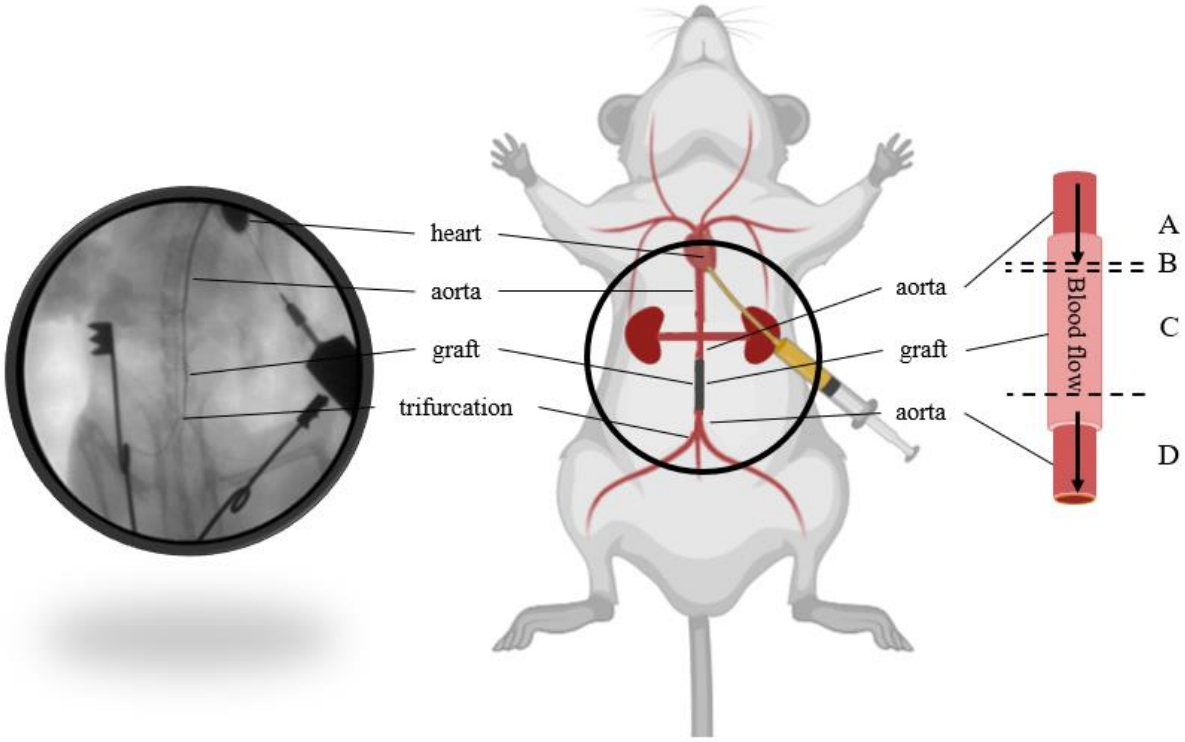

Figure 8. Depiction of angiography at explant.

Angiograms were taken to determine patency (left). Then, the grafts were explanted and divided into four sections (right): (A) proximal aorta and graft, (B) small ring, (C) medial graft, and (D) distal graft and aorta.

Angiography was used to determine graft patency with binary "patent" or "not patent" results. Successful detection of contrast distal to the graft after injection was deemed "patent," while no contrast detected was labeled "not patent" (**Figure 9**). Inconclusive angiograms occurred due to limited visibility caused by stenosis or branching arteries, in which case patency was determined with the assistance of vascular surgeon Dr. Edith Tzeng using angiogram and cross-sectional images.

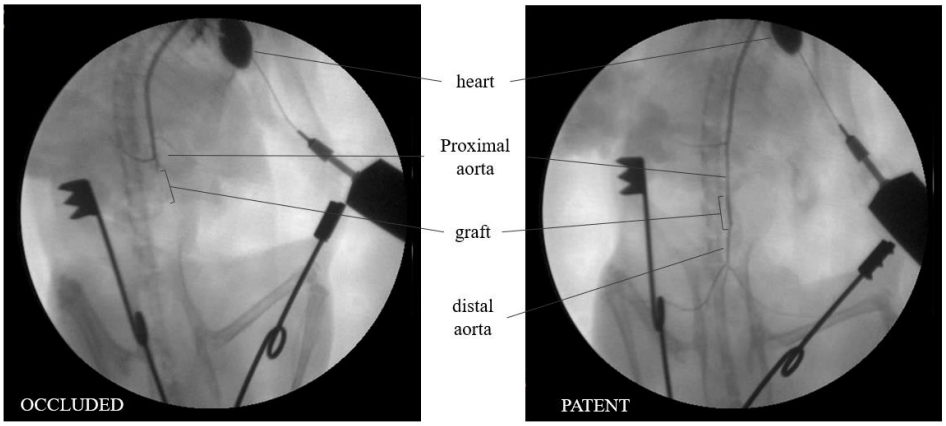

Figure 9. Angiography was used to determine the patency of each graft.

Angiograms were taken to assess patency. Images after contrast injection showed either flow through the graft (patent, left) or no flow indicated by a lack of constrast distal to the graft (occluded, right).

If grafts were removed early due to hind limb ischemia and signs of distress, no angiogram was recorded. Instead, patency was determined by isolating a portion of the aorta distal to the graft prior to euthanization and bisecting it to observe the flow. If no blood flowed out, the graft was labeled “not patent” vs. positive blood flow, meaning “patent” (**Figure 10**).

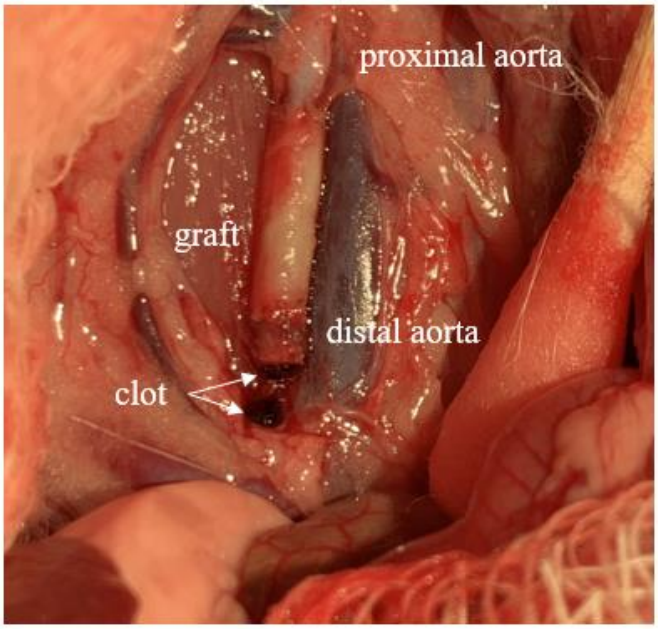

Figure 10. Depiction of graft patency determination without angiography.

Three grafts occluded due to acute thrombosis and explant was performed before the intended timepoint due to animal distress. Patency was determined by bisecting the distal aorta and observing flow through the graft. No flow indicated, not patent, and flow indicated patent.

2.1.5 Macrophage Staining

Section C (**Figure 8**, medial graft portion) of the 1-week explants was fixed in a 4% paraformaldehyde solution (FisherScientific) for 45 minutes before being paraffin-embedded and sectioned onto glass slides (McGowan Institute for Regenerative Medicine (MIRM) Histology Core). Slides were then immunofluorescently stained following the manufacturer's protocol with the following primary/secondary antibodies: CD68 (1:100 ab31630, monoclonal, Abcam)/Cy5 (1:100 ab_2340820, Jackson ImmunoReseach Laboratories Inc.), CD86 (NBP2-25208, monoclonal, Novus Biologicals)/Cy3 (1:100 ab6939, Abcam), and CD206 (1:100 18704-1-AP, polyclonal, ProteinTech) Cy5 (1:100 ab_2340820, Jackson ImmunoReseach Laboratories Inc.).

CD68 is a glycoprotein highly expressed on most macrophages, monocytes, and peripheral blood granulocytes. For this study, CD68 was used as a pan-macrophage marker to determine total macrophage quantities. The whole macrophage population within the sections was also stained for M1 (CD86) and M2 (CD206) macrophage-specific markers. All sections were co-stained with bisbenzimide H 33258 (Sigma Aldrich, St. Louis, MO), which stains DNA (cell nuclei). Each round of staining included a rat spleen (positive control) and each slide included a primary delete (negative control using secondary antibody alone, used to determine non-specific binding) to ensure true staining for each intended marker. Stained slides were imaged using an upright fluorescent microscope (Eclipse 90i, Nikon) and imaging software (NIS Elements, Nikon), and while cross-sections were imaged at 10x magnification. Each image was digitally segmented into an inner (porous layer) and outer (ES) area. For each explant, a total cell (nuclei stain), total macrophage (CD68), M1 type macrophage (CD86), and M2 type macrophage (CD206) count was determined using a custom Matlab code (**Appendix A.4**). Briefly, stained images were blinded to identity of the explant to prevent user bias. Each image was manually segmented into inner (porous) and outer (ES) layers. A separate threshold for the inner and outer layers was determined by three users and averaged (**Figures 11** and **12**). The Matlab code then determined a cell count based on the threshold chosen yielding positively stained cells per area. Significance was determined in GraphPad Prism 8 (GraphPad) using a one way ANOVA and Tukey's multiple comparison test between each group.

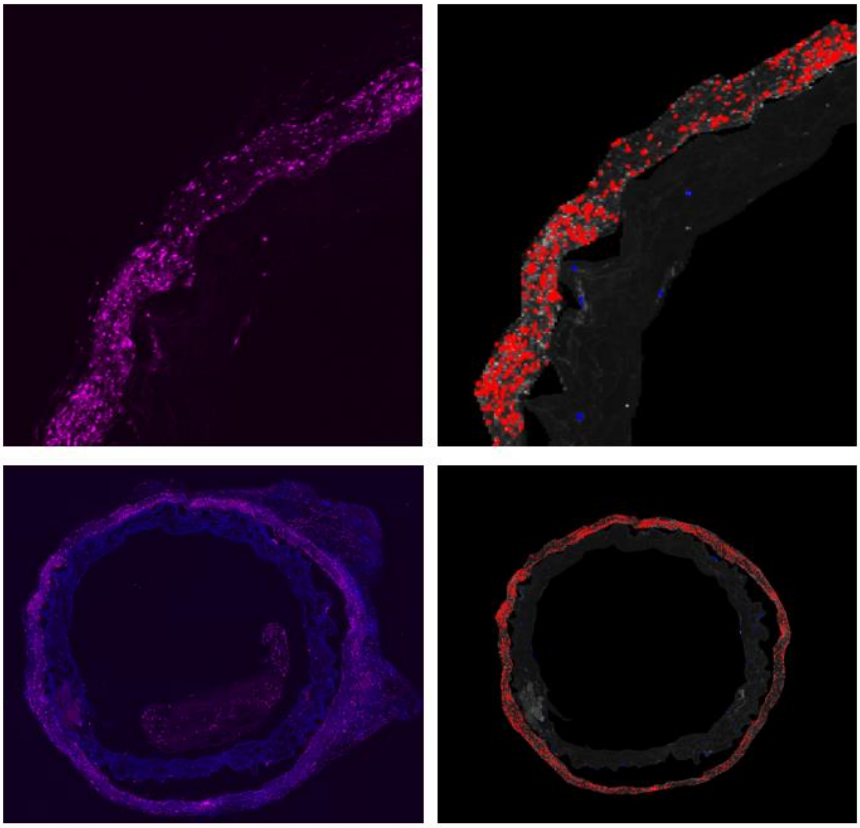

Figure 11. Representative section used for cell counting using a custom Matlab code.

Sections of the 1 week explants were stained for CD68 (pink) and DAPI (blue) to detect macropahges (left).

Images were then run through a matlab code which determine a cell count based on thresholding (right).

2.1.6 Vascular Cell and ECM Staining

Successful detection of remodeling was based on immunofluorescence (IFC) and immunohistochemistry (IHC). Positive graft remodeling was determined through the presence of three key cell types/components: (1) contractile vascular smooth muscle cells [calponin (1:100 ab46794, Abcam)/Cy5(1:100 ab150075, Abcam) and α-smooth muscle cell actin (1:100 ab7817, Abcam/Cy5 (1:100 ab_2340820, Jackson ImmunoReseach Laboratories Inc.)], (2) a full

endothelial luminal lining (von Willebrand Factor (vWF) preconjugated with FITC, Abcam), and (3) ECM deposition (hematoxylin & eosin (H&E) and Verhoeff-Van Geison (VVG)). All IFC was performed using established protocols, and all IHC was completed at the MIRM Histology Core. All 8-week stains for cell phenotypes and ECM components were qualitatively assessed.

2.2 Results

2.2.1 Silk Scaffold Characterization

All three construct types (lyogel, blank MP loaded, and CCL2 MP loaded) were ~1.5 cm long with a wall thickness of 580 ± 118 μm (490 ± 120 μm inner and 128 ± 18 μm outer layer). Each scaffold had an outer diameter of 1040 ± 82 μm and inner luminal diameter of 2194 ± 230 μm (**Figure 12**). Lyogel and MP loaded lyogel scaffolds displayed sufficient porosity, pore interconnectivity, and pore size (53 ± 30 and 43 ± 24 for lyogel and CCL2 functionalized lyogel respectively) for application as a rat TEVG. Homogeneous longitudinal distribution of MPs was observed in all sections indicating an even distribution along the length of the scaffold (**Figure 13**).

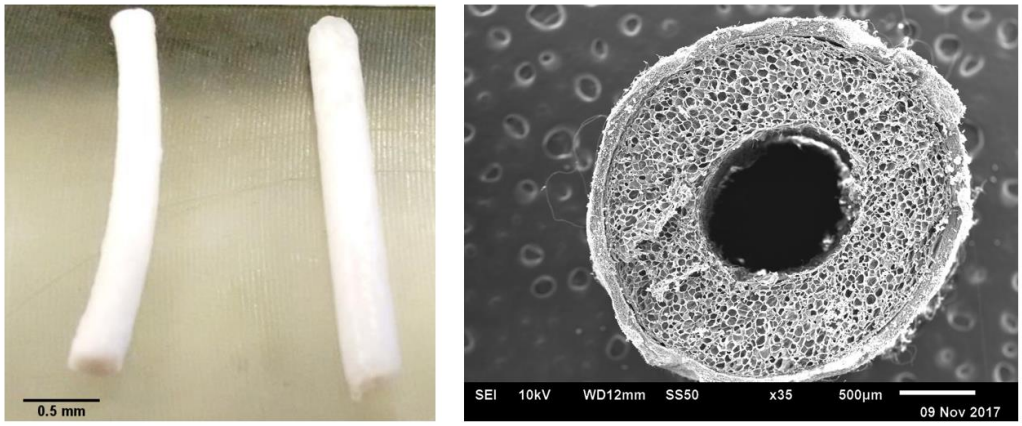

Figure 12. Lyogel scaffold macro image (left) and scanning electron microscopy image (right). Images courtesy of Prerak Gupta.

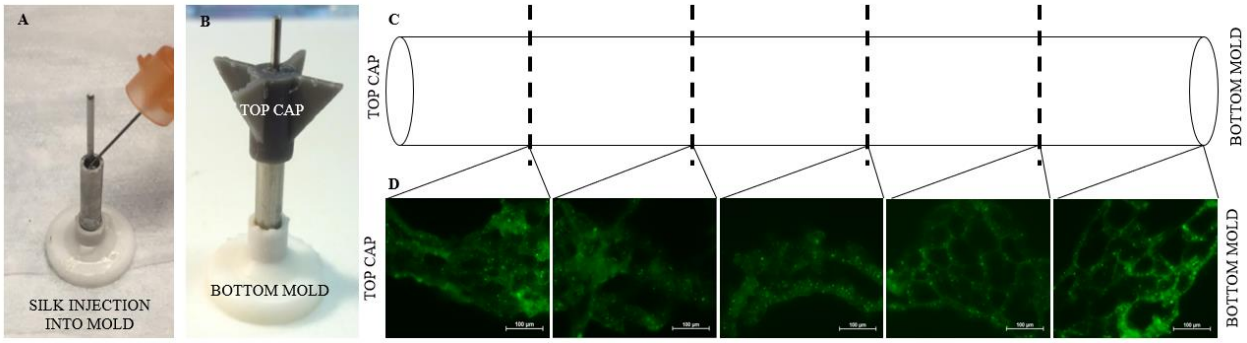

Figure 13. FITC MP loaded scaffolds were sectioned and fluorescently imaged to observe MP distribution (A) Silk solution loaded with FITC MPs was injected into a custom scaffold mold. (B) Each mold was allowed to gel while standing vertically with a top cap. (C) To test for even distrubtion of the MPs throughout the length of the mold, n=2 FITC MP loaded scaffolds were sectioned into five portions and imaged. (D) An qualitatively even distribution of MPs was observed in each section suggesting that MPs do not settle to the bottom of the mold during gelation.

2.2.2 CCL2 Loaded Scaffold Release Profile

Releasates from the CCL2 MP functionalized lyogel scaffolds were collected and measured at day 1, 4, 5, 6, and 7. An initial burst release of contents was observed within 24 hours (**Figure 14**) which was above level of detection. The initial burst release at day 1 was 567.5 pg/scaffold; however, this amount was above the level of detection so is likely higher than measured. Since samples were not collected on days 2 and 3, the day 4 sample represented the release within days 2-4 which was 28.3±16.2 pg/mg scaffold. After day 4, no CCL2 release was detected. Additional testing on diluted day 1 samples as well as releasates from days 2 and 3 were intended but omitted from this dissertation due to research restrictions during the COVID-19 pandemic outbreak.

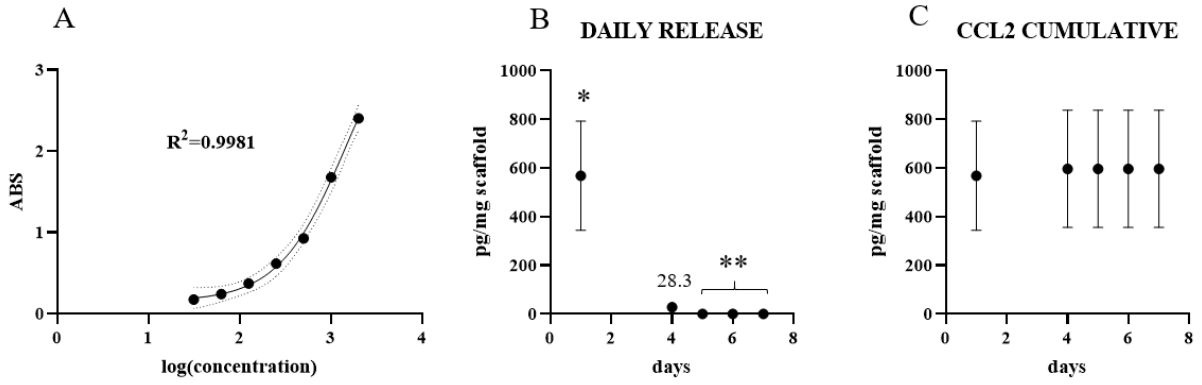

Figure 14. Release profile of CCL2 functionalized lyogel silk scaffolds.

Release from CCL2 MP loaded scaffolds (n=4) was measured using an ELISA. (A) The standard curve was analyzed in GraphPad Prism 8 following the manufactuerer's prtocol. (B) The total amount of CCL2 normalized to scaffold weight was measured within each sample collected (day 1, 4, 5, 6, and 7). (C) A cumulative profile combining the previous CCL2 measurments was also graphed. *Day 1 samples were above level of detection so the reported value of ~600 pg/mg scaffold is innaccurate and likely higher than reported. **Days 5, 6, and 7 samples were below level of detection and displayed as 0.

2.2.3 1- and 8-week Explant Patency and Gross Histology

Gross histology of the 1 week explant (**Figure 15**) showed signs of early stenosis at 1 week in one of the CCL2, one of the lyogel, and two of the Blank MP explants; however, the level of stenosis could not be quantified due to a loss of sample during tissue processing at the McGowan Institute's Histology Facility. Specifically, after paraffin embedding, neotissue was lost in ~50% of the samples, leaving only the unremodeled portions of graft. Some quantification could be performed by imaging whole cross sections of H&E stained explants; however, this analysis was not completed due to shut down of research in response to the pandemic. Therefore, cross sectional macroscopic images were used to qualitatively assess remodeling. Of all the implants in all groups, three grafts from the blank group were removed early due to loss of hind limb function (**Figure 10**) and were determined to be not patent due to acute thrombosis. Patency rates of 50% (7/14), 100% (10/10), and 100% (5/5) were observed in the Blank MP, CCL2 MP, and lyogel groups respectively after 1 week in vivo. A significant increase in patency was observed between the CCL2 and Blank groups after 1 week ($p=0.0188$) (**Appendix A.3**).

Patency for the 8-week explants was determined through angiography, consultation with Dr. Tzeng, and distal bisection of the aorta (**Figure 9**). All explants not patent before or at one week were also included within the 8-week study. Ten of the forty-eight angiograms at 8 weeks were inconclusive due to stenosis limiting flow to an undetectable amount. Explants were 40% (8/20), 54% (7/13), and 73% (11/15) patent for Blank, CCL2, and lyogel scaffolds, respectively. Overall, the 8-week patency rate for CCL2 trended higher than Blank but not significantly ($p=0.2451$). In comparison to the 1-week explants, a decrease in patency was observed in the Blank (50 to 40%), CCL2 (100 to 54%), and lyogel (100 to 73%).

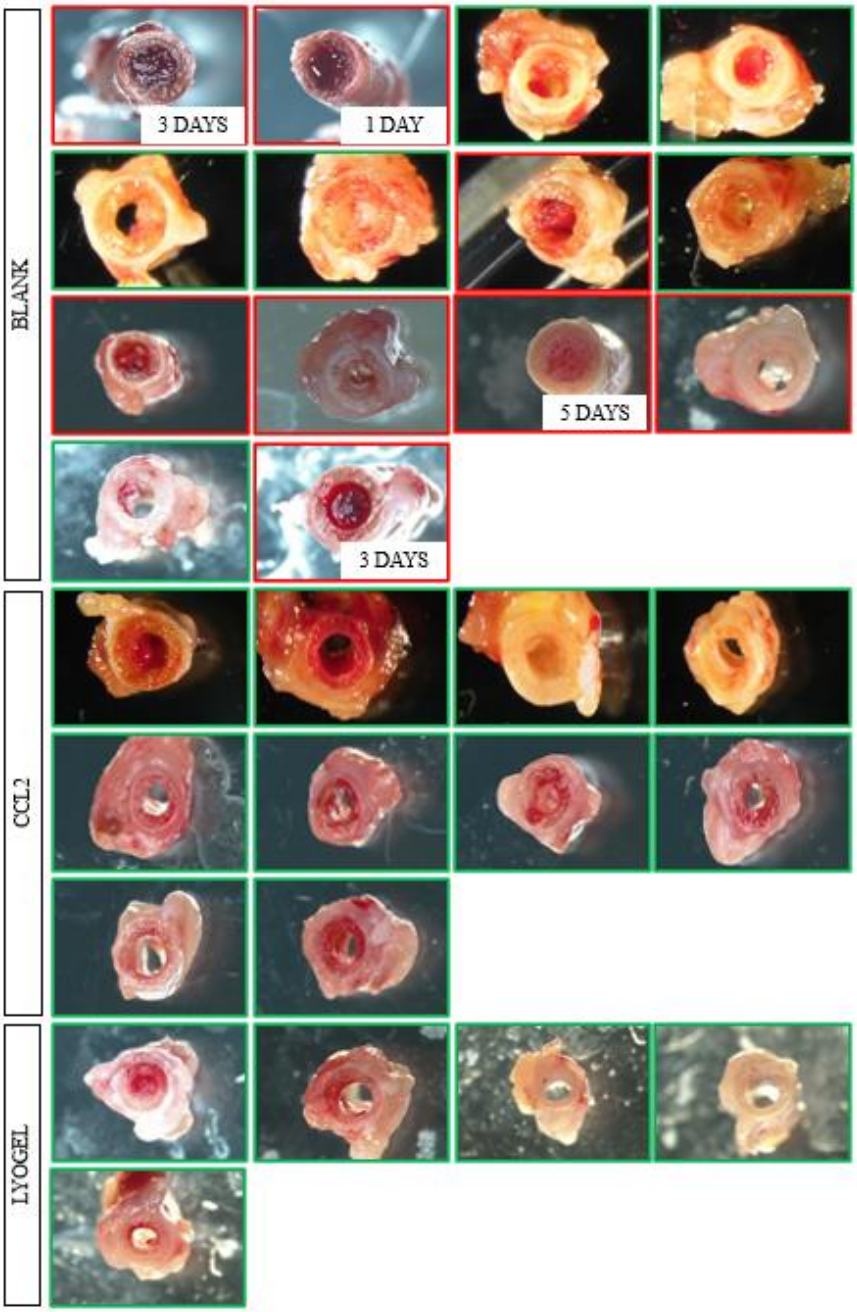

Figure 15. Macroscopic imaging of the medial portion of graft explanted after 1 week.

Grafts removed before 1 week are indicated with implant duration times in the lower right corner. Cross sectional imaging of the Blank (top 4 rows), CCL2 (middle 3 rows), and lyogel (bottom two rows) were taken to qualitatively observe signs of stenosis, neotissue, and thormbus formation. (patent = green border, not patent = red border).

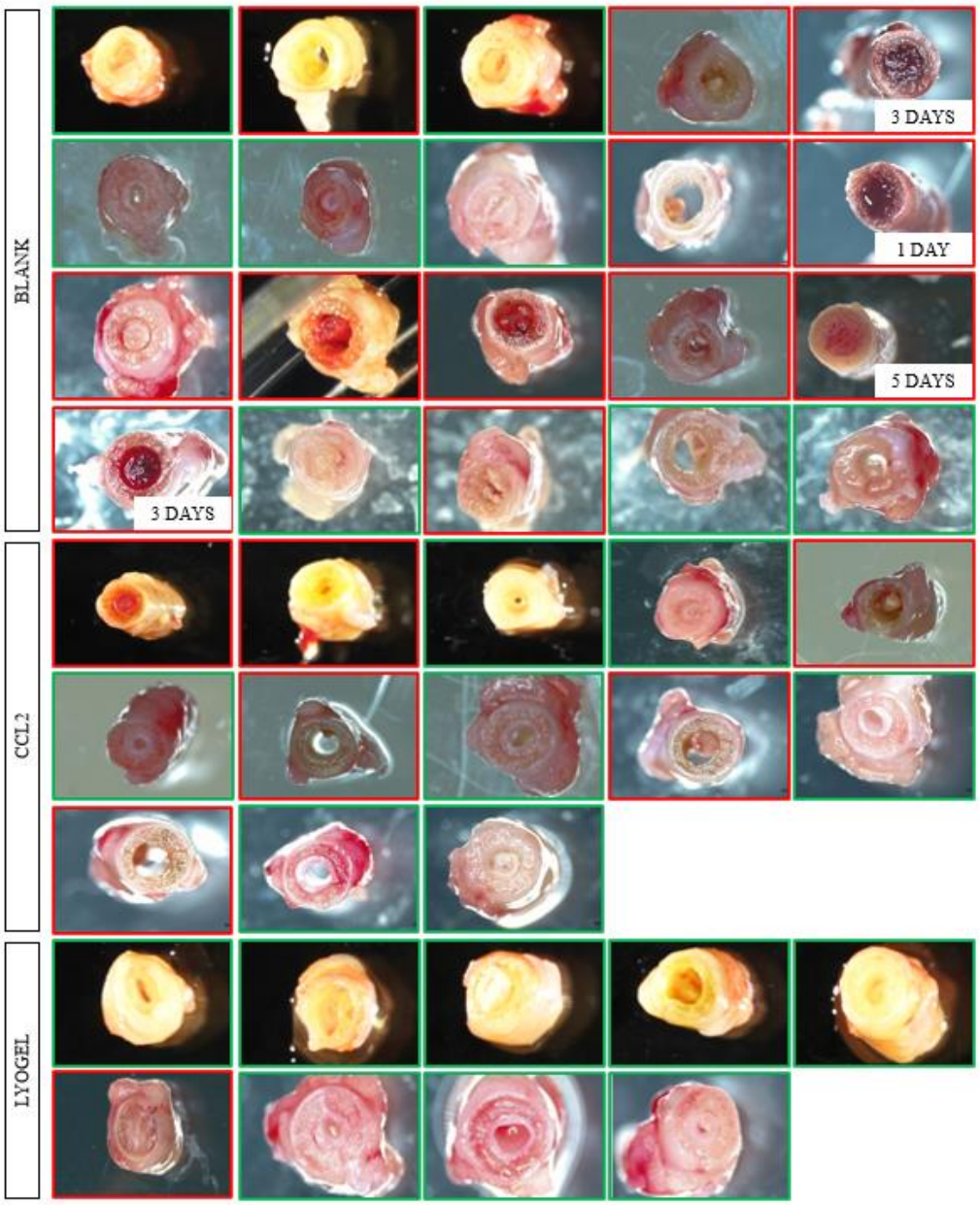

Figure 16. Macroscopic imaging of medial portions of explanted grafts after 8 weeks in vivo. Grafts removed before 1 week are indicated with implant duration times in the lower right corner. Grafts that were occluded in the 1 week explants were also included within the 8 week results. Cross-sectional images of 8-week explants showed signs of neotissue formation and stenosis in all groups.(patent = green border, not patent = red border).

2.2.4 Macrophage Activity After 1 Week In Vivo

Overall macrophage presence was indicated by positive CD68 staining. No significant difference in the density of CD68+ cells was observed between any of the groups. A significantly higher density of CD68+ cells was observed within the outer vs. inner layer of both the CCL2 and Blank MP groups ($p<0.0001$) indicated in **Figure 17**. Macrophage densities within the inner portions were 33±6 (n=11), 26±3 (n=10), and 25±2 (n=4) macrophages per square mm for the Blank, CCL2, and lyogel scaffolds respectively (error represents standard error of mean, SEM). Macrophage densities within the inner portions were 705±149, 705±61, and 383±60 macrophages per square mm Blank, CCL2, and lyogel scaffolds respectively.

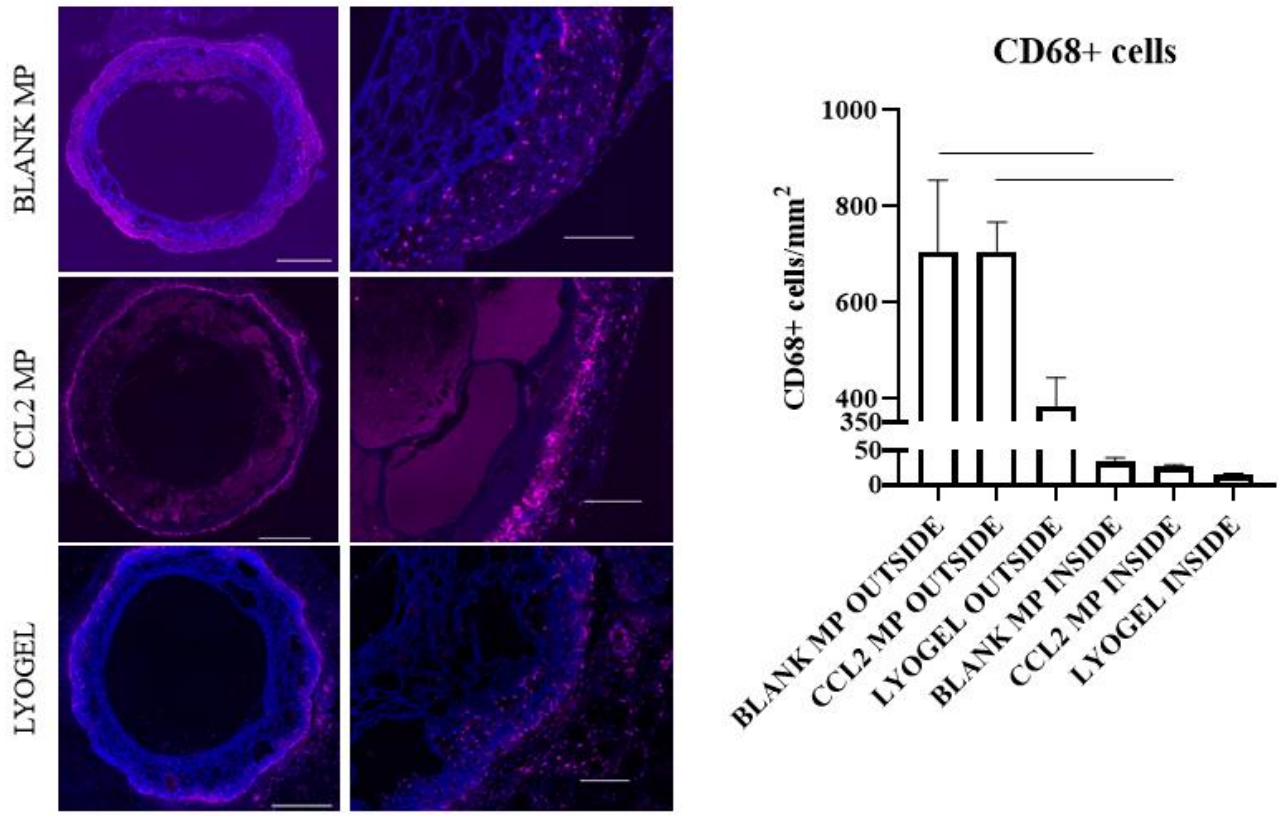

Figure 17. Quantification of CD68+ cells.

TEVGs explanted after 1 week were stained using CD68 (displayed in pink) to detect macrophages and bisbenzimide (blue) to detect all cell nuclei. Whole cross sectional images of each explant (left, each scale bar represents 500 µm) were constructed by tiling higher resultion images (middle, each scale bar represents 100 µm). Quantification of CD68+ was analyzed as positively stained cells per area of TEVG (left, shown as average CD68+ cells/area with SEM). A significantly lower density of macrophages were observed between within the inner compared to outer regions of both the CCL2 and Blank MP groups ($p<0.0001$).

2.2.5 Scaffold Remodeling After 8 Weeks In Vivo

Positive remodeling was detected in all three scaffold types that remained patent after 8 weeks in vivo. Contractile SMCs, a continuous endothelium, and early ECM deposition were detected (**Figure 18**). Qualitatively, a lower amount of calponin positive cells was observed in the blank and lyogel groups compared to the CCL2 group.

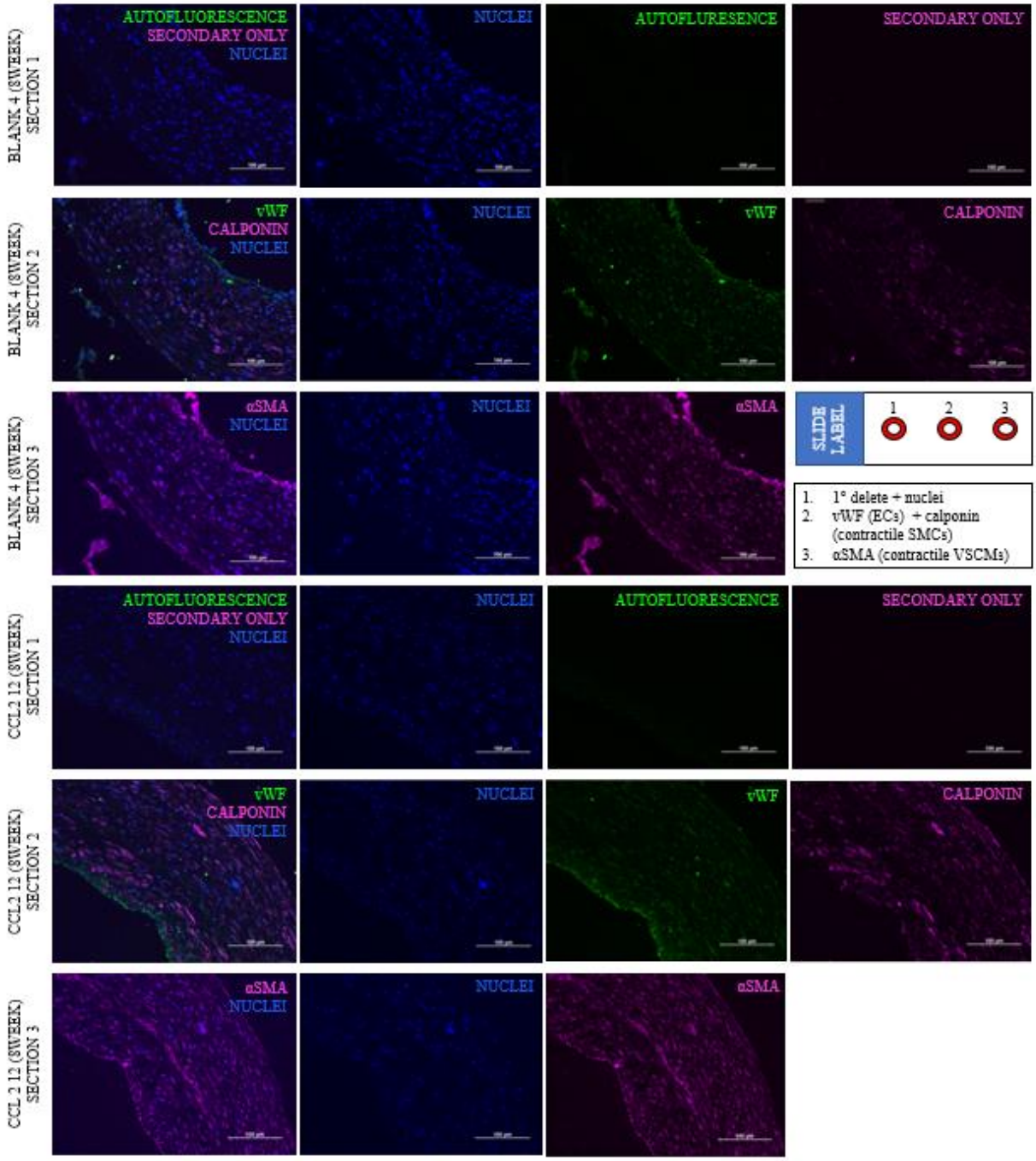
BLANK 4 (8WEEK) SECTION 1
AUTOFLUORESCENCE
SECONDARY ONLY
NUCLEI
NUCLEI
AUTOFLURESENCE
SECONDARY ONLY
BLANK 4 (8WEEK) SECTION 2
vWF
CALPONIN
NUCLEI
NUCLEI
vWF
CALPONIN
BLANK 4 (8WEEK) SECTION 3
αSMA
NUCLEI
NUCLEI
αSMA
SLIDE LABEL
1
2
3
1. 1° delete + nuclei
2. vWF (ECs) + calponin (contractile SMCs)
3. αSMA (contractile VSCMs)
CCL2 12 (8WEEK) SECTION 1
AUTOFLUORESCENCE
SECONDARY ONLY
NUCLEI
NUCLEI
AUTOFLUORESCENCE
SECONDARY ONLY
CCL2 12 (8WEEK) SECTION 2
vWF
CALPONIN
NUCLEI
NUCLEI
vWF
CALPONIN
CCL 2 12 (8WEEK) SECTION 3
αSMA
NUCLEI
NUCLEI
αSMA

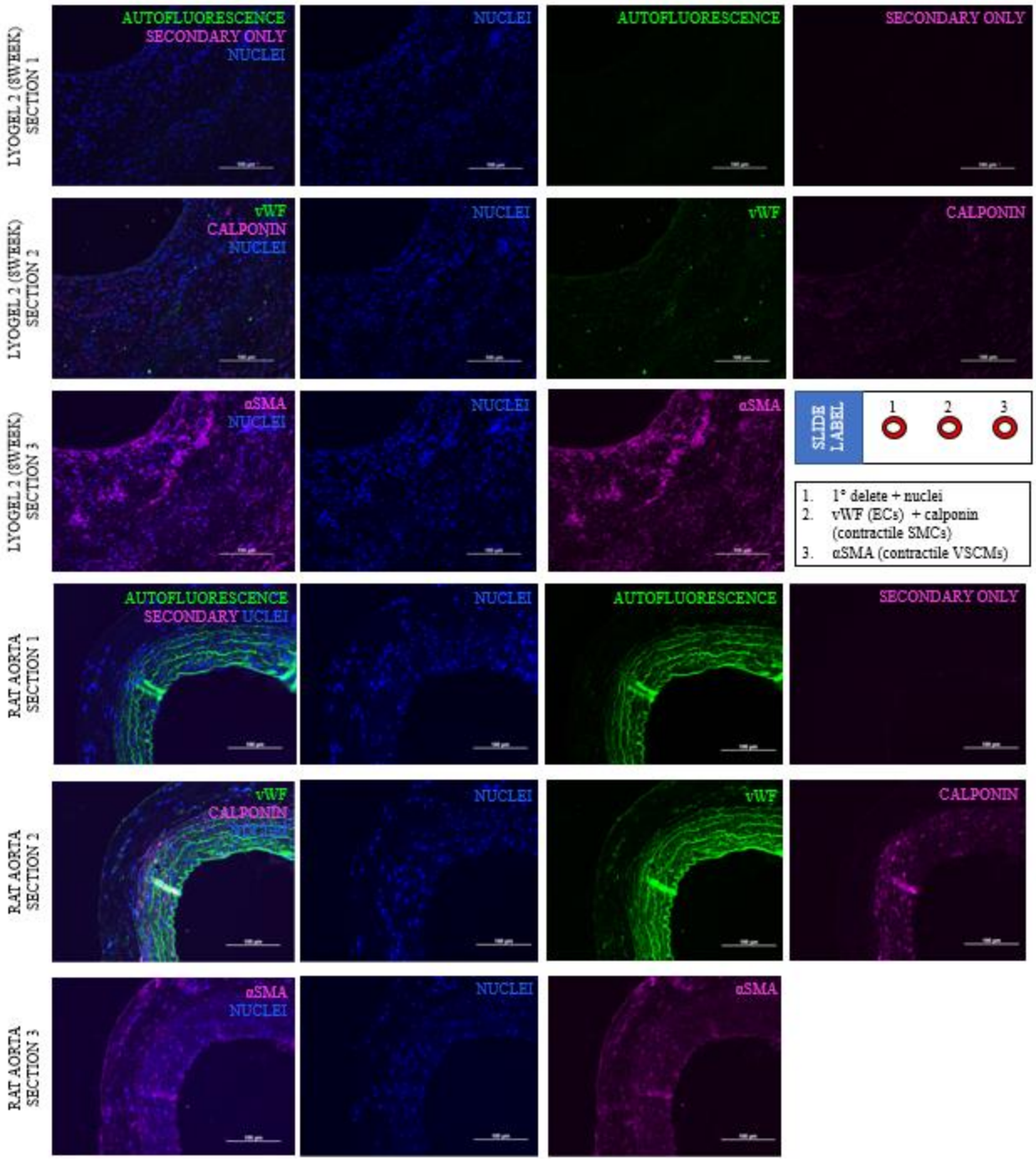

Figure 18. IFC staining of 8 week explants for VMSCs and ECs.

IFC staining showed the presence of contractile VSMCs (calponin and αSMA shown in pink) and ECs (shown in green) within all groups after 8 weeks in vivo. Nuclei of all cells were stained using bizbenzimide shown in blue. A section of rat aorta shows native tissue formation with elastic fibers autofluorescing in green.

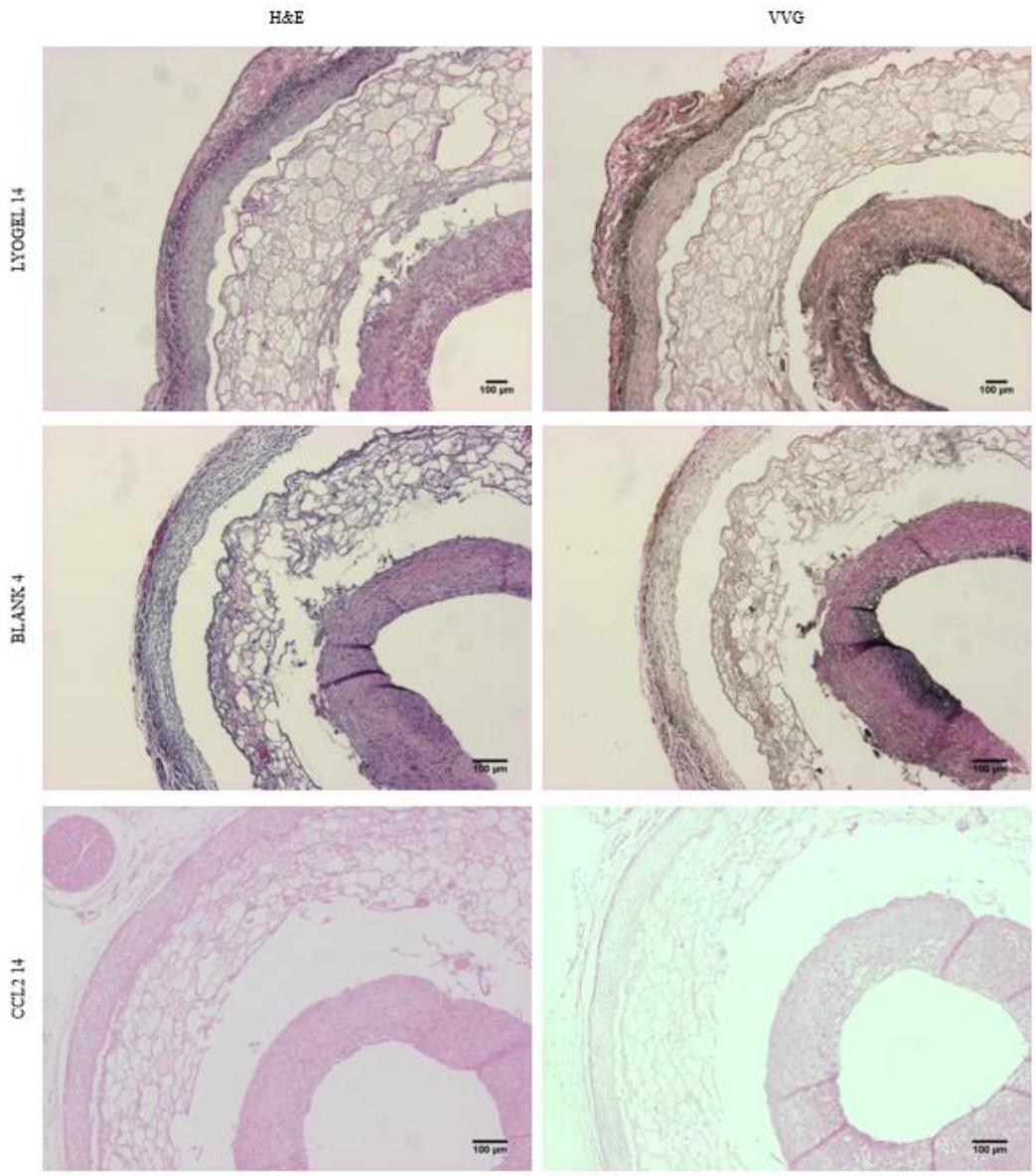

Figure 19. IHC staining of 8 week explants showed gross histology and early ECM depositon.

IHC staining for overall cellularity (H&E, left) and elastic fibers (VVG, right) of 8 week explants showed neotissue formation in all three groups and early elastic fibers within the neotissue. H&E revealed low cellularity throughout the scaffold. All scale bars represent 100µm.

2.3 Discussion

In this study, we were able to successfully fabricate novel, rat-sized silk based bilayered scaffolds functionalized with CCL2 MPs. An initial burst release of CCL2 was observed within the first four days in vitro, ensuring the release of cargo from the MPs after incorporation into the scaffold. In vivo assessment of the scaffolds revealed a significant increase in acute patency after 1 week with the delivery of CCL2 compared to Blank MPs ($p=0.0188$). After 8 weeks in vivo, no significant differences in patency were observed between the three groups (lyogel, CCL2 MPs, and Blank MPs). Additionally, no differences in neotissue cell phenotypes/ECM were observed after 8 weeks; however, differences in remodeling were qualitatively assessed through cross-sectional gross histology.

Three main types of remodeling were observed within the 8-week explants: luminal ingrowth, neotissue formation, and stenosis (**Figure 20**). The first type of remodeling was termed "luminal ingrowth," characterized by a localized infiltration of cells within the lumen forming an obstruction (**Figure 20**). Gross inspection of the explants showed the highest occurrence of "ingrowth" in the blank scaffolds (7 of the 16 explants that remained for the full 8 weeks) followed by CCL2 explants (3 of 13); however, no ingrowth cases were found in the lyogel group. IFC analysis of one luminal ingrowth explant showed infiltration of CD68 positive cells through the ES layer indicated by the cell alignment and portions of scaffold within the neotissue (**Figure 21**). This may suggest a chemotactic response from surrounding tissue-resident macrophages to the scaffold itself or rather an accumulation of circulating blood leukocytes (also CD68 positive)[258]. As previously mentioned, (**Section 2.3.3**), neotissue growth within the lumen and lack of cellularity within the scaffold itself may be due to insufficient luminal porosity. Since no luminal ingrowth was observed within the lyogel group, this may be related to the PLGA MPs or PLGA

byproducts themselves. Further, in vitro testing of cellular growth onto MP loaded scaffolds would be needed to confirm the mechanism behind luminal ingrowth.

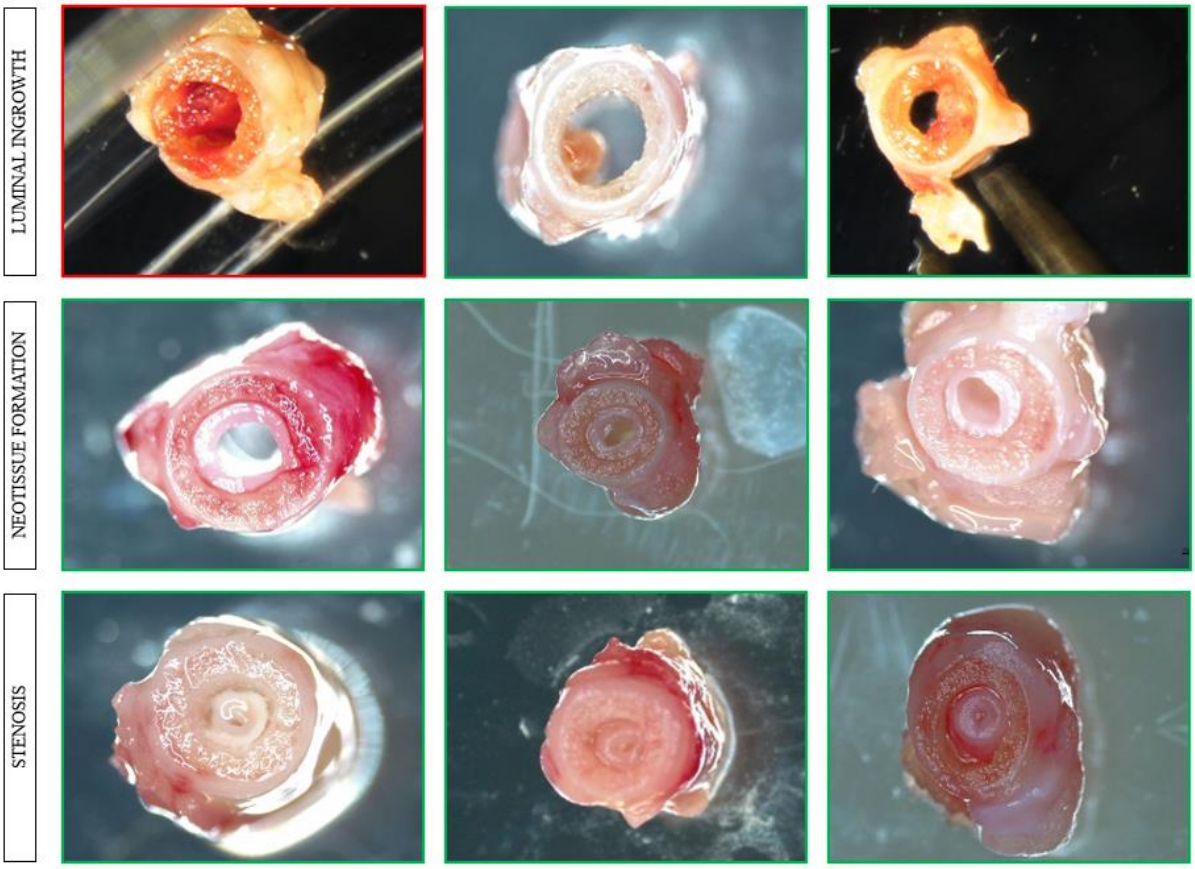

Figure 20. Depiction of the three types of graft remodeling after 8 weeks.

The three types of remodeling observed were (top) luminal ingrowth, (middle) neotissue formation, (bottom) stenosis. Representative images of each type of remodeling were chosen irrespective of TEVG construct composition.

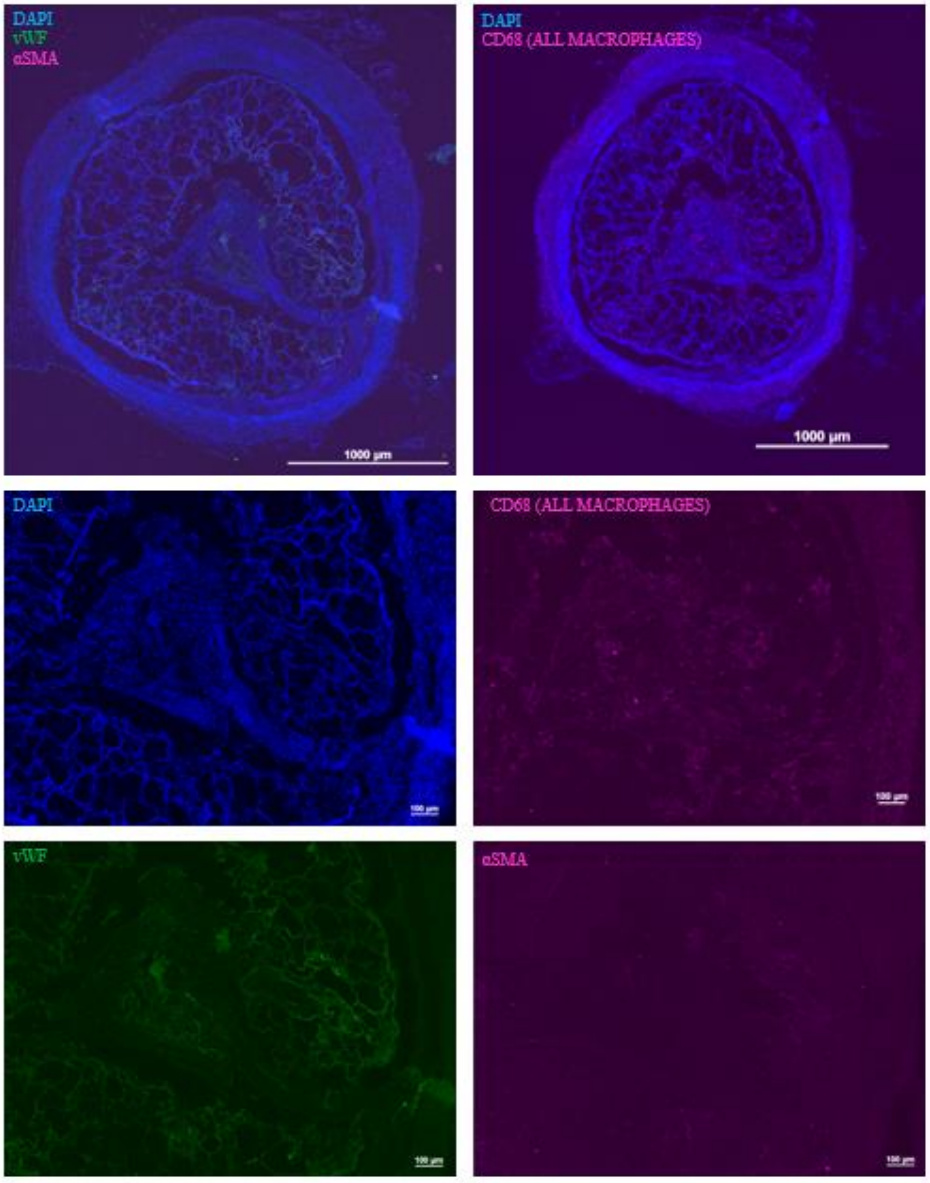

Figure 21. IFC of 8 week CCL2 functionalized lyogel scaffolds.

Total macrophages were detected using IFC for CD68 (pink in the top right and middle right). Additional staining for vWF positive cells (ECs or platelets) and VSMCs (αSMA shown in pink in the top left and bottom right) was used to detect the presence of vascular cells. The luminal neotissue was comprised of macrophages and scaffold byproducts (autofluorescent green in the bottom left) with qualitatively fewer VSMCs (αSMA, bottom right) and ECs (vWF, bottom left) observed in comparison to macrophages.

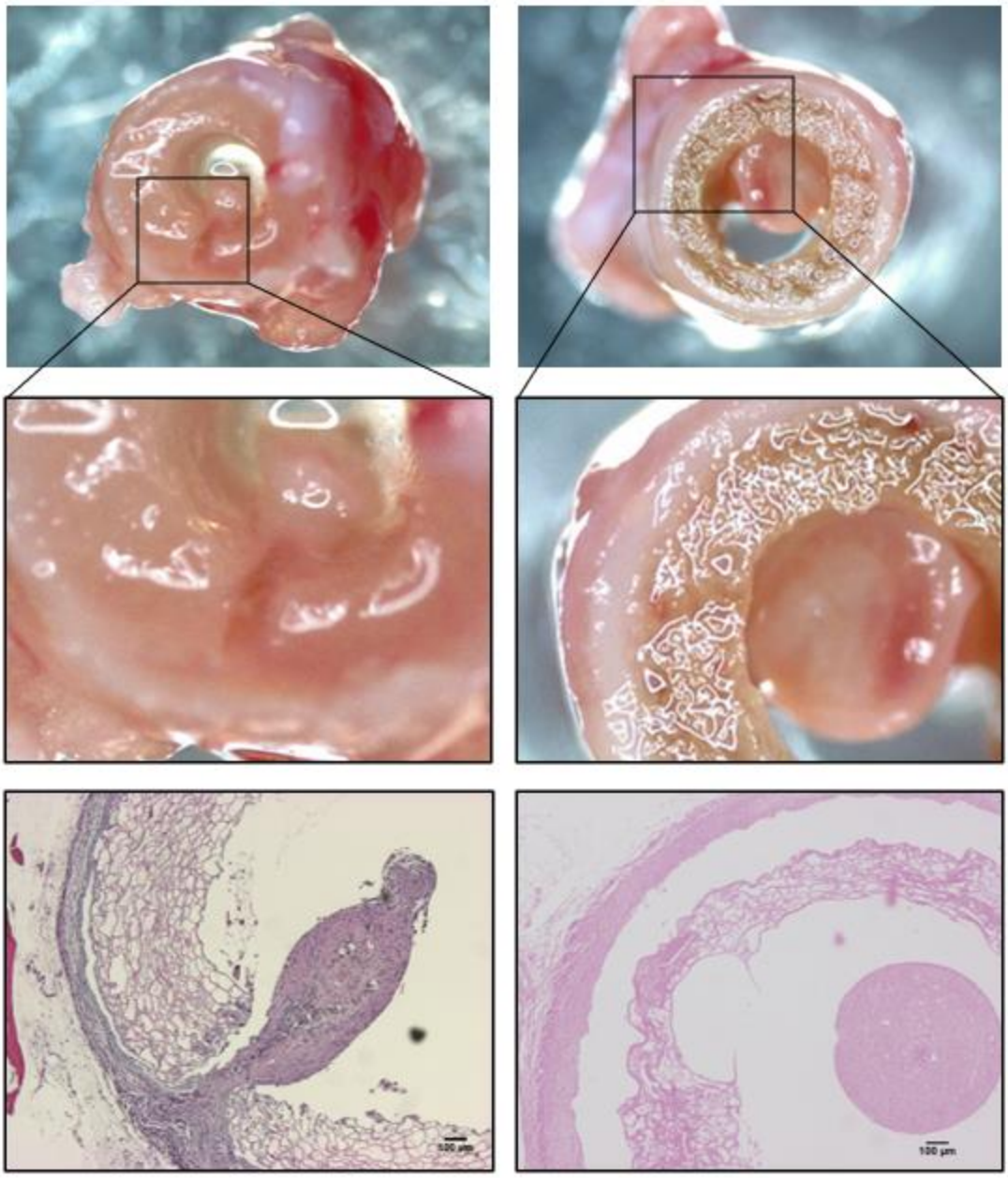

Figure 22. Histological imaging of luminal ingrowth.

Two examples of luminal ingrowth were analyzed (not TEVG type specific), Gross inspection and H&E of grafts with luminal ingrowth showed a dense cellular, circular formation anchored to the ES layer as shown in the top and middle rows. Further H&E staining showed the entire growth was cellular.

In cases of neotissue formation and stenosis, determination of neotissue formation versus stenosis was difficult after tissue processing. Results from angiography, macroscopic images, and staining confirm the main mechanism of failure in all graft types was stenosis. Previous studies in the VBL have used the presence of neotissue as an indicator of positive remodeling; however, excessive amounts can cause stenosis (as observed in this study) and eventual occlusion. Many TEVG studies from other labs have reported stenosis as the main mechanism of failure in a wide range of graft types[98,114,258,259]. However, a recent study from Dr. Breuer and Dr. Shinoka suggested the key to stenosis reduction and reversal may naturally occur through an inflammatory mediated host response over time[260].

Lastly, explants with neotissue formation but no apparent signs of stenosis showed localized infiltration of neotissue into the porous layer of the scaffold (**Figure 23**). In contrast to the cases of luminal ingrowth, the infiltration neotissue does not appear to penetrate the ES layer indicating vascular cell migration from the lumen. Although the source of vascular host cells infiltrating into the graft is still an area of study in the field of TEVGs, the leading theory suggests cellular migration from neighboring host cells from each anastomosis inwards toward the middle of the scaffold[261,262]. This theory could support the increased luminal cellularity observed in H&E images (**Figure 23**), where a distinct difference in cellularity was observed between the luminal neotissue and medial scaffold. Closer inspection of the proximal and distal ends revealed a continuous neotissue spanning both anastomoses (**Figure 24**), also suggesting cellular migration from the anastomosis.

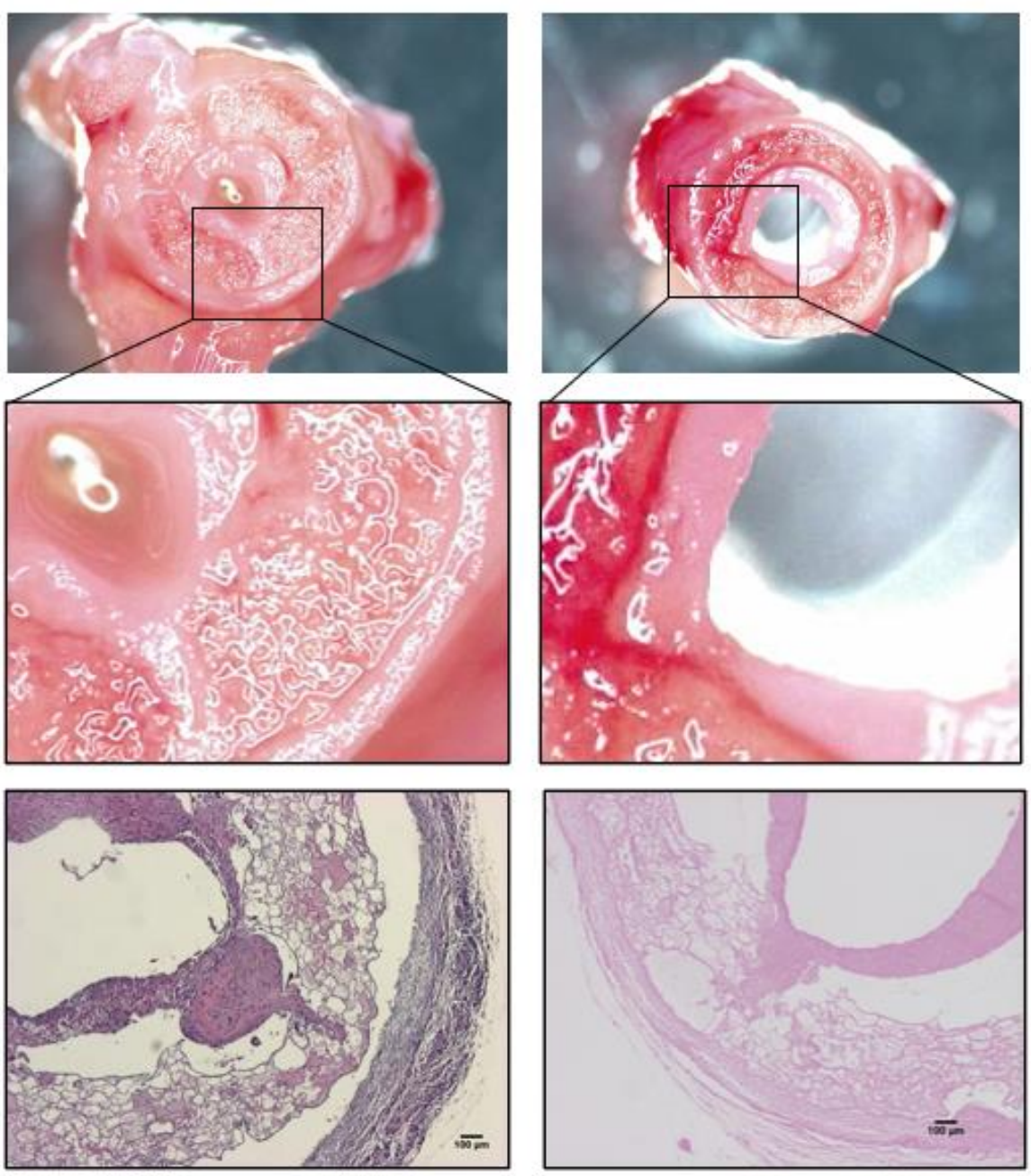

Figure 23.Histologic imaging of neotissue formation.

Two examples of neotissue formation (left=lyogel and right=CCL2) were chosen to display the histology of the explants which fell into the neotissue formation group. Gross histology (top and middle rows) showed a layer of neotissue within the lumen of the explant. Local infiltration of neotissue and localized "anchoring" of the neotissue to the porous layer of the scaffold was observed with H&E staining (bottom row).

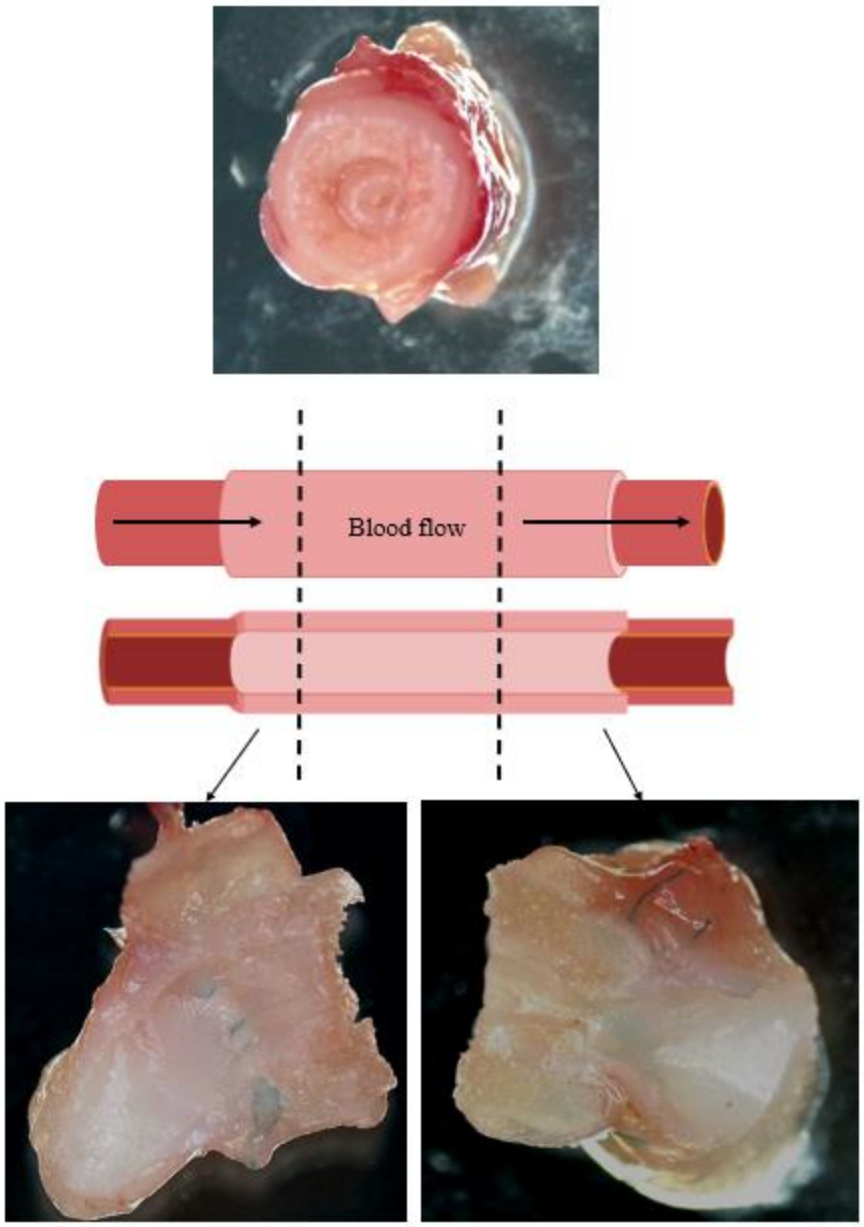

Figure 24. Macroscopic imaging of stenosis at the proximal and distal anastomoses.

The middle portion of the explant showed signs of stenosis through macroscopic cross sectional imaging (top). The proximal and distal graft portions were bisected longitudinally to observe luminal stenosis (middle and bottom). Longitudinal cross-sections showed a distinct neotissue connectin to the aorta at each end (bottom).

IHC for gross tissue structure and elastic fibers showed three distinct layers in nearly all patent explants: an inner neo-tissue, a medial portion of unremodeled graft, and an outer ES and connective tissue layer (**Figure 19**). Previous studies have shown graft recellularization from circulating vascular progenitor cells[126,263], beginning with cellular infiltration from the lumen and cellular differentiation. This potential mechanism behind cell infiltration may explain the increased luminal cellularity observed in the majority of 8-week explants. Alternatively, other studies have speculated at cellular infiltration from the anastomosis rather than the lumen[264,265]. In this case, VSMC activation and migration from the adjacent vessel is primarily immune driven due to the "injury" at each suture site. Both mechanisms would, theoretically, be enhanced by the delivery of CCL2 along the entire lumen, promoting a more rapid cellular migration towards the center of the graft. Initial patency results could be explained by the rapid formation of a cellular lining at the blood interface. To determine the true mechanism behind early graft remodeling, additional in vivo studies at earlier time points (days 1-6) are needed to observe the progression of recellularization.

Regardless of the source of infiltrating cells, graft recellularization was observed exclusively within the intima of the 8-week explants and, in most cases, displayed excessive neotissue formation. In all three types of remodeling, the excessive neo-tissue formation observed could be due to a prolonged M1 (inflammatory) immune response, resulting in chronic vascular cell activation. Recent studies in the field have switched focus from promoting vascular cell migration to mediating the immune response to the scaffold to orchestrate host cell remodeling[178,208,260]. CCL2 alone has been shown to attract and upregulate an M1 macrophage phenotype[266] which requires additional host cell signaling for later polarization. Other studies focusing on macrophage response to implanted biomaterials indicate the delivered cytokines should focus on polarizing the already present macrophages rather than attracting additional,

excessive monocytes[267]. In order to promote M2 polarization, a number of different factors could be introduced including IL-13 or IL-4[268] which have been used in previous studies. However, our previous work with MSC seeded TEVGs have benefited from the full secretome of the implanted cells which includes more than two to three factors. The encapsulation and delivery of all MSC secretions may prove more robust in mediating graft remodeling than a mixture of a few select factors.

2.4 Limitations and Future Directions

Overall, CCL2 played an early role in preventing acute thrombosis, but no additional long-term effects were detected. Below five limitations of this study are discussed in more detail – the success of lyogel without MPs, the limited time points chosen, the experimental limits of macrophage quantification, the relevance of the animal model used, and time constraints related to the COVID-19 pandemic.

First, it was unexpected based on pilot studies (**Appendix A.2**) that lyogel alone remained patent. An initial pilot study was conducted with two goals: assessing the short-term viability of lyogel TEVGs and improving surgical technique. This initial study was limited to 12 implants and only measured patency and graft cellularity. The pilot study tested the efficacy of CCL2 loaded (n=6) vs. lyogel scaffolds (n=6) in vivo (**Appendix A.2**), resulting in an 86% and 0% patency rate respectively after 1 week in vivo. Based on these promising results, the study outlined in within this chapter was performed to better assess the remodeling of a CCL2 functionalized lyogel scaffold; however, lyogel scaffolds in the full study displayed nearly 100% patency instead of 0%. Despite this finding, this study, as well as others in the field[98,114,258,259], have suggested that graft

success is defined by not only patency but also lack of significant stenosis. Taking this into account, while the lyogel scaffolds remained patent up to 8 weeks, 8 of the 9 explants displayed signs of severe stenosis. This increase in stenosis may be a result of a negative or prolonged host inflammatory response. In vitro studies observing the macrophage migration and polarization in response to CCL2 releasates could better indicate any negative effects. Future studies to address stenosis should focus on a more robust host immune response to prevent prolonged inflammation[260].

A second limitation was the limited amount of time points (1 and 8 weeks) observed. These initial two time points were chosen to observe early macrophage recruitment and late-term remodeling (since most of our previous studies showed extensive remodeling after 8 weeks [REFS]). However, further insight into the mechanism behind graft remodeling will require additional timepoints. Earlier times (1-6 days) would provide a clearer picture of the source and rate of host cell migration (both vascular and immune) and the corresponding effect on acute patency. Additionally, later time points (6-12 months) would determine longer-term graft patency and the progression of stenosis. In particular, newer studies have shown spontaneous resolution of stenosis in computational models that would need to be validated in vivo[260].

The results of the IFC staining were also limited by autofluorescence and nonspecific binding of silk to many primary antibodies. Prior to staining, several combinations of primary and secondary antibodies were tested for optimal cell staining, however, CD86 was found to bind the silk protein itself resulting in false staining. Minimal autofluorescence was observed in the CY5 channel and was therefore used for CD68 and CD206 staining. The resulting CY5 stains produced quantifiable images using CD68 primaries but very low binding for CD206 allowing for only

qualitative analysis. Future studies should use IHC or flow cytometry to better identify M1 vs. M2 macrophages.

This study was also limited by the model chosen. In this study, young (<6 months old) Lewis rats were used; however, realistically, cohorts requiring TEVGs include diseased cohorts, particularly aged and diabetic. The CDC reported a staggering ~77% of individuals over the age of 60 diagnosed with some form of CVD[93]. In response, the VBL has studied the effects of elderly cells in TEVGs[115] and shown reduced patency[19]. Another at-risk population studied in the VBL are diabetic patients with a two to four times increased risk of mortality due to CVD[93]. Previous studies from our lab have shown dysfunction in cellular migration in vitro and patency in vivo using diabetic ASC; however, additional studies observing diseased hosts (vs. cell source) are needed to explore the potential of our TEVG technology. One potential discrepancy from our "healthy, young" model to "aged or diabetic models" is the different immune responses, which could affect graft patency and stenosis[267,269]. Studies from Dr. Bryan Brown's laboratory observing the macrophage responses to CCL2 coated mesh implanted subcutaneously showed significantly different M1 and M2 host reactions within young vs. aged mice, which indicates a potential difference in graft remodeling between the two[267]. Studies show old rats contain dysfunctional tissue-resident macrophages which hinder the remodeling process. In comparison, young, healthy rats contain a host of tissue-resident macrophages already present in the surrounding tissue eliminating the need for an attractant[266,267,270,271]. This indicates the need for different cytokine treatments specific to patient age and comorbidities. Future studies could incorporate different high-risk hosts, including aged and diabetic rats, to assess TEVG acceptance among different potential recipients.

Lastly, this study was limited by the experiments not able to be completed due to the restrictions on research during the COVID-19 outbreak. Specifically, the following experiments were underway/planned but unable to be completed: (1) a second ELISA measuring the exact release profile of CCL2 from the scaffolds, (2) IHC analysis and quantification of graft stenosis, and (3) additional macrophage staining for M1 type macrophages.

Overall, this study was successful in fabricating a novel, silk based TEVG functionalized with CCL2. The delivery of CCL2 increased patency over 1 week as well as early macrophage infiltration; however, most grafts failed after 8 weeks due to stenosis. Based on these results as well as others from the field, future studies should focus on a broader immune response mediatory effect through the delivery of additional chemokines or even conditioned media (the subject of **Chapter 3**).

3.0 Chapter 3: Conditioned Media Functionalized Silk Scaffolds

Results from **Chapter 2** indicated delivery of CCL2 caused a dysfunctional graft healing response resulting in stenotic failure. **Chapter 3** aims to build upon these findings by changing the cargo from CCL2 to conditioned media in attempts to elicit a broader and more favorable host response (CM). As previously discussed in the **Introduction** (**Section 1.3.3.2)**, CM not only contains free floating factors such as cytokines and growth factors, but also EVs. The inclusion of EVs within the CM MPs introduces additional cellular communication including delivery of RNA and lipid membrane bound factors.

Previous studies by the VBL have shown patency without stenosis in MSC seeded PEUU scaffolds[17,19,86,127] in vivo, indicating an appropriate cell signaling effect when seeded prior to implant. Since CM varies with media type, cell type, and culture conditions, it is difficult to characterize the contents; however, the use of whole conditioned media ensures delivery of the entire cell secretome without the need to identify and combine individual factors. By using whole CM, we aim to replace cells seeded within the grafts without the need for living cells. For the duration of this study, lyogel scaffolds were used in combination with CM MPs to observe if the delivery of CM can offset stenosis. The use of lyogel allows for MP incorporation into the porous layer of the scaffold during fabrication while other scaffold types require vacuum seeding. Initial attempts to seed MPs into PEUU scaffolds are outlined in **Appendix A.1**. These seeding attempts were hindered by the inability of MPs to deform to fit through pores and the high pressures required to pull the rigid MPs into the scaffold resulting in burst failure of the PEUU scaffold. Additionally, the use of lyogel allowed for a direct comparison of CCL2 vs. CM in Chapters 2 and 3, respectively. Similar to Chapter 2, lyogel scaffolds were fabricated in collaboration with Dr.

Biman Mandal from the Indian Institute of Technology Guwahati and his PhD student Prerak Gupta, who spent a year working in the VBL. Silk fibroin isolation and degumming were performed by Prerak Gupta.

This Chapter focuses on the delivery of MSC-derived CM from silk TEVGs in order to produce patent grafts with fewer occurrences of stenosis when compared to the results from Chapter 2. The following sections outline the in vitro and in vivo testing of CM MP, Blank MP, and lyogel scaffolds and comparing their results.

3.1 Methods

3.1.1 CM MP Fabrication

As discussed in the **Introduction, Section 1.3.3**, conditioned media contains the important cell signaling information required to induce host cell migration, proliferation, and immune response; however, the signaling components vary with cell and media type. In order to optimize the secretome being used within this Chapter, various cell passages and media types were tested to increase the protein content within the CM. These parameters for conditioning media were optimized (**Appendix A.5**) using RoosterBio human Adipose Stem Cells (ASCs, RoosterVial-hAD-1M MSC Lot #00097, RoosterBio). This commercial source of cells was chosen based on its thorough characterization by RoosterBio and increased potential translatability when compared to patient-derived cells. ASCs were plated at 1.5 million cells at passage 3 (P3) into T175 flasks. Cells were then cultured to 40% confluency in RoosterBio RoosterNourish MSC media (KT-001, RooserBio) then rinsed with 1X Hank's buffered saline solution (HBSS, pH 7.4, Thermo Fisher

Scientific), and new 5% harvest media was applied (**Appendix A.5**). Cells were cultured in harvest media for 48 hours, during which time the cells increased from 60 to 90% confluency. The media was then collected and centrifuged (5425R refrigerated microcentrifuge, Eppendorf) at 2,040 x g and 4°C for 5 minutes to remove debris and dead cells. After centrifugation, the supernatant (CM) was isolated and stored at -80°C until use.

MP fabrication and characterization were performed in collaboration with Dr. Morgan Fedorchak, Dr. Steven Little, and Liza Bruk – a PhD student in Dr. Fedorchak's laboratory – at the University of Pittsburgh. Briefly, CM was lyophilized in 20 mL aliquots overnight and resuspended at a 10x concentration. This concentrated CM was then encapsulated in PLGA MPs using a double emulsion procedure[257]. Resulting MPs were 1-10 μm in diameter (previously measured by Dr. Jeffrey Krawiec[272]).

3.1.2 Protein Release from CM MPs

Protein release was measured from CM and Blank MPs. 10 mg of each MP was added to 1 mL PBS (pH 7.4, Gibco) in a 2 mL Eppendorf tube and mounted into an end-over-end turner. The supernatant was collected following the protocol outlined in **Section 2.1.2** and stored at -80°C until use. Using a micro BCA kit (#23235, ThermoFisher), the total protein within each supernatant sample was measured (**Figure 25**). Just prior to measurement, samples were vortexed and added (150 μl each) to triplicate wells in a 96 well plate. Standards of known concentration were also measured in triplicate following the manufacturer's protocol. 150 μL of working solution was then added to each well resulting in a colorimetric reaction. Samples were incubated at 37°C for 2 hours before resting at room temperature for 30 minutes. The samples were then analyzed (absorbance measured at 562 nm) using a plate reader (BioTek).

3.1.3 Measuring EV Release from CM MPs

To measure EV release from MPs, 10 mg of CM MPs and Blank MPs were each released into 1 mL water for 24 hours at 37°C in an end-over-end turner. The resulting releasate was centrifuged at 16,000 x g to pellet remaining MPs and degradation by-products. The supernatant was then filtered through a 0.22 μm filter (Express PES low bind membrane, Millex) to remove smaller debris and apoptotic bodies (**Section 1.3.3.3**). The filtered releasate was then measured using dynamic light scattering (DLS) using a Nano-ZS90 Zetasizer (Malvern Panalytical). 100 μL of the releasate was added to an 8.5 mm cuvette (Brandtech Scientific). Each cuvette was mounted into the Zetasizer and allowed to settle for 1 minute at 25°C. Using pre-set parameters, a refractive index, and absorption matching proteins suspended in water were set. The sample was then analyzed for the average size of particles within the sample.

3.1.4 CM MP Toxicity Assessment

The toxicity of releasates was measured using a LIVE/DEAD assay (R37601, ThermoFisher Scientific). Releasates collected from 3.0 mg MP in 1mL PBS were tested for both CM and Blank particles (**Section 3.2**). Human primary aortic smooth muscle cells (hSMCs, ATCC) were plated into a 24 well plate at 40,000 cells/well and incubated overnight in hSMC media (Cell Applications, Inc., San Diego, CA). The media was then removed, and 500μL of treatment was applied to each well for 12 hours (n=3). A positive viability control of supplemented hSMC culture media (Cell Applications) and positive cell death control of diH_2O were run in

triplicate to confirm true staining of live and dead cells. All wells were imaged using fluorescent imaging (Eclipse 90i and NIS Elements, Nikon).

3.1.5 CM MP Promotion of SMC Migration

The ability to promote cellular migration into the scaffold in vivo is an important component of TEVG remodeling and was tested in vitro using a scratch wound assay adapting protocols previously used in the VBL[115,272]. CM and Blank MPs (10mg/mL) were released into unsupplemented hSMC media (Cell Applications, Inc.). hMSCs between P8 and P12 (ATCC) were plated in a 24 well plate at 75k/well. Cells were allowed to adhere overnight in hMSC media (Cell Applications, Inc.), yielding ~70-80% confluency. A vertical scratch was created by scraping away cells with a 1000μL pipette tip down the center of each well. The media and any floating cells were then aspirated, and 500μL of unsupplemented hMSC media and 500μL of treatment was added to each well. Each well was imaged every 2 hours for 24 hours in a BioSpa 8 automated incubator and imaging system (BioTek, in collaboration with Dr. Ioannis Zervantonakis). Percent wound closure was then measured at 12, 24, and 48 hours (**Appendix A.5**). Significance was determined using a repeated measure two way ANOVA (GraphPad).

3.1.6 CM MP Promotion of SMC Proliferation

CM and Blank MP (n=6, 10mg/mL) releasates' ability to promote SMC proliferation was assessed by cellular quantification. MPs were released into unsupplemented hSMC media (Cell Applications, Inc.) for 24 hours at 37°C in an end-over-end turner. hMSCs between P8 and P12 (ATCC) were plated in a 24 well plate at 10k/well. Cells were allowed to adhere overnight in

hMSC media (Cell Applications), yielding ~30% confluency. The media was then removed, and 500μL unsupplemented hSMC media and 500μL of treatment were applied to each well. Images were taken at 0, 12, 24, and 48 hours and total cell count in each image was quantified using ImageJ. Proliferation was quantified as % cell count increase from time 0 when each treatment was applied. Significance was determined using a repeated measure two way ANOVA (GraphPad) and Dunnett's multiple comparisons test to determine significance between individual groups (95% confidence interval).

3.1.7 In Vivo Assessment of CM MP Functionalized Lyogel-based TEVG Constructs

All scaffolds were implanted as abdominal, infrarenal, interposition aortic grafts into Lewis rats for 1 and 8 weeks following the protocol in **Section 2.2.3**. Patency was assessed using angiography (dissection of the aorta distal to the graft prior to euthanasia was not required for these implantations) and consultation with Dr. Tzeng as needed after 1 and 8 weeks **(Section 2.1.4).** The medial portion of each 1-week explant was analyzed for macrophages using IFC (**Section 2.1.5**). All 8-week explants were macroscopically imaged to qualitatively observe remodeling (neotissue formation, luminal ingrowth, and stenosis) before processing at MIRM Histology Core. Sectioned samples were then analyzed using IHC and IFC for vascular cells (VSMCs, ECs) and ECM components (**Section 2.1.6**).

3.2 Results

3.2.1 Protein Release from CM MPs

A burst release of cargo was observed after the initial 24 hours of release (3.76 μg μg/mg of MPs, n=3) normalized to Blank MP release (n=1), followed by no detectable release for the following days (**Figure 25**). We had intended on running ELISAs to further characterize the presence of VEGF, TGFβ, and uPA as indicators of vascular remodeling cytokines present (**Section 1.3.3**) in the releasates but could not due to research restrictions during the Spring 2020 SARS-COVID-2 lockdown.

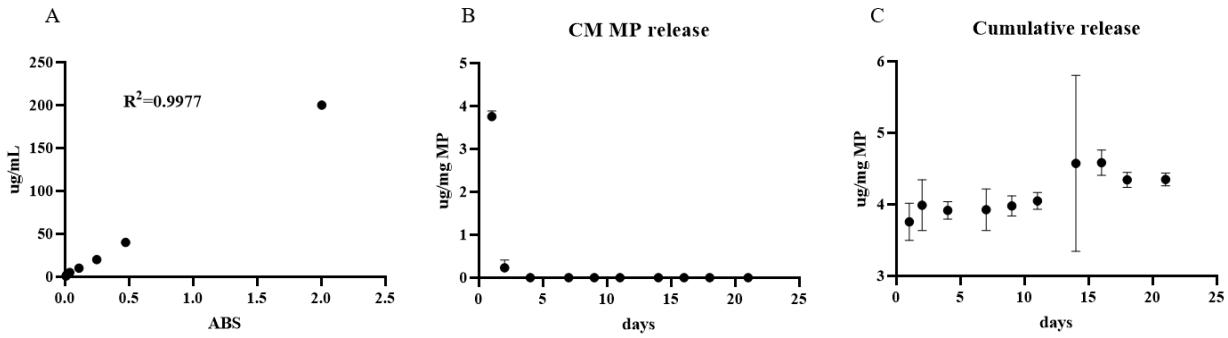

Figure 25. Release profile of CM MPs.

Protein release from MPs indicated a burst release of cargo within the first day. (A) The standard curve, (B) release within each sample, and (C) combined release over time is displayed above.

3.2.2 EV Release from CM MPs

DLS analysis showed no detectable particles within the blank releasate (note that because no particles were detected, the sample result quality report was poor). A population of particles

~243 nm in diameter was detected within the CM MP releasate (corresponding to average EV diameters ranging from 100-1000 nm OD) (**Figure 26**).

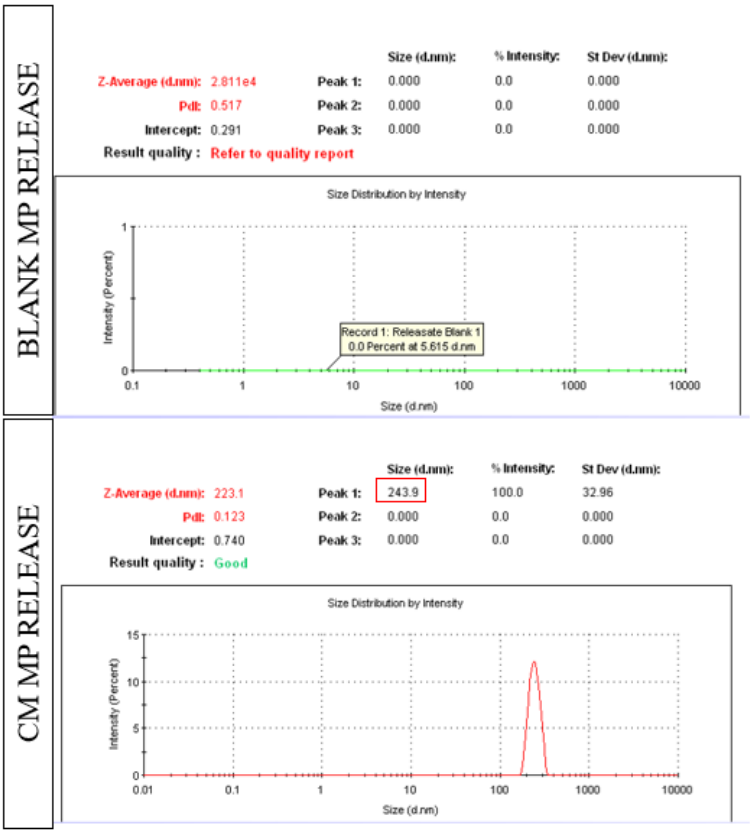

Figure 26. EV release from MPs using DLS.

DLS analysis of CM (bottom) and Blank (top) MP releasates showed no release from Blank MPs and a population of particles ~243 nm OD from the CM MPs.

3.2.3 CM MP Toxicity

Results showed some toxicity in the Blank MP release (indicated in red), and no toxicity in CM MP release (**Figure 27**). Analysis of cellular morphology using brightfield imaging (Eclipse 90i and NIS elements) showed altered cell morphology due to the treatment with Blank MPs after

24 hours (**Figure 28**). Since no toxicity was observed in response to CM MP releasates, the bioactivity was then measured.

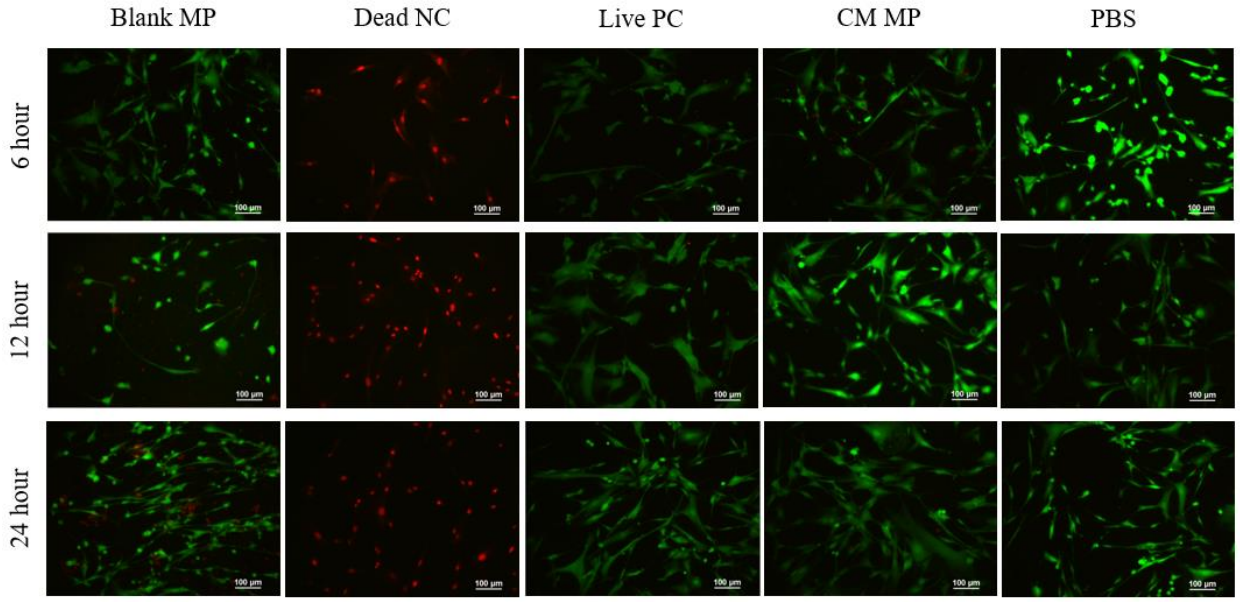

Figure 27. Toxicity of CM MP releasates on SMCs.

A LIVE/DEAD assay was used to label dead cells red and live cells green. The columns represent each treatment from left to right: releasate from Blank MPs, a cell death control (Dead NC, diH_20), a live cell control (Live PC, SMC growth media, Cell Applications), CM MP releasate (CM MPs), and PBS. The images shown are representative of the observed effect within the n=3 wells. Some cell death was observed after treatment with Blank MPs for 24 hours. No toxicity was observed in the CM MP group.

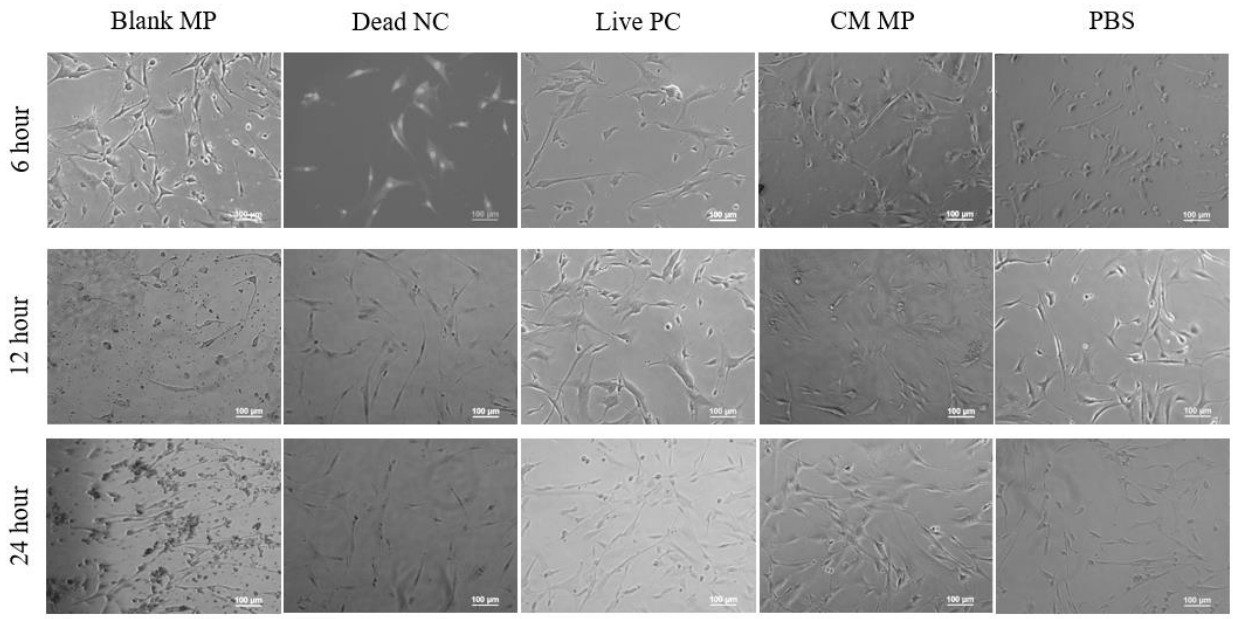

Figure 28. Morphology of cells in response to CM MP releasates.

The columns represent each treatment from left to right: releasate from Blank MPs, a cell death control (Dead NC, diH_20), a live cell control (Live PC, SMC growth media, Cell Applications), CM MP releasate (CM MPs), and PBS. The images shown are representative of the observed effect within the n=3 wells. Brightfield imaging of SMCs treated with CM MPs showed no signs of altered morphology. Only Blank MP treated cells showed any morphological differences after both 12 and 24 hours of treatment.

3.2.4 SMC Migration

SMC migration was measured in response to one batch of CM MPs (n=1) with the intention of additional iterations which were halted in response to the COVID-19 pandemic. Ideally, each n value would represent the SMC migration in response to a single CM MP batch since CM varies from flask to flask. For the purpose of this section, a single batch of CM MPs was released and applied to six wells so "n" will represent one well of SMCs measured rather than batches of CM MPs. No significant difference was observed in migration between the Blank MP (n=4) and CM

MP (n=6). A significant difference in wound closure was observed between unsupplemented media (negative control, n=6) and CM (positive control, n=4) after both 12 and 24 hours of culture, confirming the functionality of the assay ($p=0.0205$). No other significant differences were observed between groups; however, this result must be confirmed with testing of additional batches of CM MPs (**Figure 29**, additional assays were not run due to SARS-COVID-2 restrictions on research).

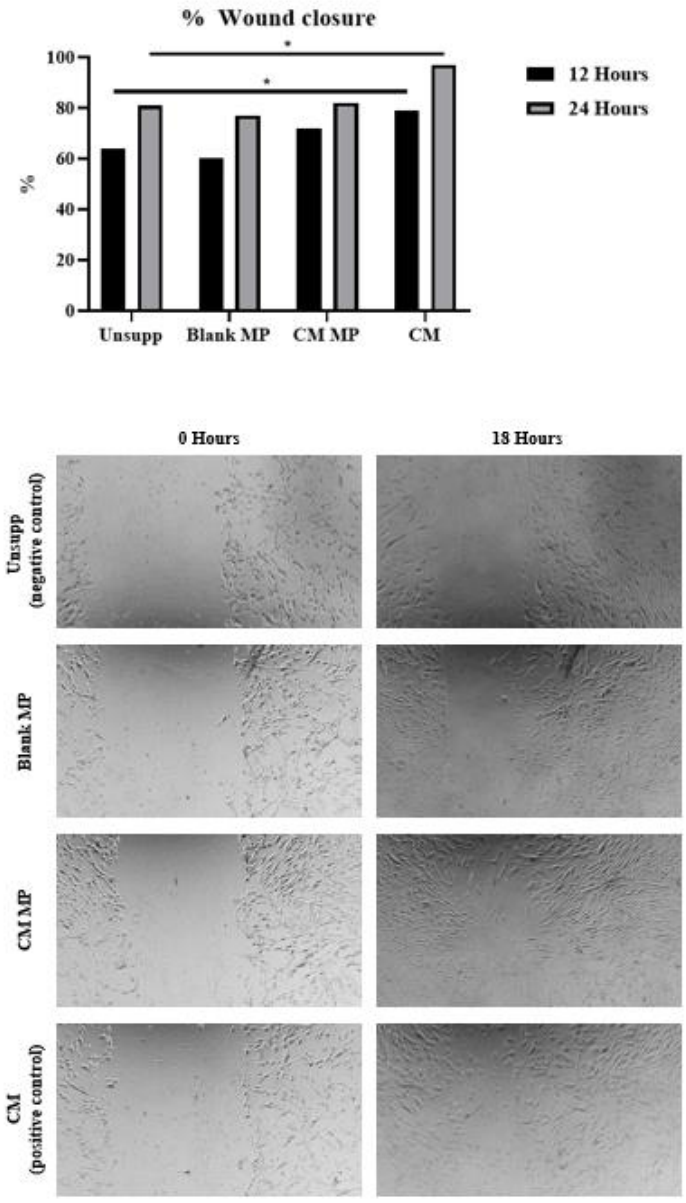

Figure 29. SMC migration measured with a scratch wound assay.

SMC migration was observed using a scratch wound assay. A wound was created within the cells (left column) and allowed to repopulate with migrating SMCs (right column). The rate of migration was measured in response to unsupplemented SMC media (top row, n=6), Blank MPs (second row, n=4), CM MPs (third row, n=6, and CM (bottom row, n=4). A significant difference was observed between the Unsupp and CM (p p=0.0205) only.

3.2.5 SMC Proliferation

Similar to **Section 2.6.4**, proliferation of SMCs was tested in response to n=1 batch of CM MPs due to limitations of the COVID-19 pandemic. For the purpose of this section, each "n" value will represent the proliferation of SMCs within a single well. A total of n=6 wells were analyzed for each of the four groups. A significant difference in proliferation (% cell count increase from time 0) after 48 hours was observed between the unsupplemented basal media (negative control) and CM groups (positive control) confirming the functionality of the assay (p=0.0043) (**Figure 30**). A significant difference was also observed between the Blank MPs and CM (p= 0.0035) and CM MP and CM groups (p=0.0115) after 48 hours. A trend towards an increase in cell proliferation was observed between the Blank and CM MP groups but was not significant (p=0.9553).

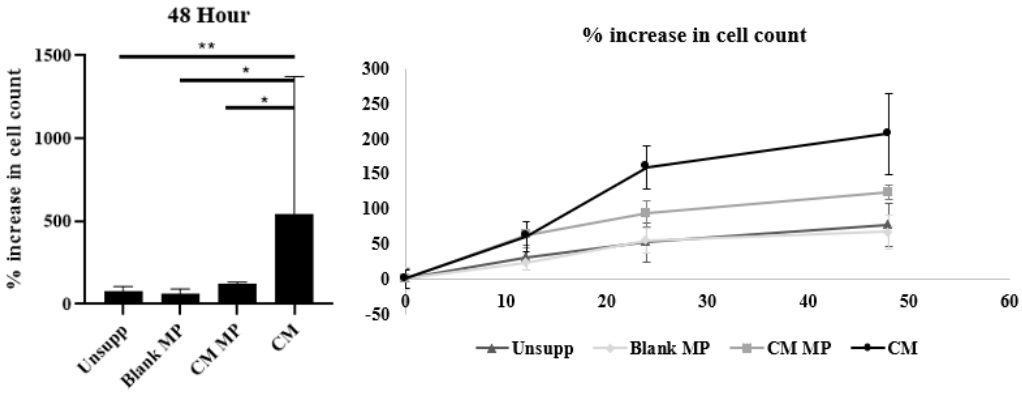

Figure 30. Proliferation image

SMC proliferation in response to unsupplemented SMC media (Unsupp, n=6), Blank MPs (n=6), CM MPs (n=6), and CM (n=6) was measured. A significant increase in proliferation was observed from the Unsupp group to CM (p=0.0043), the Blank MP group to CM (p= 0.0035), and CM MP group to CM (p=0.0115) after 48 hours of treatment (left). A trend towards overall increase in proliferation was observed with the CM MP group compared to Blank MP group but the difference was not significant (p=0.9553).

3.2.6 1- and 8-week Patency Results

Six of the nine 8-week explants displayed stenotic angiograms, and patency was assessed with the assistance of Dr. Edith Tzeng. The same Blank MP and lyogel controls were used from Chapter 2 resulting in 50% (7/14), 100% (5/5), and 100% (9/9) patency rates for Blank MPs, lyogel and CM MPs, respectively, after 1 week. Patency rates of 40% (8/2), 73% (11/15), and 56% (5/9) for Blank MPs, lyogel, and CM MPs, respectively, were observed in the 8-week explants. Cross-sectional imaging of the medial portions of each explant showed no signs of stenosis after 1 week (**Figure 30**). Four of the five patent grafts at 8 weeks showed signs of severe stenosis (**Figure 31**). Overall, CM MP scaffolds displayed similar patency rates to CCL2 MP scaffolds. All groups trended towards a decrease in patency from 1 to 8 weeks (**Figure 33**) (not significant), but a significant increase in patency was observed between the CM and Blank MP groups at 1 week ($p=0.0189$, **Appendix a.3**). As with CCL2 MPs, the CM MPs appeared to have an acute effect on thrombosis corresponding with a burst release of cargo but lacked a prolonged effect.

Figure 31. Cross-sectional images of 1 week CM MP explants

Cross sectional macroscopic imaging of the CM MP functionalized lyogel TEVGs (n=9) after 1 week in vivo showed no signs of stenosis. A thrombus was observed in one explant (bottom right) which may be due to stagnant blood within the graft during angiography. (patent explants = green border, not patent explants = red border)

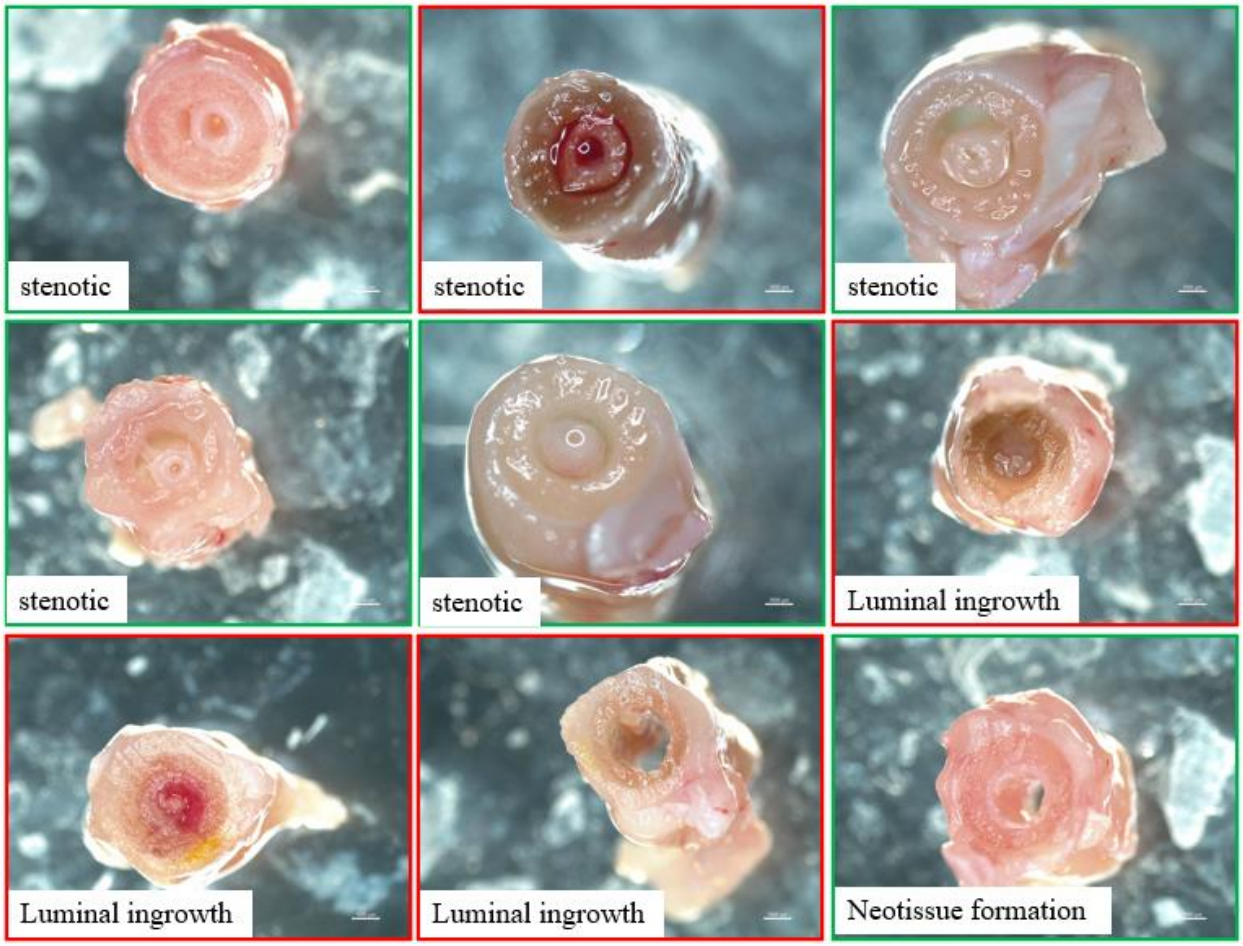

Figure 32. Cross-sectional images of 8-week CM MP explants

Macroscopic cross-sectional images of the CM MP functionalized lyogel scaffolds after 8 weeks in vivo remodeled in three ways (indicated in the lower left corner). Of the TEVGs, stenosis was the more commonly observed result. (patent = green border, not patent = red border)

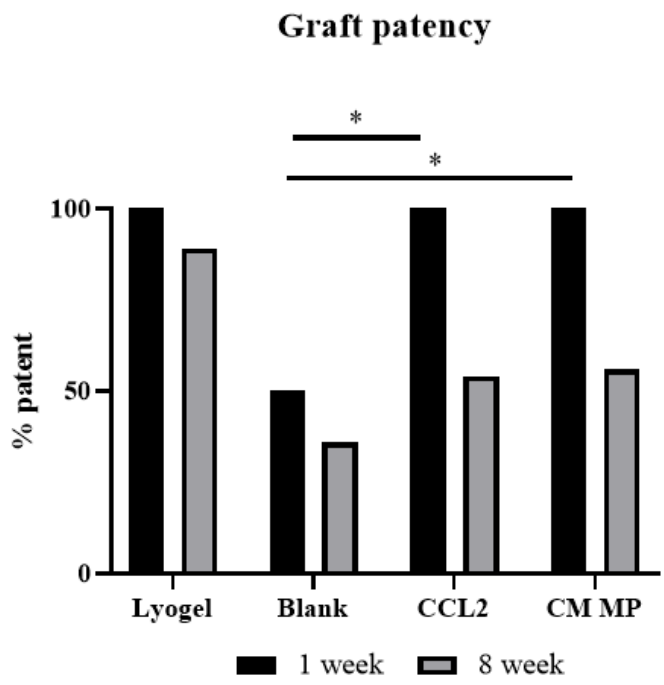

Figure 33. Patency rates for CCL2, CM MP, Blank MP, and lyogel groups at 1 and 8 weeks. A significant increase in TEVG patency was observed in the CM MP explants compared to Blank MP grafts after 1 week (p=0.0189) as well as the CCL2 to Blank MP explants (p=0.0188) after 1 week.

3.2.7 Macrophage Activity After 1 Week In Vivo

Similar to **Chapter 2, Section 2.2.4**, only CD68+ cells could be quantified in IFC images of explants (**Figure 34**). Results showed a significantly higher number of CD68+ cells within the outer layer of CCL2 vs CM MP explants (p=0.0023) indicating a dampened macrophage recruitment from CCL2 to CM delivery. Additionally, a higher number of macrophages were found in the Blank MP outer layer in comparison to the CM MP outer layer (p=0.0017) indicating a reduction of macrophage recruitment in response to CM delivery. Overall, significantly higher macrophage quantities were observed in the Blank and CCL2 outer layer vs. the inner layer

($p<0.0001$) suggesting a stronger tissue resident macrophage response vs. circulating monocyte attraction particularly in response to the PLGA microparticles themselves.

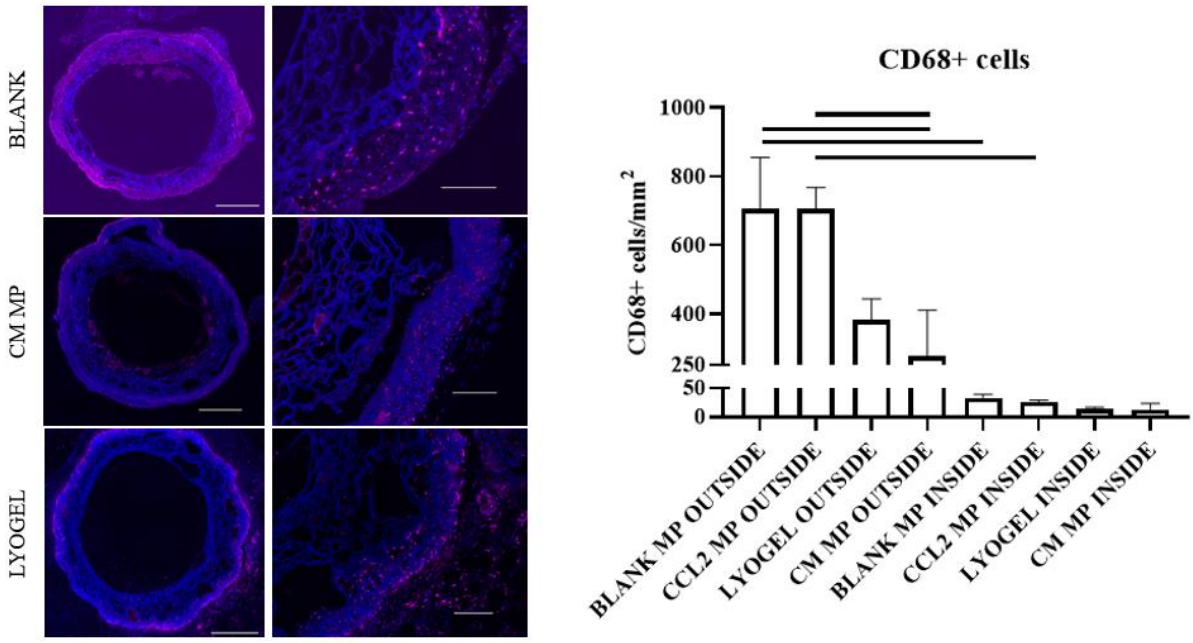

Figure 34. Macrophage response to CM MP functionalized lyogel scaffolds.

TEVGs explanted after 1 week were stained using CD68 (displayed in pink) to detect macrophages and bisbenzimide (blue) to detect all cell nuclei. Whole cross sectional images of each explant (left, each scale bar represents 500 µm) were constructed by tiling higher resultion images (middle, each scale bar represents 100 µm). Quantification of CD68+ was analyzed as positively stained cells per area of TEVG (left, shown as average CD68+ cells/area with SEM). A significantly lower density of macrophages were observed between the inner compared to outer regions of both the CCL2 and Blank MP groups ($p<0.0001$). A significantly lower density of macrophages was found in the outer layer of both the Blank MP ($p= p=0.0017$) and CCL2 ($p=0.0023$) groups in comparison to the CM MP TEVGs.

3.2.8 Scaffold Remodeling After 8 Weeks In Vivo

IFC staining of the neotissue showed contractile SMCs and a continuous endothelium present after 8 weeks (**Figure 35**). Similar to the CCL2 TEVGs (**Figure 18**), little cellularity was observed within the porous scaffold layer compared to the neotissue and ES layers (**Figure 36**). CM MP explants also showed the three distinct layers (**Chapter 2, Section 2.3, Figure 23**) found in the previous explants with definite boundaries separating each (**Figure 37**).

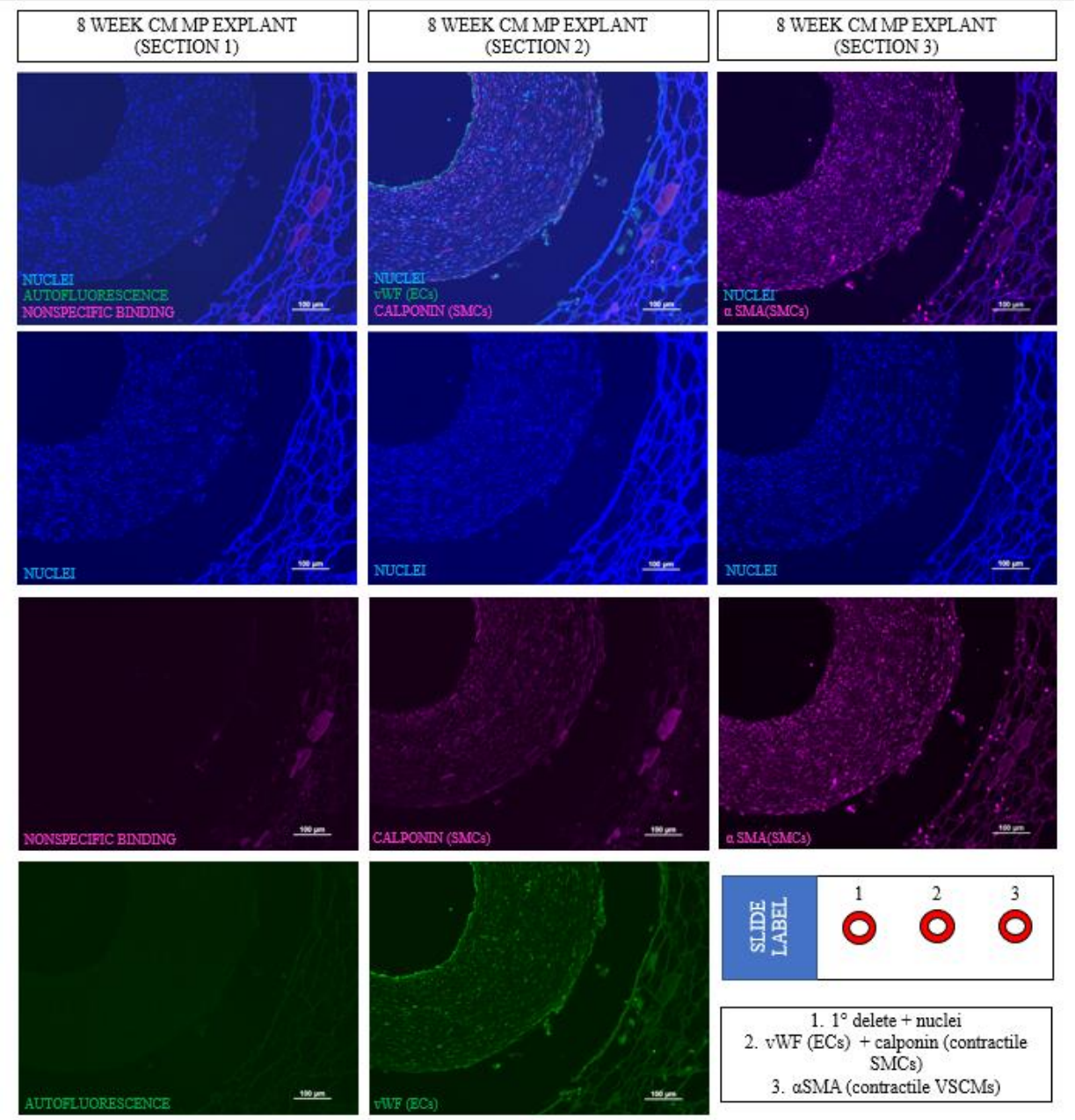

Figure 35. IFC imaging of 8 week CM MP explants.

IFC staining for SMCs (calponin and αSMA) and ECs (vWF) of the neotissue showed the presence of contractile type SMCs and an endothelial lining along the lumen. All slides were stained with secondary only (left column) to detect nonspecific binding. All three sections (shown in the lower left) were stained with DAPI to indicate cell nuclei.

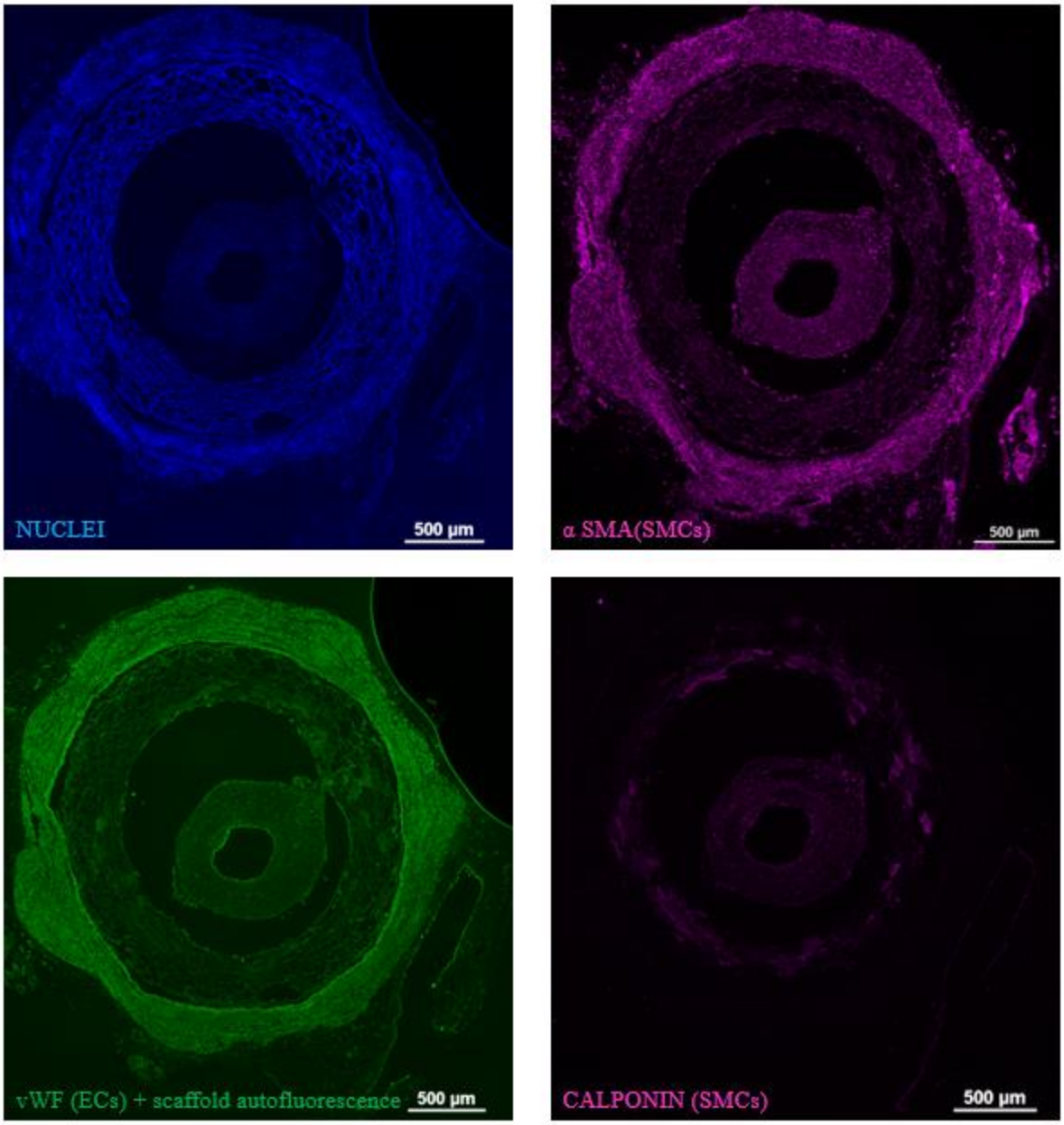

Figure 36. Cross sectional IFC of CM MP 8 week explants.

Three distinct layers were observed in the 8 week CM MP explants. Scaffold autofluorescence in the FITC and DAPI channels (left column) shows a clear outline of the three layers. VSMCs (calponin and αSMA shown in pink, left column), ECs (vWF shown in green, lower left), and nuclei (blue) were mostly detected in the neotissue and ES layers.

H&E staining confirmed cellularity within the neotissue and ES layer. VVG staining showed signs of early ECM deposition within the neotissue (**Figure 36**). As discussed in **Section 2.3.4**, neotissue appears to be "anchored" to the scaffold at localized points evident in both IFC and IHC staining (**Figure 35** and **36**). Luminal ingrowth remodeling was only observed in two of the 8-week explants (**Figure 31**), and both were occluded. Of the explants, luminal ingrowth and stenosis were indicators of graft failure.

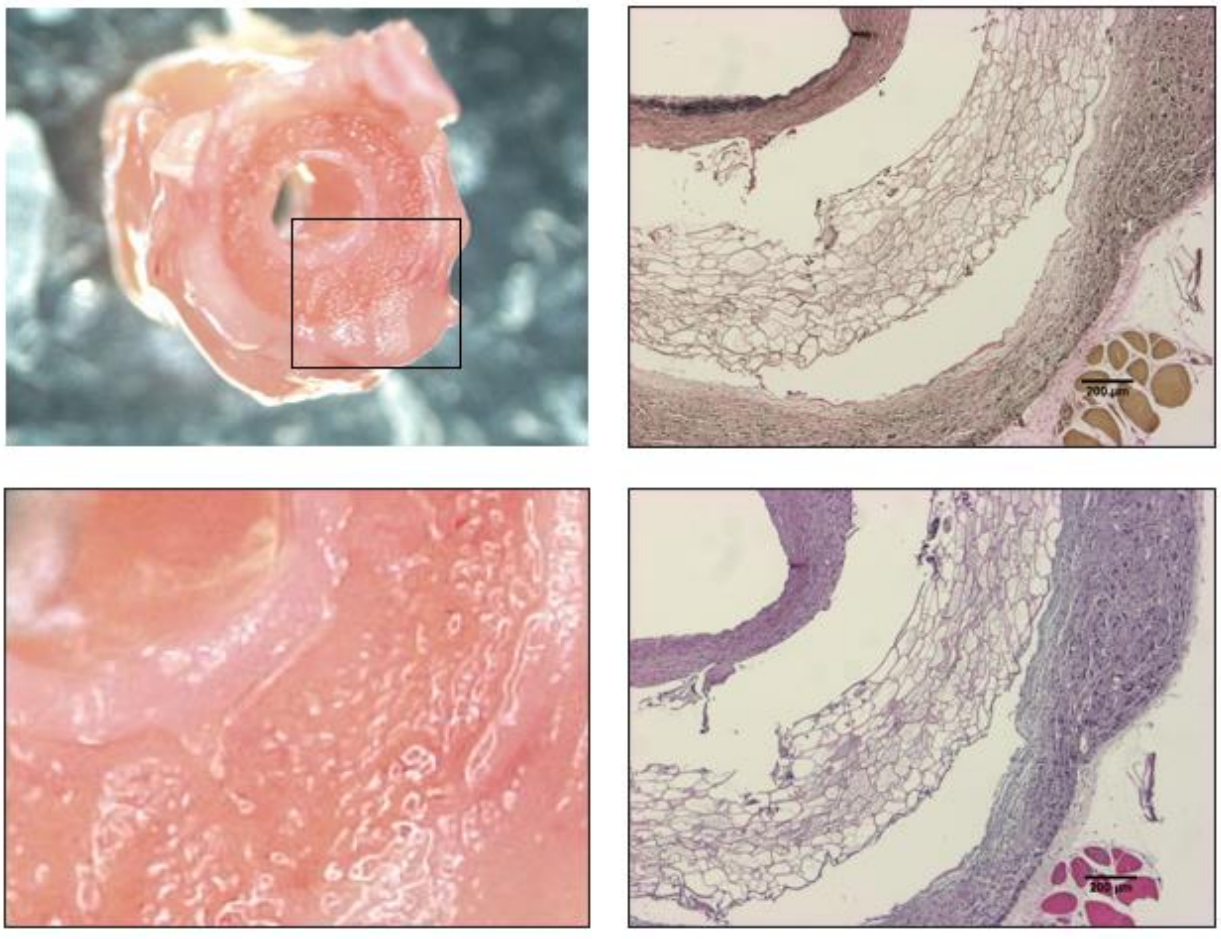

Figure 37. IHC analysis of neotissue formation within CM MP 8 week explants.

Neotissue formation was observed macroscopically (left images) as well as with H&E (bottom left) and VVG (top right) staining of a CM MP explant. Images showed cells within the neotissue and ES layers as well as early ECM deposition.

3.3 Discussion

In this study, we successfully loaded and released CM media from PLGA microparticles. A burst release of 3.7 μg/mg MP total protein was observed within the first 24 hours of release followed by no detectable amount after. Additionally, EV release from the MPs was confirmed using DLS demonstrating the successful loading and release of both free-floating proteins and vesicles from the MPs. No conclusions could be drawn from the scratch wound or proliferation assays due to limited sample size (n=1). In vivo, CM scaffolds appeared to remodel similar to CCL2 scaffolds. A significant increase in patency was observed ($p=0.0189$) with the delivery of CM MPs compared to Blank MPs. Of the five patent 8-week explants, four displayed severe stenosis confirmed through macroscopic imaging and IHC. A burst release of CM or CCL2 yielded a similar positive effect on acute patency after 1 week. Both graft types observed prevention of acute thrombosis but failed long term due mainly to stenosis. In this study, we were unsuccessful in reducing stenosis with the delivery of CM MPs in lyogel scaffolds. The potency of CM MPs in vivo may have been limited by insufficient cargo delivery or unintended components of CM being delivered resulting in dysfunctional TEVG remodeling.

The in vitro assessment revealed a burst release of cargo from CM MPs, but no additional release was seen beyond the 24 hour time point. Many labs studying the immune response to implanted materials have indicated two main stages with regards to biocompatibility: the initial attraction of immune cells (particularly macrophages within the first 3-7 days) followed by the polarization of the attracted cells towards a healing phenotype (after 5-10 days)[214,267,273,274]. In this study, we have successfully achieved an initial macrophage attraction observed through IFC staining (**Section 3.2.6**); however, the later polarization may not have occurred. This switch from a pro-inflammatory to anti-inflammatory macrophage environment is key in the progression of

TEVG remodeling. In particular, the inflammatory mediated healing depends on M2 macrophages attracting surrounding fibroblasts to aid in new ECM deposition and VSMC regulation[65,273]. In the transition from experimentation in Chapter 2 to 3 defined by shifting from CCL2 to CM MP, we aimed at dampening the M1 macrophage response and increasing M2 polarization through the delivery of the entire cell secretome. However, a more prolonged release of factors may be needed in order to fully mimic this cell signaling effect with our CM MPs.

Alternatively, the excessive stenosis and inflammatory responses observed in our CM MP scaffolds may be caused by the delivery of not only the cell secretome, but also culture media components. Previous studies have seen success with the inclusion of stem cells prior to implant and suggested that the role of these seeded cells is to signal for host cell immunomodulation and migration[19,20,65,116,250]. To mimic this signaling effect, we delivered CM in place of seeded cells in attempts to maintain the positive remodeling observed using seeded grafts without the need to the actual cells. However, delivery of conditioned media also means delivery of DMEM (Gibco, Gaithersburg, MD), FBS (Atlanta Biologics, Atlanta, GA), penicillin/streptomycin (Gibco), fungizone (Gibco), and dexamethasone (Gibco). The effects of delivering these components in vivo are unknown, and therefore the use of characterized media components could be considered in the future iterations of CM MPs.

Since the goal of CM MPs is to mimic the cell signaling effect of actual stem cells within a TEVG, further optimization to more closely match the in vivo vascular environment may result in a more similar secretome. For example, studies by Dr. Kent Leach and others have looked into the performance of stem cells after culture in varying levels of oxygen and serum[275-277]. These studies have found enhanced in vivo performance from cells cultured in hypoxic[276] and low serum conditions[275] (in bone tissue engineering applications). In a similar way, the conditioned media

could be further optimized with hypoxic conditioning to match the TEVG in vivo environment. Additionally, the excessive neotissue formation from VSMC activation may be an unintended side effect of delivering components of culture media, which are intended to enhance cellular migration and proliferation such as dexamethasone[278]. While the full characterization of cell signaling in vivo and in vitro is beyond the scope of this project, further optimization based on the desired bioactivity of the CM could address some of the excessive inflammation and vascular cell activation we observed within our implants.

3.4 Limitations and Future Directions

In summary, the use of CM MPs in lyogel scaffolds has shown some success in a rat but requires further optimization before translation into a larger in vivo model. The delivery of CM MPs within the lyogel TEVGs significantly increased patency when compared to Blank MPs after 1 week; however, no significant differences in patency were observed between CM MP, Blank MP, or lyogel groups after 8 weeks in vivo. The results within this study were limited by the lack of sustained CM release from the MPs, the use of lyogel in TEVGs, and the potency of the CM MPs.

A limiting factor of this study was the lack of sustained release from the MPs. Our current MP technology delivers a burst release of cargo to stimulate an initial host infiltration of macrophages and vascular cells, which then must take over the signaling and remodeling process. While an initial increase in patency was observed after 1 week, potentially in response to the burst release of CM, no sustained patency or positive remodeling effects were observed in the 8-week explants. Rather, a high rate of graft stenosis was observed in the 8-week explants, similar to the

results observed with CCL2 delivery in **Chapter 1**. The exact cause behind graft stenosis is unknown, however, many studies focusing on atherosclerosis and hyperplasia have indicated that macrophage polarization plays an important role in disease development and progression[279-281]. Studies[280-283] indicate a higher presence of M2 macrophages correlates to atherosclerosis regression and could potential be a target for future MP designs. A sustained release of CM timed to initiate an ideal M2 macrophage response may help reduce the occurrence of stenosis observed within the 8-week explants. A potential future direction includes the optimization of CM release from the loaded scaffold. In this case, a target release profile could be determined by assessing the retention and seeded cells within a scaffold and translating this time course to a release profile. Initial attempts towards this approach were made using ASC seeded PEUU scaffolds but were halted due low scaffold quality (**Section A.1**).

In addition to MP release optimization, the scaffold material itself must also be a consideration. Initial results from pilot studies (**Appendix A.2**) showed 100% graft occlusion due to acute thrombosis in response to an implanted lyogel scaffold, while the study in this chapter resulted in 100% patency after 1 week. This difference in results could be explained by two factors (rat age and surgical technique) which were discussed in **Section 2.4**. Additionally, a majority of the lyogel scaffolds showed signs of stenosis after 8 weeks indicating a negative host response to the material type itself rather than the MP treatment. Because of increased stenotic remodeling, the lyogel scaffold may need further optimization for use in TEVGs. Changes in both AA and BM percentages could yield a more appropriate material type. Alternatively, studies using BM silk alone have resulted in successful TEVGs without reported stenosis[15,125,149] indicating AA silk may be the cause of graft stenosis.

Lastly, this study was limited by the culture media components as mentioned in the discussion. A potential future direction could combine an early release CCL2 MP formulation (**Chapter 2**) with a later release of CM MP formulation – the aim of this approach would be to first attract host macrophage and then modulate the host macrophage response. Studies observing macrophage response to biomaterials have shown two main roles of macrophages: an early recruitment within the first days of implantations followed by a later (~1-2 weeks) polarization of the recruited cells towards an M2 phenotype[214,267,273,274]. Since increased early macrophage recruitment was observed within the CCL2 explants (**Section 2.6.7**) and previous studies from the VBL have shown positive remodeling at 8 weeks in response to seeded cells, this two-step macrophage modulation approach could be optimized with an initial recruitment of macrophages using CCL2 MPs combined with a later release of CM MPs.

Lastly, this study was limited by low n numbers due to the research restrictions during COVID-19. In progress/planned experiments which were incomplete include: (1) additional SMC as well as EC migration and proliferation assays using different batches of CM MPs, and the (2) determination of the CM MP loaded scaffold release profile using known factors within TEVG remodeling (CCL2, VEGF and uPA using ELISA kits).

Another future direction could focus on optimizing the CM itself. While the use of CM allows for entire cell secretome delivery, it also contains additional culture media components such as FBS, fungizone, and dexamethasone which may also play a role in host response. Complete purification of the intended secretome from the unwanted components could be achieved through EV isolation[226,284]. While this also eliminates free floating factors, some studies suggest the vesicles themselves play the most important signaling role due to their ability to transfer RNA, free floating proteins, and cell to cell surface signaling[226]. Additionally, the inclusion of a lipid

bilayer eliminates the need for PLGA encapsulation as the EVs themselves can adhere to the scaffold pores.

4.0 Chapter 4: EV Functionalized Silk Scaffolds

The first iteration of grafts in **Chapter 2** delivered CCL2 with the goal to promote a quicker inflammatory mediated remodeling response within the graft. However, the early delivery of cargo resulted in a corresponding early effect on patency but late term stenosis after 8 weeks in vivo. To broaden the MP effect, CM was delivered in Chapter 3 with the goal of maintaining the early patency increase observed with CCL2 (as CCL2 is present within CM) and adding additional signaling factors to induce a more wound-healing macrophage response. The delivery of CM resulted in a similar increase in patency, followed by prolonged inflammation and stenosis observed with the CCL2 grafts. Based on these results, Chapter 4 focused on providing a more robust signaling effect with increased biocompatibility between graft and host. To do this, a new MP cargo and scaffold were designed to address the biocompatibility limitations.

To increase the biocompatibility and robustness of the releasates being delivered, the PLGA MPs were replaced with purified EVs (as introduced in **Section 3.4**). The inclusion of EVs offered two distinct advantages over (1) the elimination of cell culture byproducts being delivered, and (2) a release profile which more closely mimics that of cells. As discussed in **Section 1.3.3.3**, there are three main classifications of EVs: microvesicles, exosomes, and apoptotic bodies. This study focused on the isolation of microvesicles and exosomes from the conditioned media. In Chapters 2 and 3, a custom blend of media was used based on total protein secretion detected in the CM. In Chapter 4, a new type of media was used (Protein Free RoosterNourish, RoosterBio) to eliminate supplemental proteins added by the manufacturer that cannot be filtered out. While most culture media contains FBS, this introduces unknown xenogeneic proteins as well as increased batch to batch variability which could affect the resulting EV isolate. Using a protein

free media ensures all isolated proteins intended for using are cellular secretions and not from culture media supplements.

Additionally, the scaffold material itself was also changed due to the excessive stenosis observed in response to lyogel scaffolds. Histology from the lyogel scaffolds used in Chapters 2 and 3 showed little to no cells within the porous scaffold after 8 weeks of remodeling. While a neotissue was observed, it was distinct from the scaffold itself, indicating a limited host cell infiltration into the scaffold pores. In addition, the use of EVs requires cell vacuum seeding, which causes graft rupture in lyogel scaffolds. To address both graft limitations, a different silk scaffold type was tested using only BM silk (see **Sections 1.3.1** and **2.0** for summary of the silk types considered in this thesis). Originally, AA silk was included in lyogel to increase RGD cell-binding sites; however, no increase in cellular adhesion was observed so it was eliminated from this study. Previous studies using only BM have been successful in recellularization and graft success, indicating BM silk alone is not only sufficient, but also easier to fabricate[15,16,149,285].

The following study outlines the fabrication, and in vitro/in vivo testing of EV functionalized BM silk scaffolds for use as a TEVG. A total of three groups were tested: MSC seeded, EV seeded, and unseeded BM silk scaffolds.

4.1 Methods

4.1.1 Cell Culture and EV Isolation

EV production and isolation were done in collaboration with Dr. Eoghan Cunnane – a postdoc in the VBL. RoosterBio (RoosterVial-hAD-1M MSC Lot #00097, RoosterBio) human

MSCs (P3) were cultured in growth media (RoosterNourish, SU0005, RoosterBio) in T175 flasks. Cells were then passaged into 5-layer tower flasks at 6M per flask in 75 mL growth media for 18 hours to allow for cellular adhesion. After 18 hours, growth media was removed, and cells were washed with 15 mL PBS. Harvest media (110 mL) was then applied consisting of protein-free basal media (SU006, RoosterBio) supplemented with 10% EV depleted fetal bovine serum (FBS centrifuged at 120,000 g for 18 hours at 4°C to remove EVs, Atlanta Biologics), 1% penicillin/streptomycin (5000U/mL, Gibco), 0.1% fungizone (amphotericin B, Gibco), and 10μL/L dexamethasone (Abcam). Cells were cultured in harvest media for 48 hours allowing cells to expand from 40% to 85% confluency. After 48 hours, the media was collected (now called CM). The remaining ASCs were used for the MSC seeded BM scaffold group.

EV isolation was done as described by Dr. Cunnane[286]. Briefly, CM was centrifuged at 250 x g for 20 minutes at 4°C to remove cells and large debris. The supernatant (CM free of debris) was then filtered (0.22 μm filters, Millex, Express PES low bind membrane) to remove any apoptotic bodies (**Section 1.3.3.3**) and split into six ultracentrifuge tubes (34 mL per tube, Polypropylene 25x89 mm, Beckman Coulter). Each tube was mounted into metal cases attached to a rotor (Sw28.1, 117.1g per case, Beckman Coulter) and centrifuged at 100,000 x g for 70 minutes at 4°C (L8-70M, Beckman Coulter) creating an EV pellet. The resulting supernatant (depleted CM, dCM) was removed and stored at -80°C until use. Any remaining supernatant was thoroughly drained from each tube by upturning each tube over a sterile drape and aspiration of remaining droplets. 100 μL PBS was added to each tube to resuspend pelleted EVs over 30 minutes with gentle agitation. The resuspended EVs were then diluted to 1 mL in PBS. The entire process yielded 1 μL EV isolate from 204 mL CM (n=3).

4.1.2 Scaffold Fabrication and Seeding

BM silk scaffolds were fabricated using the same protocol as lyogel scaffolds (**Section 2.1.1**), substituting lyogel silk solution with a 6% w/v BM silk solution in water for the inner layer. The resulting bilayered scaffolds have been previously characterized by the VBL[127]. BM silk scaffolds were stored in 80% EtOH at -20°C until use. Scaffolds were then washed 3 times in PBS for 10 minutes on a shaker plate before seeding.

MSCs and EV seeding was performed following established protocols within the VBL using our lab's custom rotation vacuum seeding device (RVSD)[17,19,20,88,250] (**Figure 39**). Previous studies have successfully seeded various cell types (ASCs[19], SVF[20,86], pericytes[250]) into PEUU scaffolds but not silk scaffolds. Seeding parameters including pressure, infusion volumes, and seeding times were adjusted to suit EV seeding into silk scaffolds. Briefly, scaffold mounts were made from catheter tubing (PTFE, 0.5mm ID, 1 mm OD, Aligent Technologies) cannulated with 10 μL pipette tips. Scaffolds were then secured to the mounts with 4-0 silk sutures (S-403, Sofsilk, Covidien). The mounts and scaffolds were then secured into the chamber of the seeding device, which was then sealed using an o-ring and clamps. Prior to cell seeding, each scaffold was infused with 500 μL of PBS to prime the infusion tubing. Scaffolds were then "pre-seeded" with 3 mL of PBS infused at 1 mL/min in order to wet the scaffold prior to EV delivery. During seeding, scaffolds were rotated manually, and a vacuum of -5 inHg was applied. After pre-seeding, a 1 mL EV isolate was prepared and used to prime (500 μL) and seed (500 μL) each scaffold under the same rotation and vacuum as pre-seeing. After seeding, the remaining EV suspension pulled transmurally through the scaffold and into the chamber was collected and re-seeded a total of five times.

Since this study was the first attempt to seed EVs into silk scaffolds, seeding efficiency was also measured to ensure successful EV incorporation with the RVSD. Seeding efficiency refers to the percent of EVs within the initial EV isolate that were successfully seeded into the graft. This value was assessed through total protein measurement of the EV isolate prior to seeding and the remaining unseeded isolate after seeding. A microBCA kit (Thermofisher) was used to determine total protein in each solution yielding a % protein seeded. Further confirmation of seeding was obtained using fluorescent staining and imaging of EVs following standard IFC protocols. For IFC, CD63 (1:100, 10628D, ThermoFisher) and Cy5 (1:100 ab_2340820, Jackson ImmunoReseach Laboratories Inc) were used to detect EVs.

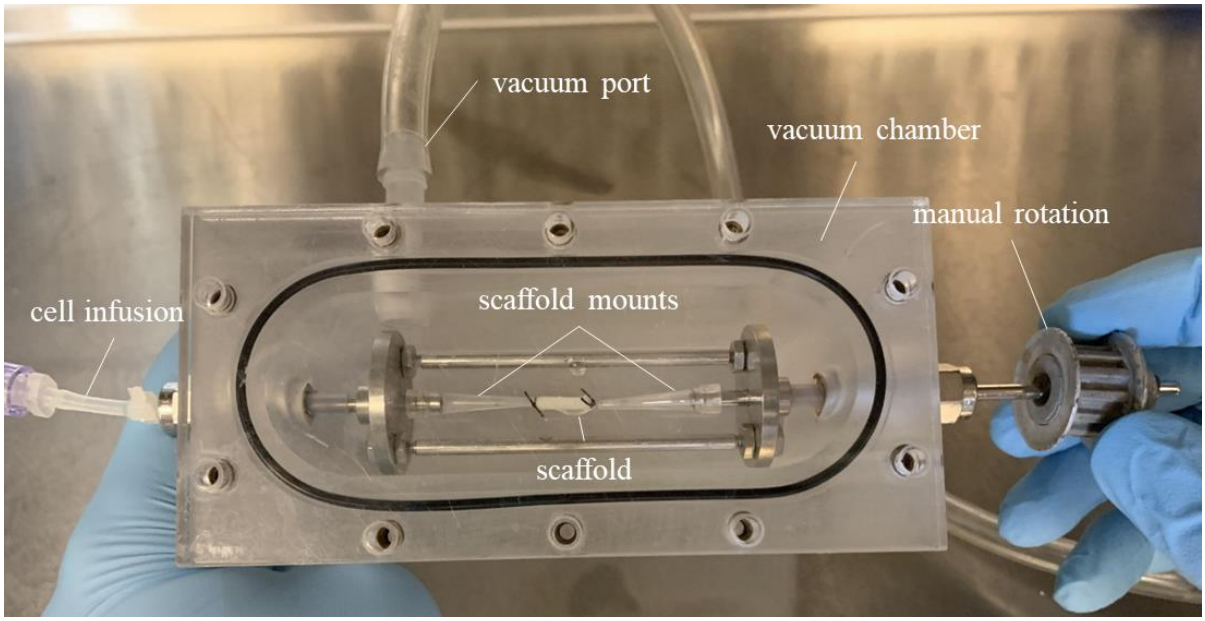

Figure 38. Depiction of the rotational vacuum seeding device.

Each scaffold was mounted into a vaccum chamber and injected with a cell or EV suspension under -5 inHg pressure. Scaffolds were rotated mannually to ensure even circumfrential distribution.

4.1.3 EV Characterization

EVs were characterized via three main measures: morphology (done by Dr. Cunnane), DLS (done by me and Dr. Cunnane), and total protein detection (done by me and Dr. Cunnane).

4.1.3.1 EV Morphology

To validate successful EV isolation, morphology was assessed by Dr. Cunnane using transmission electron microscopy (JEM-1011, JOEL, Center for Biologic Imaging, University of Pittsburgh) as described previously[286]. To summarize, 5 μL of EV isolate was dropped onto a 3 mm carbon coated grid followed by 5 μL of a 1% uranyl acetate solution to enhance contrast during imaging. Any excess liquids were removed with filter paper and the sample was analyzed.

4.1.3.2 DLS

80 μL of EV isolate was pipetted into a 8.5 mm cuvette (Brandtech Scientific). DLS was performed using the same protocol as outlined in **Section 3.1.3**. A total of n=3 samples (each difference batches of EV isolate) were assessed.

4.1.3.3 Total Protein Release from the EV Isolate

Samples of 1:9 dilution of EV isolate in PBS (regular) or sodium dodecyl sulfate (SDS, 2% in PBS, lysed) were prepared. Samples were then vortexed for 30 seconds prior to use to ensure vesicle lysing and homogenous mixing. Total protein was measured using a BCA following the same protocol in **Section 3.2.1**. Separate standard curves were measured in triplicate for the regular and lysed samples. The regular standards were suspended in PBS and lysed in 2% SDS. Samples were quantified using the corresponding standard.

4.1.4 SMC and EC Migration

Scratch assays using both SMCs (#PCS-100-012, ATCC) and ECs (#300-05a, Cell Applications Inc.) were performed to observe the effect of EVs on cellular migration. For each assay, SMCs or ECs were plated into 24 well plates (50k/well for SMCs and 90k/well for ECs) in 2 mL cell-specific growth media (**Section 4.2**) and allowed to adhere overnight. After cell adhesion, 1 mL pipette tips were dragged vertically along the bottom of the plate, creating a linear wound across the cells. The media was then removed (along with floating scraped cells), and treatment of 350 μL unsupplemented basal media (cell-specific) and 150 μL EV isolate was applied to each well (run in triplicate). The plate was then mounted into a stage top incubator (Tokai Hit Co.), maintaining 37°C and 5% CO_2 culture conditions during imaging. Wells were imaged hourly using an inverted Nikon TiE fluorescent microscope (Nikon) and NIS Elements Software (Nikon). Wound closure was quantified following the same protocol used in Section XX and outlined in **Appendix A.5** and analyzed after 24 and 48 hours. A total of five treatments were tested from n=3 batches of CM EV isolate: cell-specific unsupplemented basal media (UBM, negative control), PBS (negative control), 50μL EV isolate + 100 μL PBS (EV50), 150 μL EV isolate (EV150), and supplemented cell-specific basal media (SBM, positive control). Statistical significance between groups was performed using GraphPad Prism 8 (GraphPad Software). Normality was assessed using Shapiro-Wilk tests before analysis. After normality was assessed, significant differences in migration between groups were determined using 2-tailed unpaired t-tests (normally distributed data) and exact 2-tailed Mann-Whitney U-tests (non-normal data). One-way ANOVAs were used to determine significance between more than two groups of variables. For all tests, $p<0.05$ was considered significant.

4.1.5 SMC and EC Proliferation

Proliferation assays were also run using ECs (Cell applications) and SMCs (ATCC) at P4. Cells were plated into 48 well plates coated in collagen. To coat wells, collagen (type I rat tail collagen A10483, Gibco) was mixed in 0.02 M acetic acid at 50 μg/mL. 500 μL of the collagen solution was then placed in each well and incubated at room temperature for 1 hour before thorough washing with PBS. SMCs and ECs were plated at 4k and 5k per well, respectively, in cell-specific growth media and allowed to adhere overnight. After cellular adhesion, cell quantity at time 0 was determined using Alamar blue (DAL 1100, Invitrogen, Carlsbad, CA) diluted 11:1 in BM. 330 μL of the diluted solution was applied to each well and incubated at 37°C and 5% CO_2 for 4 hours. After incubation, 100 μL from each well was transferred to a 96 well plate, and the absorbance was measured according to the manufacturer's protocol (570/600 nm). Readings were then normalized to blank wells. Well plates containing the remaining cells were washed with PBS, and treatments were applied (Section 4.2.2) for 24 hours before re-analysis. All 24-hour readings were normalized to the initial time 0 reading for that well to account for a base number of cells. Significance was determined using the same method as cellular migration (**Section 4.1.4**).

4.1.6 In Vivo Evaluation of EV and MSC Seeded BM Silk Scaffolds

Three scaffold types were assessed for 8 weeks as abdominal aortic grafts following the protocol in **Section 2.3**: EV seeded BM silk scaffolds (EV, n=16), RoosterBio MSC seeded BM silk scaffolds (ASC, n=10), and BM silk scaffolds (BM, n=11). After 8 weeks, patency was determined through angiography (**Section 2.3**), and remodeling was observed through histology (**Section 2.3.3**).

Explants were analyzed using IFC and IHC (**Section 2.3.3**). Sections from each medial portion were analyzed for cell phenotype and ECM content (IFC performed by myself and Dr. Cunnane and IHC at the MIRM Histology Core, **Section 2.3.3**).

4.1.7 Elastin and Collagen Quantification

Insoluble elastin and collagen content of explanted TEVGs were quantified by Dr. Aneesh Ramaswamy using ninhydrin and hydroxyproline assays. Two small rings of tissue were isolated from the proximal and distal portions of the explanted graft for analysis. Soluble and insoluble elastin content of each tissue sample (normalized to weight) was then measured using previously established protocols[87,287].

4.2 Results

4.2.1 EV Characterization

TEM imaging performed by Dr. Cunnane displayed successful detection of EVs (**Figure 39**). TEM showed distinct cup like circular particles characteristic of vesicles[284]. Examples of the cup structures are indicated by the white arrows in **Figure 39**.

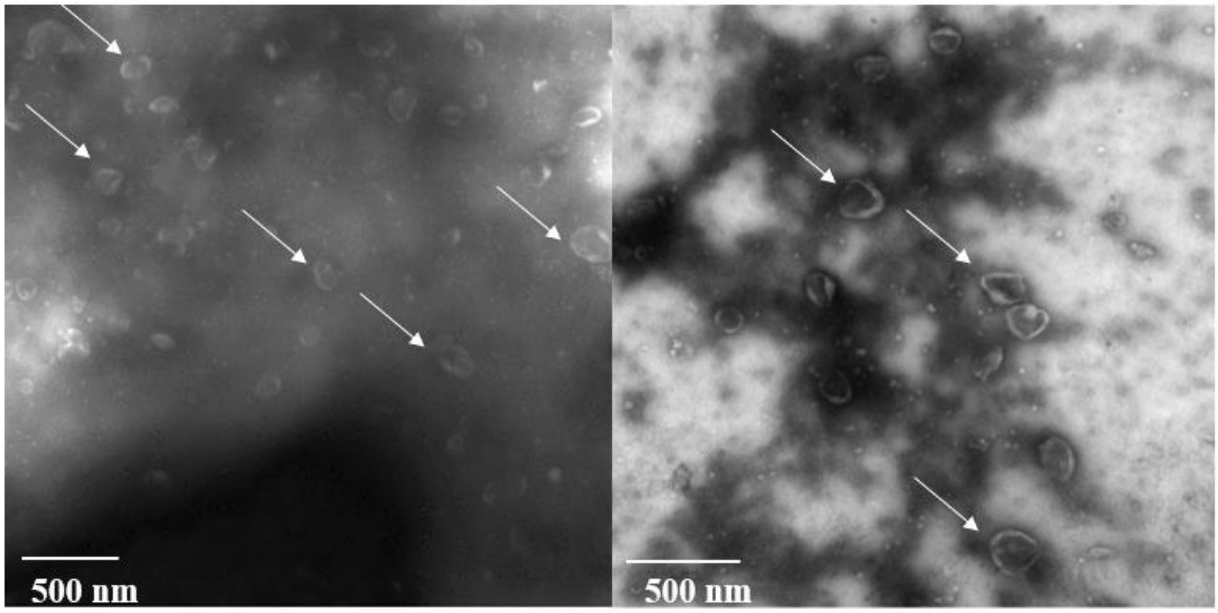

Figure 39. TEM imaging of EV isolate.

TEM imaging of the EV isolate showed distinct EVs as cup like particles. The overall size (~40 μm) indicates the imaged Evs are within the exosome and microvesicle size range[286].

Further characterization using DLS showed two distinct particle sizes: 42.67±4.09 and 215.94±34.78 nm, which correspond to exosomes and microvesicles, respectively (**Figure 409**).

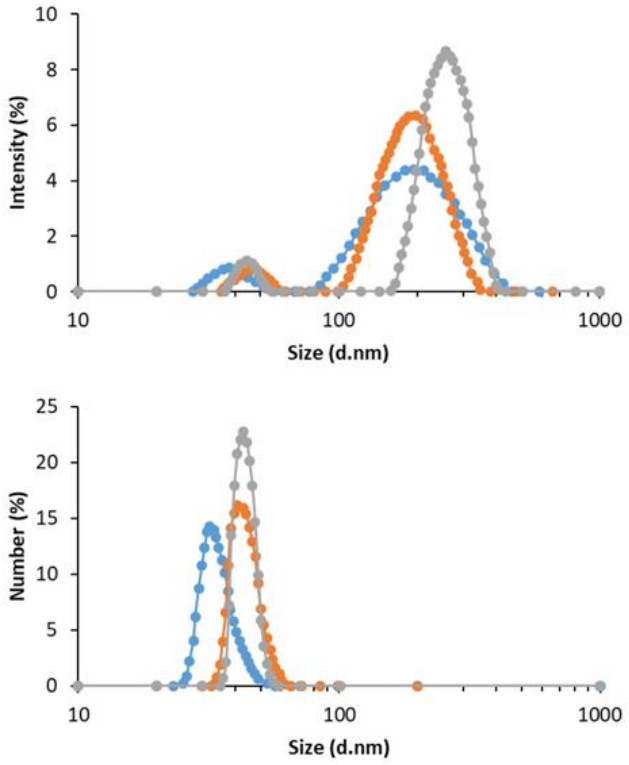

Figure 40. DLS detection of EVs.

DLS analysis of the EV isolate showed a population of exosomes (42.67±4.09 nm OD) and microvesicles (215.94±34.78 nm OD) within the isolate[286].

BCA analysis for total protein within the unlysed and lysed EV isolates resulted in 159.31±5.03 and 170.47±3.58 µg/mL of protein detected (**Figure 41**). This increase in protein due to lysing confirms the encapsulation of proteins within the vesicles themselves.

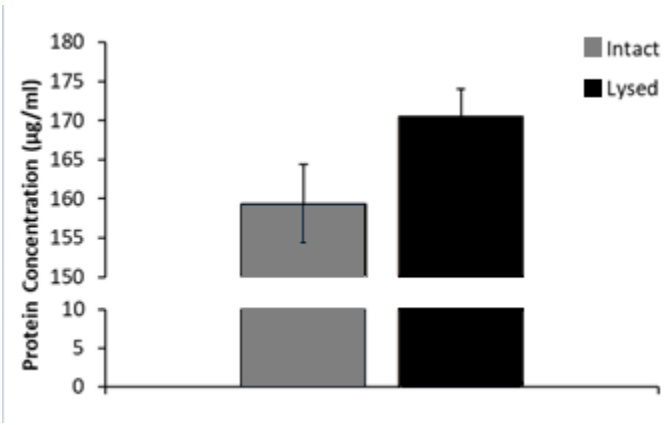

Figure 41. Total protein within the EV isolate.

Total protein increased after lysis indicating release of protein content from within the EVs[286].

4.2.2 EV Seeding

Previously published studies from the VBL have confirmed the successful seeding of ASCs into BM[127] and PEUU scaffolds[20,86,250]; however, EV seeding was first attempted in this study. All previous studies determined seeding efficiency by counting the number of cells within the isolate before and after seeding; however, this method could not be used in this study due to the small size of Evs. To determine efficiency, the total protein within the unseeded EV isolate was measured using a BCA following the manufacturer's protocol (**Section 3.1.2**), resulting in 45.69% of the total protein content from the EV isolate successfully seeded. IFC staining of seeded scaffolds showed successful incorporation of Evs throughout the entire porous layer of the construct (**Figure 42**).

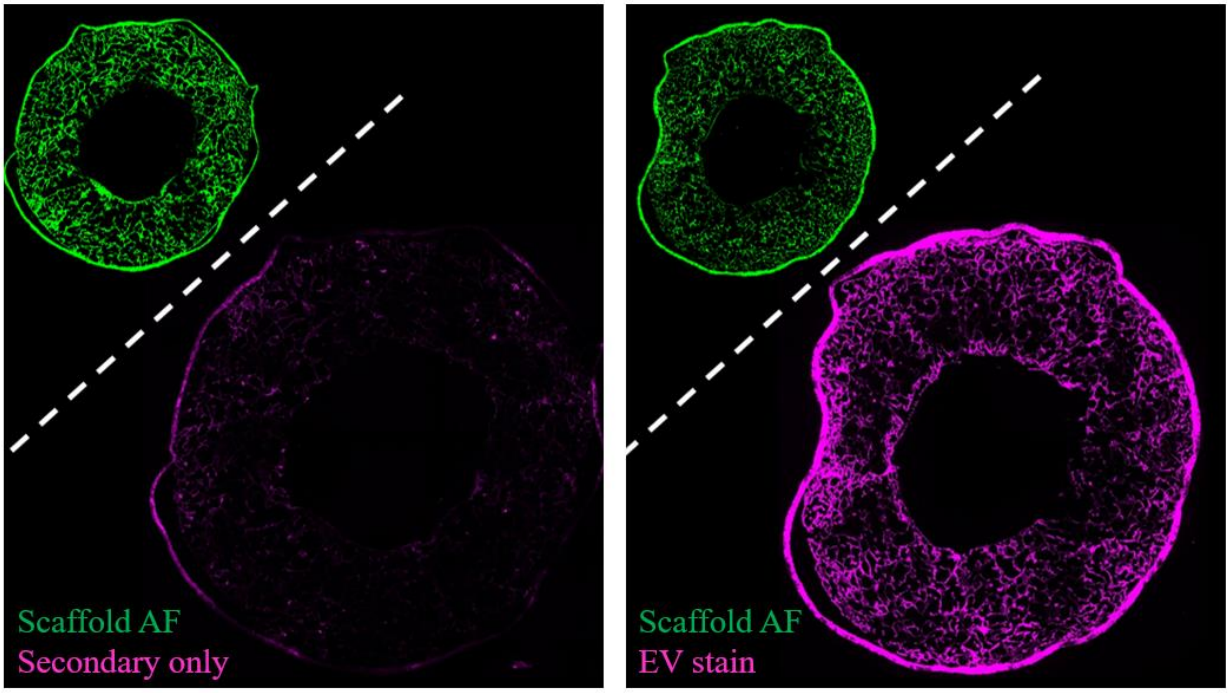

Figure 42. EV seeded scaffold IFC.

Left: staining of a seeded scaffold without a primary to detect any non-specific binding. Right: staining of an EV seeded scaffold showed homogeneous seeding throughout the porous layer of the scaffold. Pink indicates stained EVs and green indicates scaffold autofluorescence (AF)[286].

4.2.3 SMC and EC Migration

A significant increase in SMC migration was found in the EV50 group versus PBS (p=0.0209) and EV150 group versus PBS (p=0.0013). Similarly, a significant increase in EC migration was observed in the EV50 group versus PBS (p=0.047) and EV150 group versus PBS (p=0.0028) (**Figure 42**).

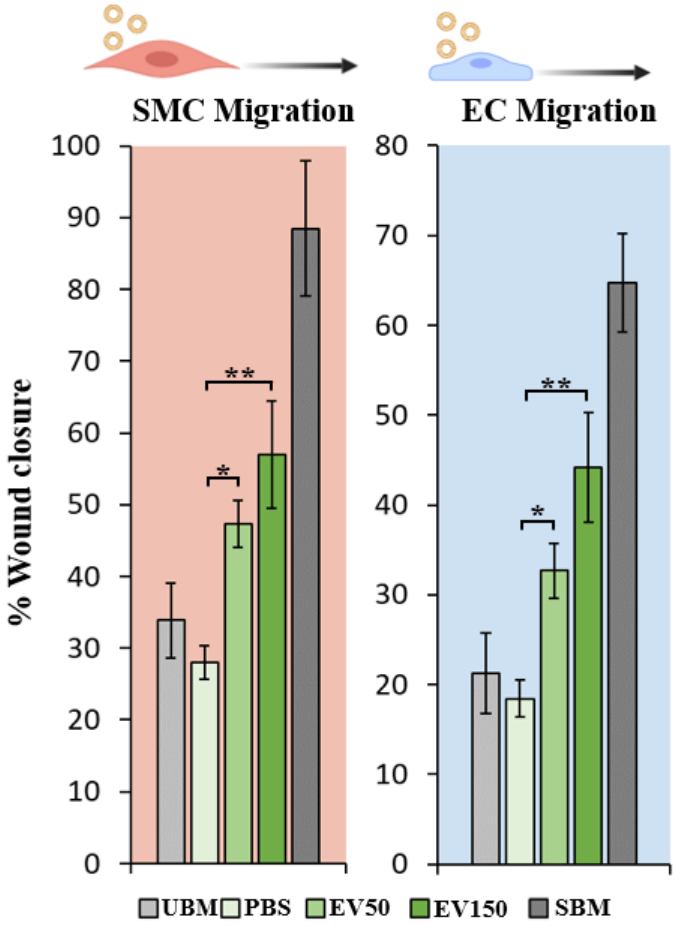

Figure 43.SMC and EC migration assay

Scratch assays showed a dose dependedent increase in cellular migration in response to EVs[286].

4.2.4 SMC and EC Proliferation

A significant increase in SMC proliferation was observed between PBS and EV150 ($p<0.0001$). A similar increase in EC proliferation was found from PBS to either EV50 ($p=0.0011$) or EV150 ($p<0.0001$) (**Figure 44**).

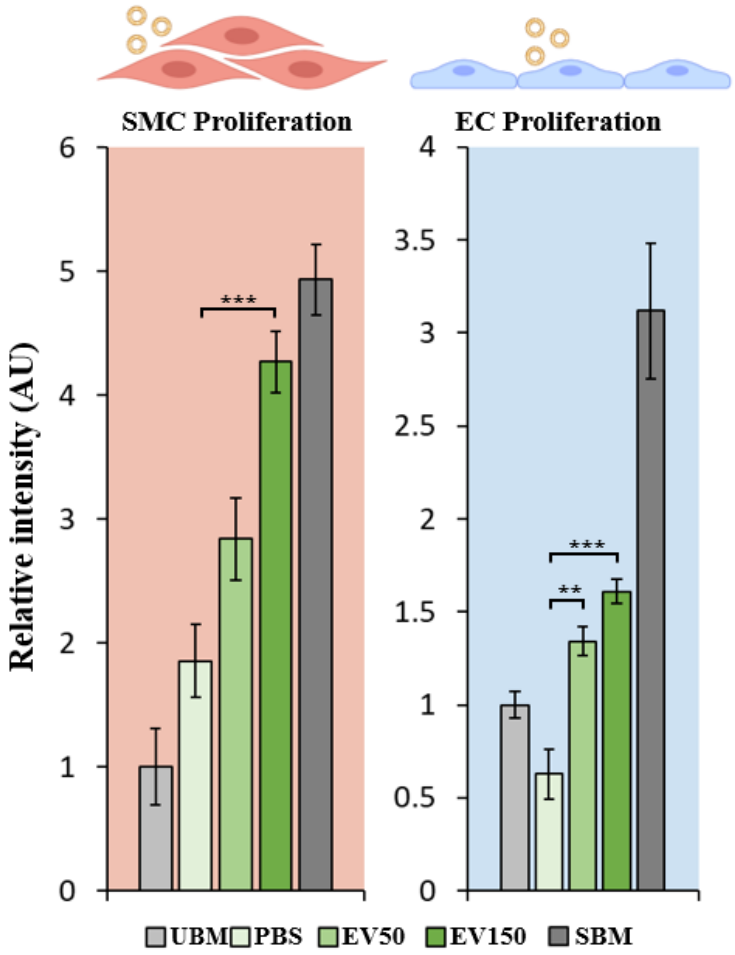

Figure 44. SMC and EC proliferation assays.

Both SMC and EC proliferation increased significantly between PBS and EV150 treatment[286].

The combined promotion of SMC and EC migration and proliferation in response to EVs suggests potential host cell chemoattractant and mitogenic roles in vivo. To test this possibility and the efficacy of EVs as a payload for our TEVG, EVs were seeded into BM silk scaffolds and assessed in vivo.

4.2.5 8-week Patency Results

Patency results showed 56% (9/16), 81% (9/11), and 100% (10/10) patency in the MSC, BM, and EV groups, respectively. A significant difference in patency was found between the MSC and EV groups (p=0.0189, **Appendix A.3**, **Figure 45**). A total of two BM TEVGs was not patent due to intimal hyperplasia. A total of seven MSC grafts failed, 3 due to acute thrombosis and 4 due to intimal hyperplasia.

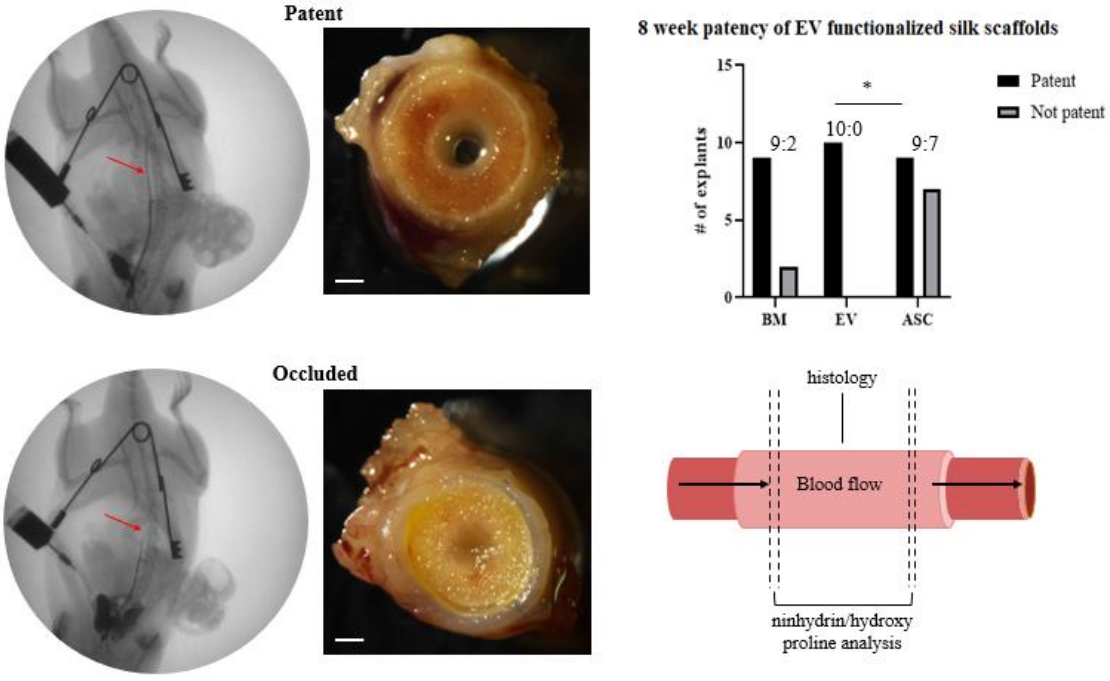

Figure 45. Patency rates of the EV functionalized BM silk scaffolds after 8 weeks.

Patency of the grafts after 8 weeks were determined through angiography (left) and cross-sectional images (middle). Patency rates showed significantly higher patency rates in the EV seeded scaffolds (p=0.0437)[286].

4.2.6 TEVG Remodeling and Histology

Medial portions of the grafts were macroscopically imaged to observe any signs of stenosis (**Figure 44**). Explants showed no obvious signs of stenosis in the cross-sectional imaging (**Figure 46**). One of the blank explants showed signs of dilation, possibly due to loss of mechanical strength as the ES layer degraded.

Histology showed similar remodeling in all grafts remaining patent until 8 weeks (**Figure 47**). Neotissue formation containing VSMCs and endothelium was detected in all groups. VVG staining showed early elastic fiber formation, and picrosirius red (PSR) staining showed aligned collagen fibers within the neotissue. IFC and IHC staining revealed VSMCs, ECs, collagen (PSR), elastin (VVG), and overall cellular infiltration (H&E) in each of the three groups after 8 weeks (**Figure 47**). Qualitative assessment showed a higher level of VSMCs (αSMA and Calponin) within the EV functionalized group when compared to both the BM and MSC groups. Additionally, an incomplete endothelium (vWF) was observed within the MSC group indicating insufficient remodeling. The highest level of cellularity was observed within some of the EV functionalized group (H&E) as well as the most elastin formation (VVG) which could suggest a greater degree of positive remodeling. Lastly, a lower level of macrophages (CD68) were observed in the EV group suggesting no prolonged inflammatory response. Overall, the higher cellularity (H&E), elastin (VVG), VSMCs (αSMA and calponin), and full endothelium (vWF) combined with the lowered macrophage presence (CD68) indicates a further level of remodeling within the EV group compared to CM and MSC groups.

Figure 46. Macroscopic imaging of the 8 week explants.

Cross-sectional images of the 8 week MSC seeded (top three rows), blank silk (middle two rows), and EV seeded (bottom two rows) showed varying levels of remodeling within each group. (patent = green border, not patent = red border).

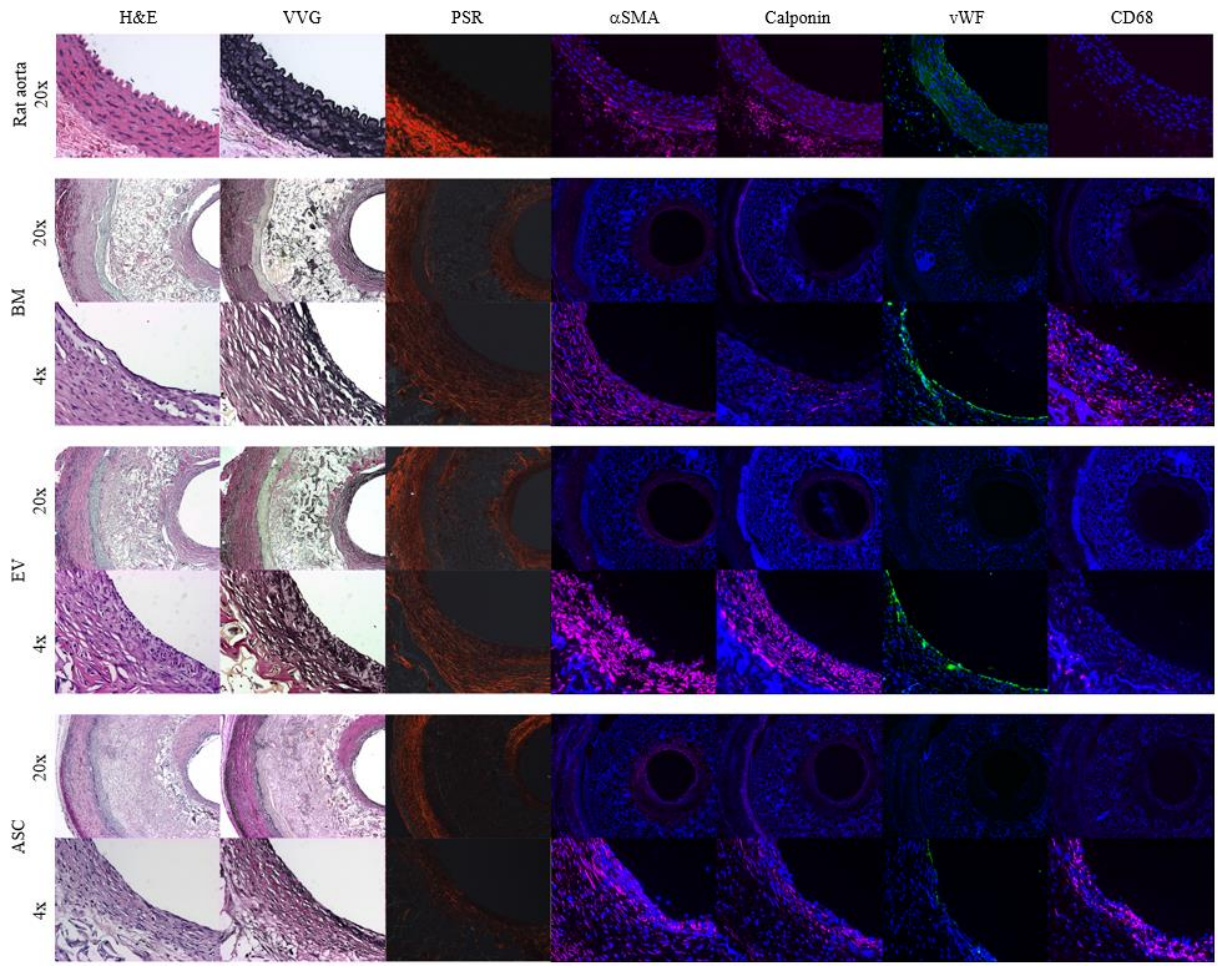

Figure 47. Histology of the explants

IHC (H&E and VVG columns) and IFC (PSR, αSMA, calponin, vWF, and CD68 columns) staining were used to observe graft remodeling after 8 weeks. All groups showed signs of cellular neotissue formation (H&E) and elastic fiber formation (VVG). A qualtitatively higher level of staining was observed in the αSMA, calponin and vWF stains within the EV seeded group possibly indicating a higher level of remodeling. A qualitatively lower amount of macrophages (CD68) was observed in the EV group possibly incdicating a more progressed remodeling stage in comparison to the CM and ASC groups.

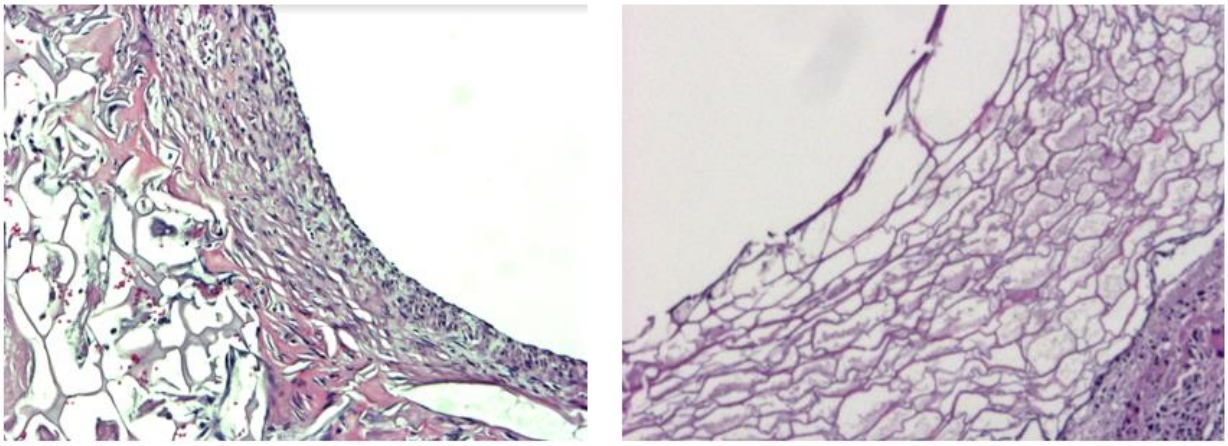

Figure 48. H&E of EV BM silk vs. CM MP lyogel silk 8-week explants

EV functionalized BM silk scaffolds showed greater cellular infiltration into the scaffold pores (left) compared to CM MP lyogel silk scaffolds (right) after 8 weeks in vivo.

4.2.7 Elastin Quantification

Results showed a significantly higher amount of elastin and collagen (126.46% p=0.0015 and 44.59% p=0.0386, respectively) in the EV group compared to UBM. No significance was determined between the ASC and BM groups (**Figure 49**).

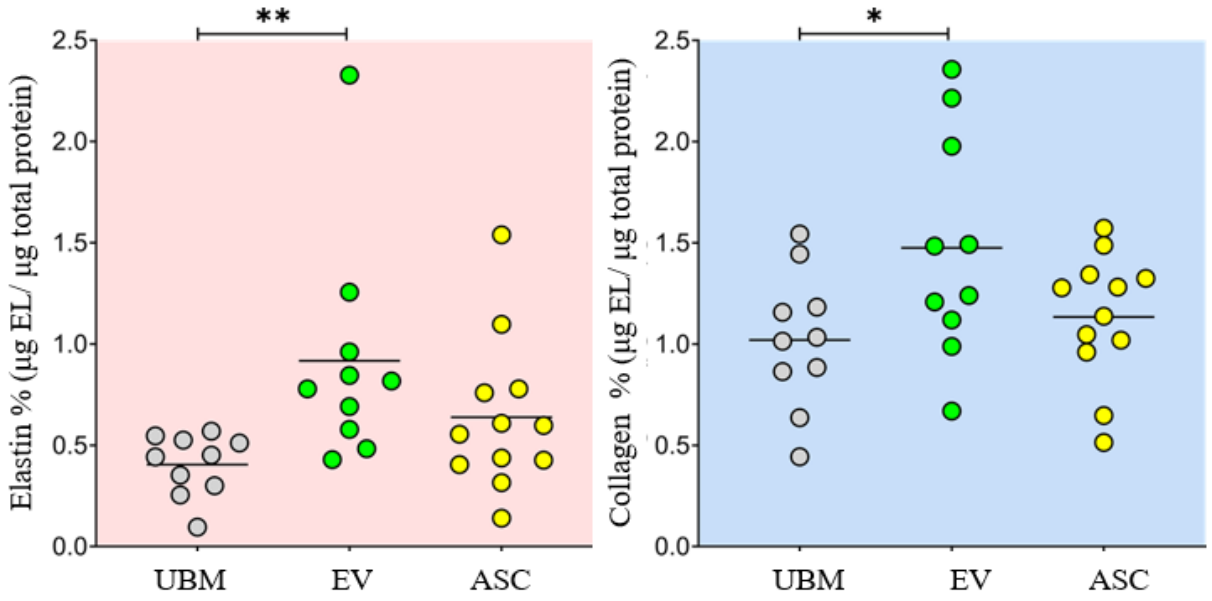

Figure 49. Ninhydrin and hydroxyproline assays were used to quantify ECM within the explant grafts[286]. Significantly more elastin (126.46, p=0.0015) and collagen (44.59%, p=0.0386) was observed in the EV group compared to the UBM.

4.3 Discussion

This chapter attempted to assess the viability of an EV functionalized silk based vascular graft. EVs were isolated from ASCs and tested for in vitro bioactivity. A significant increase in SMC and EC migration and proliferation was observed in response to EVs in comparison to PBS, indicating a positive pro-remodeling potential. Bilayered BM scaffolds were successfully fabricated, seeded with EVs, and implanted into a rat aortic model for 8 weeks. Angiography at explant showed a patency rate of 56%, 81%, and 100% for the ASC, BM, and EV groups. The delivery of EVs was successful in increasing patency and reducing stenosis in comparison to both

BM and ASC groups. Histology showed positive remodeling based on neotissue formation (VSMCs, ECs, and ECM present) in all groups without the obvious signs of stenosis observed in the TEVGs assessed in **Chapters 2** and **3**. Additionally, overall cellularity within the remaining scaffolds at 8 weeks increased in comparison to results from Chapters 2 and 3, indicating increase biocompatibility within this iteration of TEVGs. Two main changes were observed within EV seeded BM and lyogel explants from **Chapters 2** and **3**: increased cellularity within the scaffold pores and decreased stenosis after 8 weeks.

From the previous studies, the scaffold material and cargo incorporated into the scaffold were changed resulting in an increased overall biocompatibility; however, since multiple components were modified, the exact cause of behind the remodeling changes was difficult to isolate. However, when comparing the lyogel to BM silk alone after 8 weeks in vivo, a qualitative increase in cellular infiltration into the porous layer of the scaffold was observed in the BM graft (**Figure 50**). The lyogel silk explants all contained distinct boundaries between the neotissue formation and scaffold layer whereas the BM explants showed integration of the neotissue into the scaffold itself. This increase in cellularity without any treatment indicates the effect was due to the material itself rather than the treatment.

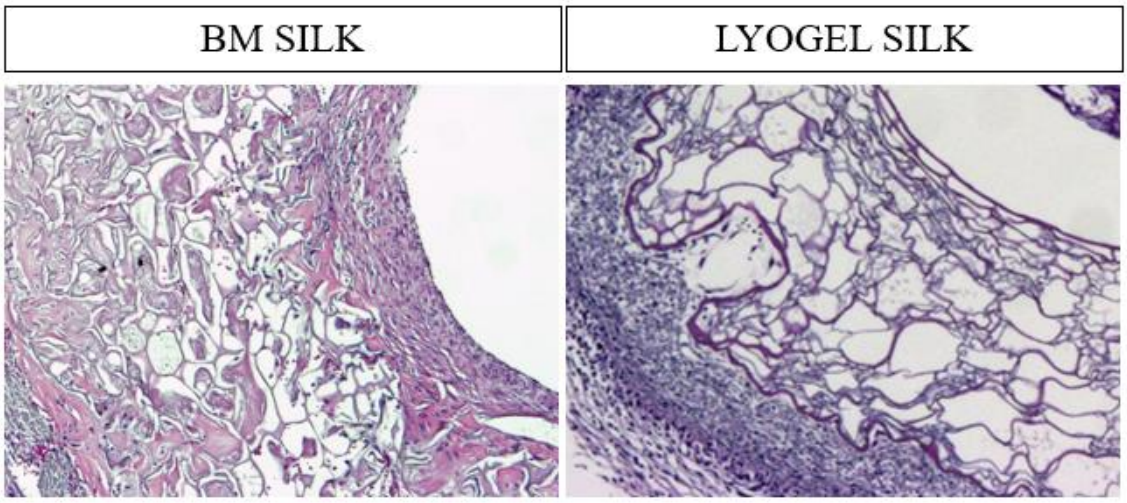

Figure 50. H&E of BM vs. Lyogel scaffolds after 8 weeks in vivo.

Initially, AA silk was utilized because of its RGD binding sites[127] to increase the potential for cellular migration and binding to the scaffold. The in vivo assessment of AA silk appears to have had the opposite effect by preventing cellular migration. This unexpected effect may be due to changes in pore interconnectivity between lyogel and BM silk or decreased luminal porosity of the lyogel scaffolds due to gelation in contact with the metal rod. Additional analysis of BM vs. lyogel porosity, pore interconnectivity, seeding, and cellular binding would be needed to gain a clearer picture of host cell infiltration.

The second difference, decreased stenosis, may be due to a decreased inflammatory response to the scaffold material and treatment. In particular, the BM silk scaffolds alone showed no signs of stenosis, while the lyogel scaffolds alone showed nearly 100% stenosis (**Figure 51**). This decrease in stenosis between lyogel and BM silk may be due to an altered immune response to the material type. While an initial immune response to any implanted graft should be characterized by an influx of macrophages, a later stage immune response (after 8 weeks) should show a decrease in macrophage presence. The inclusion of RGD binding sites within the lyogel

scaffold could have increased immune cells binding and caused a prolonged presence within the scaffold. Lastly, the decrease in stenosis could be a result of material property changes, particularly differences in scaffold stiffness and compliance, which could be determined with additional scaffold testing.

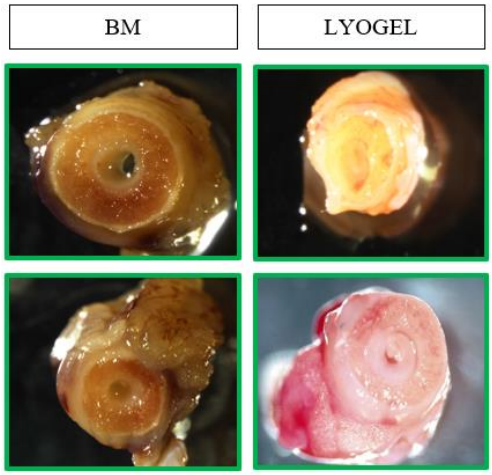

Figure 51. Cross sections of BM vs. lyogel silk scaffolds after 8 weeks in vivo.

Cross sectional images of BM silk vs lyogel silk scaffolds after 8 weeks show increased stenosis in the lyogel groups. A distinct lumen can be seen in within the BM silk grafts while a nearly occluded lumen is less visible in the lyogel grafts.

Overall, the EV functionalized BM silk scaffolds produced a patent, remodeled graft with positive neotissue formation after 8 weeks in vivo. Based on the patency, histology, and ECM characterization, EV BM scaffolds are a promising option for TEVGs. EVs offer a cell-free graft option while still leveraging the immunomodulatory effects of cell-seeded grafts.

4.4 Limitations and Future Studies

The main limitations to this study were the few timepoints observed in vivo and the healthy animal model chosen. An 8-week timepoint was chosen for in vivo studies in order to observe remodeling within a reasonable timeframe but this single timepoint fails to capture the initial host response and the long-term remodeling that would happen in a patient. Based on the promising result of this study, longer timepoints would provide information such as a timeline for full scaffold degradation, the potential of late-term stenosis, and mature ECM deposition. In addition to later timepoints, an earlier timepoint assessing the inflammatory response to EV functionalized TEVGs would provide information on the mode of graft remodeling and the host response to the EVs. While 1-week explants were included within **Chapters 2 and 3**, they were not assessed in this study due to time and cost restraints. In general, additional shorter timepoints to observe inflammation and longer timepoints to observe potential stenosis could further demonstrate the potential of EV functionalized BM silk scaffolds before testing in a larger, more expensive animal model.

These studies were also limited by the healthy model chosen. A healthy model was chosen to observe the initial potential of EV functionalized BM silk scaffolds, however, as previously discussed, the graft remodeling response is likely to vary in patients with comorbidities such as diabetes. To fully understand the potential TEVG remodeling within appropriate cohorts, the grafts should be tested in more appropriate recipients such as aged and diabetic rats (**Section 2.4**). This inclusion of high-risk cohorts and longer in vivo durations would provide a better idea of graft viability before scaling up to a more clinically relevant model.

Additional studies should also investigate different sources of EVs. Since EV application in tissue engineering is a newer field of study, no single established protocol exists for EV

isolation[284]. Because of this, additional studies testing different cell types, culture environments (hypoxia), and isolation techniques should be tested geared towards TEVG application. Similar to CM, EV signaling has been shown to change in response to culture conditions[288]. Changes in EV concentration, size, morphology, and surface markers have been observed with hypoxia[289] and must, therefore, be optimized based on the intended function.

Lastly, EV translation to a clinically relevant quantity must be considered. Current methods for EV isolation are labor and cost-intensive, yielding relatively small quantities of vesicles as displayed in this study. To translate this technology, a method for EV storage must be explored to create a stock of EVs prior to seeding. The motivation behind using RoosterBio cells throughout the entirety of this dissertation was to provide an easier path for clinical translation. Further studies towards clinical translation have been discussed with RoosterBio and potential collaborations including developing methods of EV freezing, EV viability before and after storage (SMC migration, protein content), and batch to batch variability after thawing.

5.0 Chapter 5: Additional Contributions to TEVG Translation

This chapter focuses on three collaborations focusing on different TEVG designs that the author contributed to over the course of this dissertation. These projects focused on the development and testing of a cell seeded PEUU construct (**Section 5.1**), a cell seeded large animal sized PEUU construct (**Section 5.2**), and a cell seeded silk based construct (**Section 5.3**).

A previous area of focus in the VBL has been the development of a TEVG using a cell-seeded PEUU construct[17,19,88,250]. Previous studies have used muscle derived stem cells (in collaboration with Dr. Johnny Huard)[17], pericytes (in collaboration with Dr. Huard)[250], adipose derived stem cells[19,115] (in collaboration with Dr. Kacey Marra and Dr. Peter Rubin), and the stromal vascular fraction (SVF)[86] (in collaboration with Dr. Marra and Dr. Rubin) seeded into a bilayered, PEUU scaffold (developed in collaboration with Dr. William Wagner). These scaffolds were fabricated following the paradigm shown in **Figure 52** to produce a rapidly seeded, autologous graft. The first study (**Section 5.1**) was aimed at streamlining this paradigm to produce an autologous, SVF seeded PEUU scaffold that could be fabricated within 24 hours. The work within this study was performed in collaboration with Dr. Darren Haskett (experimental design, in vitro assays, and in vivo surgeries), Dr. Marra and Dr. Rubin (SVF isolation and characterization), Dr. Wagner (PEUU scaffold fabrication), and the author (graft implantation, histology).

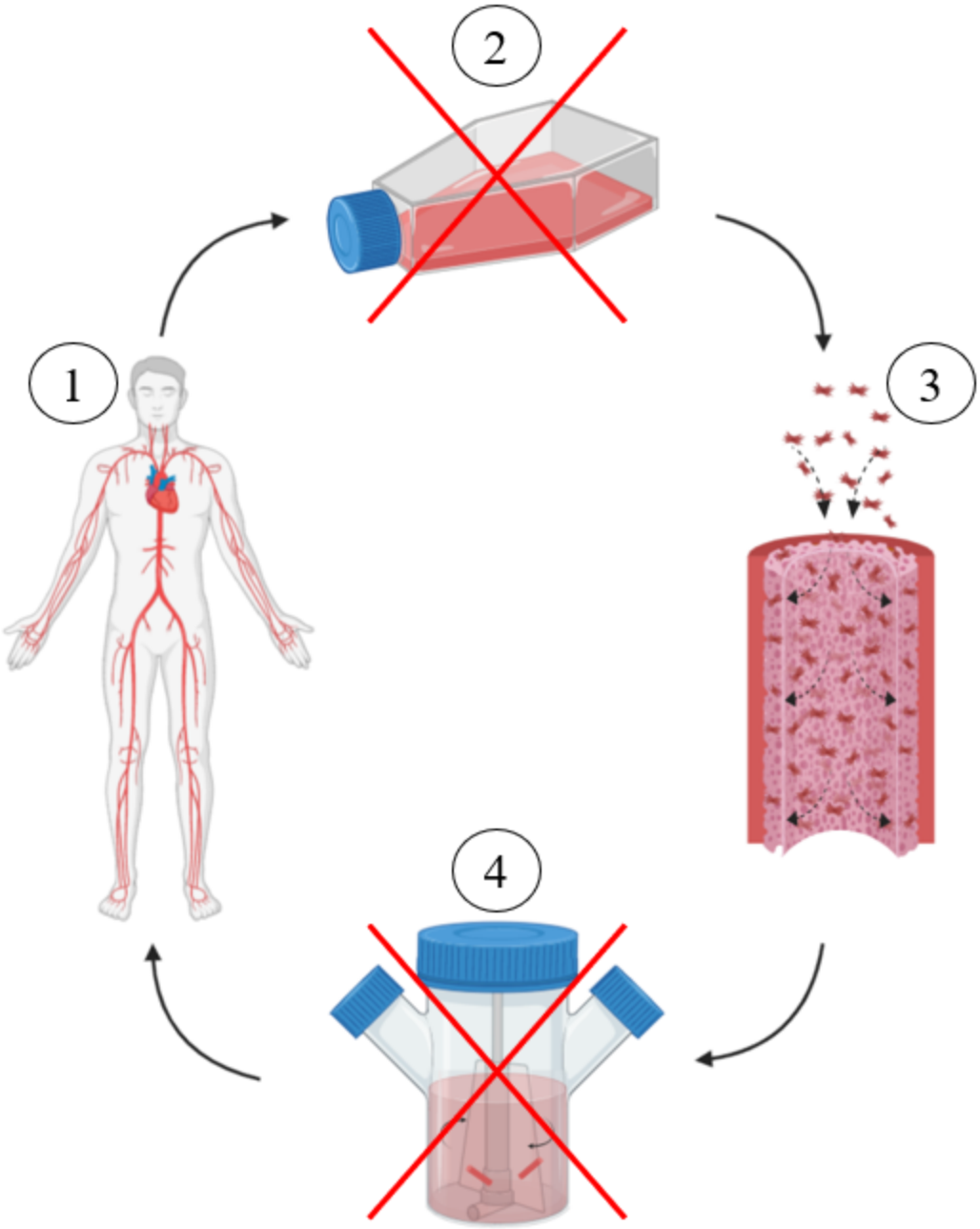

Figure 52. Cell-seeded PEUU scaffold paradigm.

(1) Cells are isolated from the patient, (2) culture expanded and purified into stem cells, (3) rapidly seeded into a PEUU scaffold, (4) cultured in a spinner flask for 48 hours to allow for cellular adhesion, then implanted back into the patient.

The second study (**Section 5.2**) built upon previous VBL studies utilizing PEUU scaffolds by scaling up the TEVGs from a rat size to a sheep size. Over the past decade, the cell seeded PEUU construct has been studied in a rat model to evaluate both the cell type and paradigm of fabrication (**Figure 52**) with the end goal of clinical translation. The multiple iterations of cell seeded PEUU constructs have demonstrated positive remodeling and 8-week patency in a rat model; however, the next step towards translation is testing a more size relevant model. Considerations when scaling up include scaffold design, seeding device scale up, cell sourcing (3 million cells for a rat vs. 200 million for a sheep), and in vivo complications associated with longer grafts (increased risk of thrombosis and graft kinking). The goal of the study outlined in **Section 5.2** was to address these concerns and scale up the cell seeded PEUU graft into a sheep model. This work was done in collaboration between the author (experimental design, graft seeding, and histology), and Dr. Cunnane (experimental design, graft seeding, mechanical testing), Dr. Wagner (large PEUU scaffold fabrication), Dr. Marra and Dr. Rubin (sheep SVF isolation), and Dr. Tzeng (implantation into a sheep model).

Lastly, in addition to the development of a cell-free, silk based TEVG described in Chapters 2-4, this dissertation included work towards a cell-seeded, silk based TEVG. **Section 5.3** outlines additional silk TEVG studies focusing on the development and in vivo testing of two cell-seeded, silk grafts fabricated with (1) BM silk alone, and (2) a combination of BM and AA silk (using a different silk percentage and fabrication technique compared to lyogel). Both scaffold types were tested in the rat model used in **Chapters 2-4** to determine their potential as a TEVG material. The work within **Section 5.3** was performed by the author (graft implantation, histology) in collaboration with Prerak Gupta (scaffold design and fabrication), Dr. Mandal (silk fibroin isolation), Dr. Haskett (graft implantation), and Dr. Ramaswamy (ECM analysis).

5.1 Same Day Cell Seeded PEUU TEVG

Previous studies within the VBL have developed and optimized an autologous, cell-seeded PEUU TEVG which has shown promising patency and remodeling in a rat model after 8 weeks[17,18,86,88,115]. Since the end goal of this technology is clinical application, considerations towards translation must be considered. The two main hurdles towards clinical translation that limited the technology were (1) FDA regulations regarding cell culture[200,202], and (2) the time constraints of construct fabrication. Specifically, FDA regulations strictly govern the implantation of stem cells that have been exposed to culture expansion due to the increased risk of cell phenotypic change and contamination[200-202]. Additionally, patients requiring a graft often cannot wait the days or weeks required for cell expansion and graft seeding. To address these limitations, a study was designed to alter the previously followed TEVG fabrication paradigm (**Figure 52**). Briefly, (1) cells were isolated from a patient, (2) culture expanded and purified into adipose derived stem cells (MSCs), (3) rapidly seeded into a PEUU scaffold, (4) cultured in a spinner flask for 48 hours to allow for cellular adhesion before implantation into the patient. This entire process takes approximately 1-2 weeks depending on culture expansion rates.

The study outlined in this section focused on modifying step 2 from **Figure 52** utilizing the stromal vascular fraction (SVF) of cells and thereby eliminating the need for culture expansion. Step 4 was also eliminated by replacing the 48-hour dynamic culture period with a 4-hour static culture. Both modifications resulted in a more translatable, “same day” TEVG which is described below.

5.1.1 SVF Isolation and Characterization

SVF describes the cellular population found within adipose tissue. Cell phenotypes within SVF include preadipocytes, adipocytes, perivascular cells, fibroblasts, adipose derived MSCs, ECs/EPCs, SMCs, and immune cells (macrophages, monocytes, lymphocytes, etc.)[290,291]. Previous studies using patient derived cells required culture purification of the stem cells, while this study utilized SVF, thereby eliminating time/culture and also introducing additional cell types known to be beneficial in TEVGs[50,185,188,265].

SVF was isolated from donor adipose tissue (<45 years old and non-diabetic) following standard protocols at the Adipose Stem Cell Center (University of Pittsburgh, Pittsburgh, PA)[292]. Within the isolate, three cell populations are most relevant to TEVGs: "mature endothelial," "endothelial stem," and "adipose stem cell," identified through surface markers $CD31^{+}/34^{-}$, $CD31^{+}/CD34^{+}$, and $CD34^{+}/CD31^{-}$ respectively[203,291,293]. The isolated cells were passaged once and characterized through flow cytometry (**Figure 53**). Two samples of 2.5 million cells were suspended in a mixture of 1 mL PBS (Gibco) and 2% FBS (Premium Select, Atlanta Biologics) in 1.5 Eppendorf tubes. Each sample was then stained for 45 minutes at 4°C in the dark. Sample 1 was mixed with one drop of compensation beads OneComp eBeads (#01-1111, Invitrogen), and stained with CD34 (mouse anti-human IgG1, #560940, BD Biosciences) and CD31 (mouse anti-human IgG, #564630, BD Biosciences). Sample 2 served as a control and was stained with a viability dye (PI, anti-all species, 556463, BD Biosciences). After 45 minutes, sample 1 was washed and resuspended in 2mL PBS + 2% FBS. Both samples were analyzed using a BDFACSAria II SORP cell sorter by the Flow Cytometry Lab in the McGowan Institute of Regenerative Medicine (University of Pittsburgh, PA). Results showed a large population of ASC phenotype cells and smaller amounts of EC and EPCs congruent with published results[293].

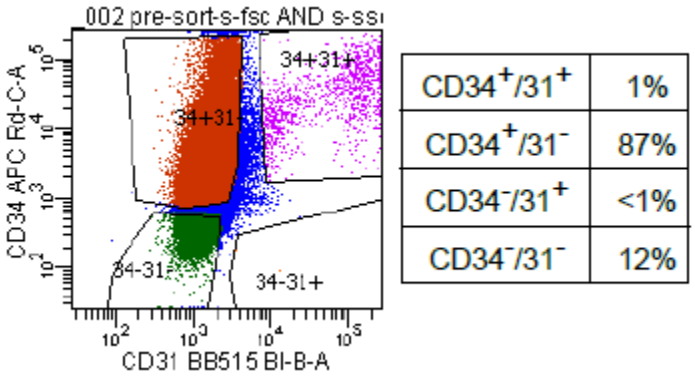

Figure 53. SVF phenotypic characterizion using flow cytrometry.

Three distince populations of cells were detected: ECs ($CD31^{+}/34^{-}$), EPCs ($CD31^{+}/CD34^{+}$), and adipose derived MSCs ($CD34^{+}/CD31^{-}$)

5.1.2 Cell Seeding into PEUU Scaffolds

PEUU scaffolds were fabricated by Dr. William Wagner's laboratory. Each scaffold was designed to fit the size of the infrarenal rat aorta (~1.3 mm ID, 1 cm long) and consisted of two layers: an inner porous layer fabricated using thermally induced phase separation (TIPS), and an outer ES layer providing mechanical support. The VBL has used this scaffold for several published studies[17,19,20,88].

SVF was resuspended at 1 million cells/mL in a 1:1 mixture of Dulbecco's modified Eagle's medium (DMEM, #11965, Gibco) and DMEM/F12 (#113300, Gibco) supplemented with 10% FBS (Premium Select, Atlanta Biologics), % penicillin/streptomycin (5000U/mL, Gibco), 0.1% fungizone (amphotericin B, Gibco), and 10µL/L dexamethasone (Abcam). The cells were then rapidly seeded into PEUU scaffolds of rat aortic size using previously established protocols (**Section 4.2.3**)[88]. Validation of successful seeding was confirmed through fluorescent staining of nuclei (bisbenzimide H 33258, Sigma Aldrich) and graft autofluorescence (**Figure 54**).

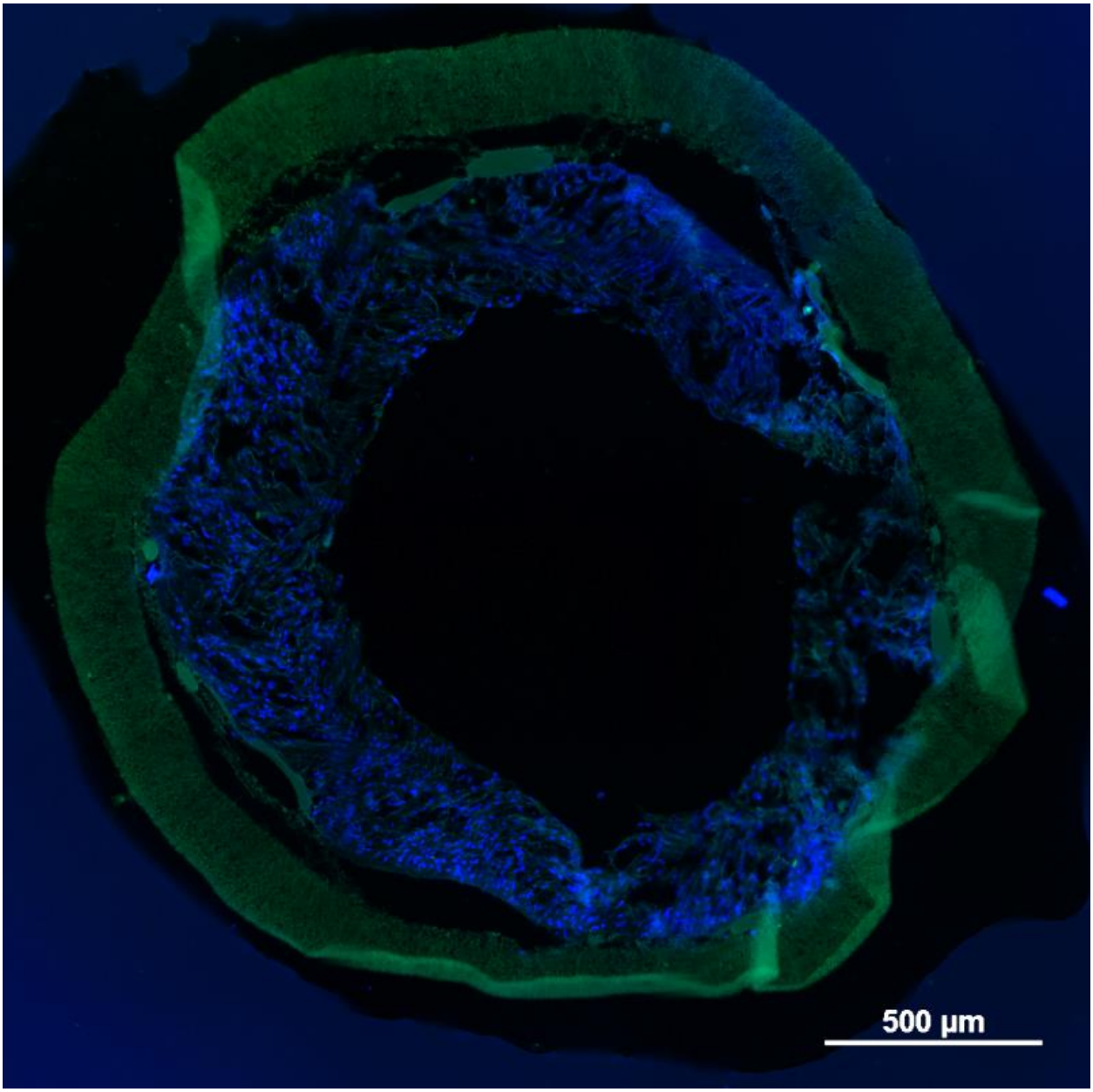

Figure 54. SVF seeded scaffolds showed homogenously seeded cells throughout the inner layer.

A section of a SVF seeded PEUU scaffold was stained with bisbenzimide to detect cell nuclei (blue). The scaffold autofluoresced (green) which showed the dense ES layer (outer) and porous TIPS layer (inner).

5.1.3 In Vivo Evaluation of SVF Seeded PEUU Scaffolds

SVF seeded grafts were assessed in an abdominal rat aortic model previously described[19,86,88,250] (**Section 2.3**) for 8 weeks in vivo (n=7 total). Angiography showed 5 of 7 grafts patent with varying degrees of remodeling (**Figure 55[20]**). Both non-patent grafts failed due to intimal hyperplasia at the anastomoses indicated by the excessive neotissue formation and lack of thrombus.

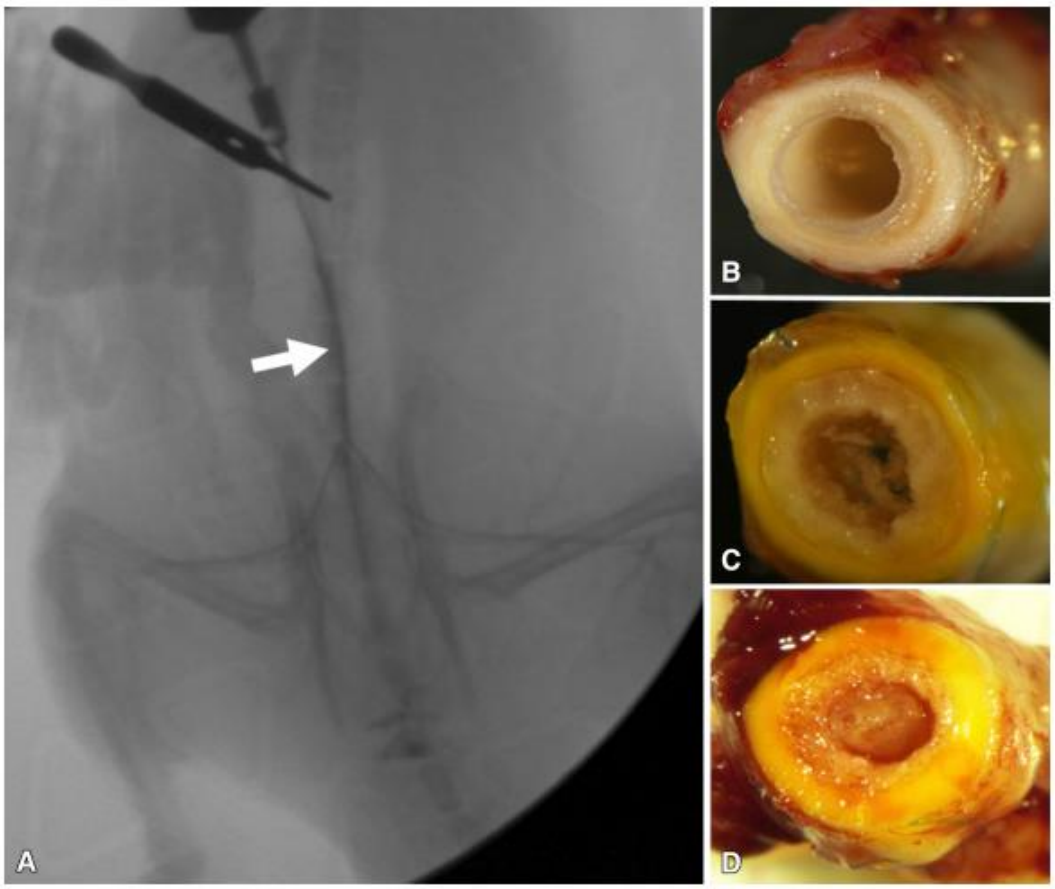

Figure 55. Patency of SVF seeded PEUU scaffolds.

(A) Angiography was used to determine graft patency after 8 weeks in vivo. Cross-sectional images revealed different levels of remodeling ranging from (B) remodeled, (C) partially remodeled, and (D) occluded due to anastomotic hyperplasia.[20]

5.1.4 Overview and Future Directions

The concept of a "same day" vascular graft was validated through this study with the close coordination and collaboration between Dr. Marra and Dr. Rubin with the Adipose Stem Cell Research Laboratory (SVF isolation) and the VBL (author included, graft seeding and implantation). SVF isolation expertise from the Adipose Stem Cell Research Laboratory and improvements in surgical techniques and skill made a 24-hour scaffold fabrication and implantation possible[20].

In summary, similar patency rates were observed with SVF compared to previously published results using adipose derived MSCs[19,20], with the added benefit of reduced time and culture. Future studies towards translation include scaling of the technology into a clinically relevant size. Preliminary work has been done towards this translation outlined in **Section 5.2**. Additional studies may include observing the effects of frozen SVF to eliminate the need for same-day cell isolation and further streamline the benchtop to the bedside process.

5.2 Large Scaffold and TEVG Pilot Study

Using the concept of cell seeded PEUU TEVGs, the VBL has been working towards the end goal of clinical translation for the past 10 years. From graft seeding optimization to efficient cell sourcing, each iteration of the technology has produced a faster, more relevant model. The recent design of the TEVG summarized in **Section 5.1**, comprised of SVF seeded PEUU scaffolds, can be created and implanted on the same day without cell culture, making it one appealing option

for translation[20]; however, ultimately all combinations of cells/cell replacements and scaffolds could be tested in a larger model to assess the translational potential of each.

One remaining step in testing the potential of seeded grafts is scaling the technology towards a clinically relevant size. The study outlined here focused on scaling the cell source and graft size to a sheep carotid graft. This bulk of this study was done in collaboration with Dr. Cunnane (scaled up seeding device design, mechanical testing, and scaffold seeding) and Dr. Haskett (scaled up seeding device design), two post-docs in the VBL.

5.2.1 Scaling Up of the Scaffold Design and Cell Source

Sheep sized biodegradable, bilayered PEUU scaffolds were fabricated in collaboration with Dr. William Wagner using modified protocols[294] previously described for rat size scaffold fabrication[17,88]. The tubular scaffolds were 4.7 mm ID and 10 cm in length (compared to ~4-5mm ID of native sheep carotid). A custom seeding device to mimic the rapid rotational vacuum seeding device used for rat size scaffolds was designed by former VBL PhD graduate, Dr. Lorenzo Soletti[294], and built and validated by Drs. Cunnane and Haskett. The device seeded cells through a diffuser stylet, which moved linearly and coaxially through the lumen, spraying a cell suspension as the scaffold rotated under -5inHg vacuum pressure. The linear speed of the stylet (2.5 mm/s) and cell quantity (200 million cells/scaffold) was optimized by Dr. Cunnane using RoosterBio MSCs (RoosterBio). Scaffold seeding using RoosterBio cells was observed (n=2) along the length and circumference of the scaffold (**Figure 56**) with H&E. Even seeding was observed along the length with some variation in circumferential distribution. Metabolic activity for each section was also assessed by Dr. Cunnane using Alamar Blue (DAL 1025, ThermoFisher Scientific) with no difference between sections indicating even quantities of cells within each portion.

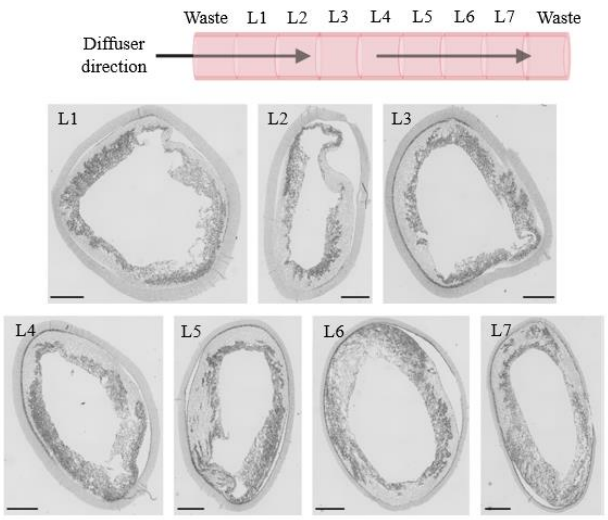

Figure 56. Histological imaging of the allogenic ASC seeded PEUU scaffold after 10 weeks in vivo. Seeded scaffolds were divided into seven sections, and cellularity was observed through H&E staining.

Seeding optimization was performed using RoosterBio cells due to ease of access, however, the end goal was an autologous seeded scaffold using sheep SVF. Sheep SVF isolation was performed using the same protocol as human SVF isolation[292]. Cells were isolated from the adipose tissue of one donor sheep and cultured in a 1:1 mixture of Dulbecco's modified Eagle's medium (DMEM, #11965, Gibco) and DMEM/F12 (#113300, Gibco) supplemented with 10% FBS (Premium Select, Atlanta Biologics), % penicillin/streptomycin (5000U/mL, Gibco), 0.1% fungizone (amphotericin B, Gibco), and 10μL/L dexamethasone (Abcam). Due to the increased cell quantities required, culture expansion was required for a trial run due to limited adipose tissue available. Cells were cultured on collagen-coated (rat tail type I, Sigma) T175 flasks for a single passage. After P1, cells were cultured in collagen-coated 5-layer tower flasks to P4, at which point a sufficient quantity of cells was achieved.

5.2.2 Pilot In Vivo Testing of a Seeded "Human-sized" Scaffold in a Large Animal Model

An initial pilot study of a single sheep was performed to assess the potential of the large scaffold design. Two million cells were seeded into a 9cm long scaffold and incubated at 37°C in culture media overnight. The seeded construct was then placed on ice during surgery for ease of access. The scaffold was implanted as a carotid bypass graft in a 9-month-old Suffolk sheep (Rojo Stock Farm, New Castle, PA) by Dr. Tzeng at the McGowan Institute of Regenerative Medicine facilities. The sheep was intubated and anesthetized with atropine (0.03-0.06 mg/kg), oxytetracycline (20-27 mg/kg) and heparin (5000 IU). Just prior to surgery, morphine was administered (0.2-0.5 mg/kg). Throughout the procedure, anesthesia was maintained with isoflurane (1.5-5% inhaled) and monitored through vitals. The operation site was shaved and prepared with a 7.5% povidone-iodine solution and by 70% ethanol. A 14 cm incision was made longitudinally along the neck over the sternocleidomastoid muscle over the carotid. A 10 cm portion of the carotid was exposed and isolated from surrounding tissues. Vascular clamps were placed at each end of the isolated vessel to stop blood flow, and an 8 cm portion of the carotid was removed. The 9 cm construct was implanted in the void space as a carotid interposition graft, sutured to the carotid at each end using a running suture (7-0 prolene, Ethicon 8696G, Cincinnati, OH) (**Figure 57**). The additional 1 cm of scaffold (8 cm void bypassed using a 9 cm construct) allowed for graft stretching after clamp removal. The clamps were then removed, and flow was confirmed through graft distention and ultrasound. The skin and muscle layers were closed, using 2-0 and 3-0 vicryl running sutures Ethicon J317H and J316H, Ethicon).

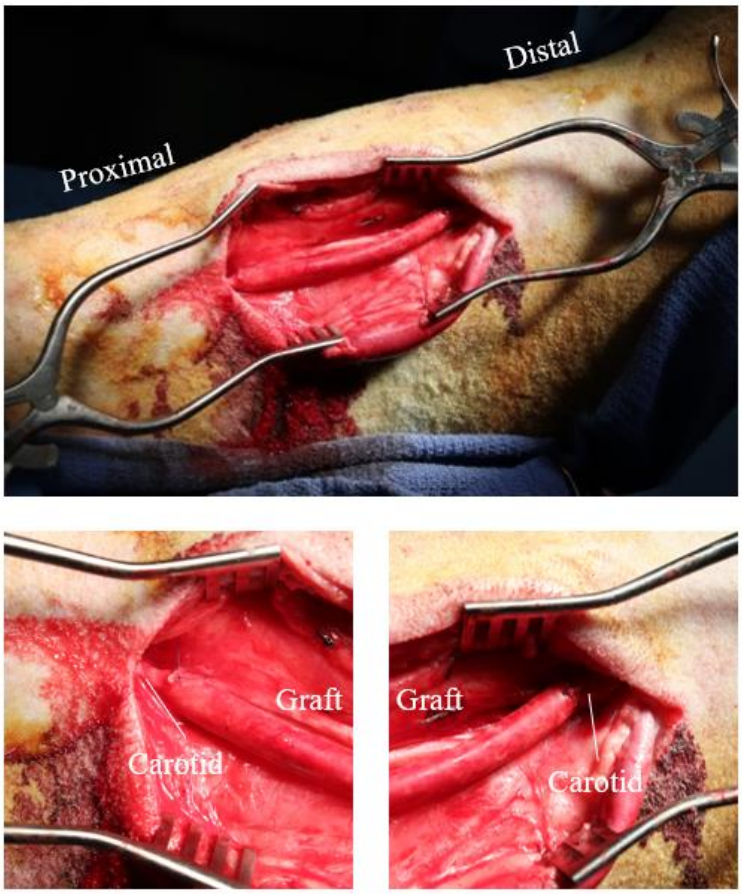

Figure 57. Depiction of an ASC seeded PEUU graft implant as a carotid bypass graft in a sheep model. The graft maintained flow after clamp removal (top) with no signs of leaking. Graft diameter was slightly larger than the native carotid as observed in the proximal (lower left) and distal (lower right) anastomoses.

After the implant, graft patency was monitored weekly with ultrasound (Titan, Sonosite) with no detection of occlusion. After 10 weeks, the sheep was euthanized, and the graft explanted. Euthanasia was performed in accordance with the IACUCs regulation of ethical treatment. After euthanasia, the initial incision site was re-opened, and the graft was isolated (**Figure 58**). The TEVG and surrounding carotid was isolated and divided into 7 portions for histological analysis (**Figure 59**).

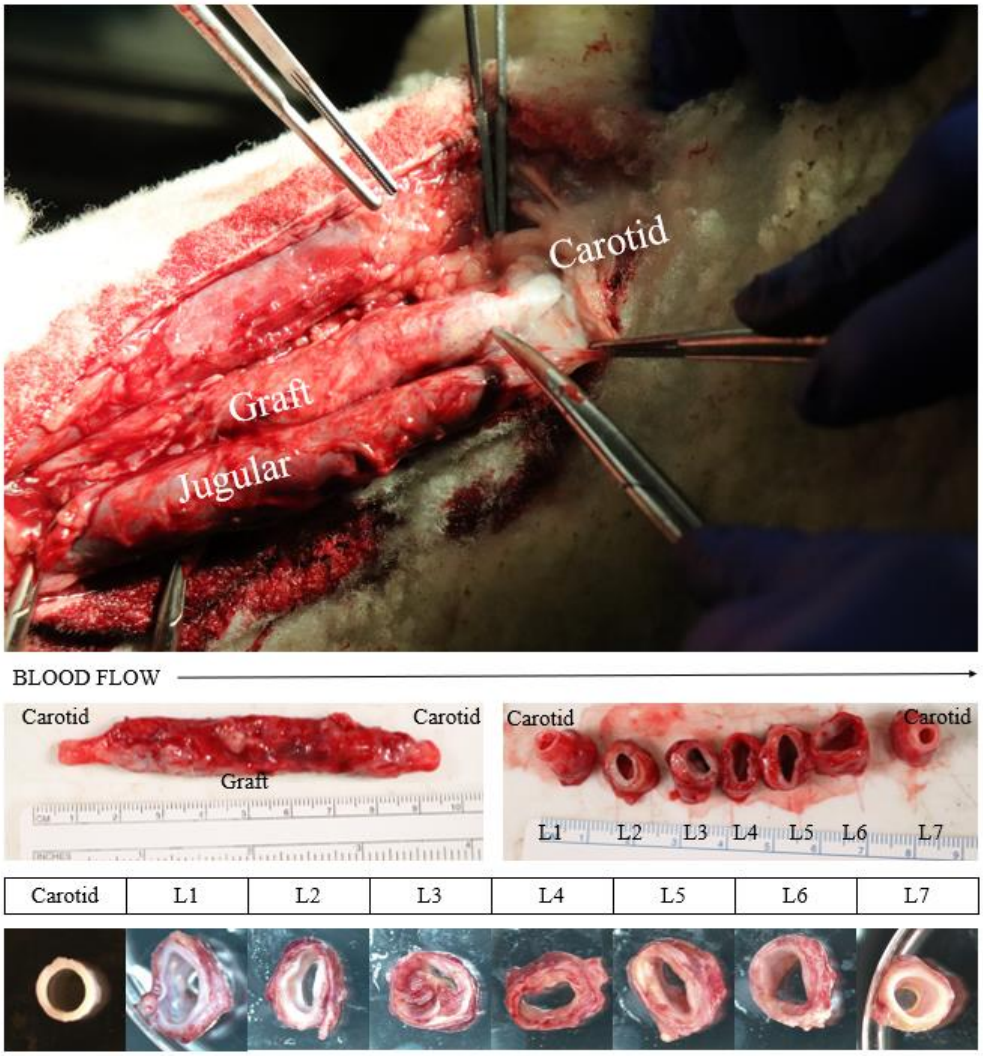

Figure 58. Explant and macroscopic imaging of the ASC seeded PEUU TEVG after 10 weeks in vivo. The graft at explant (top) was covered in a thin, fibrous layer of connective tissue. The graft diameter appeared to have increased and was comprable in diameter to the jugular vein after 10 weeks in vivo (top). The explanted graft was ~7.5 cm in length (middle left) and ranged in diameter due to graft dilation (middle right). The graft appeared slightly more dilated towards the ends of the explants in sections L1 (proximal) and L6 (distal). A luminal ingrowth was observed in the medial L3 portion of the explant. *Blood flow direction for the entire figure is displayed by the black arrow.

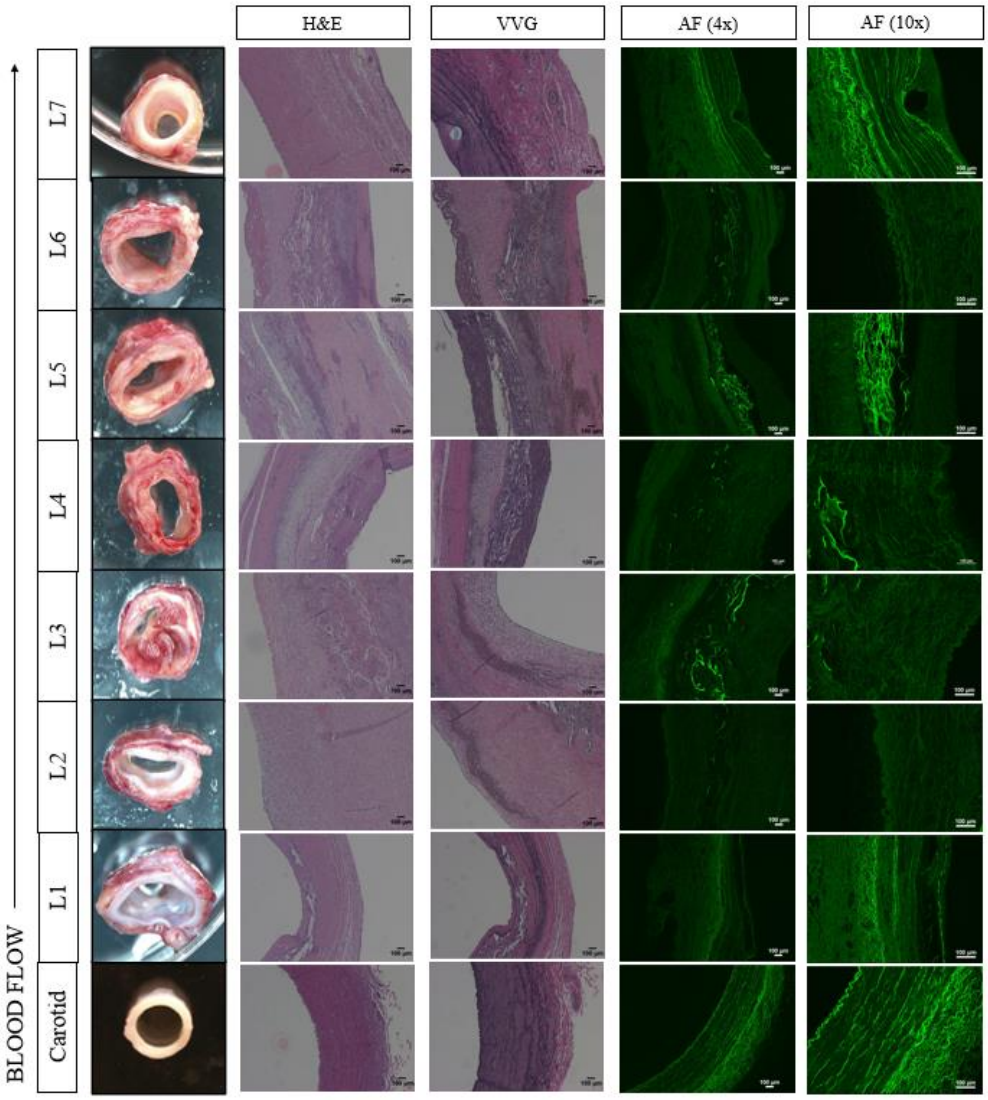

Figure 59. IFC and IHC imaging of the explanted ASC seeded PEUU scaffold.

Each section of explanted TEVG (far left column) was stained for cellularity (H&E), elastin (VVG) and remaining scaffold portions/elastin (FITC autofluorescence). Higher amounts of elastic fiber formation (VVG) were observed towards the anastomoses (L1, 2, 6, and 7) indicating cellular infiltration from the surrounding vasculature. Cells were observed within each portion of the graft (H&E) indicating successful recellularization. Elastin was observed in the L1 and L7 portions, likely due to overlapping carotid tissue. Autofluoresence showed more remaining scaffold within the middle portion of the graft (L3,4, and 5) compared to the ends (L1,2,6 and 7).

Cross-sectional imaging of each explant section showed no signs of stenosis except in L3. The sections closest to each anastomosis (L1 and L7) appeared dilated with a noticeably increased ID in comparison to the medial portion of the TEVG and carotid. IHC staining for cellularity (H&E) showed full re-cellularization of the scaffold throughout the length and circumference. Varying levels of remodeling was observed with distance from the anastomosis. VVG staining showed early elastin deposition within the neotissue with qualitatively more deposition towards the ends of the scaffold (L1 and L7). Scaffold sections were also imaged in the FITC channel for autofluorescence of both elastin and remaining scaffold. Portions of the remaining scaffold were found mostly within the center of the TEVG (L3-5) with higher levels of scaffold degradation towards the anastomoses (**Figure 58**).

5.2.3 Overview and Future Directions

We were able to successfully develop and test a scaled-up model of our cell-seeded PEUU scaffold both in vitro and in vivo. Initial in vitro results demonstrated the ability to rapidly vacuum seed SVF and MSCs into the pores of a bilayered scaffold. Histologic analysis showed even cellularity along the length, however, an uneven distribution of cells was observed radially. Additional optimization of seeding parameters (linear speed, rotational speed, injection rate, vacuum pressure) specific to cell type may improve radial distribution but may not be required if the current quantities and distribution of cells is sufficient in promoting in vivo patency and remodeling as indicated by a pilot study.

Pilot in vivo testing of a single allogenic ASC seeded PEUU scaffold resulted in a patent, partially remodeled graft after 10 weeks. Even cellularity and neotissue formation were present in each longitudinal section and with evidence of early ECM deposition throughout; however, vessel

dilation was observed in cross-sectional images of each section. A slight diameter difference was observed (4.7 mm construct ID vs. ~4 mm carotid ID) at the time of implant, which, in cases of more drastic mismatch, often leads to flow disruption and stenosis which was observed within the L3 potion of the graft. While carotid diameter varies from animal to animal, future studies should use ultrasound prior to scaffold preparation to determine diameter and adjust the scaffold accordingly. The explanted TEVG also appeared dilated, potentially due to a compliance difference between carotid and construct. Future studies may include testing more compliant matched grafts to reduce dilation. Overall, this pilot study showed promising results in graft seeding and early observations of remodeling.

5.3 Cell Seeded Silk Scaffolds

A study exploring cell-seeded silk scaffolds[127] was performed in collaboration with Dr. Biman Mandal at the Indian Institute of Technology Guwahati and Prerak Gupta, his PhD student who was a visiting scientist in the VBL for a year. This study combined the VBL's cell seeding technology with Dr. Mandal's silk scaffold design and fabrication expertise.

5.3.1 BA and BM Silk Scaffold Fabrication and Seeding

Two bi-layered silk based TEVGs were fabricated for testing by Prerak Gupta. The first type consisted of BM (6% w/v) silk protein isolated from silk cocoons and the second from a 1:1 blend of BM (10% w/v) and AA (2% w/v) silk. The inner layer of both types was fabricated by injecting the silk solution into custom molds (see **Section 2.1**), forming a tubular structure with a

lumen defined by a center rod. The filled molds were sealed with a cap and frozen at -20°C overnight. After freezing, the mold cap and center rods were removed the scaffolds were lyophilized for 24 hours. After lyophilization, the scaffolds were removed from the molds and soaked in 80% (v/v) EtOH producing a tubular structure of ~40 μm pores. This inner layer was ES with a mixture of PCL and BM silk following the protocol in **Section 2.1**. Mechanical characterization and in vitro assessment of scaffold properties was done by Prerak Gupta to ensure scaffold suitability for TEVG implant. Briefly, both scaffolds had a 918±82 μm ID and 718±65μm wall thickness. The porosity of the inner layer was 53±30μm and 43±24μm for BM and BA scaffolds respectively with an overall porosity of ~90% for both. Suitable suture retention and burst strengths were observed (827±68 mmHg for BM and 798±100 mmHg for BA).

Scaffolds were seeded with human SVF isolated from healthy donors under 45 years old following established protocols[292]. Silk scaffolds were seeded using the VBL's custom rotational vacuum seeding[88]. A 1 million/mL cell suspension of SVF was luminally injected at 1mL/min, and a -5inHg vacuum pressure was applied. Successful seeding (>90% efficiency) was achieved in both scaffold types. After validation of graft seeding, the constructs were tested in a rat model.

5.3.2 In Vivo Assessment of BA and BM Scaffolds

Four groups were tested in vivo: (1) unseeded BA (n=2), (2) unseeded BM (n=3), (3) BA seeded with SVF (n=9), and (4) BM seeded with SVF (n=8). SVF constructs were seeded and placed in culture 48 hours before surgery to allow for cellular adhesion. The constructs were implanted as abdominal aortic interposition grafts (**Section 2.2**) for 1 and 8 weeks, followed by an angiogram to determine patency (**Figure 60**[127]). No significant difference in patency was observed between any of the groups (Fisher's test, **Appendix A.3**, p=0.4894). In summary, 0% (n=0/2,

patent/total), 66% (2/3), 43% (3/7), and 33% (3/9) of the explanted grafts were patent for BA, BM, BA+SVF, and BM+SVF respectively. Of the 13 not patent grafts, 6 failed due to acute thrombosis and 7 due to hyperplasia.

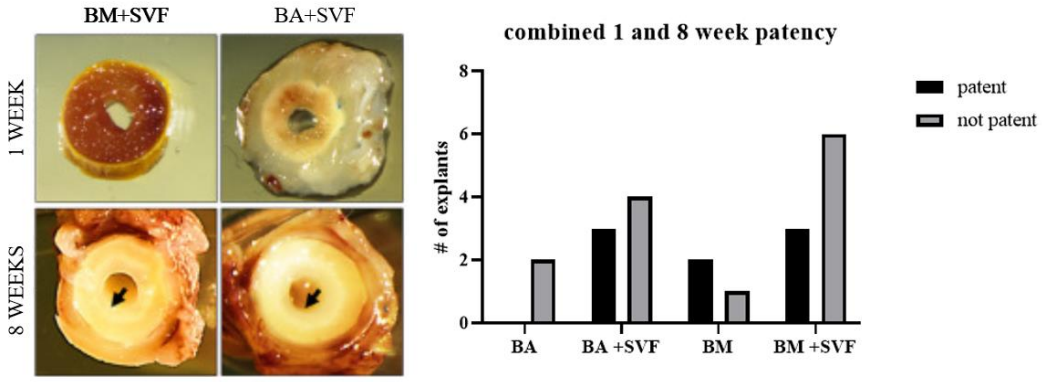

Figure 60. Patency of BM and BA cell seeded silk scaffolds.

Macroscopic imaging of explant cross sections showed neotissue formation after 8 weeks indicated by the black arrows. Patency (graph) based on angiography was assessed for all explants. No significant differences in patency was observed (p=0.4894).

All medial portions of the grafts were sectioned and stained following established protocols (Section 2.3.3) for VSMCs (1:100, calponin and αSMA), ECs (1:100 vWF), and macrophages (1:100 CD68) (**Figure 60**, from published manuscript[127]). Explants increased in overall cellularity from 1 to 8 weeks in both the BA+SVF and BM+SVF groups. After 8 weeks, neotissue within the remodeled grafts contained VSMCs (shown by calponin and αSMA) and an endothelial lining (vWF). Additionally, a decrease in macrophage presence was observed from 1 to 8 weeks in both SVF scaffold types. The highest quantity of positive macrophage staining was found in BA+SVF scaffolds after 1 week.

IHC for overall structure and cellularity (H&E), collagen (PCRO), and elastin (VVG) showed increased graft remodeling from 1 to 8 weeks indicated by increased cell count and ECM

positive staining (**Figure 61**). Additional elastin and collagen quantification using a ninhydrin and hydroxyproline assay (performed by Dr. Ramaswamy) also showed a higher amount of collagen production within both SVF groups after 1 week ($p<0.05$, **Figure 62**). Increased elastin was found within the BA+SVF group after 8 weeks ($p<0.05$) in comparison to the BM+SVF group. All results were analyzed using a one-way ANOVA and Tukey's post hoc testing using Origin 8.0 software.

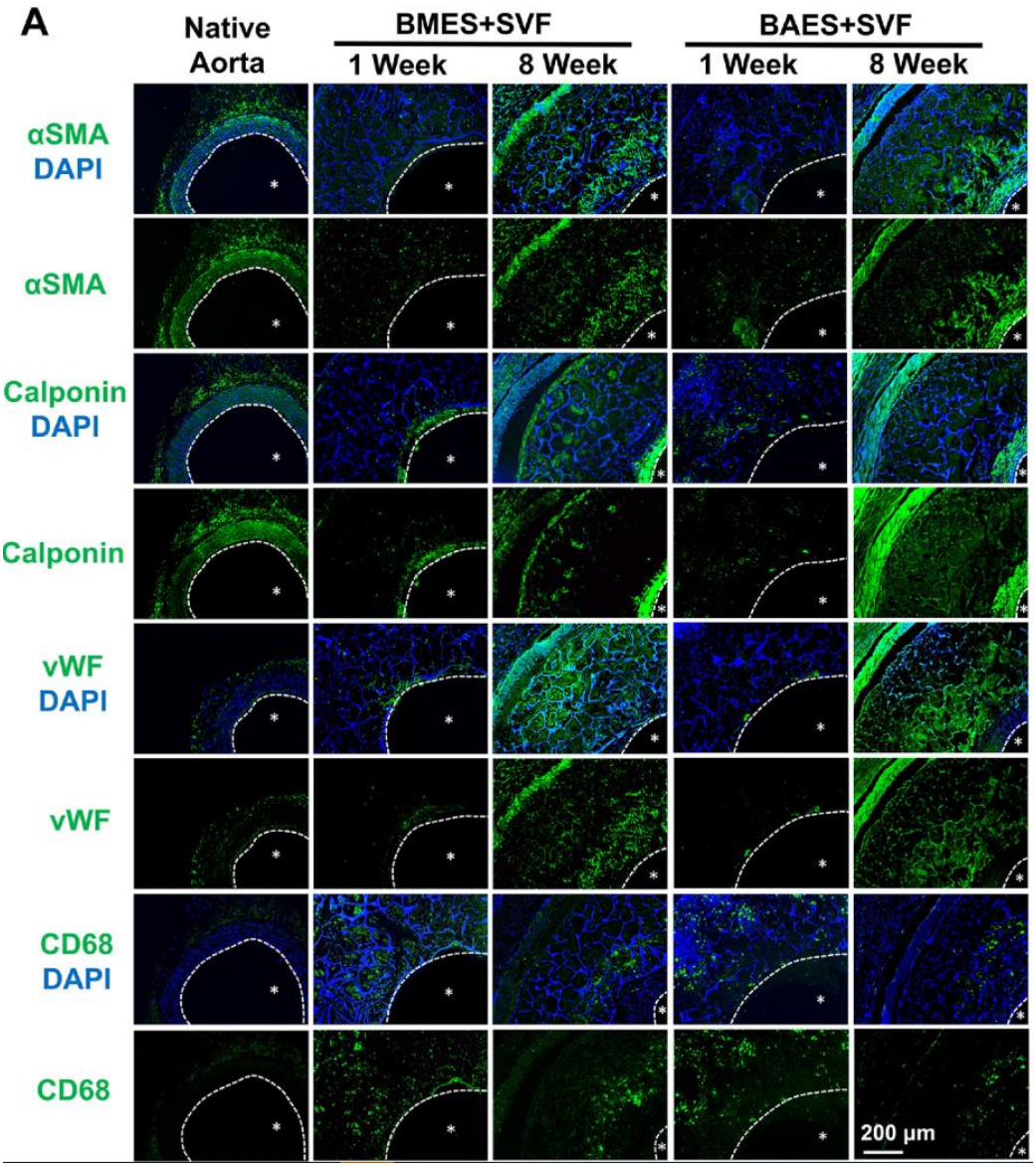

Figure 61. IFC analysis of BM and BA cell seeded silk scaffolds after 1 and 8 weeks in vivo.

IFC staining showed increase cellularity between 1 to 8 weeks in vivo in both the BMES+SVF and BAES+SVF groups. Neotissue after 8 weeks stained positive for VMSCs (calponin, αSMA) and an endothelial lining (vWF). All sections were costained for cell nuclei shown in blue.

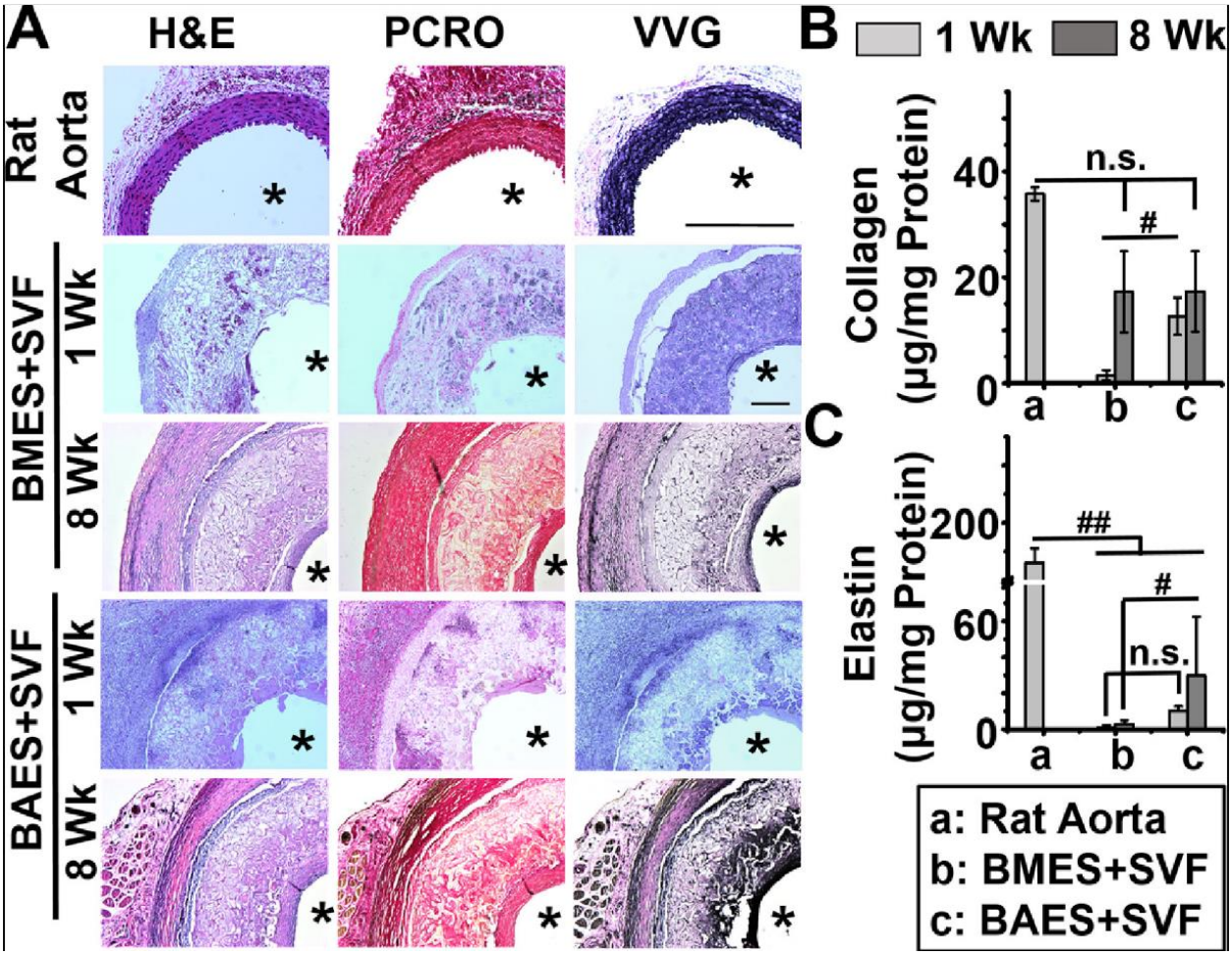

Figure 62. IHC analysis of BA and BM cell seeded scaffold after 1 and 8 weeks in vivo.

(A) IHC staining of explants for cellularity (H&E), collagen (PCRO), and elastin (VVG) showed an increased level of ECM deposition and cellularity in the 8-week explants of both seeded scaffold types. (B) A significantly higher collagen content was measured within BAES+WVF samples vs. BMES+SVF after 1 week in vivo. (C)ECM quantification showed a significantly higher amount of elastin deposition in the BAES+SVF group vs. BMES+SVF after 8 weeks. #p<0.05, ##p<0.01, n.s.= not significant.

5.3.3 Overview and Future Directions

This study tested the viability of cell-seeded silk scaffolds for use as TEVGs. Previous studies of cell-seeded synthetic scaffolds have shown increased patency and remodeling with the inclusion of cells leading to the question: Will cell seeding also improve patency and remodeling of silk, a natural material? To answer this question, each graft type was tested in vivo with unseeded controls and measured for patency (angiography), immune response (macrophage staining), and quality of remodeling (presence of contractile VSMCs, and EC lining, and ECM deposition) within a rat aortic model. Analysis of each of these components was aimed at observing two particular effects of cells within TEVGs: (1) antithrombogenicity, and (2) encouragement of early host macrophage infiltration to mediate graft remodeling.

No significant differences in patency were observed between any of the four groups. In contrast to the previous cell seeded PEUU studies, the inclusion of SVF had no significant effect on graft patency. No antithrombotic effect was observed in cell-seeded scaffolds; rather, acute thrombosis was the mode of failure for 5 (n=4 for BM and n=1 for BA) of the 10 failed grafts. Of the patent grafts, an increased macrophage presence was found in BA+SVF grafts after 1 week possibly due to the presence of RGD binding sites (**Section 1.3.1.1**) associated with AA silk; however, this additional biocompatibility attribute did not increase patency in the blank (n=0/2 patent) or seeded scaffolds (n=3/9 patent). In addition to thrombosis, grafts also failed due to hyperplasia localized around the anastomosis indicating damage to the intima during implant. Because of the higher degree of hyperplasia at the suture sites, failure of grafts due to hyperplasia could be associated with surgical technique rather than graft properties. Despite this, the grafts maintaining patency to 8 weeks contained remodeled neotissue with contractile VSMCs, ECs, and ECM deposition.

This study was able to demonstrate rapid cell seeding of silk scaffolds and in vivo assessment of remodeling after 10 weeks. Future studies exploring a higher number of implants are needed to determine significance in patency between seeded and unseeded groups. Additionally, longer time points would allow for better characterization of whole scaffold degradation, ECM maturation, and any prolonged inflammatory response.

6.0 Chapter 6: Overall Summary and Future Directions

Cardiovascular disease is currently the leading cause of death worldwide[21] encompassing many different afflictions requiring revascularization. Current revascularization strategies utilize a synthetic or autologous graft which are associated with high failure rates mainly due to re-occlusion over time[66,99,103-105]; thus, there is a need for a more suitable vascular graft option. This dissertation focused on the development and testing of three different graft types for use in small diameter vascular bypass surgeries: (1) lyogel silk functionalized with CCL2, (2) lyogel silk functionalized with conditioned media, and (3) bombyx mori silk functionalized with extracellular vesicles.

The studies outlined in Chapters 2-4 focusing on the development of a cell-free, silk based TEVG showed a successful increase in acute (1 week) patency with the delivery of either CCL2 or CM from a lyogel scaffold. Despite this initial effect, the increased patency was not maintained after 8 weeks, and all four (Blank MP, CCL2 MP, CM MP, and lyogel) scaffolds showed similar patency rates. Remodeling of the lyogel scaffolds after 8 weeks was characterized by the presence of new tissue vascular tissue formation within the scaffold combined with scaffold degradation. In comparison, graft failure occurred through acute thrombosis, and excessive tissue growth into the lumen of the graft without scaffold degradation leading to stenotic failure. A high occurrence of stenosis was observed in response to the lyogel itself, which was reduced when we introduced a scaffold made of BM silk alone. Overall, an increase in patency and reduction in stenosis after 8 weeks in vivo was observed using EV functionalized BM silk scaffolds in comparison to all lyogel groups. Chapter 5 outlined three additional TEVG studies performed with collaborators: (1) testing of an autologous cell seeded graft fabricated and implanted within 1 day, (2) design and testing of

a sheep sized allogeneic cell seeded graft, and (3) design and testing of cell seeded silk scaffold. Studies 5.1 and 5.2 were a continuation of a well-established TEVG design previously developed in the VBL where a PEUU bilayered scaffold was rapidly seeded with allogenic ASCs and implanted into rat (**Chapter 5.1**) and sheep (**Chapter 5.2**) models. Both studies showed promising results which will serve as the foundation for future studies to optimize a clinically relevant sized graft. Additionally, **Chapter 5.3** focused on applying similar cell seeding to silk scaffolds resulting in a decrease in graft remodeling and patency with the inclusion of cells. This study emphasized the interconnected nature of the scaffold treatment (i.e., cells, coatings or MPs) and material type. While previous PEUU scaffolds observed an increase in patency and remodeling with cell seeding, the opposite effect occurred in silk-based scaffold.

The varied results of **Chapters 2-4** and **5.3** focusing on silk based scaffolds lend to many different future directions, including an extended-release of cargo from the MPs, incorporation of the MPs into a different base scaffold type, scaling up of the EV functionalized scaffold, and considerations towards clinical translation (i.e. shelf life, reproducibility, etc.). The studies utilizing PEUU and cells (**Chapter 5.1-5.2**) have also shown promise towards clinical translation. The next steps using this technology include large scaffold optimization and additional in vivo testing. Additionally, while this dissertation includes two distinct graft types (silk and PEUU) with many different treatment types (CCL2, CM, EVs, autologous cells, and allogeneic cells), future studies may look at testing various combinations to produce the most translatable option. Overall, future studies can be divided into silk-based grafts, PEUU based grafts, combination grafts, and translational considerations.

Silk based scaffolds functionalized with CCL2 and CM MPs showed a burst release of cargo within the first 24 hours of release, which corresponded to an increase in 1-week patency

but not 8-week patency. One potential future direction could explore the effects of a sustained release of cargo from the MPs. A high tissue-resident macrophage response was observed after 1 week with the delivery of CCL2 and CM; however, very little macrophage infiltration into the porous layer of the scaffold was observed, resulting in low scaffold cellularity. A longer release of either cargo may increase cellular infiltration into the porous layer through the recruitment of circulating macrophages which may then lead to increased graft remodeling. Future studies focusing on a sustained release should start with CCL2 rather than CM due to its higher translatability. Additionally, a more porous scaffold could encourage cellular infiltration of the host cells. As previously discussed (**Section 1.3.1**), scaffold porosity plays an important role in graft remodeling by encouraging host cell migration into the pores; however, ideal porosity can vary with different material types and treatments. Future studies should test different pore sizes to better optimize the ideal pore size for lyogel, BM, and BA silk scaffolds. Alternatively, a combined early release of CCL2 to first recruit macrophages followed by a later release of an immunoregulatory factor, such as IL-4, to polarize the cells may also increase graft remodeling. While the exact mechanism behind remodeling is still unknown, many studies focusing on biomaterial and host interactions indicate that macrophage polarization towards an M2 phenotype is key in successful biomaterial incorporation[213,267,280,281]. The combined release of two characterized factors may provide sufficient remodeling (i.e. neotissue formation and reduced stenosis) and would be a more clinical translatable option due to the elimination of unknown and xenogeneic factors present within CM (FBS, apoptotic bodies). Additionally, the use of two known factors could be easily characterized reducing potential FDA hurdles. Another important consideration for future studies utilizing MPs is the scaffold material itself. The increased stenosis

observed in Chapters 2 and 3 was observed in the majority of lyogel explants indicating a negative response to the lyogel rather than the MPs.

The studies focusing on cell seeded PEUU grafts also showed positive patency, remodeling and potential for clinical translation within a rat model resulting in scaling up of the technology and pilot testing within a sheep model (more clinically appropriate sizing). The initial large scaffold fabrication and implant resulted in a patent graft with vascular neotissue formation and no signs of stenosis indicating the potential as a new TEVG option. Future studies should test additional scaffolds at longer timepoints to better observe the risk of stenosis since it is a main mode of failure in clinically available grafts. Additionally, a slight dilation was observed after implantation of the graft for 10 weeks possibly due to rapid degradation of the ES layer and loss of mechanical stability before sufficient neotissue formation (i.e. before collagen deposition). A prolonged presence of the ES by increasing the thickness could prevent this dilation and should be explored in future attempts.

Overall, many different scaffolds and treatments were assessed within this study with varying levels of patency and remodeling. Since the time, funds, and effort was spent to develop and test each element (silk, PEUU, CCL2 MPs, CM MPs, EV isolations, cell seeding, etc.), future studies should observe combinations of different scaffold bases and treatment types. For example, both the CCL2 and CM MPs successfully prevented acute thrombosis, a common mode of small diameter TEVG failure, but later failed due to stenosis from the lyogel. Future studies should test the anti-thrombotic properties of the CCL2 and CM MPs in a new scaffold type (PEUU or BM silk previously used in the VBL) to observe if a reduction in stenosis can be achieved through altering the graft material. Another future study should observe the potential of EVs within a PEUU

scaffold since previous studies within the VBL have focused on cell seeded PEUU scaffolds with consistent success.

The last consideration for future studies is the potential for clinical translation. All future studies based on the work outlined in this dissertation should account for the potential for clinical translation. These factors may include existing FDA regulations (i.e. BM silk is already approved but lyogel silk is not), shelf life and storage of the resulting graft (i.e. can pre-seeded grafts be stored? For how long?), and feasibility in a clinically relevant sized graft (i.e. can enough cells/MPs, or EVs be isolated for a large scaffold?). For example, future studies building upon the EV functionalized BM silk scaffold (**Chapter 4**) results should focus on: (1) scaling up the EV isolation from rat-sized to a clinically relevant model (e.g. sheep size), (2) scaling up the graft itself from rat aorta dimensions to human/sheep dimensions, and (3) the potential storage and longevity of the resulting large TEVGs. While rat size scaffolds were seeded with an isolate from ~200mL of CM, scaling to a clinically relevant size would require cell culture on a mass scale. Initial attempts towards increased EV isolation have been made in collaboration with RoosterBio resulting in a grant to explore the use of EVs within TEVGs. Future studies with RoosterBio should explore the potential of both a scaled-up cell culture method and EV storage in order to obtain enough isolate for large scaffold seeding. The optimization of EV storage would also determine the potential storage method and shelf life of a EV functionalized BM silk scaffold.

Overall, many future directions could be pursued focusing on the work within this dissertation. With each of these potential studies, the potential for clinical translation must be the main consideration during experimental design. Such considerations include the cost of fabrication, batch to batch variability (CM), shelf life (silk vs. PEUU, MPs vs EVs), and potential

FDA regulations (cell culture byproducts, already approved vs. new material). All future studies based on this work should keep the end goal of a clinically viable, small diameter TEVG in mind.

Appendix A Supplementary Materials and Experiments

Appendix A.1 PEUU Scaffold Optimization and Troubleshooting Quality Control Issues

The development and translation of a bilayered, biomimetic PEUU scaffold have been studied through a collaborative effort between Dr. William Wagner's laboratory and the VBL. Previous studies within the collaboration have demonstrated that PEUU scaffolds alone fail due to acute thrombosis nearly 100% of the time while cell-seeded (pericyte, SVF, adipose derived MSCs, MSCs) PEUU scaffolds remain patent nearly 100% of the time[20,86,88,250]. Chapters 2-4 of this dissertation mimicked this effect artificially through scaffold functionalization with cytokine loaded MPs or MSC-derived EVs in silk scaffolds. This section outlines the early attempts towards functionalizing PEUU scaffolds with MPs to determine the potential of cytokine loaded MPs for use in different graft materials.

Appendix A.1.1 MP-seeded PEUU Graft and Seeding Considerations

This study focused on the development of CM MP-seeded and RoosterBio MSC-seeded PEUU scaffolds to directly compare the differences in patency and remodeling between delivery of seeded cells (RoosterBio MSCs (RBMSCs)) vs. CM (RoosterBio MSC CM). The development of both types required changes in both the seeding method and graft qualities from previous studies.

The previously mentioned rapid cell seeding (**Section 3.2.2**) method has been used with pericytes[250], SVF[20,86], and adipose derived MSCs[19] because the cells can deform and squeeze

through smaller pores. In comparison, rigid MPs cannot deform requiring not only smaller diameters of the particles themselves, but also a higher external vacuum to force the MPs into the pores. The standard protocol for cell seeding uses -5 inHg pressure which was insufficient for MP seeding. In collaboration with Dr. Krawiec, an increased seeding pressure of -10 inHg was found to successfully seed MPs but also increase of risk of graft rupture and pore damage during seeding. Additionally, initial attempts at RBMSCs seeding also resulted in an increased occurrence of graft rupture and pore damage due to the larger size of RBMSCs compared to previous cell types (**Appendix Figure 1**). Seeding these larger cells resulted in either graft rupture or only luminal seeding due to the inability of the cells to fit through the pores (**Appendix Figure 2).**

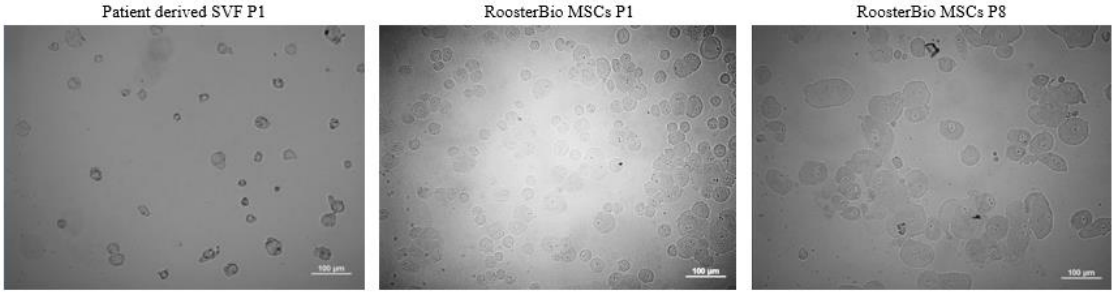

Appendix Figure 1. Imaging of cell morphology before seeding.

Brightfield imaging of SVF at passage 1 (left), RoosterBio MSCs at passage 1 (middle), and RoosterBio MSCs at passage 8 (right), were used to assess cell diameters. SVF cell diameters were smaller than RoosterBio cells. RB cell diameters also increased with passage.

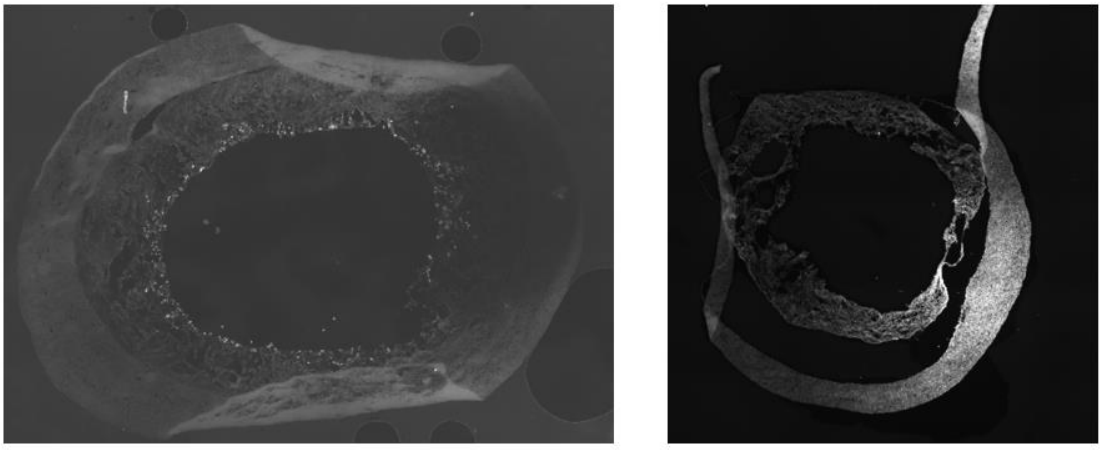

Appendix Figure 2. Cross-sectional images of failed PEUU graft seeding.

PEUU scaffolds seeded with P3 RBMSCs resulted in either luminal seeding only (left) or graft rupture (right).

Based on these results, a new type of PEUU scaffold was developed by Dr. William Wagner's group to increase porosity. All previous PEUU scaffolds were consisted of an inner porous layer formed using TIPS and an outer ES layer for mechanical stability (Appendix A.1.2). To increase the pore size and interconnectivity, the inner layer was instead formed using a combination of TIPS and salt leaching, then ES. The resulting SL+TIP+ES scaffolds were able to successfully seed RBMSCs (**Appendix Figure 3**); however, in vivo pilot implantation studies resulted in aneurysmal graft dilation **(Appendix Figure 4**) observed macroscopically. Cross-sections of the explanted grafts appeared showed nearly 3x graft dilation (**Appendix Figure 4E**) in comparison to previously explanted TEVGs (**Appendix Figure 4F**, note scale bar). Additionally, upon implantation, grafts were similar in diameter to native rat aorta but markedly larger at explant (**Appendix Figure 4A-D**). Grafts explanted after 8 weeks showed apparent signs of an aneurysm in both angiography and cross-sectional imaging.

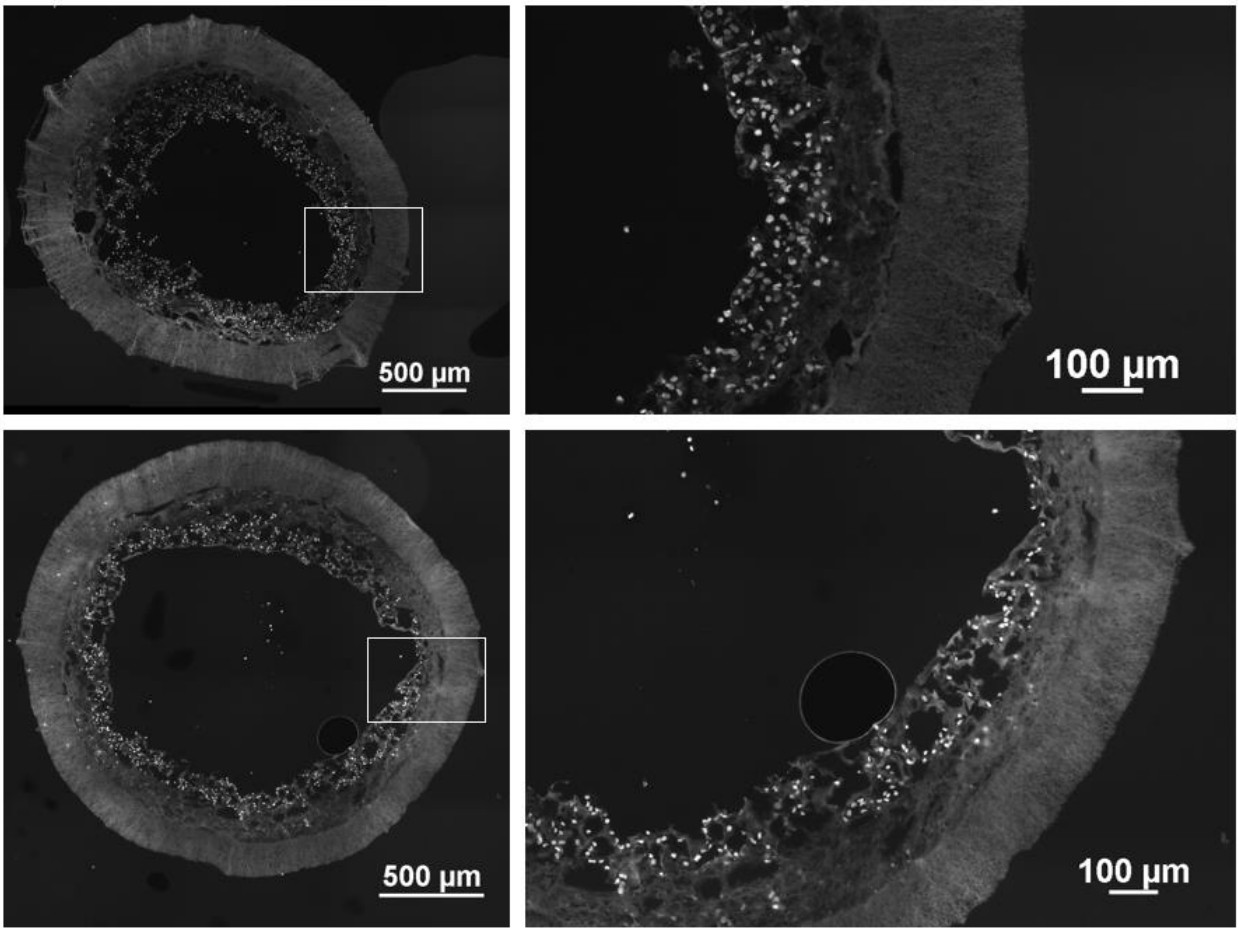

Appendix Figure 3. Cross-sections imaging of SL + TIPS cell seeding

SL+TIPS+ES scaffolds seeded with P3 RBMSCs showed improved cell seeding and less graft damage compared to previous TIPS + SL grafts (Appendix Figure 4).

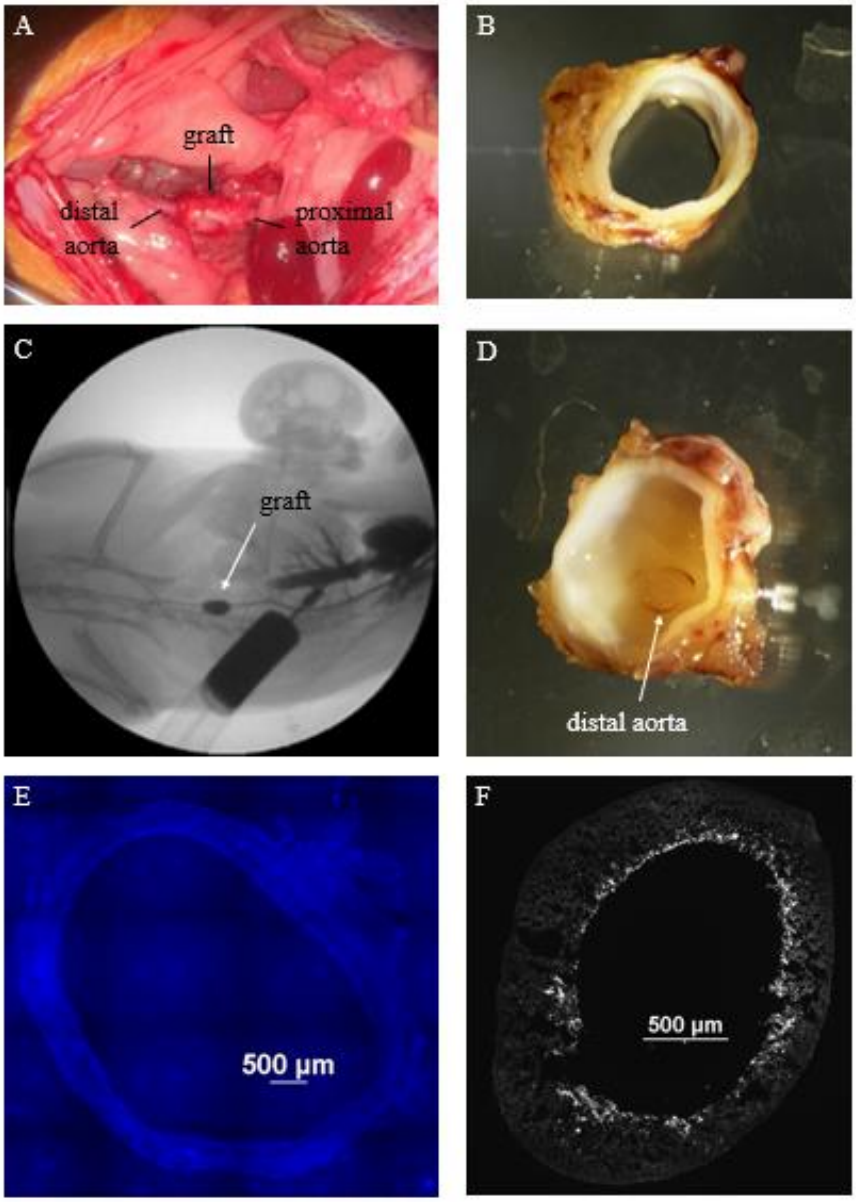

Appendix Figure 4. Patency and macroscopic imaging of SL + PEUU scaffolds implanted for 8 weeks. Implantation of SL+TIPS+ES scaffolds (unseeded) resulted in graft dilation. (A) A depiction of the graft after 8 weeks just prior to explant shows graft dilation which was confirmed using (C) angiography and macroscopic analysis of the (B) cross section of the explanted graft. (D) A cross section of the distal portion of the graft showed a drastically dilated graft in comparison to the distal aorta. This difference was confirmed using IFC to compare medial cross sections of the (E) SL+TIPS+ES explanted graft from this study vs. (F) previously explanted TIPS+ES grafts.

Appendix A.1.2 Overview and Future Directions

The new approach to fabrication incorporating salt leaching was successful in increasing inner layer porosity but also produced a mechanically weaker graft compared to previous TIPS+ES models. A new iteration of SL+TIPS+ES grafts is under development, focusing on increasing the strength of the ES layer to prevent graft dilation. Future studies in this project include continued graft optimization with the long-term goal of assessing patency and graft remodeling between RBMSC and CM MP seeded SL+TIPS+ES scaffolds in a rat model.

Appendix A.2 Pilot Studies Observing CCL2 Loaded vs. Unloaded Lyogel Scaffolds as Abdominal Aortic Grafts

An initial pilot study was performed where CCL2 MP loaded lyogel, and lyogel scaffolds were tested in 10-12-month-old Lewis rats as abdominal aortic interposition grafts following the procedure in **Section 2.3**. Lyogel (n=5) and CCL2 loaded lyogel (n=4) grafts were implanted for 1 week, and patency was measured. Additionally, n=2 CCL2 loaded scaffolds were implanted for 8 weeks to determine their long-term potential. At 1 week, all the lyogel scaffolds failed due to acute thrombosis determined through the presence of a clot while only one CCL2 functionalized graft (1/7) similarly clotted. A summary of the total implants is displayed in **Appendix Table 1** below. Of the attempted implants recorded, five were excluded due to surgical error. Note: implants were performed by myself and Dr. Haskett and were early attempts (i.e. before I became fully comfortable with the surgeries) leading to higher surgical complications. All excluded attempts denoted “Euthanized due to surgical error” in **Appendix Table 1** correspond to signs of

leaking at the anastomosis upon explant or signs of damage to surrounding organs during implant (obstructed bowels, leak in vena cava).

Appendix Table 1 Pilot study summary of implanted lyogel and CCL2 functionalized lyogel scaffolds. The rows highlighted in green represented successful surgeries while those in were elimated from the study due to surgical error (indicaed in the last column).

Scaffold type	Intended duration	Explant duration	Result
Lyogel	8 weeks	2 days	Euthanized due to infection
Lyogel	8 weeks	2 days	Acute thrombosis
Lyogel	8 weeks	2 days	Acute thrombosis
Lyogel	8 weeks	1 day	Euthanized due to hernia
Lyogel	8 weeks	1 day	Acute thrombosis
Lyogel	8 weeks	1 day	Acute thrombosis
Lyogel	8 weeks	1 day	Acute thrombosis
Lyogel+CCL2	8 weeks	8 weeks	Patent
Lyogel+CCL2	8 weeks	8 weeks	Patent
Lyogel+CCL2	1 week	1 week	Patent
Lyogel+CCL2	1 week	5 days	Euthanized due to surgical error
Lyogel+CCL2	1 week	5 days	Euthanized due to surgical error
Lyogel+CCL2	1 week	1 week	Patent
Lyogel+CCL2	1 week	1 day	Euthanized due to surgical error
Lyogel+CCL2	1 week	1 day	Euthanized due to surgical error
Lyogel+CCL2	1 week	1 week	Not patent
Lyogel+CCL2	1 week	1 week	Patent

Total macrophage staining using CD68 IFC staining (1:100 ab31630, monoclonal, Abcam)/Cy5 (1:100 ab_2340820, Jackson ImmunoReseach Laboratories Inc.) showed qualitatively more macrophages within the CCL2 group (**Appendix Figure 5**); however, an equal time comparison was not possible since none of the lyogel scaffolds remained in vivo until the intended explant date.

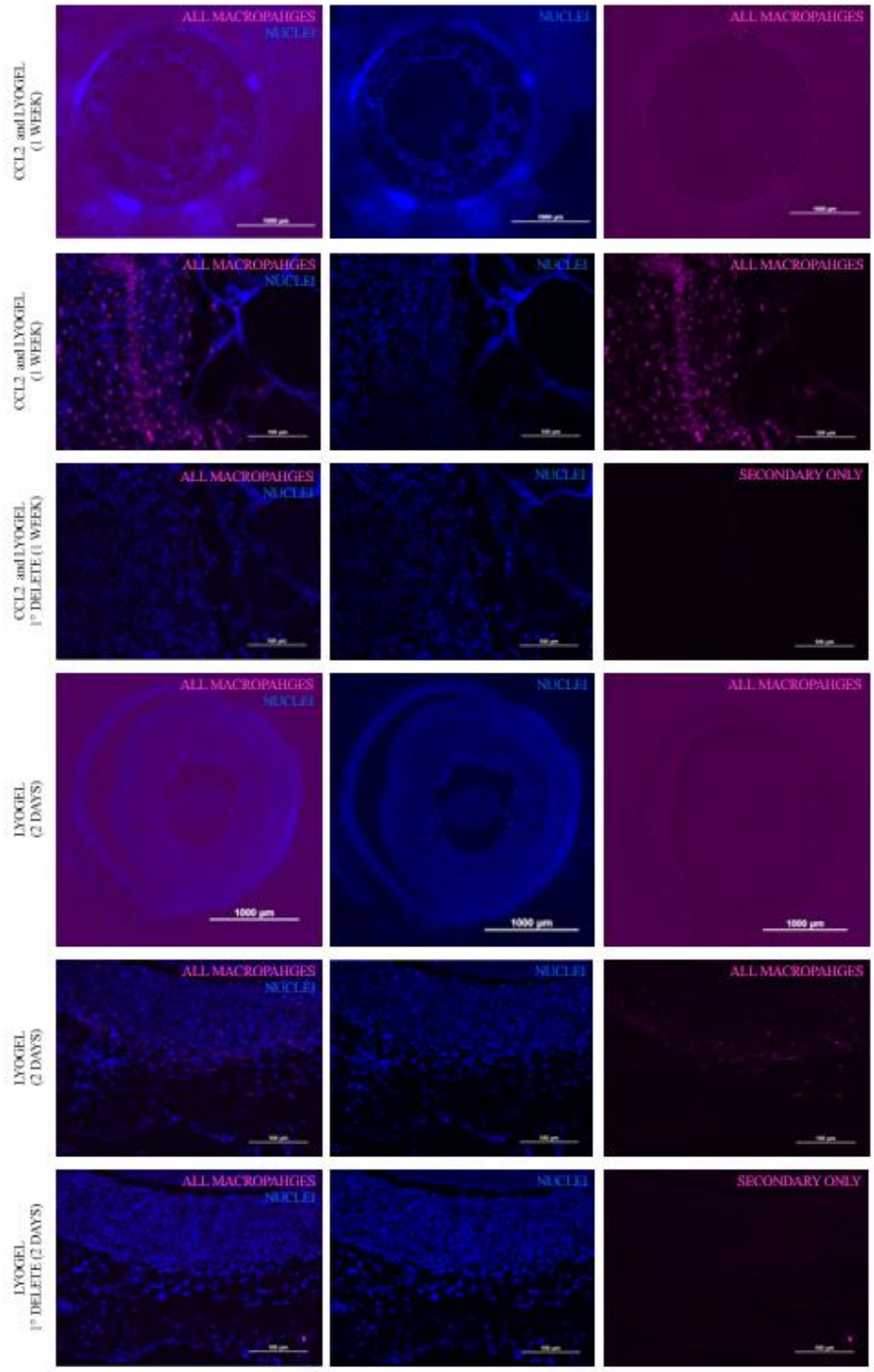

Appendix Figure 5. IFC staining for total macrophages within explant CCL2 lyogel scaffolds

IFC staining of all macrophages (CD68 in pink) showed qualitatively higher amounts of macrophages within the CCL2 explants vs. lyogel alone.

Two CCL2 scaffolds were implanted for 8 weeks and remained patent during this time. One showed promising signs of recellularization while the other showed signs of stenosis (**Appendix Figure 6**). The promising early patency and potential for long term remodeling lead to a more robust study of CCL2 functionalized scaffolds (**Chapter 2**).

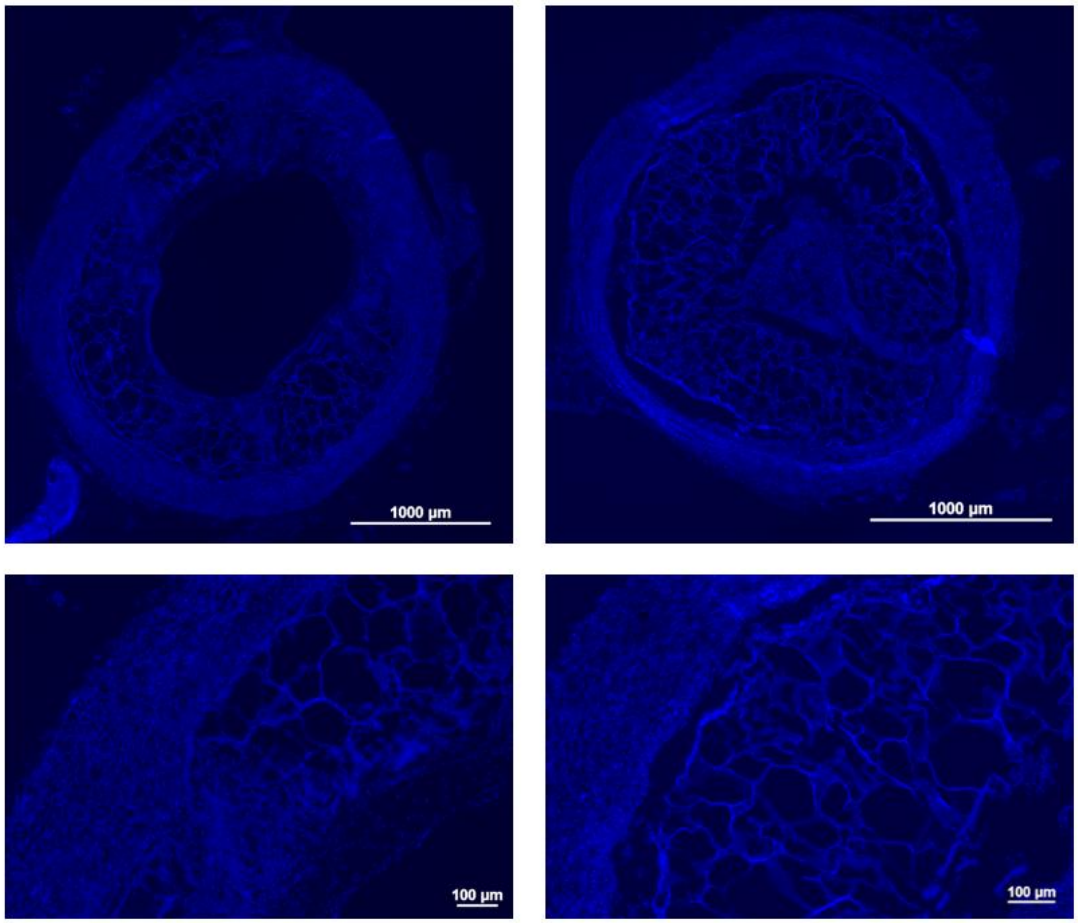

Appendix Figure 6. IFC imaging of CCL2 functionalized grafts after 8 weeks in vivo.

Two CCL2 scaffolds were explanted after 8 weeks showing different levels of remodeling. One scaffold showed signs of recellularization (left) while the other contained fewer engrafted cells and showed signs of stenosis.

Appendix A.2.1 Surgical Technique and Progress

A major component of this study and indeed the entire dissertation was implantation of various scaffolds into a rat model. This microsurgery procedure and technique improved with practice, as can be seen in this study (**Appendix Table 1** showed many instances of euthanasia due to surgical error early in the process). In each surgery, the success was dependent on three main components: (1) limiting the time that blood supply was restricted to the lower extremities after aortic clamping, (2) limiting disruption of the endothelium at each anastomosis through practiced suturing, and (3) aligning the sutures from graft to the aorta to avoid "folds" which may cause disruptions in blood flow.

Initial surgeries, such as the pilot studies described in this section, were limited by surgical technique. In the context of the three success criteria, these early surgeries (1) required ~45-60 minutes of restricted blood flow, (2) had more damage at each anastomosis due to multiple suture attempts, and (3) may have been slightly unaligned. All these factors resulted in increased graft failure due to occlusion at the anastomoses rather than failure due to graft material/treatment itself. Over the course of this dissertation (including studies within the appendices) and additional studies for other collaborations, a total of ~200 surgeries were performed, resulting in improved outcomes based on technique alone. Later surgeries (such as those from **Chapter 4**), required only (1) 15-20 minutes of limited flow due to clamping, (2) had little damage to the aortic endothelium due to practiced suturing, and (3) were aligned due to practice which could be observed through a 10x microscope. The overall time of each surgery decreased from ~90 minutes to 25-40 minutes total allowing for faster recovery as well. This decreased time also allowed for a higher level or rigor within each experiment as implants could be performed in larger numbers from the same litter of

rats. Overall, surgical technique and progress was a major component of this study and was reflected in the design and outcome of each study.

Appendix A.3 Statistical Analysis of Binary Results

Graft patency was assessed as binary data where outcomes must be "patent" or "not patent." Using GraphPad Prism 8 (GraphPad Software), patency data was entered into a contingency table and analyzed using a Fisher's exact test to determine significance (**Appendix Figure 7**). This test is used to determine significance between two classifications (patent vs. not patent) in small sample sizes of categorical data (i.e., data that can only have a small, consistent number of outcomes). Fisher's exact test was used to determine differences in patency. Each test calculates the significance of deviation from H_0: there is a similarity in patency between each graft type.

Table format: Contingency		Outcome A	Outcome B
		Patent	Not Patent
1	Lyogel	5	0
2	Blank	7	7
3	CCL2	10	0

Appendix Figure 7. GraphPad input of patency data to determine significance.

All 1 week explants were labeled patent or not patent and entered into Graphpad as binary data

Fisher's exact test for 1-week explants resulted in p=0.0115, indicating a significant difference between the three groups. Additional Fisher's tests were performed between each group

to determine significance between individual groups. A significant difference in patency was determined between the CCL2 and Blank scaffolds ($p=0.0188$) but no other groups.

The same method was used to determine significant differences in 8-week explant patency. A Fisher's exact test determined a significant difference between the three groups ($p=0.040$) and between Blank MP and Lyogel groups ($p=0.0288$).

Appendix A.4 Macrophage Stain Optimization and Quantification

First, IFC staining of macrophages was optimized using rat spleens. Sections of rat spleens were stained by IFC following standard protocols. After testing, total macrophage or CD68 (1:100 ab31630, monoclonal, Abcam)/Cy5 (1:100 ab_2340820, Jackson ImmunoReseach Laboratories Inc.), M1 type macrophages or CD86 (NBP2-25208, monoclonal, Novus Biologicals)/Cy3 (1:100 ab6939, Abcam), and M2 type macrophages or CD206 (1:100 18704-1-AP, polyclonal, ProteinTech)/Cy5 (1:100 ab_2340820, Jackson ImmunoReseach Laboratories Inc.) markers were chosen and optimized (**Appendix Figure 8**).

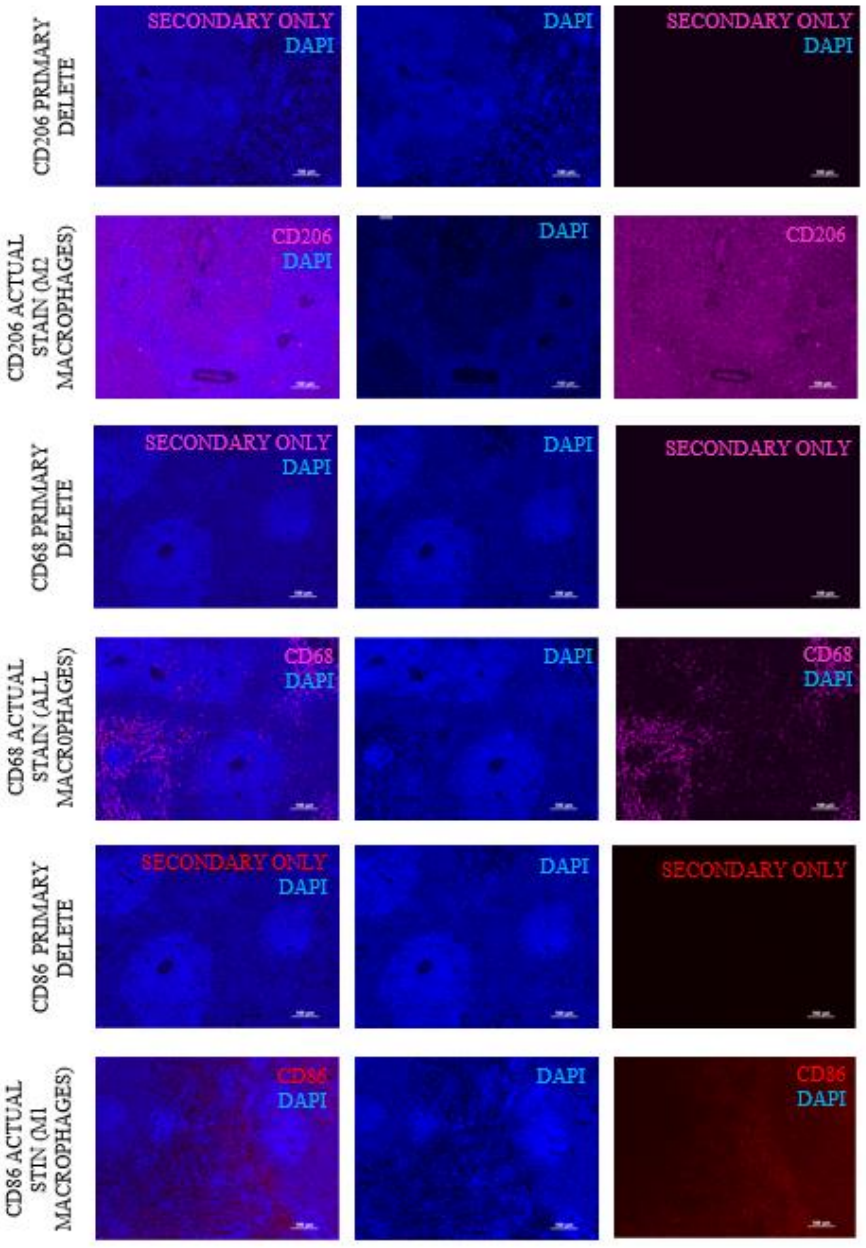

Appendix Figure 8. IFC staining for macrophages was optimized using rat spleens.

An M2 type macrophage marker (CD206, row 2), a pan macrophage marker (CD68, row 4) and an M1 type macrophage marker (CD86, row 6) were tested. Each stain was run with a section of spleen only stained with secondary antibody (rows 1, 3, and 5) to determine nonspecific binding. Positive staining for all three markers was observed using rat spleens.

Each CD68 image was then manually segmented into “inner” and “outer” portions containing the porous and ES layers of the scaffold, respectively (**Appendix Figure 9**). Since distinctly different densities of macrophages were observed in inner vs. outer, each was quantified separately.

Appendix Figure 9. Image segmentation to quantify macrophages.

Each stained section was imaged (left) for macrophages (pink) and cell nuclei (blue). Images were then manually segmented into inner (middle) and outer (left) masks.

The inner and outer masks were then applied to both the DAPI and stained images (CD68, 86 or 206). The nuclei stain corresponding to each of the three stains were used to determine an overall cellularity. Each image was then run through a custom Matlab code developed by Dr. Timothy Chung (**Appendix B.2**), producing a series of 80 images for each image with varying levels of thresholds applied in incremental steps (**Appendix Figure 10**).

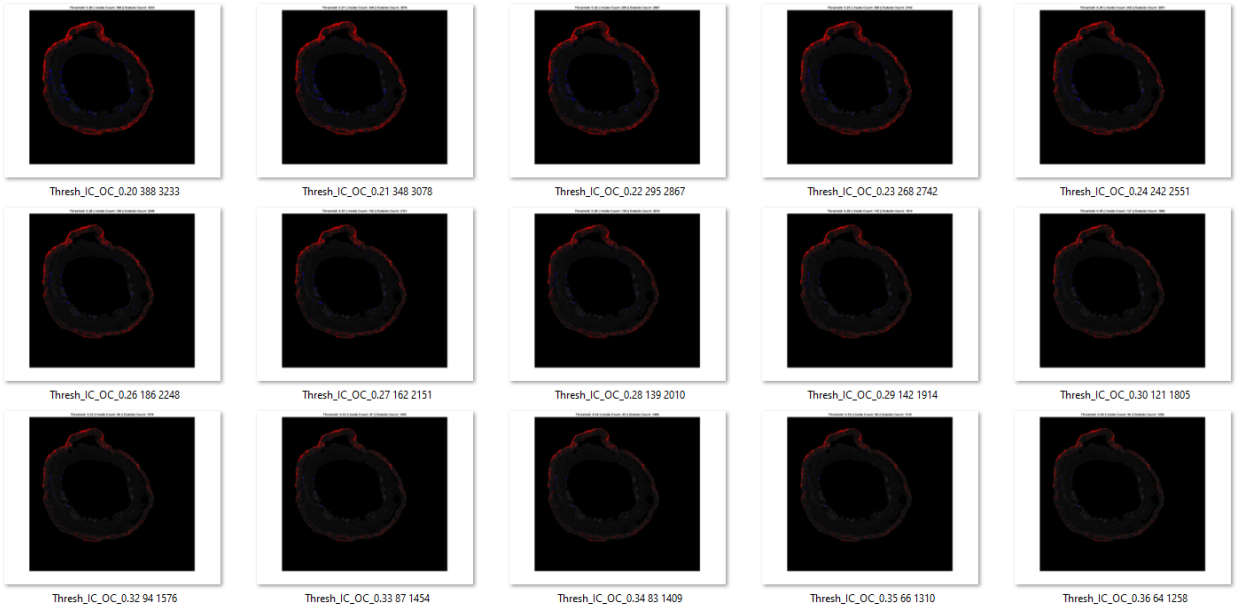

Appendix Figure 10. Thresholded images for macrophage quantification.

Fluorescently stained images for CD68 and DAPI were run through a custom Matlab code which provided varying thresholds with corresponding cell counts.

Each file was then blinded by assigning a random number to each. A threshold for each image was determined by comparing the original image to the different level of threshold (**Appendix Figure 11**).

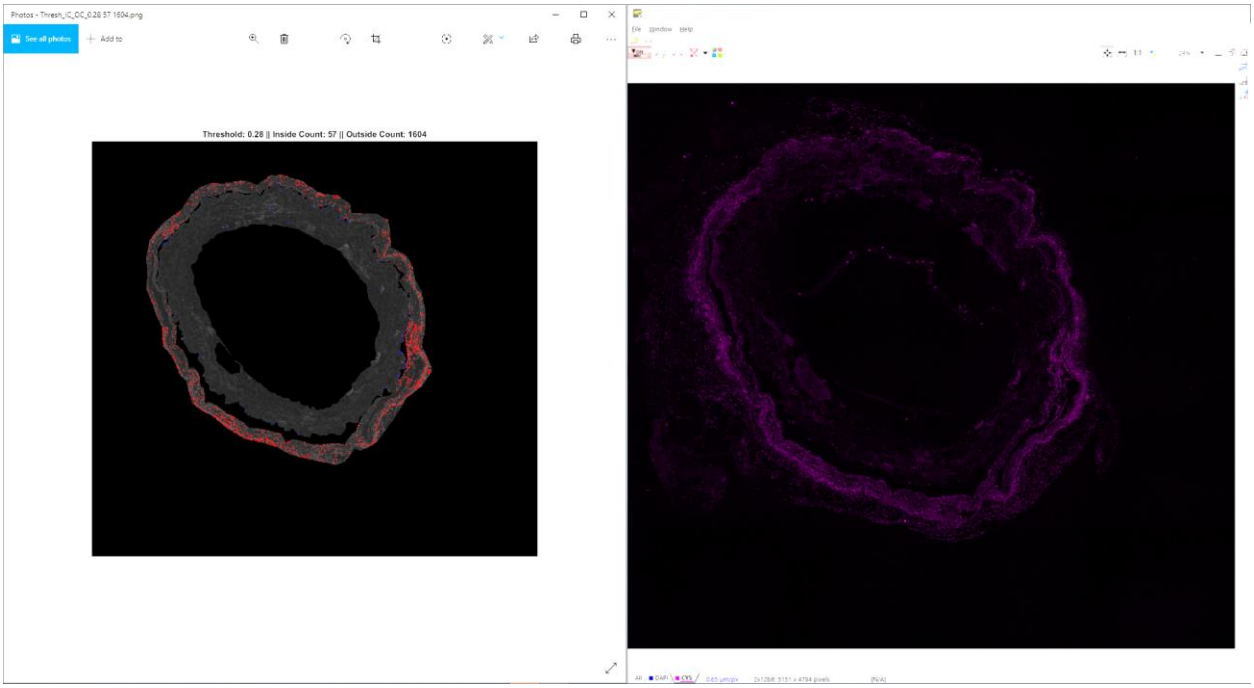

Appendix Figure 11. Determining a threshold for each IFC image.

Threshold IFC images were blinded and compared to the original to determine a threshold which best fit.

The custom Matlab code assessed cellularity based on the chosen threshold for each image yielding cell counts per area for each of the twelve images. Images were then unblinded and overall cell counts were calculated. Significance was determined using GraphPad Prism 8 (GraphPad) via a one-way ANOVA followed by Tukey post hoc testing between groups.

Appendix A.5 CM Optimization

CM was optimized in two ways: determining the passage at which the highest amounts of protein secretions were observed and basal media formula. Both tests were aimed at maximizing

cellular secretions to produce a more potent CM. Both metrics were optimized using RoosterBio MSCs (RoosterBio).

Appendix A.5.1 Determining Cell Passage Secretions

RoosterBio MSCs were purchased at passage 0 (P0). With each passage, cells were grown to 40% confluency in T175 flasks and rinsed. New media (RoosterBio RoosterNourish MSC (KT-001, RooserBio, Fedrick, MD)) was then applied and conditioned for 48 hours at which time cells reached 80-90% confluency. Conditioned media was collected and centrifuged at 2,040 x g and 4°C for 5 minutes to remove debris and dead cells. After centrifugation, the supernatant (CM) was isolated and stored at -80°C until use. Remaining cells were lifted using 5mL per flask 0.025% EDTA trypsin (ThermoFisher Scientific) incubated at 37°C for 3-5 minutes. After cell detachment was observed, trypsin was quenched with a 1:5 ratio of FBS (Atlanta Biologics, Flowery Branch, GA). Cells were then replated at 1.5M/T175 flask, and the process was repeated for 7 passages.

ELISAs were performed on the CM to observe protein levels: VEGF (DVE00, R&D Systems), HGF (DHG00, , R&D Systems), IL-8 (D8000C, , R&D Systems), TIMP1(DTM100, R&D Systems), and TIMP2 (DTM200, R&D Systems). These proteins were chosen based on relevance to vascular remodeling (VEGF and HGF) and comparison to RoosterBio pre-characterized data (IL-8, TIMP1, and TIMP2). ELISA results showed increased secretions of all factors between P2-P4. Based on these results, P3 was chosen (**Appendix Figure 12**).

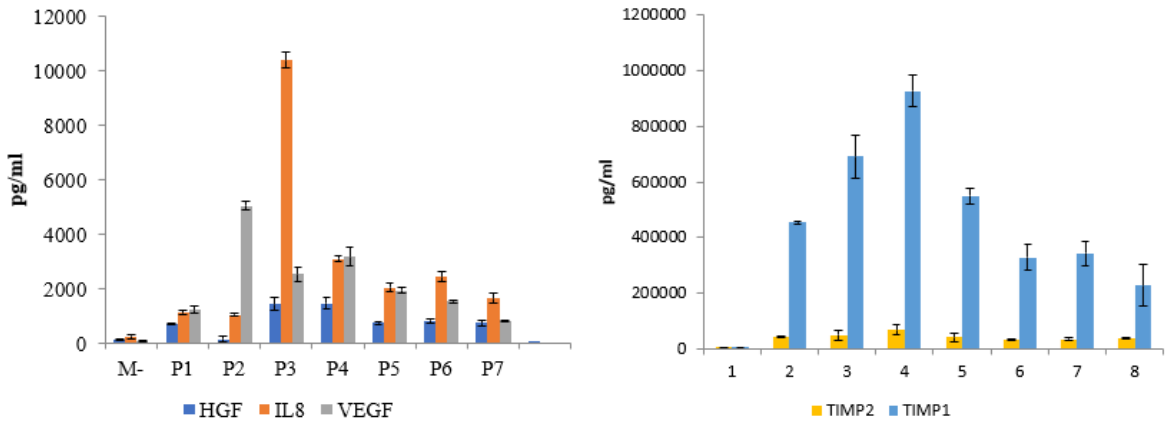

Appendix Figure 12. Characterization of cellular secretions based on the cellular passage of RBMSCs. Conditioned media from RoosterBio cells was collected at passages 1-8. The amount of HGF (left, blue), IL8 (left, orange), VEGF (left, grey), TIMP1 (right, blue), and TIMP2 (right, yellow) was determined for each sample using ELISA kits. The highest overall levels were detected in passage 3 conditioned media.

Appendix A.5.2 Determining Basal Media Type

Six types of media were tested (n=4):

1. RoosterBio Media – RoosterBio RoosterNourish MSC (KT-001, RoosterBio, Fedrick, MD)
2. RoosterBio Conditioned Media – RoosterBio RoosterNourish MSC media (KT-001, RoosterBio, Fedrick, MD) conditioned for 48 hours on RoosterBio ASC (P3)
3. 10% FBS Harvest media:

- DMEM, high glucose, HEPES, no phenol red (Lot 2046800, Gibco, Gaithersburg, MD) (+4.5 g/L D-Glucose, + L-Glutamine, +25 mM HEPES, - Sodium Pyruvate)
- 10% FBS (Lot K17139, Atlanta Biologics, Flowery Branch, GA)
- 1% P/S (Gibco)
- 0.1% Fungazone (Gibco)
- 10 uL/L dexamethasone (Gibco)

4. 10% FBS Harvest media conditioned for 48 hours on RoosterBio MSCs (P3)
5. 5% Harvest Media:
    - DMEM, high glucose, HEPES, no phenol red (Lot 2046800, Gibco, Gaithersburg, MD) (+4.5 g/L D-Glucose, + L-Glutamine, +25 mM HEPES, - Sodium Pyruvate)
    - 5% FBS (Lot K17139, Atlanta Biologics, Flowery Branch, GA)
    - 1% P/S (Gibco)
    - 0.1% Fungazone (Gibco)
    - 10 uL/L dexamethasone (Gibco)
6. 5% Harvest Media conditioned for 48 hours on RoosterBio MSCs (P3)

A scratch assay was performed following the protocol outlined in **Chapter 3.1.5**. Results were quantified based on the percent wound closure in response to treatment. For each image, a wounded region of interest (ROI) was manually segmented using ImageJ (Madison, Wisconsin). For images with ragged boundaries, a line was estimated to represent the level of overall migration (**Appendix Figure 13**). The ROI area was then measured, and percent wound closure determined.

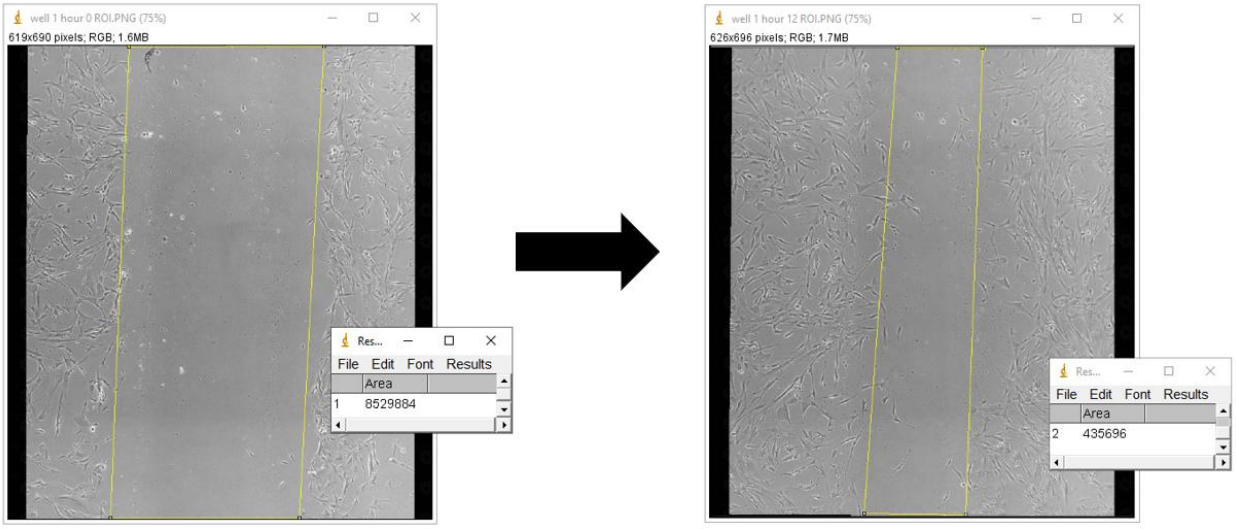

Appendix Figure 13. A wounded ROI was manually segmented for each image at 0 (left) and 12 hours (right) to determine percent wound closure after 12 hours.

$$\%\, wound\ closure\ = \frac{(initial\ ROI\ area - 12\ hour\ ROI\ area)}{initial\ ROI\ area} \times 100 \qquad \textbf{Appendix Eq. 1}$$

Samples were run in n=6 wells and analyzed in GraphPad Prism (GraphPad). All values were entered at percent wound closures as grouped sets of data and analyzed using a two-way, repeated measures ANOVA to determine significance. Significant differences between groups was determined using Dunnett's test ($p<0.05$).

The largest difference basal and conditioned media was observed in the cells conditioned with 5% Harvest Media (**Appendix Figure 14**). Additionally, the highest percent wound closure was measured in response to 5% Harvest Media. Based on these results, 5% Harvest Media was used throughout this study.

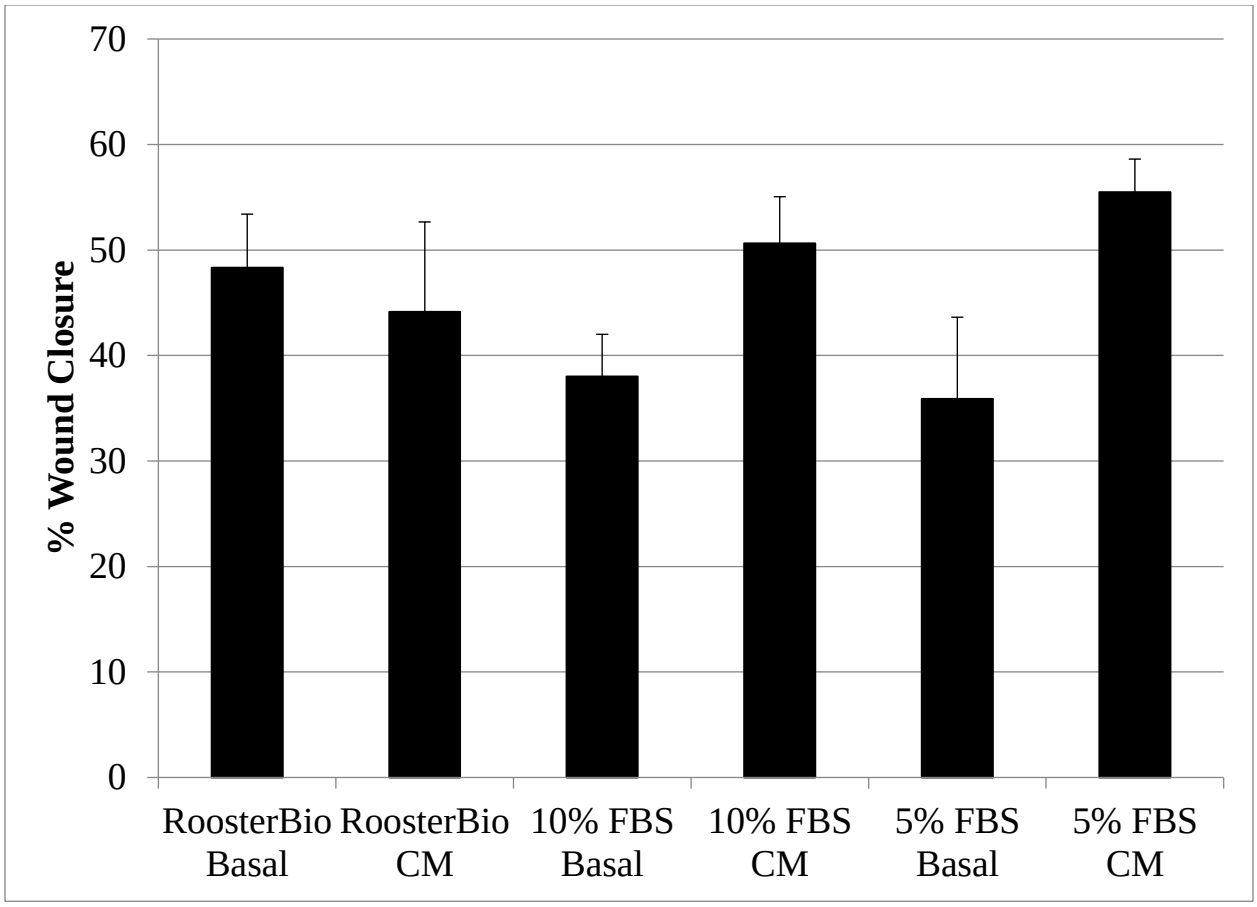

Appendix Figure 14. SMC migration after treatment with different conditioned media types.

SMC migration in response to conditioned media was tested between six groups. Increased migration was observed in the 5% Harvest CM group.

Appendix B Raw Data

Appendix B.1 CCL2 Release Profile ELISA Data

A release profile of CCL2 functionalized scaffolds was performed using an ELISA kit (R&D Systems). Total CCL2 release was measured normalized to scaffold weight prior to release (n=12, **Appendix Table 2**). Raw data is displayed in **Appendix Table 3,** with each well labeled "tube # D (day) #."

Appendix Table 2. Dry weights of each scaffold prior to release for protein quantification.

CCL2		**Lyogel**		**Blank**	
tube #	weight (mg)	tube #	weight (mg)	tube #	weight (mg)
1	14.8	13	25.6	25	18.5
2	20.3	14	23.2	26	14.3
3	10.3	15	20.7	27	21.8
4	19.6	16	22.5	28	18.2
5	19.2	17	23.2	29	23.7
6	23.1	18	16.9	30	14.4
7	17.8	19	25.6	31	14.2
8	17.2	20	15.9	32	13
9	10.4	21	23.6	33	16.9
10	13.5	22	23.4	34	17.5
11	14	23	27.1	35	15.4
12	10.6	24	27.7	36	15.4

Appendix Table 3. ELISA raw data and standards.

Three separate 96 well plates were analyzed. The plate set up, raw data and corresponding standards are shown above. All data highlighted in red represents data below the level of detection. The working range of the assay is bolded in each standard shown on the right.

PLATE 1 RAW DATA

	1	2	3	4	5	6	7	8	9	10	11	12
A	2.689	3.749	3.627	3.732	3.586	3.664	3.507	3.709	3.554	3.406	3.095	3.424
B	0.113	0.114	0.113	0.107	0.112	0.118	0.114	0.122	0.113	0.115	0.12	0.129
C	0.197	0.126	0.13	0.151	0.132	0.125	0.129	0.132	0.194	0.124	0.125	0.12
D	0.223	0.761	0.772	0.859	1.333	0.601	1.258	1.298	0.661	0.87	0.743	1.227
E	0.048	0.107	0.11	0.108	0.116	0.112	0.132	0.117	0.109	0.117	0.123	0.115
F	0.105	0.108	0.113	0.1	0.107	0.123	0.114	0.131	0.121	0.114	0.119	0.124
G	2.358	1.693	1.114	0.597	0.37	0.232	0.176	0.115				
H	2.448	1.663	0.738	0.633	0.37	0.249	0.173	0.119				

PLATE 2 SETUP

	1	2	3	4	5	6	7	8	9	10	11	12
A	1 D5	2 D5	3 D5	4 D5	5 D5	6 D5	7 D5	8 D5	9 D5	10 D5	11 D5	12 D5
B	13 D5	14 D5	15 D5	16 D5	17 D5	18 D5	19 D5	20 D5	21 D5	22 D5	23 D5	24 D5
C	25 D5	26 D5	27 D5	28 D5	29 D5	30 D5	31 D5	32 D5	33 D5	34 D5	35 D5	36 D5
D	1 D6	2 D6	3 D6	4 D6	5 D6	6 D6	7 D6	8 D6	9 D6	10 D6	11 D6	12 D6
E	13 D6	14 D6	15 D6	16 D6	17 D6	18 D6	19 D6	20 D6	21 D6	22 D6	23 D6	24 D6
F	25 D6	26 D6	27 D6	28 D6	29 D6	30 D6	31 D6	32 D6	33 D6	34 D6	35 D6	36 D6
G	A	B	C	D	E	F	G	H				
H	A	B	C	D	E	F	G	H				

	pg/mL	abs
A	**2000**	**2.403**
B	**1000**	**1.678**
C	**500**	**0.926**
D	**250**	**0.615**
E	**125**	**0.37**
F	**62.5**	**0.2405**
G	**31.3**	**0.1745**
H	0	0.117

Appendix Table 3 (continuted)

PLATE 2 SETUP

	1	2	3	4	5	6	7	8	9	10	11	12
A	1 D5	2 D5	3 D5	4 D5	5 D5	6 D5	7 D5	8 D5	9 D5	10 D5	11 D5	12 D5
B	13 D5	14 D5	15 D5	16 D5	17 D5	18 D5	19 D5	20 D5	21 D5	22 D5	23 D5	24 D5
C	25 D5	26 D5	27 D5	28 D5	29 D5	30 D5	31 D5	32 D5	33 D5	34 D5	35 D5	36 D5
D	1 D6	2 D6	3 D6	4 D6	5 D6	6 D6	7 D6	8 D6	9 D6	10 D6	11 D6	12 D6
E	13 D6	14 D6	15 D6	16 D6	17 D6	18 D6	19 D6	20 D6	21 D6	22 D6	23 D6	24 D6
F	25 D6	26 D6	27 D6	28 D6	29 D6	30 D6	31 D6	32 D6	33 D6	34 D6	35 D6	36 D6
G	A	B	C	D	E	F	G	H				
H	A	B	C	D	E	F	G	H				

PLATE 2 RAW DATA

	1	2	3	4	5	6	7	8	9	10	11	12
A	0.077	0.094	0.082	0.077	0.115	0.082	0.063	0.097	0.06	0.077	0.099	0.112
B	0.067	0.09	0.068	0.072	0.084	0.056	0.059	0.058	0.056	0.055	0.062	0.069
C	0.075	0.078	0.088	0.066	0.068	0.05	0.061	0.065	0.087	0.079	0.072	0.071
D	0.063	0.095	0.084	0.06	0.075	0.089	0.075	0.067	0.077	0.076	0.08	0.103
E	0.054	0.066	0.093	0.072	0.069	0.078	0.073	0.057	0.062	0.059	0.079	0.099
F	0.058	0.065	0.065	0.078	0.072	0.07	0.074	0.087	0.091	0.066	0.067	0.089
G	1.172	1.29	0.761	0.483	0.247	0.167	0.138	0.069				
H	1.499	1.326	0.756	0.464	0.263	0.171	0.123	0.064				

	pg/mL	abs
A	**2000**	**1.3355**
B	**1000**	**1.326**
C	**500**	**0.756**
D	**250**	**0.464**
E	**125**	**0.263**
F	**62.5**	**0.171**
G	**31.3**	**0.123**
H	0	0.064

PLATE 3 SETUP

	1	2	3	4	5	6	7	8	9	10	11	12
A	1 D7	2 D7	3 D7	4 D7	5 D7	6 D7	7 D7	8 D7	9 D7	10 D7	11 D7	12 D7
B	13 D7	14 D7	15 D7	16 D7	17 D7	18 D7	19 D7	20 D7	21 D7	22 D7	23 D7	24 D7
C	25 D7	26 D7	27 D7	28 D7	29 D7	30 D7	31 D7	32 D7	33 D7	34 D7	35 D7	36 D7
D	1 D8	2 D8	3 D8	4 D8	5 D8	6 D8	7 D8	8 D8	9 D8	10 D8	11 D8	12 D8
E	13 D8	14 D8	15 D8	16 D8	17 D8	18 D8	19 D8	20 D8	21 D8	22 D8	23 D8	24 D8
F	25 D8	26 D8	27 D8	28 D8	29 D8	30 D8	31 D8	32 D8	33 D8	34 D8	35 D8	36 D8
G	A	B	C	D	E	F	G	H				
H	A	B	C	D	E	F	G	H				

Appendix Table 3 (continuted)

PLATE 4 RAW DATA

	1	2	3	4	5	6	7	8	9	10	11	12
A	0.065	0.071	0.064	0.057	0.072	0.084	0.078	0.085	0.074	0.064	0.081	0.069
B	0.08	0.076	0.087	0.08	0.119	0.067	0.088	0.072	0.08	0.067	0.079	0.081
C	0.14	0.083	0.098	0.065	0.079	0.07	0.097	0.088	0.148	0.074	0.078	0.067
D	0.085	0.167	0.135	0.122	0.23	0.15	0.124	0.179	0.124	0.092	0.116	0.072
E	0.097	0.072	0.094	0.095	0.1	0.083	0.092	0.105	0.082	0.067	0.064	0.061
F	0.072	0.102	0.086	0.077	0.08	0.101	0.14	0.075	0.08	0.08	0.08	0.071
G	1.116	1.102	0.797	0.464	0.32	0.193	0.121					
H	1.59	1.212	0.788	0.421	0.25	0.143	0.11					

	pg/mL	abs
A	**2000**	**1.353**
B	**1000**	**1.212**
C	**500**	**0.788**
D	**250**	**0.421**
E	**125**	**0.25**
F	**62.5**	**0.143**
G	**31.3**	**0.11**
H	0	0.063

Appendix B.2 Macrophage Quantification for 1-week CCL2 Explants

Macrophages were counted using based on thresholding averaged between two blinded users (**Appendix Table 4**).

Appendix Table 4. Macrophage qunatifiation data for 1 week CCL2 explants.

INSIDE CD68 USER 1	INSIDE CD68 USER 2	INSIDE CD68 AVG	OUTSIDE CD68 USER 1	OUTSIDE CD68 USER 2	OUTSIDE CD68 AVG	INSIDE CD68/mm^2	OUTSIDE CD68/mm^2	EXPLANT TYPE
889	153	521	1235	1369	1302	50	202	BLANK
73	676	374.5	585	367	476	55	74	BLANK
230	107	168.5	2388	2969	2678.5	31	702	BLANK
88	489	288.5	3415	4280	3847.5	66	1588	BLANK
610	248	429	3565	4949	4257	41	1115	BLANK
640	329	484.5	3581	3390	3485.5	39	1144	BLANK
220	162	191	3562	3286	3424	23	743	BLANK
485	107	296	4207	3473	3840	36	1078	BLANK
235	79	157	4350	3655	4002.5	22	517	BLANK
7	5	6	88	12	50	1	23	BLANK
55	15	35	1286	1449	1367.5	3	568	BLANK
338	238	288	2640	1779	2209.5	33	566	CCL2
134	77	105.5	2077	2376	2226.5	13	701	CCL2
334	512	423	1395	1675	1535	37	545	CCL2
359	113	236	3417	4944	4180.5	22	1044	CCL2
286	276	281	4382	4877	4629.5	36	985	CCL2
167	203	185	1232	1551	1391.5	19	593	CCL2
298	229	263.5	1696	1577	1636.5	22	853	CCL2
379	440	409.5	1100	1218	1159	39	558	CCL2
254	112	183	989	1297	1143	22	495	CCL2
294	239	266.5	2292	2377	2334.5	22	714	CCL2
15	65	40	763	478	620.5	6	161	CM MP
65	38	51.5	954	338	646	7	190	CM MP
555	47	301	2394	1376	1885	34	311	CM MP
79	91	85	1215	1336	1275.5	7	243	CM MP
551	81	316	2493	1593	2043	23	483	CM MP
39	212	125.5	306	371	338.5	15	222	CM MP
36	19	27.5	2438	651	1544.5	3	151	CM MP
169	151	160	1241	1567	1404	19	507	CM MP

Appendix Table 4 (continued)

51	25	38	1258	750	1004	4	229	CM MP
136	181	158.5	1545	1317	1431	21	384	LYOGEL
143	69	106	1942	3270	2606	12	290	LYOGEL
118	77	97.5	1526	1801	1663.5	13	551	LYOGEL
168	19	93.5	949	870	909.5	12	306	LYOGEL

Cell counts were then generated using a custom code written by Dr. Timothy Chung:

```
%MAIN Run through all Images
clear
all_files = inside_files;
inside_files   = all_files(:,1)
outsides_files = all_files(:,2)
RGB_files      = all_files(:,3)

%%
%get masks
% parpool('local',16)
% parpool(8);

for i = 1:length(RGB_files);

   try
      temp_inside  = char(inside_files{i});
      temp_outside = char(outsides_files{i});
      temp_RGB     = char(RGB_files{i});

      where_space = strfind(temp_RGB,' ');
      tag = temp_RGB(1:where_space(2)-1);

      TI = imread(temp_inside);
      TI = TI(1:end,1:end,end);
      TI(TI >0) = 1; TI = logical(TI);

      TO = imread(temp_outside);
      TO = TO(1:end,1:end,end);
      TO(TO >0) = 1; TO = logical(TO);

      TRGB = imread(temp_RGB);
      TR = TRGB(1:end,1:end,1); %DAPI
      TG = TRGB(1:end,1:end,2); %BLANK
```

```
        TB = TRGB(1:end,1:end,3); %RED

        TI_DAPI = TB.*uint8(TI);
        TO_DAPI = TB.*uint8(TO);

        TI_RED  = TR.*uint8(TI);
        TO_RED  = TR.*uint8(TO);

        tkc_get_inside_outside([tag '_DAPI'], TI_DAPI, TO_DAPI);
        cd ..

        tkc_get_inside_outside([tag '_206'], TI_RED, TO_RED);
        cd ..
    catch
      disp('Something went wrong');
      wrong_cases(i,:) = 1;
      cd ..
    end
end



function tkc_get_inside_outside(tag, TI, TO);


TII = TI; %make copy of inner mask
TOO = TO; %make copy of outer mask

TII(TII >0) = 1; TII = logical(TII); %create binary regions
TOO(TOO >0) = 1; TOO = logical(TOO); %create binary regions
inside_pixel_area = sum(sum(TII));   %calculate inner pixel area
outside_pixel_area = sum(sum(TOO));  %calculat outer pixel area
%%
mkdir(tag) %Creates a new folder of cell image of interest
cd(tag)
fid = fopen([ tag '_data.csv'],'w+'); %create data file
fprintf(fid,'Inside Pixel Area, Outside Pixel Area, Inside Cell Count (Area), Outside Cell
Count (Area), Inside Cell Count (Boundaries), Outside Cell Count (Boundaries),threshold\n');
%create headers for data file.
fclose('all');

for i = 1:1:82 %threshold ranges from 1 to 82

    try
    threshold = i/100; %threshold rescaling from i, to be between 0.00 - 1.00
    temp_TI = im2bw(TI,threshold); %im2bw to binarize image
```

```
temp_TO = im2bw(TO,threshold);

temp_inside_borders = bwboundaries(temp_TI); %retrieves boundary regions from inner cross-section
temp_outside_borders = bwboundaries(temp_TO); %retrieves boundary regions from outer cross section

for j = 1:length(temp_inside_borders);
   inside_lengths(j,:) = length(temp_inside_borders{j}); %retrieve boundary lengths
end

for k = 1:length(temp_outside_borders);
   outside_lengths(k,:) = length(temp_outside_borders{k}); %retrieve boundary lengths
end

where_is_bad = inside_lengths >= 5; %filter out non cell regions
where_is_bad_2 = outside_lengths >=3; %filter out non cell regions for outer

final_inside  = temp_inside_borders(where_is_bad,:);
final_outside = temp_outside_borders(where_is_bad_2,:);

h = figure; %create new image
imshow(TI+TO,[]); hold on; %show combined image

for l=1:length(final_inside) %plot cell boundaries
  b = final_inside{l};
  plot(b(:,2),b(:,1),'b','LineWidth',1); hold on;
end

for m=1:length(final_outside) %plot cell boundaries
  b = final_outside{m};
  plot(b(:,2),b(:,1),'r','LineWidth',1); hold on;
end
set(gcf,'color','black');

title_stuff = sprintf('Threshold: %0.2f || Inside Count: %d || Outside Count: %d',threshold, length(final_inside), length(final_outside));
image_title = sprintf('Thresh_IC_OC_%0.2f %d %d.png',threshold, length(final_inside), length(final_outside));
title(title_stuff)
set(h, 'Color',[1, 1 ,1])
saveas(gcf,[image_title]);

dlmwrite([tag '_data.csv'],[inside_pixel_area outside_pixel_area sum(sum(TI)) sum(sum(TO)) length(final_inside) length(final_outside) threshold],'-append'); %appends to csv file stats per threshold
```

```
            close('all')
            clear final_inside final_outside temp_inside_borders temp_outside_borders
outside_lengths inside_lengths %reset variables for conflict reduction
            catch
              disp('There are no cells at this threshold level');
            end
        end



        function [maximum second] = tkc_get_2_boundaries(inside_boundaries);

            for i = 1:length(inside_boundaries);
               lengths(i,:) = length(inside_boundaries{i}); %creates list of boundaries
            end

        maximum = dsearchn(lengths, max(lengths)); %recovers max length
        max_copy = maximum;

        lengths_copy = lengths;
        lengths_copy(lengths_copy == max(lengths_copy)) = []; %removes max length

        second = dsearchn(lengths, max(lengths_copy)); %retrieves second max length of entire
set
        sec_copy = second;

        temp_1 = inside_boundaries{maximum}; %boundary cell to array
        temp_2 = inside_boundaries{second};  %boundary cell to array

        area_1 = polyarea(temp_1(:,1), temp_1(:,2)); %Measures area that the boundary
encompasses
        area_2 = polyarea(temp_2(:,1), temp_2(:,2)); %Measures area that the boundary
encompasses

        if area_2 > area_1
            maximum = sec_copy;
            second = max_copy;
        end
```

Appendix B.3 Protein Release from CM MPs

Samples of 10 mg of CM MPs were released into 0.5 mL PBS (pH 7.4, Gibco) in triplicate. Appendix Table 5 displays the well plate set up and raw data. The samples were normalized to the Blank MP releasates. In each well label, N refers to the replicate number and D refers to the date of measure.

Appendix Table 5. Protein release from CM MPs raw data.

The well plate setup (top) used the nomenclature: sample number (N#) day of releasate collection (D#) or standard label (STD) which corresponds to the standards displayed in the bottom table. Raw data is displayed in the middle table.

	1	2	3	4	5	6	7	8	9
A	STD A	STD A	STD A	STD I	STD I	STD I	N1 D16	N2 D16	N3 D16
B	STD B	STD B	STD B	N1 D1	N2 D1	N3 D1	N1 D18	N2 D18	N3 D18
C	STD C	STD C	STD C	N1 D2	N2 D2	N3 D2	N1 D21	N2 D21	N3 D21
D	STD D	STD D	STD D	N1 D4	N2 D4	N3 D4	B D1	B D2	B D4
E	STD E	STD E	STD E	N1 D7	N2 D7	N3 D7	B D7	B D9	B D11
F	STD F	STD F	STD F	N1 D9	N2 D9	N3 D9	B D14	B D16	B D18
G	STD G	STD G	STD G	N1 D11	N2 D11	N3 D11	B D21		
H	STD H	STD H	STD H	N1 D14	N2 D14	N3 D14			
	1	**2**	**3**	**4**	**5**	**6**	**7**	**8**	**9**
A	2.139	2.077	2.09	0.099	0.098	0.099	0.108	0.14	0.11
B	0.588	0.554	0.574	0.499	0.467	0.519	0.128	0.135	0.149
C	0.357	0.343	0.34	0.179	0.117	0.117	0.148	0.151	0.165
D	0.211	0.209	0.204	0.108	0.104	0.127	0.107	0.104	0.11
E	0.134	0.133	0.138	0.111	0.11	0.161	0.116	0.122	0.108
F	0.118	0.11	0.111	0.142	0.122	0.149	0.137		
G	0.105	0.106	0.106	0.117	0.139	0.12			
H	0.104	0.106	0.106	0.131	0.126	0.343			

Appendix Table 5 (continued)

Standard		
STD	ug/mL	Abs
A	200	2.102
B	40	0.572
C	20	0.347
D	10	0.208
E	5	0.135
F	2.5	0.113
G	1	0.106
H	0.5	0.105
I	0	0.099

Appendix B.4 CM MP Scratch Assay Migration Quantification

SMC migration was assessed using a scratch wound assay (**Section 3.1.5**). Treatments of unsupplemented SMC media (negative control, Cell Applications), RoosterBio CM (positive control, RoosterBio), 500 μL of 10 mg/mL Blank MP releasate, and 500 μL of 10 mg/mL CM MP releasate were applied to SMCs. All images were blinded before quantification to ensure non-biased measurements. Percent wound closure after 18 and 24 hours were quantified (**Appendix A.5.2**) by two separate people and average (**Appendix Table 6**).

Appendix Table 6. Scratch assay quantification represented as % wound closure after 18 and 24 hours.

User #1 Measurements				
	18H %	18H STD	24H %	24H STD
UNSUPP	68	28	83	20
BLANK MP	62	26	73	19
CM MP	72	23	87	14
CM	86	17	97	6
User #2 Measurements				
UNSUPP	59	16	78	25
BLANK	59	28	82	22
CM MP	71	23	77	19
CM	71	8	96	8
Combined Measurements				
UNSUPP	64	6	81	4
BLANK	60	2	77	7
CM MP	72	1	82	7
CM	79	10	97	1

Appendix B.5 CM MP Proliferation Quantification

SMC proliferation in response to CM MPs was quantified in **Section 3.2.5**. **Appendix Table 7** displays the raw data.

Appendix Table 7. CM MP SMC proliferation quantification.

Cell count at time 0	Cell count at time 12	% increase after 12 hours	Cell count after 24 hours	% increase after 24 hours	Cell count after 48 hours	% increase after 48 hours
32	39	22	51	59	60	88
63	79	25	81	29	90	43
49	64	31	68	39	100	104
73	89	22	101	38	114	56
61	100	64	125	105	132	116
54	63	17	77	43	82	52
27	36	33	40	48	42	56
56	61	9	76	36	75	34
30	35	17	46	53	51	70
57	74	30	103	81	114	100
29	35	21	49	69	55	90
22	27	23	30	36	33	50
32	52	63	65	103	71	122
34	52	53	76	124	82	141
39	56	44	76	95	86	121
28	34	21	50	79	64	129
35	41	17	65	86	77	120
26	31	19	45	73	55	112
15	29	93	46	207	56	273
40	71	78	106	165	112	180
48	72	50	118	146	128	167
16	24	50	41	156	57	256
31	42	35	66	113	70	126
37	58	57	99	168	125	238

Appendix B.6 EV Scratch Assay Migration

Averages of percent wound closure after 24 hours are listed in **Appendix Table 8** (SMCs) and **9** (ECs). Each row represents one batch of EV isolate.

Appendix Table 8. . SMC migration with EV treatment.

Values represent percent wound closure after 24 hours. SBM=supplemented basal media, CM=conditioned media, dCM=conditioned media with EVs depleted, nCM=non conditioned media, PBS=phosphate buffered saline, UBM=unsupplemented basal media (SMC specific), EV150= 150µL of EV isolate, EV50=100µL PBS + 50µL EV isolate.

SBM	CM	dCM	nCM	PBS	UBM	EV150	EV50
78.8	66.6	43.6	41.2	27.9	27.9	48.7	50.6
88.9	88.2	60.0	43.1	30.3	37.1	63.2	47.3
97.7	67.9	56.1	40.7	25.8	36.7	59.1	44.0

Appendix Table 9. EC migration with EV treatment.

Values represent percent wound closure after 24 hours. SBM=supplemented basal media, CM=conditioned media, dCM=conditioned media with EVs depleted, nCM=non conditioned media, PBS=phosphate buffered saline, UBM=unsupplemented basal media (EC specific), EV150= 150µL of EV isolate, EV50=100µL PBS + 50µL EV isolate.

SBM	UBM	PBS	EV150	EV50	nCM	CM	dCM
65.6	18.4	17.0	48.5	36.1	59.9	99.0	72.5
58.9	26.4	19.9	39.9	31.8	78.6	84.2	71.1
69.8	19.1			30.2	78.5	86.4	63.8

Appendix B.7 EV Stimulation of Cell Proliferation

Averages of cellular proliferation measured using Alamar blue assays (**Chapter 4.2.4**) after 24 hours are listed in **Appendix Table 10** (SMCs) and **11** (ECs). Each row represents one batch of EV isolate.

Appendix Table 10. SMC proliferation with EV treatment.

Values represent SMC proliferation measured using alamar blue after 24 hours of treatment. SBM=supplemented basal media, UBM=unsupplemented basal media (SMC specific), PBS=phosphate buffered saline, EV150= 150µL of EV isolate, EV50=100µL PBS + 50µL EV isolate, nCM=non conditioned media, CM=conditioned media, and dCM=conditioned media with EVs depleted. Each column represents one EV isolation and black boxes indcate no sample was run for that assay.

SBM	UBM	PBS	EV150	EV50	nCM	CM	dCM
0.134						0.598	0.276
0.111	0.692	0.932		0.898		0.650	0.210
0.174	0.659		0.753	0.689		0.583	0.324
0.217	0.718	1.083	0.964		0.407		0.274
0.113	0.755	1.073	0.986		0.454		0.243
0.109		0.816		0.757	0.358		

Appendix Table 11. EC profilferation with EV treatment.

Values represent EC proliferation measured using alamar blue after 24 hours of treatment. SBM=supplemented basal media, UBM=unsupplemented basal media (SMC specific), PBS=phosphate buffered saline, EV150= 150µL of EV isolate, EV50=100µL PBS + 50µL EV isolate, nCM=non conditioned media, CM=conditioned media, and dCM=conditioned media with EVs depleted. Each column represents one EV isolation and black boxes indcate no sample was run for that assay.

SBM	BM	PBS	EV150	EV50	nCM	CM	dCM
0.465	1.1			0.986	0.665	0.577	0.356
0.413	1.23	1.196	1.051	1.061	0.657	0.588	0.268
0.387	1.26	1.213	1.1976	1.032	0.706	0.526	0.27
0.448	1.3	1.335	1.36	1.185			0.27
0.416	1.52	1.263	1.2181	1.152			0.186
0.391	1.46	1.275	1.1927	0.943			0.233

Appendix B.8 EV Functionalized Lyogel Explants Elastin and Collagen Quantification

Elastin was quantified by Dr. Ramaswamy using a ninhydrin assay. Raw data is displayed in **Appendix Table 12** in μg ELN/μg Total Protein.

Appendix Table 12. Elastin quantification of 8 week explanted EV funcionalized TEVGs. Elastin content of 8 week explanted TEVGs was measured for the Blank (BM silk alone), MSCs (MSCs seeded BM silk), and EV (EV functionalized BM silk) groups. Measurements are in μg ELN/μg Total Protein. Black boxes represent no sample or damaged sample with no quantification.

Blank	MSC	EV
0.25455	0.13994	1.256
0.09562	1.53869	0.77858
0.352	0.60799	0.57855
0.44249	0.42626	0.84499
	0.31541	0.429
0.30031	0.77829	2.3275
0.51079	1.09735	0.69113
0.56923	0.43749	0.48298
0.52518	0.40403	0.96114
0.45109	0.59783	0.81695
0.54665	0.55469	
	0.7592	

Collagen was quantified by Dr. Ramaswamy using a hydroxyproline assay. Raw data is displayed in **Appendix Table 13** in μg COL/μg Total Protein.

Appendix Table 13. Collagen quantification of explanted 8 week EV functionalized TEVGs. Collagen content of 8 week explanted TEVGs was measured for the Blank (BM silk alone), ASC (adipose stem cell seeded BM silk), and EV (EV functionalized BM silk) groups. Measurements are in µg ELN/µg Total Protein. Black boxes represent no sample or damaged sample with no quantification.

Blank	MSC	EV
1.03302	1.13763	1.49222
1.18234	0.96027	1.20808
0.44285	1.32416	2.21491
0.88415	0.51389	0.98837
0.63624	1.34319	2.35643
1.15698	1.01944	1.11923
1.54355	1.047	1.48447
0.86367	1.2778	1.9777
1.44409	1.48796	0.66902
1.01422	0.6472	1.23973
	1.5727	
	1.28167	

Appendix B.9 EV Seeding Efficiency

Seeding efficiency was measured by comparing the protein content of the EV isolate before and after seeding. Raw data is displayed in **Appendix Table 14** in μg/mL.

Appendix Table 14. Protein content of EV isolate pre and post seeding.

Seeding efficiency was measured by detecting the amount of protein within the EV isolate before and after seeding. A portion of each sample was also lysed to release protein content previously encapsulated within the vesicles. Values are shown in μg/mL.

Post infusion	Post infusion lysed	Pre infusion	Post infusion lysed
57.238	84.65461	163.879	170.8257
77.8568	92.41623	160.132	166.729
73.0037	68.0177	153.922	173.8641

Appendix C Summary of Accomplishments

The work within this dissertation resulted in the following manuscripts:

1. Darren G Haskett, Kamiel S Saleh, **Katherine L Lorentz**, Alexander D Josowitz, Samuel K Lueketich, Justin S Weinbaum, Lauren E Kokai, Antonio D'Amore, Kacey G Marra, J Peter Rubin, William R Wagner, David A Vorp; An exploratory study on the preparation and evaluation of a "same-day" adipose stem cell-based tissue-engineered vascular graft (JTCVS, November 2018)
2. Aneesh K Ramaswamy, Rachel E Sides, Eoghan M Cunnane, **Katherine L Lorentz**, Leila M Reines, David A Vorp, Justin S Weinbaum; Adipose-Derived Stromal Cell Secreted Factors Induce the Elastogenesis Cascade within 3D Aortic Smooth Muscle Cell Constructs (Matrix Biology Plus, Sept 2019)
3. Prerak Gupta, **Katherine L Lorentz**, Darren G Haskett, Eoghan M Cunnane, Aneesh K Ramaswamy, Justin S Weinbaum, David A Vorp, Biman B Mandal; Bioresorbable Silk Grafts for Small Diameter Vascular Tissue Engineering Applications: In vitro and In vivo Functional Analysis (Acta Biomaterialia, March 2020)
4. Eoghan M Cunnane, **Katherine L Lorentz**, Aneesh K Ramaswamy, Prerak Gupta, Biman B Mandal, Fergal J O'Brien, Justin S Weinbaum, David A Vorp; Extracellular vesicles enable remodeling of cell-free silk vascular scaffolds in rat aortae (ACS, accepted May 2020)
5. Eoghan M Cunnane, Niall F Davis, Alan J Ryan, **Katherine L Lorentz**, Jochen Hess, Justin S Weinbaum, Michael T Walsh, Fergal J O'Brien, David A Vorp;

Biomechanical and micromorphological characterization of the human male urethra for the development of a biomimetic tissue engineered urethral scaffold (in preparation)

6. **Katherine L Lorentz**, Eoghan M Cunnane, Aneesh K Ramaswamy, Timothy K Chung, Darren G Haskett, Samuel K Luketich, Lorenzo Soletti, Edith T Tzeng, Antonio D'Amore, William R Wagner, Justin S Weinbaum, David A Vorp; Seeding Tubular Scaffolds with Adipose Stromal Cells for Large Animal Model Implantation of Tissue Engineered Vascular Grafts (in preparation)
7. **Katherine L Lorentz**, Prerak Gupta, Mostafa S Shehabeldin, Emily M Lickert, Brittany R Rodriguez, Eoghan M Cunnane, Aneesh K Ramaswamy, Morgan V Fedorchak, Steven R Little, Justin S Weinbaum, Charles S Sfier, Biman B Mandal, David A Vorp; Testing the efficacy of CCL2 to prevent acute thrombosis in silk vascular grafts in vivo (in preparation)
8. **Katherine Lorentz**, Liza A Bruk, Prerak Gupta, Eoghan M Cunnane, Aneesh K Ramaswamy, Biman B Mandal, Morgan V Fedorchak, Steven R Little, Justin S Weinbaum, David A Vorp; Validation of artificial MSCs for use in tissue engineered vascular grafts (in preparation)

The following patent applications were filed as a result of this work:

1. Artificial cells and delivery devices for use in tissue engineering, and related methods (PCT/US2017/039973)
2. Biodegradable, porous, tubular silk scaffold for tissue engineering applications (in preparation)
3. Extracellular vesicle augmentation of vascular grafts (in preparation)

The following research grants and awards were earned by the author, mentored student during the work described in this dissertation, or PI with contributions from the author:

1. NIH R01 HL130077; Artificial Stem Cells for Vascular Tissue Engineering. National Institutes of Health grant to the Vascular Bioengineering laboratory awarded July 2016.
2. Bevier Award, Swanson School of Engineering, University of Pittsburgh, awarded to author September 2016.
3. World Congress of Biomechanics Grant; Retention of seeded mesenchymal stem cells within an implanted elastomeric vascular scaffold, awarded to author in July 2018.
4. Undergraduate Summer Research Internship; Swanson School of Engineering, University of Pittsburgh 6/2018-8/2018, awarded to Abigail Snyder (mentored undergraduate student).
5. Undergraduate Summer Research Internship; Swanson School of Engineering, University of Pittsburgh 6/2018-8/2018, awarded to Meara Sedlak (mentored undergraduate student).
6. Undergraduate Summer Research Internship; Swanson School of Engineering, University of Pittsburgh 6/2019-8/2019, awarded to Emily Lickert (mentored undergraduate student).

Bibliography

1. Isenberg BC, Williams C and Tranquillo RT. Small-diameter artificial arteries engineered in vitro. *Circ Res*. 2006;98:25-35.

2. U.S. National Institutes of Health NCI. SEER Training Modules, Introduction to the Cardiovascular System.

3. Docherty B. The arteriovenous system. Part one--the anatomy. *Nurs Times*. 2005;101:28-9.

4. Susan Standring HG. Grey's Anatomy 40th Edition: The Anatomical Basis of Clinical Practice. 2008.

5. J Charles Jennette JRS. *Cellular and Molecular Pathobiology of Cardiovascular Disease*. London: Elsevier; 2014.

6. Heart Disease Facts. 2019.

7. Kirkton RD, Santiago-Maysonet M, Lawson JH, Tente WE, Dahl SLM, Niklason LE and Prichard HL. Bioengineered human acellular vessels recellularize and evolve into living blood vessels after human implantation. *Sci Transl Med*. 2019;11.

8. Gong Z and Niklason LE. Blood vessels engineered from human cells. *Trends Cardiovasc Med*. 2006;16:153-6.

9. Sugiura T, Matsumura G, Miyamoto S, Miyachi H, Breuer CK and Shinoka T. Tissue-engineered Vascular Grafts in Children With Congenital Heart Disease: Intermediate Term Follow-up. *Semin Thorac Cardiovasc Surg*. 2018;30:175-179.

10. Best C, Strouse R, Hor K, Pepper V, Tipton A, Kelly J, Shinoka T and Breuer C. Toward a patient-specific tissue engineered vascular graft. *J Tissue Eng*. 2018;9:2041731418764709.

11. Sugiura T, Tara S, Nakayama H, Kurobe H, Yi T, Lee YU, Lee AY, Breuer CK and Shinoka T. Novel Bioresorbable Vascular Graft With Sponge-Type Scaffold as a Small-Diameter Arterial Graft. *Ann Thorac Surg*. 2016;102:720-727.

12. Breuer CK. The development and translation of the tissue-engineered vascular graft. *J Pediatr Surg*. 2011;46:8-17.

13. Grassl ED, Oegema TR and Tranquillo RT. A fibrin-based arterial media equivalent. *J Biomed Mater Res A*. 2003;66:550-61.

14. Syedain ZH, Graham ML, Dunn TB, O'Brien T, Johnson SL, Schumacher RJ and Tranquillo RT. A completely biological "off-the-shelf" arteriovenous graft that recellularizes in baboons. *Sci Transl Med*. 2017;9.

15. Tanaka K, Fukuda D, Higashikuni Y, Hirata Y, Komuro I, Saotome T, Yamashita Y, Asakura T and Sata M. Biodegradable Extremely-Small-Diameter Vascular Graft Made of Silk Fibroin can be Implanted in Mice. *J Atheroscler Thromb*. 2020.

16. Soffer L, Wang X, Zhang X, Kluge J, Dorfmann L, Kaplan DL and Leisk G. Silk-based electrospun tubular scaffolds for tissue-engineered vascular grafts. *J Biomater Sci Polym Ed*. 2008;19:653-64.

17. Nieponice A, Soletti L, Guan J, Deasy BM, Huard J, Wagner WR and Vorp DA. Development of a tissue-engineered vascular graft combining a biodegradable scaffold, muscle-derived stem cells and a rotational vacuum seeding technique. *Biomaterials*. 2008;29:825-33.

18. Nieponice A, Soletti L, Guan J, Hong Y, Gharaibeh B, Maul TM, Huard J, Wagner WR and Vorp DA. In vivo assessment of a tissue-engineered vascular graft combining a biodegradable elastomeric scaffold and muscle-derived stem cells in a rat model. *Tissue Eng Part A*. 2010;16:1215-23.

19. Krawiec JT, Weinbaum JS, Liao HT, Ramaswamy AK, Pezzone DJ, Josowitz AD, D'Amore A, Rubin JP, Wagner WR and Vorp DA. In Vivo Functional Evaluation of Tissue-Engineered Vascular Grafts Fabricated Using Human Adipose-Derived Stem Cells from High Cardiovascular Risk Populations. *Tissue Eng Part A*. 2016;22:765-75.

20. Haskett DG, Saleh KS, Lorentz KL, Josowitz AD, Luketich SK, Weinbaum JS, Kokai LE, D'Amore A, Marra KG, Rubin JP, Wagner WR and Vorp DA. An exploratory study on the preparation and evaluation of a "same-day" adipose stem cell-based tissue-engineered vascular graft. *J Thorac Cardiovasc Surg*. 2018;156:1814-1822 e3.

21. Benjamin EJ, Muntner P, Alonso A, Bittencourt MS, Callaway CW, Carson AP, Chamberlain AM, Chang AR, Cheng S, Das SR, Delling FN, Djousse L, Elkind MSV, Ferguson JF, Fornage M, Jordan LC, Khan SS, Kissela BM, Knutson KL, Kwan TW, Lackland DT, Lewis TT, Lichtman JH, Longenecker CT, Loop MS, Lutsey PL, Martin SS, Matsushita K, Moran AE, Mussolino ME, O'Flaherty M, Pandey A, Perak AM, Rosamond WD, Roth GA, Sampson UKA, Satou GM, Schroeder EB, Shah SH, Spartano NL, Stokes A, Tirschwell DL, Tsao CW, Turakhia MP, VanWagner LB, Wilkins JT, Wong SS, Virani SS, American Heart Association Council on E, Prevention Statistics C and Stroke Statistics S. Heart Disease and Stroke Statistics-2019 Update: A Report From the American Heart Association. *Circulation*. 2019;139:e56-e528.

22. Fryar CD, Chen TC and Li X. Prevalence of uncontrolled risk factors for cardiovascular disease: United States, 1999-2010. *NCHS Data Brief*. 2012:1-8.

23. Libby P and Theroux P. Pathophysiology of coronary artery disease. *Circulation*. 2005;111:3481-8.

24. Boudoulas KD, Triposciadis F, Geleris P and Boudoulas H. Coronary Atherosclerosis: Pathophysiologic Basis for Diagnosis and Management. *Prog Cardiovasc Dis*. 2016;58:676-92.

25. Simpson CF. Comparative morphology of intimal and adventitial hyperplasia of the arteriosclerotic turkey aorta. *Exp Mol Pathol*. 1972;17:65-76.

26. Newby AC and Zaltsman AB. Molecular mechanisms in intimal hyperplasia. *J Pathol*. 2000;190:300-9.

27. Insull W, Jr. The pathology of atherosclerosis: plaque development and plaque responses to medical treatment. *Am J Med*. 2009;122:S3-S14.

28. Patel RS, Asselbergs FW, Quyyumi AA, Palmer TM, Finan CI, Tragante V, Deanfield J, Hemingway H, Hingorani AD and Holmes MV. Genetic variants at chromosome 9p21 and risk of first versus subsequent coronary heart disease events: a systematic review and meta-analysis. *J Am Coll Cardiol*. 2014;63:2234-45.

29. Beckman JA and Creager MA. Vascular Complications of Diabetes. *Circ Res*. 2016;118:1771-85.

30. Siasos G, Tsigkou V, Kokkou E, Oikonomou E, Vavuranakis M, Vlachopoulos C, Verveniotis A, Limperi M, Genimata V, Papavassiliou AG, Stefanadis C and Tousoulis D. Smoking and atherosclerosis: mechanisms of disease and new therapeutic approaches. *Curr Med Chem*. 2014;21:3936-48.

31. Palmefors H, DuttaRoy S, Rundqvist B and Borjesson M. The effect of physical activity or exercise on key biomarkers in atherosclerosis--a systematic review. *Atherosclerosis*. 2014;235:150-61.

32. Siri-Tarino PW and Krauss RM. Diet, lipids, and cardiovascular disease. *Curr Opin Lipidol*. 2016;27:323-8.

33. Kruger-Genge A, Blocki A, Franke RP and Jung F. Vascular Endothelial Cell Biology: An Update. *Int J Mol Sci*. 2019;20.

34. Cines DB, Pollak ES, Buck CA, Loscalzo J, Zimmerman GA, McEver RP, Pober JS, Wick TM, Konkle BA, Schwartz BS, Barnathan ES, McCrae KR, Hug BA, Schmidt AM and Stern DM. Endothelial cells in physiology and in the pathophysiology of vascular disorders. *Blood*. 1998;91:3527-61.

35. Aird WC. Endothelial cell heterogeneity. *Cold Spring Harb Perspect Med*. 2012;2:a006429.

36. Galley HF and Webster NR. Physiology of the endothelium. *Br J Anaesth*. 2004;93:105-13.

37. dela Paz NG and D'Amore PA. Arterial versus venous endothelial cells. *Cell Tissue Res*. 2009;335:5-16.

38. Wu KK and Thiagarajan P. Role of endothelium in thrombosis and hemostasis. *Annu Rev Med*. 1996;47:315-31.

39. Yau JW, Teoh H and Verma S. Endothelial cell control of thrombosis. *BMC Cardiovasc Disord*. 2015;15:130.

40. Busse R, Trogisch G and Bassenge E. The role of endothelium in the control of vascular tone. *Basic Res Cardiol*. 1985;80:475-90.

41. Zhao Y, Vanhoutte PM and Leung SW. Vascular nitric oxide: Beyond eNOS. *J Pharmacol Sci*. 2015;129:83-94.

42. Mundi S, Massaro M, Scoditti E, Carluccio MA, van Hinsbergh VWM, Iruela-Arispe ML and De Caterina R. Endothelial permeability, LDL deposition, and cardiovascular risk factors-a review. *Cardiovasc Res*. 2018;114:35-52.

43. Velnar T and Gradisnik L. Tissue Augmentation in Wound Healing: the Role of Endothelial and Epithelial Cells. *Med Arch*. 2018;72:444-448.

44. Newby AC. An overview of the vascular response to injury: a tribute to the late Russell Ross. *Toxicol Lett*. 2000;112-113:519-29.

45. Maus U, Henning S, Wenschuh H, Mayer K, Seeger W and Lohmeyer J. Role of endothelial MCP-1 in monocyte adhesion to inflamed human endothelium under physiological flow. *Am J Physiol Heart Circ Physiol*. 2002;283:H2584-91.

46. Salcedo R, Ponce ML, Young HA, Wasserman K, Ward JM, Kleinman HK, Oppenheim JJ and Murphy WJ. Human endothelial cells express CCR2 and respond to MCP-1: direct role of MCP-1 in angiogenesis and tumor progression. *Blood*. 2000;96:34-40.

47. Munaron L and Fiorio Pla A. Endothelial calcium machinery and angiogenesis: understanding physiology to interfere with pathology. *Curr Med Chem*. 2009;16:4691-703.

48. Pawlowski KJ, Rittgers SE, Schmidt SP and Bowlin GL. Endothelial cell seeding of polymeric vascular grafts. *Front Biosci*. 2004;9:1412-21.

49. Melchiorri AJ, Bracaglia LG, Kimerer LK, Hibino N and Fisher JP. In Vitro Endothelialization of Biodegradable Vascular Grafts Via Endothelial Progenitor Cell Seeding and Maturation in a Tubular Perfusion System Bioreactor. *Tissue Eng Part C Methods*. 2016;22:663-70.

50. Dunn PF, Newman KD, Jones M, Yamada I, Shayani V, Virmani R and Dichek DA. Seeding of vascular grafts with genetically modified endothelial cells. Secretion of recombinant TPA results in decreased seeded cell retention in vitro and in vivo. *Circulation*. 1996;93:1439-46.

51. Tucker WD and Mahajan K. Anatomy, Blood Vessels *StatPearls* Treasure Island (FL); 2020.

52. Lacolley P, Regnault V, Nicoletti A, Li Z and Michel JB. The vascular smooth muscle cell in arterial pathology: a cell that can take on multiple roles. *Cardiovasc Res*. 2012;95:194-204.

53. Mark A. Creager JAB, Joseph Loscalzo. *Vascular Medicine: A Companion to Braunwald's Heart Disease*. Second ed. ELSEVIER Inc.: Saunders; 2013.

54. Wang G, Jacquet L, Karamariti E and Xu Q. Origin and differentiation of vascular smooth muscle cells. *J Physiol*. 2015;593:3013-30.

55. Beamish JA, He P, Kottke-Marchant K and Marchant RE. Molecular regulation of contractile smooth muscle cell phenotype: implications for vascular tissue engineering. *Tissue Eng Part B Rev*. 2010;16:467-91.

56. Thyberg J, Blomgren K, Hedin U and Dryjski M. Phenotypic modulation of smooth muscle cells during the formation of neointimal thickenings in the rat carotid artery after balloon injury: an electron-microscopic and stereological study. *Cell Tissue Res*. 1995;281:421-33.

57. Touyz RM, Alves-Lopes R, Rios FJ, Camargo LL, Anagnostopoulou A, Arner A and Montezano AC. Vascular smooth muscle contraction in hypertension. *Cardiovasc Res*. 2018;114:529-539.

58. Rzucidlo EM, Martin KA and Powell RJ. Regulation of vascular smooth muscle cell differentiation. *J Vasc Surg*. 2007;45 Suppl A:A25-32.

59. Bennett MR, Sinha S and Owens GK. Vascular Smooth Muscle Cells in Atherosclerosis. *Circ Res*. 2016;118:692-702.

60. Doran AC, Meller N and McNamara CA. Role of smooth muscle cells in the initiation and early progression of atherosclerosis. *Arterioscler Thromb Vasc Biol*. 2008;28:812-9.

61. Brown IAM, Diederich L, Good ME, DeLalio LJ, Murphy SA, Cortese-Krott MM, Hall JL, Le TH and Isakson BE. Vascular Smooth Muscle Remodeling in Conductive and Resistance Arteries in Hypertension. *Arterioscler Thromb Vasc Biol*. 2018;38:1969-1985.

62. Sterpetti AV, Cucina A, D'Angelo LS, Cardillo B and Cavallaro A. Shear stress modulates the proliferation rate, protein synthesis, and mitogenic activity of arterial smooth muscle cells. *Surgery*. 1993;113:691-9.

63. Qiu J, Zheng Y, Hu J, Liao D, Gregersen H, Deng X, Fan Y and Wang G. Biomechanical regulation of vascular smooth muscle cell functions: from in vitro to in vivo understanding. *J R Soc Interface*. 2014;11:20130852.

64. Otsuka F, Yasuda S, Noguchi T and Ishibashi-Ueda H. Pathology of coronary atherosclerosis and thrombosis. *Cardiovasc Diagn Ther*. 2016;6:396-408.

65. Hibino N, Yi T, Duncan DR, Rathore A, Dean E, Naito Y, Dardik A, Kyriakides T, Madri J, Pober JS, Shinoka T and Breuer CK. A critical role for macrophages in neovessel formation and the development of stenosis in tissue-engineered vascular grafts. *FASEB J*. 2011;25:4253-63.

66. Buccheri D, Piraino D, Andolina G and Cortese B. Understanding and managing in-stent restenosis: a review of clinical data, from pathogenesis to treatment. *J Thorac Dis*. 2016;8:E1150-E1162.

67. Frismantiene A, Philippova M, Erne P and Resink TJ. Smooth muscle cell-driven vascular diseases and molecular mechanisms of VSMC plasticity. *Cell Signal*. 2018;52:48-64.

68. Opitz F, Schenke-Layland K, Cohnert TU and Stock UA. Phenotypical plasticity of vascular smooth muscle cells-effect of in vitro and in vivo shear stress for tissue engineering of blood vessels. *Tissue Eng*. 2007;13:2505-14.

69. Wagenseil JE and Mecham RP. Vascular extracellular matrix and arterial mechanics. *Physiol Rev*. 2009;89:957-89.

70. Cocciolone AJ, Hawes JZ, Staiculescu MC, Johnson EO, Murshed M and Wagenseil JE. Elastin, arterial mechanics, and cardiovascular disease. *Am J Physiol Heart Circ Physiol*. 2018;315:H189-H205.

71. Fratzl P. *Collagen : structure and mechanics*. New York: Springer; 2008.

72. Xie SA, Zhang T, Wang J, Zhao F, Zhang YP, Yao WJ, Hur SS, Yeh YT, Pang W, Zheng LS, Fan YB, Kong W, Wang X, Chiu JJ and Zhou J. Matrix stiffness determines the phenotype of vascular smooth muscle cell in vitro and in vivo: Role of DNA methyltransferase 1. *Biomaterials*. 2018;155:203-216.

73. *Biochemistry of Collagens, Laminins and Elastin: Structure, Function and Biomarkers*; 2016.

74. Ponticos M and Smith BD. Extracellular matrix synthesis in vascular disease: hypertension, and atherosclerosis. *J Biomed Res*. 2014;28:25-39.

75. Patel A, Fine B, Sandig M and Mequanint K. Elastin biosynthesis: The missing link in tissue-engineered blood vessels. *Cardiovasc Res*. 2006;71:40-9.

76. Li DY, Brooke B, Davis EC, Mecham RP, Sorensen LK, Boak BB, Eichwald E and Keating MT. Elastin is an essential determinant of arterial morphogenesis. *Nature*. 1998;393:276-80.

77. Shapiro SD, Endicott SK, Province MA, Pierce JA and Campbell EJ. Marked longevity of human lung parenchymal elastic fibers deduced from prevalence of D-aspartate and nuclear weapons-related radiocarbon. *J Clin Invest*. 1991;87:1828-34.

78. Zarkovic K, Larroque-Cardoso P, Pucelle M, Salvayre R, Waeg G, Negre-Salvayre A and Zarkovic N. Elastin aging and lipid oxidation products in human aorta. *Redox Biol*. 2015;4:109-17.

79. Just M, Ribera M, Monso E, Lorenzo JC and Ferrandiz C. Effect of smoking on skin elastic fibres: morphometric and immunohistochemical analysis. *Br J Dermatol*. 2007;156:85-91.

80. Abraham PA, Perejda AJ, Carnes WH and Uitto J. Marfan syndrome. Demonstration of abnormal elastin in aorta. *J Clin Invest*. 1982;70:1245-52.

81. Wong CS, Liu X, Xu Z, Lin T and Wang X. Elastin and collagen enhances electrospun aligned polyurethane as scaffolds for vascular graft. *J Mater Sci Mater Med*. 2013;24:1865-74.

82. Wise SG, Byrom MJ, Waterhouse A, Bannon PG, Weiss AS and Ng MK. A multilayered synthetic human elastin/polycaprolactone hybrid vascular graft with tailored mechanical properties. *Acta Biomater*. 2011;7:295-303.

83. Syedain Z, Reimer J, Lahti M, Berry J, Johnson S and Tranquillo RT. Tissue engineering of acellular vascular grafts capable of somatic growth in young lambs. *Nat Commun*. 2016;7:12951.

84. Kothapalli CR, Taylor PM, Smolenski RT, Yacoub MH and Ramamurthi A. Transforming growth factor beta 1 and hyaluronan oligomers synergistically enhance elastin matrix regeneration by vascular smooth muscle cells. *Tissue Eng Part A*. 2009;15:501-11.

85. Davidson JM, Zoia O and Liu JM. Modulation of transforming growth factor-beta 1 stimulated elastin and collagen production and proliferation in porcine vascular smooth muscle cells and skin fibroblasts by basic fibroblast growth factor, transforming growth factor-alpha, and insulin-like growth factor-I. *J Cell Physiol*. 1993;155:149-56.

86. Krawiec JT, Liao HT, Kwan LL, D'Amore A, Weinbaum JS, Rubin JP, Wagner WR and Vorp DA. Evaluation of the stromal vascular fraction of adipose tissue as the basis for a stem cell-based tissue-engineered vascular graft. *J Vasc Surg*. 2017;66:883-890 e1.

87. Ramaswamy AK, Vorp DA and Weinbaum JS. Functional Vascular Tissue Engineering Inspired by Matricellular Proteins. *Front Cardiovasc Med*. 2019;6:74.

88. Soletti L, Hong Y, Guan J, Stankus JJ, El-Kurdi MS, Wagner WR and Vorp DA. A bilayered elastomeric scaffold for tissue engineering of small diameter vascular grafts. *Acta Biomater*. 2010;6:110-22.

89. Johnson R, Ding Y, Nagiah N, Monnet E and Tan W. Coaxially-structured fibres with tailored material properties for vascular graft implant. *Mater Sci Eng C Mater Biol Appl*. 2019;97:1-11.

90. Fischer GM, Swain ML and Cherian K. Increased vascular collagen and elastin synthesis in experimental atherosclerosis in the rabbit. Variation in synthesis among major vessels. *Atherosclerosis*. 1980;35:11-20.

91. Bishop JE and Lindahl G. Regulation of cardiovascular collagen synthesis by mechanical load. *Cardiovasc Res*. 1999;42:27-44.

92. McKavanagh P, Zawadowski G, Ahmed N and Kutryk M. The evolution of coronary stents. *Expert Rev Cardiovasc Ther*. 2018;16:219-228.

93. Virani SS, Alonso A, Benjamin EJ, Bittencourt MS, Callaway CW, Carson AP, Chamberlain AM, Chang AR, Cheng S, Delling FN, Djousse L, Elkind MSV, Ferguson JF, Fornage M, Khan SS, Kissela BM, Knutson KL, Kwan TW, Lackland DT, Lewis TT, Lichtman JH, Longenecker CT, Loop MS, Lutsey PL, Martin SS, Matsushita K, Moran AE, Mussolino ME, Perak AM, Rosamond WD, Roth GA, Sampson UKA, Satou GM, Schroeder EB, Shah SH, Shay CM, Spartano NL, Stokes A, Tirschwell DL, VanWagner LB, Tsao CW, American Heart Association Council on E, Prevention Statistics C and Stroke Statistics S. Heart Disease and Stroke Statistics-2020 Update: A Report From the American Heart Association. *Circulation*. 2020;141:e139-e596.

94. Chhabra L, Zain MA and Siddiqui WJ. Coronary Stents *StatPearls* Treasure Island (FL); 2020.

95. Alexander JH and Smith PK. Coronary-Artery Bypass Grafting. *N Engl J Med*. 2016;375:e22.

96. Park DW, Kim YH, Song HG, Ahn JM, Kim WJ, Lee JY, Kang SJ, Lee SW, Lee CW, Park SW, Yun SC, Chung SH, Choo SJ, Chung CH, Lee JW and Park SJ. Long-term outcome of stents versus bypass surgery in diabetic and nondiabetic patients with multivessel or left main coronary artery disease: a pooled analysis of 5775 individual patient data. *Circ Cardiovasc Interv*. 2012;5:467-75.

97. Ravi S and Chaikof EL. Biomaterials for vascular tissue engineering. *Regen Med*. 2010;5:107-20.

98. Seifu DG, Purnama A, Mequanint K and Mantovani D. Small-diameter vascular tissue engineering. *Nat Rev Cardiol*. 2013;10:410-21.

99. Tatterton M, Wilshaw SP, Ingham E and Homer-Vanniasinkam S. The use of antithrombotic therapies in reducing synthetic small-diameter vascular graft thrombosis. *Vasc Endovascular Surg*. 2012;46:212-22.

100. de Mel A, Cousins BG and Seifalian AM. Surface modification of biomaterials: a quest for blood compatibility. *Int J Biomater*. 2012;2012:707863.

101. Barner HB. Conduits for coronary bypass: internal thoracic artery. *Korean J Thorac Cardiovasc Surg*. 2012;45:351-67.

102. Nwaejike N, Tennyson C, Mosca R and Venkateswaran R. Reusing the patent internal mammary artery as a conduit in redo coronary artery bypass surgery. *Interact Cardiovasc Thorac Surg*. 2016;22:346-50.

103. Virk HUH, Lakhter V, Ahmed M, B OM and Chatterjee S. Radial Artery Versus Saphenous Vein Grafts in Coronary Artery Bypass Surgery: a Literature Review. *Curr Cardiol Rep*. 2019;21:36.

104. Klinkert P, Post PN, Breslau PJ and van Bockel JH. Saphenous vein versus PTFE for above-knee femoropopliteal bypass. A review of the literature. *Eur J Vasc Endovasc Surg*. 2004;27:357-62.

105. Altshuler P and Welle NJ. Saphenous Vein Grafts *StatPearls* Treasure Island (FL); 2020.

106. Gaudino M, Lorusso R, Rahouma M, Abouarab A, Tam DY, Spadaccio C, Saint-Hilary G, Leonard J, Iannaccone M, D'Ascenzo F, Di Franco A, Soletti G, Kamel MK, Lau C, Girardi LN, Schwann TA, Benedetto U, Taggart DP and Fremes SE. Radial Artery Versus Right Internal Thoracic Artery Versus Saphenous Vein as the Second Conduit for Coronary Artery Bypass Surgery: A Network Meta-Analysis of Clinical Outcomes. *J Am Heart Assoc*. 2019;8:e010839.

107. Barner HB, Swartz MT, Mudd JG and Tyras DH. Late patency of the internal mammary artery as a coronary bypass conduit. *Ann Thorac Surg*. 1982;34:408-12.

108. Harskamp RE, Alexander JH, Ferguson TB, Jr., Hager R, Mack MJ, Englum B, Wojdyla D, Schulte PJ, Kouchoukos NT, de Winter RJ, Gibson CM, Peterson ED, Harrington RA, Smith PK and Lopes RD. Frequency and Predictors of Internal Mammary Artery Graft Failure and Subsequent Clinical Outcomes: Insights From the Project of Ex-vivo Vein Graft Engineering via Transfection (PREVENT) IV Trial. *Circulation*. 2016;133:131-8.

109. Harskamp RE, Williams JB, Hill RC, de Winter RJ, Alexander JH and Lopes RD. Saphenous vein graft failure and clinical outcomes: toward a surrogate end point in patients following coronary artery bypass surgery? *Am Heart J*. 2013;165:639-43.

110. El-Kurdi M, Soletti L, McGrath J, Linhares S, Rousselle S, Greisler H, Edelman E and Schoen FJ. Functional remodeling of an electrospun polydimethylsiloxane-based polyether urethane external vein graft support device in an ovine model. *J Biomed Mater Res A*. 2019;107:2135-2149.

111. Zhang Y, Janssen L and Chu FV. Atherosclerosis of radial arterial graft may increase the potential of vessel spasm in coronary bypass surgery. *J Thorac Cardiovasc Surg*. 2005;130:1477-8.

112. Siminelakis S, Karfis E, Anagnostopoulos C, Toumpoulis I, Katsaraki A and Drossos G. Harvesting radial artery and neurologic complications. *J Card Surg*. 2004;19:505-10.

113. Weinberg CB and Bell E. A blood vessel model constructed from collagen and cultured vascular cells. *Science*. 1986;231:397-400.

114. Radke D, Jia W, Sharma D, Fena K, Wang G, Goldman J and Zhao F. Tissue Engineering at the Blood-Contacting Surface: A Review of Challenges and Strategies in Vascular Graft Development. *Adv Healthc Mater*. 2018;7:e1701461.

115. Krawiec JT, Weinbaum JS, St Croix CM, Phillippi JA, Watkins SC, Rubin JP and Vorp DA. A cautionary tale for autologous vascular tissue engineering: impact of human demographics on the ability of adipose-derived mesenchymal stem cells to recruit and differentiate into smooth muscle cells. *Tissue Eng Part A*. 2015;21:426-37.

116. Miyachi H, Reinhardt JW, Otsuru S, Tara S, Nakayama H, Yi T, Lee YU, Miyamoto S, Shoji T, Sugiura T, Breuer CK and Shinoka T. Bone marrow-derived mononuclear cell seeded bioresorbable vascular graft improves acute graft patency by inhibiting thrombus formation via platelet adhesion. *Int J Cardiol*. 2018;266:61-66.

117. Best C, Tara S, Wiet M, Reinhardt J, Pepper V, Ball M, Yi T, Shinoka T and Breuer C. Deconstructing the Tissue Engineered Vascular Graft: Evaluating Scaffold Pre-Wetting, Conditioned Media Incubation, and Determining the Optimal Mononuclear Cell Source. *ACS Biomater Sci Eng*. 2017;3:1972-1979.

118. Lee CJ and Ansell JE. Direct thrombin inhibitors. *Br J Clin Pharmacol*. 2011;72:581-92.

119. Salvagnini C, Gharbi S, Boxus T and Marchand-Brynaert J. Synthesis and evaluation of a small library of graftable thrombin inhibitors derived from (L)-arginine. *Eur J Med Chem*. 2007;42:37-53.

120. Qu Z, Muthukrishnan S, Urlam MK, Haller CA, Jordan SW, Kumar VA, Marzec UM, Elkasabi Y, Lahann J, Hanson SR and Chaikof EL. A biologically active surface enzyme assembly that attenuates thrombus formation. *Adv Funct Mater*. 2011;21:4736-4743.

121. Lumsden AB, Morrissey NJ, Comparison of S, Primary Patency Between the FBH-CVG and Co-investigators ESeT. Randomized controlled trial comparing the safety and efficacy between the FUSION BIOLINE heparin-coated vascular graft and the standard expanded polytetrafluoroethylene graft for femoropopliteal bypass. *J Vasc Surg*. 2015;61:703-12 e1.

122. Iijima M, Aubin H, Steinbrink M, Schiffer F, Assmann A, Weisel RD, Matsui Y, Li RK, Lichtenberg A and Akhyari P. Bioactive coating of decellularized vascular grafts with a temperature-sensitive VEGF-conjugated hydrogel accelerates autologous endothelialization in vivo. *J Tissue Eng Regen Med*. 2018;12:e513-e522.

123. Koens MJ, Krasznai AG, Hanssen AE, Hendriks T, Praster R, Daamen WF, van der Vliet JA and van Kuppevelt TH. Vascular replacement using a layered elastin-collagen vascular graft in a porcine model: one week patency versus one month occlusion. *Organogenesis*. 2015;11:105-21.

124. Shojaee M, Wood KB, Moore LK and Bashur CA. Peritoneal pre-conditioning reduces macrophage marker expression in collagen-containing engineered vascular grafts. *Acta Biomater*. 2017;64:80-93.

125. Fukayama T, Takagi K, Tanaka R, Hatakeyama Y, Aytemiz D, Suzuki Y and Asakura T. Biological reaction to small-diameter vascular grafts made of silk fibroin implanted in the abdominal aortae of rats. *Ann Vasc Surg*. 2015;29:341-52.

126. Enomoto S, Sumi M, Kajimoto K, Nakazawa Y, Takahashi R, Takabayashi C, Asakura T and Sata M. Long-term patency of small-diameter vascular graft made from fibroin, a silk-based biodegradable material. *J Vasc Surg*. 2010;51:155-64.

127. P. Gupta KLL, D.G. Haskett, et al. Bioresorbable Silk Grafts for Small Diameter Vascular Tissue Engineering Applications: In vitro and In vivo Functional Analysis. *Acta Biomater*. 2020.

128. Li J, Ding M, Fu Q, Tan H, Xie X and Zhong Y. A novel strategy to graft RGD peptide on biomaterials surfaces for endothelization of small-diamater vascular grafts and tissue engineering blood vessel. *J Mater Sci Mater Med*. 2008;19:2595-603.

129. Antonova LV, Silnikov VN, Sevostyanova VV, Yuzhalin AE, Koroleva LS, Velikanova EA, Mironov AV, Godovikova TS, Kutikhin AG, Glushkova TV, Serpokrylova IY, Senokosova EA, Matveeva VG, Khanova MY, Akentyeva TN, Krivkina EO, Kudryavtseva YA and Barbarash LS. Biocompatibility of Small-Diameter Vascular Grafts in Different Modes of RGD Modification. *Polymers (Basel)*. 2019;11.

130. Chandy T, Das GS, Wilson RF and Rao GH. Use of plasma glow for surface-engineering biomolecules to enhance bloodcompatibility of Dacron and PTFE vascular prosthesis. *Biomaterials*. 2000;21:699-712.

131. Zhou Z and Meyerhoff ME. Preparation and characterization of polymeric coatings with combined nitric oxide release and immobilized active heparin. *Biomaterials*. 2005;26:6506-17.

132. Wang N, Zheng W, Cheng S, Zhang W, Liu S and Jiang X. In Vitro Evaluation of Essential Mechanical Properties and Cell Behaviors of a Novel Polylactic-co-Glycolic Acid (PLGA)-Based Tubular Scaffold for Small-Diameter Vascular Tissue Engineering. *Polymers (Basel)*. 2017;9.

133. Miller DC, Haberstroh KM and Webster TJ. PLGA nanometer surface features manipulate fibronectin interactions for improved vascular cell adhesion. *J Biomed Mater Res A*. 2007;81:678-84.

134. Li Y, Fan P, Ding XM, Tian XH, Feng XS, Yan H, Pan XM, Tian PX, Zheng J, Ding CG and Xue WJ. Polyglycolic Acid Fibrous Scaffold Improving Endothelial Cell Coating and Vascularization of Islet. *Chin Med J (Engl)*. 2017;130:832-839.

135. Wen SJ, Zhao LM, Wang SG, Li JX, Chen HY, Liu JL, Liu Y, Luo Y and Changizi R. Human vascular smooth muscle cells and endothelial cells cocultured on polyglycolic acid (70/30) scaffold in tissue engineered vascular graft. *Chin Med J (Engl)*. 2007;120:1331-5.

136. Tara S, Kurobe H, Rocco KA, Maxfield MW, Best CA, Yi T, Naito Y, Breuer CK and Shinoka T. Well-organized neointima of large-pore poly(L-lactic acid) vascular graft coated with poly(L-lactic-co-epsilon-caprolactone) prevents calcific deposition compared to small-pore electrospun poly(L-lactic acid) graft in a mouse aortic implantation model. *Atherosclerosis*. 2014;237:684-91.

137. Li C, Wang F, Douglas G, Zhang Z, Guidoin R and Wang L. Comprehensive mechanical characterization of PLA fabric combined with PCL to form a composite structure vascular graft. *J Mech Behav Biomed Mater*. 2017;69:39-49.

138. Sugiura T, Tara S, Nakayama H, Yi T, Lee YU, Shoji T, Breuer CK and Shinoka T. Fast-degrading bioresorbable arterial vascular graft with high cellular infiltration inhibits calcification of the graft. *J Vasc Surg*. 2017;66:243-250.

139. Fiqrianti IA, Widiyanti P, Manaf MA, Savira CY, Cahyani NR and Bella FR. Poly-L-lactic Acid (PLLA)-Chitosan-Collagen Electrospun Tube for Vascular Graft Application. *J Funct Biomater*. 2018;9.

140. Sevostyanova VV, Antonova LV, Velikanova EA, Matveeva VG, Krivkina EO, Glushkova TV, Mironov AV, Burago AY and Barbarash LS. Endothelialization of Polycaprolactone Vascular Graft under the Action of Locally Applied Vascular Endothelial Growth Factor. *Bull Exp Biol Med*. 2018;165:264-268.

141. van Uden S, Vanerio N, Catto V, Bonandrini B, Tironi M, Figliuzzi M, Remuzzi A, Kock L, Redaelli ACL, Greco FG and Riboldi SA. A novel hybrid silk-fibroin/polyurethane three-layered vascular graft: towards in situ tissue-engineered vascular accesses for haemodialysis. *Biomed Mater*. 2019;14:025007.

142. Yang X, Wei J, Lei D, Liu Y and Wu W. Appropriate density of PCL nano-fiber sheath promoted muscular remodeling of PGS/PCL grafts in arterial circulation. *Biomaterials*. 2016;88:34-47.

143. Lee KW, Johnson NR, Gao J and Wang Y. Human progenitor cell recruitment via SDF-1alpha coacervate-laden PGS vascular grafts. *Biomaterials*. 2013;34:9877-85.

144. Lee KW and Wang Y. Elastomeric PGS scaffolds in arterial tissue engineering. *J Vis Exp*. 2011.

145. Naito Y, Shinoka T, Duncan D, Hibino N, Solomon D, Cleary M, Rathore A, Fein C, Church S and Breuer C. Vascular tissue engineering: towards the next generation vascular grafts. *Adv Drug Deliv Rev*. 2011;63:312-23.

146. Badimon L, Badimon JJ, Turitto VT, Vallabhajosula S and Fuster V. Platelet thrombus formation on collagen type I. A model of deep vessel injury. Influence of blood rheology, von Willebrand factor, and blood coagulation. *Circulation*. 1988;78:1431-42.

147. Gupta P, Adhikary M, M JC, Kumar M, Bhardwaj N and Mandal BB. Biomimetic, Osteoconductive Non-mulberry Silk Fiber Reinforced Tricomposite Scaffolds for Bone Tissue Engineering. *ACS Appl Mater Interfaces*. 2016;8:30797-30810.

148. Liu H, Li X, Zhou G, Fan H and Fan Y. Electrospun sulfated silk fibroin nanofibrous scaffolds for vascular tissue engineering. *Biomaterials*. 2011;32:3784-93.

149. Lovett M, Eng G, Kluge JA, Cannizzaro C, Vunjak-Novakovic G and Kaplan DL. Tubular silk scaffolds for small diameter vascular grafts. *Organogenesis*. 2010;6:217-24.

150. Schaner PJ, Martin ND, Tulenko TN, Shapiro IM, Tarola NA, Leichter RF, Carabasi RA and Dimuzio PJ. Decellularized vein as a potential scaffold for vascular tissue engineering. *J Vasc Surg*. 2004;40:146-53.

151. Conklin BS, Richter ER, Kreutziger KL, Zhong DS and Chen C. Development and evaluation of a novel decellularized vascular xenograft. *Med Eng Phys*. 2002;24:173-83.

152. Hoenicka M, Schrammel S, Bursa J, Huber G, Bronger H, Schmid C and Birnbaum DE. Development of endothelium-denuded human umbilical veins as living scaffolds for tissue-engineered small-calibre vascular grafts. *J Tissue Eng Regen Med*. 2013;7:324-36.

153. Gui L, Muto A, Chan SA, Breuer CK and Niklason LE. Development of decellularized human umbilical arteries as small-diameter vascular grafts. *Tissue Eng Part A*. 2009;15:2665-76.

154. Row S, Peng H, Schlaich EM, Koenigsknecht C, Andreadis ST and Swartz DD. Arterial grafts exhibiting unprecedented cellular infiltration and remodeling in vivo: the role of cells in the vascular wall. *Biomaterials*. 2015;50:115-26.

155. Porzionato A, Stocco E, Barbon S, Grandi F, Macchi V and De Caro R. Tissue-Engineered Grafts from Human Decellularized Extracellular Matrices: A Systematic Review and Future Perspectives. *Int J Mol Sci*. 2018;19.

156. L'Heureux N, Dusserre N, Konig G, Victor B, Keire P, Wight TN, Chronos NA, Kyles AE, Gregory CR, Hoyt G, Robbins RC and McAllister TN. Human tissue-engineered blood vessels for adult arterial revascularization. *Nat Med*. 2006;12:361-5.

157. Gui L, Dash BC, Luo J, Qin L, Zhao L, Yamamoto K, Hashimoto T, Wu H, Dardik A, Tellides G, Niklason LE and Qyang Y. Implantable tissue-engineered blood vessels from human induced pluripotent stem cells. *Biomaterials*. 2016;102:120-9.

158. Morin KT, Smith AO, Davis GE and Tranquillo RT. Aligned human microvessels formed in 3D fibrin gel by constraint of gel contraction. *Microvasc Res*. 2013;90:12-22.

159. Quint C, Kondo Y, Manson RJ, Lawson JH, Dardik A and Niklason LE. Decellularized tissue-engineered blood vessel as an arterial conduit. *Proc Natl Acad Sci U S A*. 2011;108:9214-9.

160. Afewerki T, Ahmed S and Warren D. Emerging regulators of vascular smooth muscle cell migration. *J Muscle Res Cell Motil*. 2019;40:185-196.

161. Bruzauskaite I, Bironaite D, Bagdonas E and Bernotiene E. Scaffolds and cells for tissue regeneration: different scaffold pore sizes-different cell effects. *Cytotechnology*. 2016;68:355-69.

162. Loh QL and Choong C. Three-dimensional scaffolds for tissue engineering applications: role of porosity and pore size. *Tissue Eng Part B Rev*. 2013;19:485-502.

163. Golden MA, Hanson SR, Kirkman TR, Schneider PA and Clowes AW. Healing of polytetrafluoroethylene arterial grafts is influenced by graft porosity. *J Vasc Surg*. 1990;11:838-44; discussion 845.

164. Gade PS, Lee K, Pfaff BN, Wang Y and Robertson AM. Degradation and erosion mechanisms of bioresorbable porous acellular vascular grafts: an in vitro investigation. *J R Soc Interface*. 2017;14.

165. Tamimi E, Ardila DC, Haskett DG, Doetschman T, Slepian MJ, Kellar RS and Vande Geest JP. Biomechanical Comparison of Glutaraldehyde-Crosslinked Gelatin Fibrinogen Electrospun Scaffolds to Porcine Coronary Arteries. *J Biomech Eng*. 2016;138.

166. El-Kurdi MS, Hong Y, Stankus JJ, Soletti L, Wagner WR and Vorp DA. Transient elastic support for vein grafts using a constricting microfibrillar polymer wrap. *Biomaterials*. 2008;29:3213-20.

167. L'Heureux N, McAllister TN and de la Fuente LM. Tissue-engineered blood vessel for adult arterial revascularization. *N Engl J Med*. 2007;357:1451-3.

168. Palombo C and Kozakova M. Arterial stiffness, atherosclerosis and cardiovascular risk: Pathophysiologic mechanisms and emerging clinical indications. *Vascul Pharmacol*. 2016;77:1-7.

169. Emoto M, Nishizawa Y, Kawagishi T, Maekawa K, Hiura Y, Kanda H, Izumotani K, Shoji T, Ishimura E, Inaba M, Okuno Y and Morii H. Stiffness indexes beta of the common carotid and femoral arteries are associated with insulin resistance in NIDDM. *Diabetes Care*. 1998;21:1178-82.

170. Thomas LV, Lekshmi V and Nair PD. Tissue engineered vascular grafts--preclinical aspects. *Int J Cardiol*. 2013;167:1091-100.

171. Zhang L, Ao Q, Wang A, Lu G, Kong L, Gong Y, Zhao N and Zhang X. A sandwich tubular scaffold derived from chitosan for blood vessel tissue engineering. *J Biomed Mater Res A*. 2006;77:277-84.

172. McAllister TN, Maruszewski M, Garrido SA, Wystrychowski W, Dusserre N, Marini A, Zagalski K, Fiorillo A, Avila H, Manglano X, Antonelli J, Kocher A, Zembala M, Cierpka L, de la Fuente LM and L'Heureux N. Effectiveness of haemodialysis access with an autologous tissue-engineered vascular graft: a multicentre cohort study. *Lancet*. 2009;373:1440-6.

173. Koch S, Flanagan TC, Sachweh JS, Tanios F, Schnoering H, Deichmann T, Ella V, Kellomaki M, Gronloh N, Gries T, Tolba R, Schmitz-Rode T and Jockenhoevel S. Fibrin-polylactide-based tissue-engineered vascular graft in the arterial circulation. *Biomaterials*. 2010;31:4731-9.

174. Lee KW, Stolz DB and Wang Y. Substantial expression of mature elastin in arterial constructs. *Proc Natl Acad Sci U S A*. 2011;108:2705-10.

175. von Bornstadt D, Wang H, Paulsen MJ, Goldstone AB, Eskandari A, Thakore A, Stapleton L, Steele AN, Truong VN, Jaatinen K, Hironaka C and Woo YJ. Rapid Self-Assembly of Bioengineered Cardiovascular Bypass Grafts From Scaffold-Stabilized, Tubular Bilevel Cell Sheets. *Circulation*. 2018;138:2130-2144.

176. Wang Y, Kim YM and Langer R. In vivo degradation characteristics of poly(glycerol sebacate). *J Biomed Mater Res A*. 2003;66:192-7.

177. Lee KW, Gade PS, Dong L, Zhang Z, Aral AM, Gao J, Ding X, Stowell CET, Nisar MU, Kim K, Reinhardt DP, Solari MG, Gorantla VS, Robertson AM and Wang Y. A biodegradable synthetic graft for small arteries matches the performance of autologous vein in rat carotid arteries. *Biomaterials*. 2018;181:67-80.

178. Wu W, Allen RA and Wang Y. Fast-degrading elastomer enables rapid remodeling of a cell-free synthetic graft into a neoartery. *Nat Med*. 2012;18:1148-53.

179. Pitt CG, Marks TA and Schindler A. Biodegradable drug delivery systems based on aliphatic polyesters: application to contraceptives and narcotic antagonists. *NIDA Res Monogr*. 1981;28:232-53.

180. Simionescu A, Schulte JB, Fercana G and Simionescu DT. Inflammation in cardiovascular tissue engineering: the challenge to a promise: a minireview. *Int J Inflam*. 2011;2011:958247.

181. Weinbaum J.S. HDG, Mandelkern T.F., Vorp D.A. *Advances in Cell Seeding of Tissue Engineered Vascular Grafts*: Springer; 2020.

182. Bai H, Dardik A and Xing Y. Decellularized Carotid Artery Functions as an Arteriovenous Graft. *J Surg Res*. 2019;234:33-39.

183. Wang L, Hu J, Sorek CE, Chen EY, Ma PX and Yang B. Fabrication of tissue-engineered vascular grafts with stem cells and stem cell-derived vascular cells. *Expert Opin Biol Ther*. 2016;16:317-30.

184. Bajpai VK and Andreadis ST. Stem cell sources for vascular tissue engineering and regeneration. *Tissue Eng Part B Rev*. 2012;18:405-25.

185. Foxall TL, Auger KR, Callow AD and Libby P. Adult human endothelial cell coverage of small-caliber Dacron and polytetrafluoroethylene vascular prostheses in vitro. *J Surg Res*. 1986;41:158-72.

186. Roh JD, Nelson GN, Udelsman BV, Brennan MP, Lockhart B, Fong PM, Lopez-Soler RI, Saltzman WM and Breuer CK. Centrifugal seeding increases seeding efficiency and cellular distribution of bone marrow stromal cells in porous biodegradable scaffolds. *Tissue Eng*. 2007;13:2743-9.

187. Krawiec JT and Vorp DA. Adult stem cell-based tissue engineered blood vessels: a review. *Biomaterials*. 2012;33:3388-400.

188. Kang TY, Lee JH, Kim BJ, Kang JA, Hong JM, Kim BS, Cha HJ, Rhie JW and Cho DW. In vivo endothelization of tubular vascular grafts through in situ recruitment of endothelial and endothelial progenitor cells by RGD-fused mussel adhesive proteins. *Biofabrication*. 2015;7:015007.

189. Bowlin GL, Meyer A, Fields C, Cassano A, Makhoul RG, Allen C and Rittgers SE. The persistence of electrostatically seeded endothelial cells lining a small diameter expanded polytetrafluoroethylene vascular graft. *J Biomater Appl*. 2001;16:157-73.

190. Park PK, Jarrell BE, Williams SK, Carter TL, Rose DG, Martinez-Hernandez A and Carabasi RA, 3rd. Thrombus-free, human endothelial surface in the midregion of a Dacron vascular graft in the splanchnic venous circuit--observations after nine months of implantation. *J Vasc Surg*. 1990;11:468-75.

191. Herring M, Gardner A and Glover J. Seeding human arterial prostheses with mechanically derived endothelium. The detrimental effect of smoking. *J Vasc Surg*. 1984;1:279-89.

192. Shirota T, He H, Yasui H and Matsuda T. Human endothelial progenitor cell-seeded hybrid graft: proliferative and antithrombogenic potentials in vitro and fabrication processing. *Tissue Eng*. 2003;9:127-36.

193. Rotmans JI, Heyligers JM, Stroes ES and Pasterkamp G. Endothelial progenitor cell-seeded grafts: rash and risky. *Can J Cardiol*. 2006;22:1113-6.

194. Cherubino M, Rubin JP, Miljkovic N, Kelmendi-Doko A and Marra KG. Adipose-derived stem cells for wound healing applications. *Ann Plast Surg*. 2011;66:210-5.

195. Tsuji W, Rubin JP and Marra KG. Adipose-derived stem cells: Implications in tissue regeneration. *World J Stem Cells*. 2014;6:312-21.

196. Ayatollahi M, Geramizadeh B, Zakerinia M, Ramzi M, Yaghobi R, Hadadi P, Rezvani AR, Aghdai M, Azarpira N and Karimi H. Human Bone Marrow-derived Mesenchymal Stem Cell: A Source for Cell-Based Therapy. *Int J Organ Transplant Med*. 2012;3:32-41.

197. Nagamura-Inoue T and He H. Umbilical cord-derived mesenchymal stem cells: Their advantages and potential clinical utility. *World J Stem Cells*. 2014;6:195-202.

198. da Silva Meirelles L, Caplan AI and Nardi NB. In search of the in vivo identity of mesenchymal stem cells. *Stem Cells*. 2008;26:2287-99.

199. Hibino N, Duncan DR, Nalbandian A, Yi T, Qyang Y, Shinoka T and Breuer CK. Evaluation of the use of an induced puripotent stem cell sheet for the construction of tissue-engineered vascular grafts. *J Thorac Cardiovasc Surg*. 2012;143:696-703.

200. Halme DG and Kessler DA. FDA regulation of stem-cell-based therapies. *N Engl J Med*. 2006;355:1730-5.

201. Lee MH, Arcidiacono JA, Bilek AM, Wille JJ, Hamill CA, Wonnacott KM, Wells MA and Oh SS. Considerations for tissue-engineered and regenerative medicine product development prior to clinical trials in the United States. *Tissue Eng Part B Rev*. 2010;16:41-54.

202. Administration FaD. Regulatory Considerations for Human Cells, Tissues, and Cellular and Tissue-Based Products: Minimal Manipulation and Homologous Use. 2017.

203. Zimmerlin L, Donnenberg VS, Pfeifer ME, Meyer EM, Peault B, Rubin JP and Donnenberg AD. Stromal vascular progenitors in adult human adipose tissue. *Cytometry A*. 2010;77:22-30.

204. Roh JD, Sawh-Martinez R, Brennan MP, Jay SM, Devine L, Rao DA, Yi T, Mirensky TL, Nalbandian A, Udelsman B, Hibino N, Shinoka T, Saltzman WM, Snyder E, Kyriakides TR, Pober JS and Breuer CK. Tissue-engineered vascular grafts transform into mature blood vessels via an inflammation-mediated process of vascular remodeling. *Proc Natl Acad Sci U S A*. 2010;107:4669-74.

205. Luke Brewster EB, Howard Greisler. *Principles of Tissue Engineering*. 4th ed: Academic Press; 2014.

206. Zhao Y, Zhang S, Zhou J, Wang J, Zhen M, Liu Y, Chen J and Qi Z. The development of a tissue-engineered artery using decellularized scaffold and autologous ovine mesenchymal stem cells. *Biomaterials*. 2010;31:296-307.

207. Zhang L, Zhou J, Lu Q, Wei Y and Hu S. A novel small-diameter vascular graft: in vivo behavior of biodegradable three-layered tubular scaffolds. *Biotechnol Bioeng*. 2008;99:1007-15.

208. Hibino N, Mejias D, Pietris N, Dean E, Yi T, Best C, Shinoka T and Breuer C. The innate immune system contributes to tissue-engineered vascular graft performance. *FASEB J*. 2015;29:2431-8.

209. Weiss ARR and Dahlke MH. Immunomodulation by Mesenchymal Stem Cells (MSCs): Mechanisms of Action of Living, Apoptotic, and Dead MSCs. *Front Immunol*. 2019;10:1191.

210. Wu Q, Fang T, Lang H, Chen M, Shi P, Pang X and Qi G. Comparison of the proliferation, migration and angiogenic properties of human amniotic epithelial and mesenchymal stem cells and their effects on endothelial cells. *Int J Mol Med*. 2017;39:918-926.

211. Iso Y, Usui S, Toyoda M, Spees JL, Umezawa A and Suzuki H. Bone marrow-derived mesenchymal stem cells inhibit vascular smooth muscle cell proliferation and neointimal hyperplasia after arterial injury in rats. *Biochem Biophys Rep*. 2018;16:79-87.

212. Minutti CM, Knipper JA, Allen JE and Zaiss DM. Tissue-specific contribution of macrophages to wound healing. *Semin Cell Dev Biol*. 2017;61:3-11.

213. Ley K. M1 Means Kill; M2 Means Heal. *J Immunol*. 2017;199:2191-2193.

214. Brown BN, Ratner BD, Goodman SB, Amar S and Badylak SF. Macrophage polarization: an opportunity for improved outcomes in biomaterials and regenerative medicine. *Biomaterials*. 2012;33:3792-802.

215. Kehl D, Generali M, Mallone A, Heller M, Uldry AC, Cheng P, Gantenbein B, Hoerstrup SP and Weber B. Proteomic analysis of human mesenchymal stromal cell secretomes: a systematic comparison of the angiogenic potential. *NPJ Regen Med*. 2019;4:8.

216. Smith RJ, Jr., Yi T, Nasiri B, Breuer CK and Andreadis ST. Implantation of VEGF-functionalized cell-free vascular grafts: regenerative and immunological response. *FASEB J*. 2019;33:5089-5100.

217. Lee YU, de Dios Ruiz-Rosado J, Mahler N, Best CA, Tara S, Yi T, Shoji T, Sugiura T, Lee AY, Robledo-Avila F, Hibino N, Pober JS, Shinoka T, Partida-Sanchez S and Breuer CK. TGF-beta receptor 1 inhibition prevents stenosis of tissue-engineered vascular grafts by reducing host mononuclear phagocyte activation. *FASEB J*. 2016;30:2627-36.

218. Cooley BC, Nevado J, Mellad J, Yang D, St Hilaire C, Negro A, Fang F, Chen G, San H, Walts AD, Schwartzbeck RL, Taylor B, Lanzer JD, Wragg A, Elagha A, Beltran LE, Berry C, Feil R, Virmani R, Ladich E, Kovacic JC and Boehm M. TGF-beta signaling mediates endothelial-to-mesenchymal transition (EndMT) during vein graft remodeling. *Sci Transl Med*. 2014;6:227ra34.

219. Kowalewski R, Zimnoch L, Wojtukiewicz MZ, Glowinski J and Glowinski S. Evaluation of urokinase-type plasminogen activator and its receptor in neointima of polyester vascular grafts. *Pathophysiol Haemost Thromb*. 2005;34:23-8.

220. Wysocki SJ, Zheng MH, Smith A and Norman PE. Vascular endothelial growth factor (VEGF) expression during arterial repair in the pig. *Eur J Vasc Endovasc Surg*. 1998;15:225-30.

221. Bao P, Kodra A, Tomic-Canic M, Golinko MS, Ehrlich HP and Brem H. The role of vascular endothelial growth factor in wound healing. *J Surg Res*. 2009;153:347-58.

222. Dimmeler S and Zeiher AM. Nitric oxide-an endothelial cell survival factor. *Cell Death Differ*. 1999;6:964-8.

223. Walshe TE, Saint-Geniez M, Maharaj AS, Sekiyama E, Maldonado AE and D'Amore PA. TGF-beta is required for vascular barrier function, endothelial survival and homeostasis of the adult microvasculature. *PLoS One*. 2009;4:e5149.

224. Gong D, Shi W, Yi SJ, Chen H, Groffen J and Heisterkamp N. TGFbeta signaling plays a critical role in promoting alternative macrophage activation. *BMC Immunol*. 2012;13:31.

225. Neubauer K, Kruger M, Quondamatteo F, Knittel T, Saile B and Ramadori G. Transforming growth factor-beta1 stimulates the synthesis of basement membrane proteins laminin, collagen type IV and entactin in rat liver sinusoidal endothelial cells. *J Hepatol*. 1999;31:692-702.

226. Lawson C, Vicencio JM, Yellon DM and Davidson SM. Microvesicles and exosomes: new players in metabolic and cardiovascular disease. *J Endocrinol*. 2016;228:R57-71.

227. Antonova LV, Seifalian AM, Kutikhin AG, Sevostyanova VV, Krivkina EO, Mironov AV, Burago AY, Velikanova EA, Matveeva VG, Glushkova TV, Sergeeva EA, Vasyukov GY, Kudryavtseva YA, Barbarash OL and Barbarash LS. Bioabsorbable Bypass Grafts Biofunctionalised with RGD Have Enhanced Biophysical Properties and Endothelialisation Tested In vivo. *Front Pharmacol*. 2016;7:136.

228. Zheng W, Wang Z, Song L, Zhao Q, Zhang J, Li D, Wang S, Han J, Zheng XL, Yang Z and Kong D. Endothelialization and patency of RGD-functionalized vascular grafts in a rabbit carotid artery model. *Biomaterials*. 2012;33:2880-91.

229. Lee JS, Lee K, Moon SH, Chung HM, Lee JH, Um SH, Kim DI and Cho SW. Mussel-inspired cell-adhesion peptide modification for enhanced endothelialization of decellularized blood vessels. *Macromol Biosci*. 2014;14:1181-9.

230. Peng G, Yao D, Niu Y, Liu H and Fan Y. Surface Modification of Multiple Bioactive Peptides to Improve Endothelialization of Vascular Grafts. *Macromol Biosci*. 2019;19:e1800368.

231. Tang C, Kligman F, Larsen CC, Kottke-Marchant K and Marchant RE. Platelet and endothelial adhesion on fluorosurfactant polymers designed for vascular graft modification. *J Biomed Mater Res A*. 2009;88:348-58.

232. Bastijanic JM, Marchant RE, Kligman F, Allemang MT, Lakin RO, Kendrick D, Kashyap VS and Kottke-Marchant K. In vivo evaluation of biomimetic fluorosurfactant polymer-coated expanded polytetrafluoroethylene vascular grafts in a porcine carotid artery bypass model. *J Vasc Surg*. 2016;63:1620-1630 e4.

233. Hsu SH, Sun SH and Chen DC. Improved retention of endothelial cells seeded on polyurethane small-diameter vascular grafts modified by a recombinant RGD-containing protein. *Artif Organs*. 2003;27:1068-78.

234. Wissink MJ, Beernink R, Pieper JS, Poot AA, Engbers GH, Beugeling T, van Aken WG and Feijen J. Immobilization of heparin to EDC/NHS-crosslinked collagen. Characterization and in vitro evaluation. *Biomaterials*. 2001;22:151-63.

235. Larm O, Larsson R and Olsson P. A new non-thrombogenic surface prepared by selective covalent binding of heparin via a modified reducing terminal residue. *Biomater Med Devices Artif Organs*. 1983;11:161-73.

236. Tseng PY, Rele SS, Sun XL and Chaikof EL. Membrane-mimetic films containing thrombomodulin and heparin inhibit tissue factor-induced thrombin generation in a flow model. *Biomaterials*. 2006;27:2637-50.

237. Gao J, Jiang L, Liang Q, Shi J, Hou D, Tang D, Chen S, Kong D and Wang S. The grafts modified by heparinization and catalytic nitric oxide generation used for vascular implantation in rats. *Regen Biomater*. 2018;5:105-114.

238. Cummings I, George S, Kelm J, Schmidt D, Emmert MY, Weber B, Zund G and Hoerstrup SP. Tissue-engineered vascular graft remodeling in a growing lamb model: expression of matrix metalloproteinases. *Eur J Cardiothorac Surg*. 2012;41:167-72.

239. Nakayama Y, Furukoshi M, Terazawa T and Iwai R. Development of long in vivo tissue-engineered "Biotube" vascular grafts. *Biomaterials*. 2018;185:232-239.

240. Ju YM, Ahn H, Arenas-Herrera J, Kim C, Abolbashari M, Atala A, Yoo JJ and Lee SJ. Electrospun vascular scaffold for cellularized small diameter blood vessels: A preclinical large animal study. *Acta Biomater*. 2017;59:58-67.

241. Deutsch M, Meinhart J, Fischlein T, Preiss P and Zilla P. Clinical autologous in vitro endothelialization of infrainguinal ePTFE grafts in 100 patients: a 9-year experience. *Surgery*. 1999;126:847-55.

242. Wystrychowski W, McAllister TN, Zagalski K, Dusserre N, Cierpka L and L'Heureux N. First human use of an allogeneic tissue-engineered vascular graft for hemodialysis access. *J Vasc Surg*. 2014;60:1353-1357.

243. Torikai K, Ichikawa H, Hirakawa K, Matsumiya G, Kuratani T, Iwai S, Saito A, Kawaguchi N, Matsuura N and Sawa Y. A self-renewing, tissue-engineered vascular graft for arterial reconstruction. *J Thorac Cardiovasc Surg*. 2008;136:37-45, 45 e1.

244. Grus T, Lambert L, Mlcek M, Chlup H, Honsova E, Spacek M, Burgetova A and Lindner J. In Vivo Evaluation of Short-Term Performance of New Three-Layer Collagen-Based Vascular

Graft Designed for Low-Flow Peripheral Vascular Reconstructions. *Biomed Res Int*. 2018;2018:3519596.

245. Syedain Z, Reimer J, Lahti M, Berry J, Johnson S, Bianco R and Tranquillo RT. Corrigendum: Tissue engineering of acellular vascular grafts capable of somatic growth in young lambs. *Nat Commun*. 2017;8:14297.

246. Koobatian MT, Row S, Smith RJ, Jr., Koenigsknecht C, Andreadis ST and Swartz DD. Successful endothelialization and remodeling of a cell-free small-diameter arterial graft in a large animal model. *Biomaterials*. 2016;76:344-58.

247. Fukayama T, Ozai Y, Shimokawatoko H, Kimura Y, Aytemiz D, Tanaka R, Machida N and Asakura T. Evaluation of endothelialization in the center part of graft using 3 cm vascular grafts implanted in the abdominal aortae of the rat. *J Artif Organs*. 2017;20:221-229.

248. Fukayama T, Ozai Y, Shimokawadoko H, Aytemiz D, Tanaka R, Machida N and Asakura T. Effect of fibroin sponge coating on in vivo performance of knitted silk small diameter vascular grafts. *Organogenesis*. 2015;11:137-51.

249. Sugiura T, Agarwal R, Tara S, Yi T, Lee YU, Breuer CK, Weiss AS and Shinoka T. Tropoelastin inhibits intimal hyperplasia of mouse bioresorbable arterial vascular grafts. *Acta Biomater*. 2017;52:74-80.

250. He W, Nieponice A, Soletti L, Hong Y, Gharaibeh B, Crisan M, Usas A, Peault B, Huard J, Wagner WR and Vorp DA. Pericyte-based human tissue engineered vascular grafts. *Biomaterials*. 2010;31:8235-44.

251. Gupta P, Kumar M, Bhardwaj N, Kumar JP, Krishnamurthy CS, Nandi SK and Mandal BB. Mimicking Form and Function of Native Small Diameter Vascular Conduits Using Mulberry and Non-mulberry Patterned Silk Films. *ACS Appl Mater Interfaces*. 2016;8:15874-88.

252. Mandal BB and Kundu SC. Non-mulberry silk gland fibroin protein 3-D scaffold for enhanced differentiation of human mesenchymal stem cells into osteocytes. *Acta Biomater*. 2009;5:2579-90.

253. S. Jasmine BBM. *Silk Biomaterials for Tissue Engineering and Regenerative Medicine*: Woodhead Publishing Limited; 2014.

254. Mandal BB, Kapoor S and Kundu SC. Silk fibroin/polyacrylamide semi-interpenetrating network hydrogels for controlled drug release. *Biomaterials*. 2009;30:2826-36.

255. P. Gupta JCM, B.B. Mandal. Surface Patterning and Innate Physicochemical Attributes of Silk Films Concomitantly Govern Vascular Cell Dynamics. *ACS Biomaterials Science & Engineering*. 2018.

256. Zhuang Z, Yoshizawa-Smith S, Glowacki A, Maltos K, Pacheco C, Shehabeldin M, Mulkeen M, Myers N, Chong R, Verdelis K, Garlet GP, Little S and Sfeir C. Induction of M2 Macrophages Prevents Bone Loss in Murine Periodontitis Models. *J Dent Res*. 2019;98:200-208.

257. Rothstein SN, Kay JE, Schopfer FJ, Freeman BA and Little SR. A retrospective mathematical analysis of controlled release design and experimentation. *Mol Pharm*. 2012;9:3003-11.

258. Strobl H, Scheinecker C, Riedl E, Csmarits B, Bello-Fernandez C, Pickl WF, Majdic O and Knapp W. Identification of CD68+lin- peripheral blood cells with dendritic precursor characteristics. *J Immunol*. 1998;161:740-8.

259. Hibino N, McGillicuddy E, Matsumura G, Ichihara Y, Naito Y, Breuer C and Shinoka T. Late-term results of tissue-engineered vascular grafts in humans. *J Thorac Cardiovasc Surg*. 2010;139:431-6, 436 e1-2.

260. Drews JD, Pepper VK, Best CA, Szafron JM, Cheatham JP, Yates AR, Hor KN, Zbinden JC, Chang YC, Mirhaidari GJM, Ramachandra AB, Miyamoto S, Blum KM, Onwuka EA, Zakko J, Kelly J, Cheatham SL, King N, Reinhardt JW, Sugiura T, Miyachi H, Matsuzaki Y, Breuer J, Heuer ED, West TA, Shoji T, Berman D, Boe BA, Asnes J, Galantowicz M, Matsumura G, Hibino N, Marsden AL, Pober JS, Humphrey JD, Shinoka T and Breuer CK. Spontaneous reversal of stenosis in tissue-engineered vascular grafts. *Sci Transl Med*. 2020;12.

261. Sandusky GE, Jr., Badylak SF, Morff RJ, Johnson WD and Lantz G. Histologic findings after in vivo placement of small intestine submucosal vascular grafts and saphenous vein grafts in the carotid artery in dogs. *Am J Pathol*. 1992;140:317-24.

262. Sugimura Y, Schmidt AK, Lichtenberg A, Assmann A and Akhyari P. (*) A Rat Model for the In Vivo Assessment of Biological and Tissue-Engineered Valvular and Vascular Grafts. *Tissue Eng Part C Methods*. 2017;23:982-994.

263. Yokota T, Ichikawa H, Matsumiya G, Kuratani T, Sakaguchi T, Iwai S, Shirakawa Y, Torikai K, Saito A, Uchimura E, Kawaguchi N, Matsuura N and Sawa Y. In situ tissue regeneration using a novel tissue-engineered, small-caliber vascular graft without cell seeding. *J Thorac Cardiovasc Surg*. 2008;136:900-7.

264. Tillman BW, Yazdani SK, Neff LP, Corriere MA, Christ GJ, Soker S, Atala A, Geary RL and Yoo JJ. Bioengineered vascular access maintains structural integrity in response to arteriovenous flow and repeated needle puncture. *J Vasc Surg*. 2012;56:783-93.

265. Kaushal S, Amiel GE, Guleserian KJ, Shapira OM, Perry T, Sutherland FW, Rabkin E, Moran AM, Schoen FJ, Atala A, Soker S, Bischoff J and Mayer JE, Jr. Functional small-diameter neovessels created using endothelial progenitor cells expanded ex vivo. *Nat Med*. 2001;7:1035-40.

266. Ruytinx P, Proost P, Van Damme J and Struyf S. Chemokine-Induced Macrophage Polarization in Inflammatory Conditions. *Front Immunol*. 2018;9:1930.

267. Hachim D, Iftikhar A, LoPresti ST, Nolfi AL, Ravichandar S, Skillen CD and Brown BN. Distinct release strategies are required to modulate macrophage phenotype in young versus aged animals. *J Control Release*. 2019;305:65-74.

268. Yu T, Gan S, Zhu Q, Dai D, Li N, Wang H, Chen X, Hou D, Wang Y, Pan Q, Xu J, Zhang X, Liu J, Pei S, Peng C, Wu P, Romano S, Mao C, Huang M, Zhu X, Shen K, Qin J and Xiao Y. Modulation of M2 macrophage polarization by the crosstalk between Stat6 and Trim24. *Nat Commun*. 2019;10:4353.

269. Hachim D, Wang N, Lopresti ST, Stahl EC, Umeda YU, Rege RD, Carey ST, Mani D and Brown BN. Effects of aging upon the host response to implants. *J Biomed Mater Res A*. 2017;105:1281-1292.

270. Linehan E, Dombrowski Y, Snoddy R, Fallon PG, Kissenpfennig A and Fitzgerald DC. Aging impairs peritoneal but not bone marrow-derived macrophage phagocytosis. *Aging Cell*. 2014;13:699-708.

271. Stout RD and Suttles J. Immunosenescence and macrophage functional plasticity: dysregulation of macrophage function by age-associated microenvironmental changes. *Immunol Rev*. 2005;205:60-71.

272. Krawiec JT. FUNCTIONAL STEM-CELL BASED TISSUE ENGINEERED VASCULAR GRAFTS FOR HIGH-RISK DONOR POPULATIONS. *Swanson School of Engineering Department of Bioengineering*. 2015;Doctor of Philosophy:279.

273. CP Molina RG, RM Gandhi, BM Sicari, R Londono, GS Hussey, JG Bartolacci, LM Quijano Luque, MC Cramer, JL Dziki, PM Crap, SF Badylak. Comparison of the host macrophage response to synthetic and biologic surgical meshes used for ventral hernia repair. *Journal of Immunology and Regenerative Medicine*. 2019:13-25.

274. Brown BN, Londono R, Tottey S, Zhang L, Kukla KA, Wolf MT, Daly KA, Reing JE and Badylak SF. Macrophage phenotype as a predictor of constructive remodeling following the implantation of biologically derived surgical mesh materials. *Acta Biomater*. 2012;8:978-87.

275. Binder BY, Sagun JE and Leach JK. Reduced serum and hypoxic culture conditions enhance the osteogenic potential of human mesenchymal stem cells. *Stem Cell Rev Rep*. 2015;11:387-93.

276. Ho SS, Hung BP, Heyrani N, Lee MA and Leach JK. Hypoxic Preconditioning of Mesenchymal Stem Cells with Subsequent Spheroid Formation Accelerates Repair of Segmental Bone Defects. *Stem Cells*. 2018;36:1393-1403.

277. Ferreira JR, Teixeira GQ, Santos SG, Barbosa MA, Almeida-Porada G and Goncalves RM. Mesenchymal Stromal Cell Secretome: Influencing Therapeutic Potential by Cellular Pre-conditioning. *Front Immunol*. 2018;9:2837.

278. Xiao Y, Peperzak V, van Rijn L, Borst J and de Bruijn JD. Dexamethasone treatment during the expansion phase maintains stemness of bone marrow mesenchymal stem cells. *J Tissue Eng Regen Med*. 2010;4:374-86.

279. Yarnazari A, Hassanpour P, Hosseini-Fard SR, Amirfarhangi A and Najafi M. The sdLDL Reduces MRC1 Expression Level and Secretion of Histamin e in Differentiated M2-macrophages from Patients with Coronary Artery Stenosis. *Cardiovasc Hematol Disord Drug Targets*. 2017;17:28-32.

280. Bi Y, Chen J, Hu F, Liu J, Li M and Zhao L. M2 Macrophages as a Potential Target for Antiatherosclerosis Treatment. *Neural Plast*. 2019;2019:6724903.

281. de Gaetano M, Crean D, Barry M and Belton O. M1- and M2-Type Macrophage Responses Are Predictive of Adverse Outcomes in Human Atherosclerosis. *Front Immunol*. 2016;7:275.

282. Lavin B, Gomez M, Pello OM, Castejon B, Piedras MJ, Saura M and Zaragoza C. Nitric oxide prevents aortic neointimal hyperplasia by controlling macrophage polarization. *Arterioscler Thromb Vasc Biol*. 2014;34:1739-46.

283. Lee SG, Oh J, Bong SK, Kim JS, Park S, Kim S, Park S, Lee SH and Jang Y. Macrophage polarization and acceleration of atherosclerotic plaques in a swine model. *PLoS One*. 2018;13:e0193005.

284. Lotvall J, Hill AF, Hochberg F, Buzas EI, Di Vizio D, Gardiner C, Gho YS, Kurochkin IV, Mathivanan S, Quesenberry P, Sahoo S, Tahara H, Wauben MH, Witwer KW and Thery C. Minimal experimental requirements for definition of extracellular vesicles and their functions: a position statement from the International Society for Extracellular Vesicles. *J Extracell Vesicles*. 2014;3:26913.

285. Filipe EC, Santos M, Hung J, Lee BSL, Yang N, Chan AHP, Ng MKC, Rnjak-Kovacina J and Wise SG. Rapid Endothelialization of Off-the-Shelf Small Diameter Silk Vascular Grafts. *JACC Basic Transl Sci*. 2018;3:38-53.

286. Eoghan Cunnane KL, Aneesh Ramaswammy, Prerak Gupta, Biman Mandal, Fergal O'Brien, Justin Weinbuam, David Vorp. Extracellular vesicles enhance remodeling of cell-free silk vascular scaffolds in rat aortae. *ACS Applied Materials & Interfaces*. in press.

287. Ahmann KA, Weinbaum JS, Johnson SL and Tranquillo RT. Fibrin degradation enhances vascular smooth muscle cell proliferation and matrix deposition in fibrin-based tissue constructs fabricated in vitro. *Tissue Eng Part A*. 2010;16:3261-70.

288. Patton MC, Zubair H, Khan MA, Singh S and Singh AP. Hypoxia alters the release and size distribution of extracellular vesicles in pancreatic cancer cells to support their adaptive survival. *J Cell Biochem*. 2020;121:828-839.

289. Almeria C, Weiss R, Roy M, Tripisciano C, Kasper C, Weber V and Egger D. Hypoxia Conditioned Mesenchymal Stem Cell-Derived Extracellular Vesicles Induce Increased Vascular Tube Formation in vitro. *Front Bioeng Biotechnol*. 2019;7:292.

290. Ramakrishnan VM and Boyd NL. The Adipose Stromal Vascular Fraction as a Complex Cellular Source for Tissue Engineering Applications. *Tissue Eng Part B Rev*. 2018;24:289-299.

291. Minteer D, Marra KG and Rubin JP. Adipose-derived mesenchymal stem cells: biology and potential applications. *Adv Biochem Eng Biotechnol*. 2013;129:59-71.

292. Kokai LE, Marra K and Rubin JP. Adipose stem cells: biology and clinical applications for tissue repair and regeneration. *Transl Res*. 2014;163:399-408.

293. Li H, Zimmerlin L, Marra KG, Donnenberg VS, Donnenberg AD and Rubin JP. Adipogenic potential of adipose stem cell subpopulations. *Plast Reconstr Surg*. 2011;128:663-72.

294. Soletti L. Development of a Stem Cell-Based Tissue Engineered Vascular Graft. *Swanson School of Engineering Department of Bioengineering*. 2009;Doctor of Philosophy.